OPTIMISATION OF PERIPHERAL VISUAL FUNCTION USING STIMULUS-BASED MANIPULATIONS

Jonathan Antony Patrick, MSc BSc (Hons)

Thesis submitted to the University of Nottingham for the degree of

Doctor of Philosophy

February 2017

Abstract

Ocular disorders that restrict visual capacity in the centre of the visual field, such as age-related macular degeneration (AMD) and Stargardt's disease, force patients to perform important visual tasks in the periphery. It is well documented that visual performance is progressively limited as the peripheral eccentricity at which the task is performed increases. Since many of the disorders that cause central vision loss currently have no cure, adaptive techniques to optimise the remaining visual function are required.

This thesis describes a series of psychophysical experiments that aim to optimise stimulus perception using manipulations to the stimulus input. Super-resolution (SR) is a form of image processing wherein multiple low-resolution images are merged over time to form a higher-resolution image. In many situations, the low-resolution sequence of images is produced by motion. Because of this, the effect of motion on peripheral acuity is first examined. The benefit of motion on acuity observed within 10° in the healthy periphery was very limited to specific combinations of target speed and retinal location. Thus, the investigation was extended to artificially undersampled stimuli. Spatial undersampling was achieved by presenting stimuli behind partially opaque masks. A significant benefit of motion was identified for the partially occluded stimuli, indicating a SR mechanism that operates when the visual input is sufficiently undersampled. In further experiments, it was established that smooth motion, originating from the target, is a key condition required for peripheral SR to be most effective.

Since motion was shown to be insufficient to significantly improve resolution in the typical periphery, the effects of additional temporal modulations applied to

static and moving stimuli were examined. Applying periodic temporal modulations to stimuli has the effect of creating temporal harmonics of the stimulus in the Fourier domain. The purpose of these experiments was thus to examine whether the visual system is capable of utilising these harmonics to better resolve the target. Temporally subsampling the stimulus, such that it appears with blank temporal intervals, was shown to drastically reduce the motion-related loss of acuity. However, at low target speeds, resolution thresholds were higher in the more subsampled conditions. It was shown that the loss at low speeds was driven by a reduction in the time-averaged contrast that accompanies temporal subsampling. Next, the effect of contrast polarity reversal was examined, whereby the target switches between black and white at periodic intervals, thus preserving the time-averaged contrast. Contrast polarity reversal diminished the motion-related loss, while also providing an overall reduction in resolution thresholds across speeds. Certain temporal modulations may therefore improve peripheral acuity for static and moving targets.

To test whether the benefit of temporal modulations may be of use in a patient population, the effect of modulating the stimulus on resolution thresholds was examined in simulated conditions of ocular disease. A common comorbid symptom of central vision loss is exaggerated ocular jitter. The effects of subsampling and contrast polarity reversal were examined on resolution thresholds for targets jittering in accordance with ocular motion, multiplied by a variable gain factor. Temporal subsampling, as for smooth motion, was a hindrance to resolution. Contrast polarity reversal, however, was shown to improve performance at all levels of jitter. Contrast polarity reversal was also examined in simulated conditions of neuro-retinal matrix disorder (NRMD),

whereby targets appear with spatial undersampling. There was no significant improvement in resolution for undersampled targets. Thus, while temporal modulations may be beneficial in some central vision loss disorders, the results do not support its use in NRMD patients.

Additional temporal stimulus modulations therefore have diverse effects on resolution. To investigate the mechanisms driving these effects, a model was created to examine how the temporal modulations were influencing the perception of the stimulus. In the development of the model, the spatiotemporal characteristics of the stimulus were assessed. By calculating the extent to which the stimulus was compromised of frequencies to which the visual system is sensitive, an estimate of how visible the target should be in each condition was estimated. In assessment of the spatiotemporal characteristics of the stimuli, it was confirmed that contrast alone is not sufficient to explain the benefits of contrast polarity reversal. Further, the model indicated that the extended spectral range additional temporal modulations provide the stimulus is a reasonable explanation of the effects the modulations have on resolution, when combined with a description of the retinal response to temporally modulating stimuli.

Finally, to confirm the use of contrast polarity reversal as a technique to optimise peripheral function in vision loss disorders, it was examined in a more salient task for patients: peripheral reading. Reading speed and accuracy were assessed for peripheral sentences with and without temporal modulation, in healthy observers and in patients with central vision loss. Both healthy observers and patients made significantly fewer errors in the contrast polarity reversal conditions than in the unmodulated conditions. However, only the healthy observers demonstrated a

reduction in reading speed. While the results do not wholly support contrast polarity reversal, it was postulated that patients with more severe symptoms of AMD may reveal a stronger benefit.

Thus, the experiments in this thesis have demonstrated that performance on several peripheral visual tasks can be improved by applying additional temporal modulations to the stimulus. Further, it has been indicated that this benefit stems from a combination of the contrast of the stimulus, and the effect of the modulation on the spatiotemporal characteristics of the target.

Acknowledgements

I would like to thank my supervisors, Neil Roach and Paul McGraw, for their tireless assistance throughout this work. My thanks also go to everyone in office C68, Nottingham Visual Neuroscience, and the Human Vision Laboratory at the University of Western Australia. This thesis would not have been possible without endless support from my friends, my family, and Lucy.

This project was funded by Fight for Sight.

"Data! Data! Data!" he cried impatiently. "I cannot make bricks without clay!"

Sherlock Holmes*, The Adventure of the Copper Beeches.*

Contents

Chapter 1: Introduction

1.1 Outline

There are over 20,000 people in the UK with a registered visual impairment, many of which are permanent and untreatable (Bunce & Wormald, 2006). This makes it very important to seek methods of optimising the use of the remaining visual capacity. This thesis describes a series of psychophysical experiments on visual performance in healthy and diseased eyes, aiming to develop and characterise a non-invasive technique for maximising resolution capacity in patients for whom performing visual tasks can be increasingly challenging.

This introduction provides a brief outline of the anatomy of the visual system, and how visual performance is assessed in humans. Then, the characteristics of visual perception are discussed, with specific focus on the capacity for resolving static and moving peripheral targets. Next, the influence that specific forms of ocular disease have on visual perception is discussed, and existing techniques for optimising the remaining visual capacity in patients that have suffered vision loss are explained. Finally, an overview of the experiments in this thesis is provided.

1.2 Vision

The basis of visual perception is light. The human visual system is sensitive to electromagnetic radiation in the wavelength range 400-700nm. Photons within this range travel through the cornea to the lens, whereby the photon path is corrected to produce an in-focus image on the retina. Photons outside this range are not detected, because they pass unaffected through retina, are absorbed by the

cornea, or are not energetic enough to activate the photoreceptive cells. The ability to focus on an image is reliant on the ability of the cornea and the lens to refract light onto the retinal surface. The quality of focus is contingent on the linespread function of the eye, a measure of the extent to which the retinal image of an object is degraded by the optical qualities of the eye (Campbell & Gubisch, 1966). The linespread function widens, i.e. focus is degraded, as pupil size is increased. This results in an optical blurring of a visual object prior to it reaching the retina.

The retina consists of arrays of photoreceptor cells, which convert incident photons into electrical energy. These pulses of electrical energy are collected by bipolar cells and transmitted to ganglion cells. The axons of ganglion cells transmit electrical information through the optic nerve to the brain (Curcio & Allen, 1990). There are two classes of photoreceptors: rod cells and cone cells. Rod photoreceptors detect low-intensity monochrome light, whilst cones are responsible for the detection of higher-intensity light, and can distinguish between different wavelengths. Cone cells are clustered at the fovea, an anatomical region that subtends approximately 1° 10’ across the centre of the visual field. The fovea is contained within the larger macula, which has a diameter of approximately 5° (Yanoff & Sassani, 2009). In humans, there are three types of cone cell sensitive to the shorter, middle and long-wavelengths of the visible spectrum, allowing for a vast number of distinguishable hues (Kuehni, 2016). Unlike rod cells, foveal cone cells synapse on a single bipolar cell, which in turn connects to a single ganglion cell (Curcio & Allen, 1990; Polyak, 1941). Because of this, the signals propagated by cone cells have high spatial precision. Owing to this increased spatial resolution possible through cone cells, the macula is responsible for high

acuity tasks such as reading and identifying small objects. Beyond the fovea, retinal ganglion cells begin to receive projections from multiple cone cells, which places an additional restraint on resolution (Rossi & Roorda, 2010). Bipolar cells synapse onto a far higher number of rod cells, resulting in poorer spatial resolution.

The relative densities of photoreceptor cells change greatly with retinal eccentricity, with the greatest changes occurring in the central 10° of the visual field (Curcio, Sloan, Kalina, & Hendrickson, 1990). At the fovea, the ratio is strongly in favour of cone cells but cone density decreases rapidly, reaching a low stasis from 20° in both nasal and temporal fields. Rod density increases drastically into the periphery, peaking at 20° before steadily reducing, while remaining an order of magnitude above cone density even as far out as 80° (Curcio et al., 1990). The relative densities of rod and cone photoreceptors are shown in Figure 1. Rod density is still very high in the periphery, but the signals from many rods converge onto a single neuron, which implies the high rod density is not designed to improve spatial resolution but sensitivity to low-intensity stimuli. Cone cells, however, project signals to far fewer ganglion cells, allowing them to produce high spatial resolution (Rossi & Roorda, 2010).

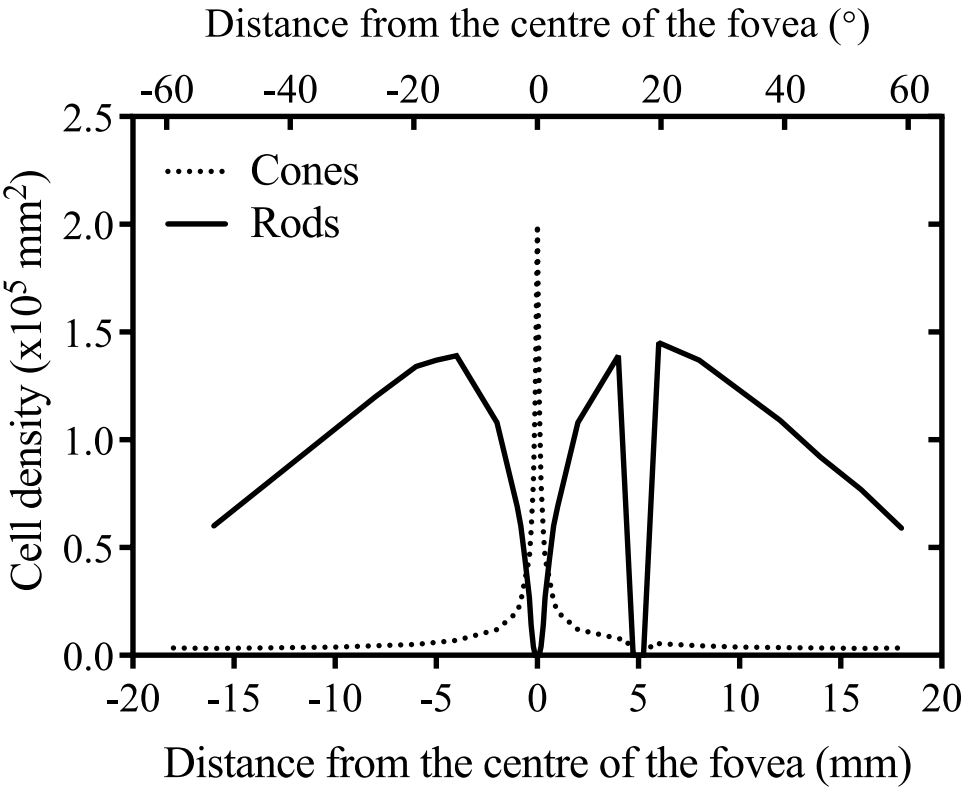

Figure 1: Density of cone and rod photoreceptors as a function of retinal eccentricity on the horizontal meridian (in the temporal and nasal visual fields). Cone receptors are dominant in the centre of the fovea, but are rapidly overtaken by rods in the periphery. Note the physiological blind spot in the temporal retina, whereby the retinal surface is obscured by the optic nerve. Data adapted from Curcio et al. (1990).

The physiological inhomogeneity in receptor layout leads to inhomogeneous visual performance across the visual field. The loss of spatial resolution with eccentricity is well documented (e.g. see Thibos, Cheney, & Walsh, 1987; Thibos, Walsh, & Cheney, 1987; Westheimer, 2009). Resolution has also been shown to diminish as retinal eccentricity is increased. At the centre of the fovea, resolution is mediated by the spacing between cone cells. However, as the retinal eccentricity increases, the retinal surface begins to become dominated by rod cells, and resolution is instead limited by the receptive field size of retinal ganglion cells (Rossi & Roorda, 2010). Retinal inhomogeneity has therefore

resulted in inhomogeneous performance. Performance in several other visual tasks has also been shown to diminish with increasing retinal eccentricity. For example, critical print size is increased, reading speed is slower, and letter identification is less accurate (Chung, Legge, & Tjan, 2002; Legge, Mansfield, & Chung, 2001).

The distribution of photoreceptor cells across the retina is anisotropic as well as inhomogeneous. The spatial density of both rod and cone cells, as well as ganglion cells are higher at the same distance left or right of the fovea than superior or inferior, most distinctly toward the temporal retina (Curcio & Allen, 1990; Curcio et al., 1990). Accordingly, anisotropic performance has been identified in several situations.

The contrast between adjacent areas in a visual image is determined by the difference in their luminance, and the capability of an observer to detect this is known as contrast sensitivity (CS). Rijsdijk, Kroon, and van der Wildt (1980) demonstrated psychophysically that CS closely follows the pattern of photoreceptor cell density. CS to sinusoidally modulated luminance targets was examined at several eccentric locations. Sensitivity for low spatial frequency targets is highest in the nasal visual field (the temporal retina), followed by the temporal field, and then by similar performance in the superior and inferior fields. However, for higher spatial frequencies the performance bias along the horizontal meridian evens out, while remaining consistently more sensitive than locations on the vertical meridian. Similar results have been found by Regan and Beverly (1983) and Rovamo, Virsu, Laurinen, and Hyvärinen (1982). Pointer and Hess (1989) also reported that the decline in CS with retinal eccentricity depends on the spatial frequency of the grating, and that the rate of decline differs between the

horizontal and vertical meridians. However, there was no difference in the rate of decline between the nasal and temporal fields at any of the target spatial frequencies. Alternatively, Khuu and Kalloniatis (2015) found that for sufficiently large targets, there was no significant difference in CS between the cardinal axes (on the horizontal and vertical meridians) and the oblique (diagonal) axes. However, larger targets increase the area of the retinal surface across which they are displayed, obscuring estimates of the photoreceptor density at the target location.

Similarly, motion detection shows anisotropic properties. The direction of motion to which sensitivity is highest corresponds to the spatial meridian along which the target is presented (i.e. when motion direction is along the axis joining the point of fixation with the target location) (Van De Grind, Koenderink, Van Doorn, Milders, & Voerman, 1993).

Acuity, a measure of sensitivity to fine detail, has also been shown to depend on the retinal location of the target. Altpeter, Mackeben, and Trauzettel-Klosinski (2000) found peripheral letter identification was better in the horizontal than the vertical meridian, and that this was consistent in healthy eyes and in central vision loss. Similarly, Carrasco, Williams, and Yeshurun (2002) reported that peripheral Landolt rings appearing on the vertical meridian were generally resolved less accurately and slower than those on the horizontal meridian, but that this relationship was dependent on the size of the target and the eccentricity at which it was presented.

Thus, the perception of visual images is contingent on many covarying factors. However, the relationships between many of these factors and the accuracy of the

perceived image are well documented. While the effects of some visual attributes remain uncertain or untested, several key methods of examining these relationships have been described.

1.3 Psychophysical measures of visual performance

Visual performance is often quantified using psychophysical procedures. Psychophysics refers to an experimental method of recording reactions participants make in response to specific visual stimulation. A typical psychophysical experiment may consist of presenting the participant with a visual stimulus with very specific and precise features and characteristics, then measuring the speed, sensitivity, or accuracy of the participant's perception of the stimulus. Stimulus characteristics commonly measured using psychophysics include the contrast of the stimulus against an isoluminant background, the speed, the retinal location, and the spatial and temporal frequencies of the stimulus.

Acuity is a common measure of the perceived clarity of an image, and is usually established psychophysically. It refers to the sensitivity of the visual system to the high spatial frequency information present in the stimulus, such as the borders or edges. Acuity is often measured in terms of the threshold size of a visual target at which it can be accurately identified. Resolution threshold is the reciprocal of visual acuity. One common way to measure acuity is to examine Vernier acuity (Westheimer, 1979), which attempts to quantify the observer's ability to detect a misalignment between two adjoining line segments. Examples of Vernier targets are shown in Figure 2A. Vernier acuity thresholds are a simple and robust way of assessing visual performance, but performance relies heavily on the

characteristics of the lines such as length and thickness, and not just the magnitude of the misalignment.

Resolution thresholds are also estimated using two-line separation tasks (Westheimer, 1987). This method increases the separation of a pair of line sources until the observer can report a separation. Like Vernier acuity, observers' discrimination criteria may not rely exclusively on the critical detail, but may be being estimated based on a perception of a blurring or widening of the stimuli. This can be controlled for, as in Westheimer and Beard (1998) by using a control bar of width matching the double-line stimulus, although a variation in intensity my be detectable without resolution of a gap. An example of a two-line separation target and control bar are shown in Figure 2B. Alternatively, König bars provide an assessment of spatial resolution without a confounding uneven distribution of luminous intensity (Westheimer, 1987). König bars are a pair of parallel lines, of fixed width in relation to the size of the target. The width of the bars and the gap is one third of the total width. The observers' task is to decide if they appear horizontally or vertically. Examples of König bars are shown in Figure 2C.

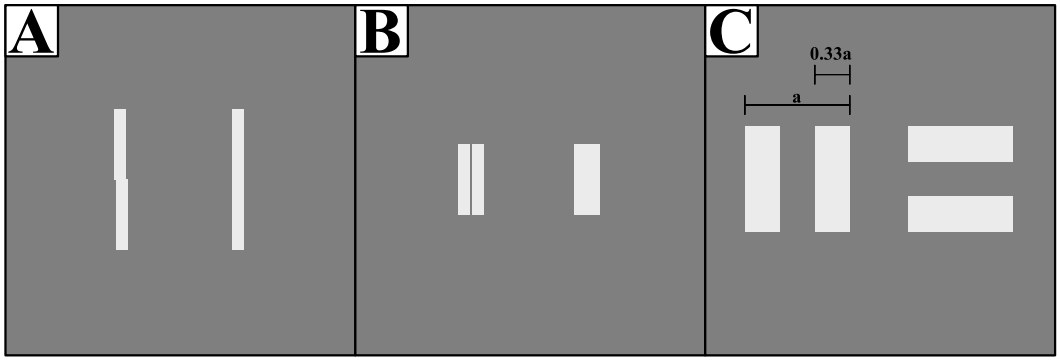

Figure 2: Examples of line stimuli. (A) Example Vernier targets (Westheimer, 1979). Observers are tasked with identifying misaligned (left) from aligned (right) lines. (B) Example two-line separation targets (Westheimer, 1987). Observers report on perceived separation between bars (left). In some studies (e.g. Westheimer & Beard, 1998), separated lines are distinguished from a control bar of matching width (right). (C) König bars (Westheimer, 1987) are an example of lines being used in a resolution task. The width of the bar and gap are a fixed relationship. Observers indicate perceived bar orientation, vertical (left) or horizontal (right).

Sensitivity to grating stimuli is often examined in vision studies. Gratings with luminance or contrast modulations of both square- and sinusoidal-wave are used, and paradigms can ask several different questions, such as if the grating was detectable, or for an indication of the orientation of the lines. Gabor patches are a special case of grating in which contrast is modulated sinusoidally and contained in a Gaussian window. An example Gabor patch is shown in Figure 3. Gabor patches are often used in detection tasks, in which the threshold patch contrast is reduced until it can no longer be detected from the background. Alternatively, a task in which the observers estimate the orientation of the lines, or distinguish between patches at different orientations can provide an estimate of the resolvability of the patch. Studies often compare performance at these tasks at different spatial and temporal frequencies of the patch. Spatial and temporal frequency sensitivity provides a useful indication of visual ability and how it changes under different conditions, for example with moving stimuli, or at

different visual field locations (Burr & Ross, 1982; Burr, Ross, & Morrone, 1986a; Koenderink, Bouman, de Mesquita, & Slappendel, 1978).

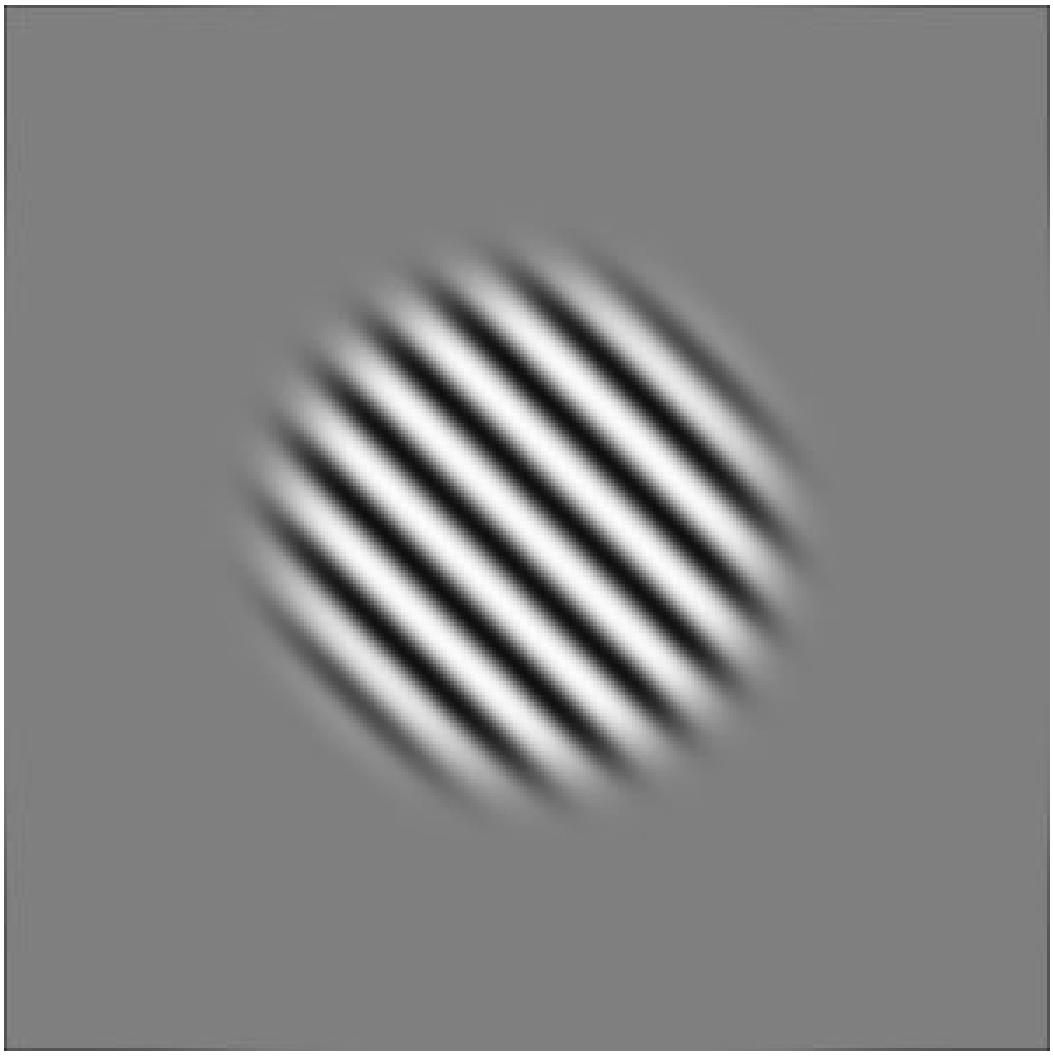

Figure 3: Example of a Gabor patch. It is a sinusoidal variation in luminance of fixed and predetermined spatial frequency that is contained within a Gaussian window.

The part of the target vital to its identification in visual experiments is often referred to as the critical detail. These are often high spatial frequency, such as line edges or gaps in Landolt rings, so the loss of sensitivity to high spatial frequencies has an important effect on performance in many acuity tasks. While gratings are useful for identifying the constraints of the visual system, more

naturalistic stimuli such as letter detection tasks can provide insight into the mechanisms of the visual system under normal viewing conditions.

Letter discrimination tasks are examples of more naturalistic stimuli, better representing the ability to perform an everyday task such as reading under the given conditions. Letter discrimination tasks are used for finding the conditions under which reading becomes most difficult. Standardised letter targets are used clinically as a measure of acuity, such as in Snellen letter charts (Ferris, Kassoff, Bresnick, & Bailey, 1982), in which observers identify letters that decrease in height until they can no longer be identified. An advantage of letter targets is that they are highly familiar to observers, and are easily standardised.

Landolt ring tasks are often used to quantify the ability of an observer to obtain information from a small part of the stimulus. A Landolt ring is a capital letter C in Sloan font (Pelli, Robson, & Wilkins, 1988). It is circular, with the stroke width fixed at one fifth of the ring diameter. The critical detail of the Landolt ring is the gap, a square break in the ring, the sides of which are also one fifth the diameter. An example Landolt ring is shown in Figure 4A. Orientation information can be obtained from any point on a grating, but in a Landolt ring task the critical detail is much more localised, making up less than 9% of the total stimulus.

A Tumbling E target is an alternative to the Landolt ring. It is a capital letter E in Sloan font. It is square, with the stroke width one fifth of the letter height. An example of a Tumbling E target is shown in Figure 4B. Observers are often tasked with identifying the orientation of the critical details (the gaps created by the strokes), or discriminating the Tumbling E from three parallel bars (Anderson & Thibos, 1999a). Reich and Ekabutr (2002) suggested that for healthy eyes with

normal visual acuity, the Landolt ring and the Tumbling E provide comparable estimates of visual acuity. However, the circular Landolt ring can be presented at any orientation without providing visual cues aside from the critical detail. As the Tumbling E is square, there are only four possible directions the critical details can face without altering the orientation of the entire target.

Vanishing optotypes are a type of acuity test letter in which high spatial frequency filters have greatly diminished the interval between detection and resolution thresholds for letter charts (Frisén, 1986). Letter targets are high-pass filtered, such that low spatial frequency information is diminished. They are presented on a uniform grey background and the minimum contrast at which they can be detected, and at which the letter can be identified, is assessed. An advantage of filtering targets in this manner is that it limits the broad range of spatial frequencies typically contained within a letter target (Bondarko & Danilova, 1997). High-pass filtered letter targets are used clinically in the Moorfields Acuity Chart (Shah et al., 2016).

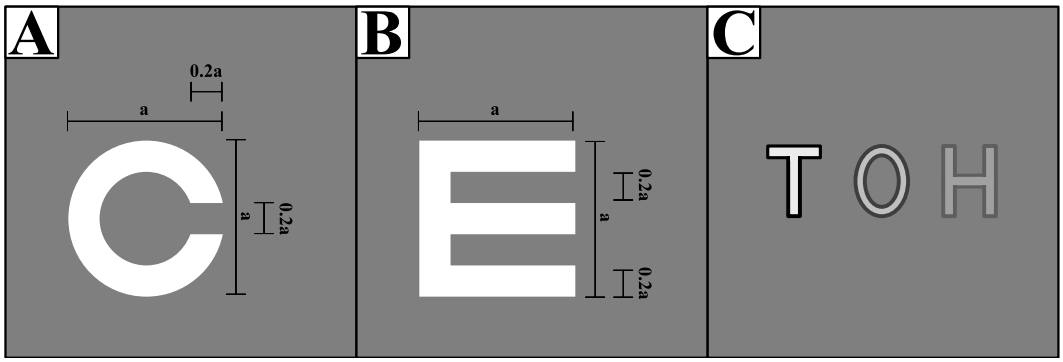

Figure 4: Examples of stimuli used in examining acuity. (A) a Landolt ring is a capital letter C in Sloan font. The stroke width of the ring is fixed at one fifth of the diameter. The gap in the ring (the critical detail) is a square, the sides of which are one fifth the ring diameter. (B) a Tumbling E, a capital letter E in Sloan font. The stroke width is one fifth of the height of the target. (C) Vanishing optotypes (Frisén, 1986) are capital letters in Ariel Bold font, which have been high-pass filtered.

1.4 Describing visual stimuli in the Fourier domain

CS is typically measured using sinusoidal gratings, alternating black and white bars of fixed width. Gratings are useful in examining visual function due to their precise spatial frequency profile, which is easily manipulated, and usually assessed in the Fourier domain. Sensitivity to spatial and temporal frequency are often quantified using a contrast sensitivity function (CSF), indicating the relationship between the spatial or temporal frequency of a grating and the viewer's ability to distinguish the grating from the background.

The optimum spatial and temporal frequencies for accurate perception are well documented. Kelly (1979, 1985) mathematically described the spatiotemporal sensitivity surface, a three-dimensional plane indicating sensitivity to a stimulus at each possible combination of spatial and temporal frequency. Watson, Ahumada, and Farrell (1986) used such a model to create the spatiotemporal window of visibility, a description of the visual sensitivity of an idealised observer. The

description of the window of visibility has been extended to include how it is affected by certain stimulus characteristics (Watson, 2013; Watson & Ahumada, 2005). For example, they showed that the spatial limits of the window shrinks with increasing eccentricity, as has been demonstrated psychophysically (Berkley, Kitterle, & Watkins, 1975; Johnson, Keltner, & Balestrery, 1978). The comprehensive account of the spatiotemporal window of visibility and factors affecting it provides a useful template for estimating the accuracy of stimulus perception, based on its own spectral profile.

More spatially-complex stimuli such as Landolt ring targets can also be assessed in terms of the constituent frequencies using Fourier analysis (e.g. Bondarko & Danilova, 1997). Fourier analysis is a mathematical technique used for converting a two-dimensional image that changes with time into a depiction of its constituent spatial and temporal frequencies. Van Santen and Sperling (1985) described how stimulus characteristics can affect the Fourier spectrum of the stimulus. The Fourier spectrum of a static sinusoidal grating is shown in Figure 5A. Since it is static, the temporal frequency component is zero. Gratings have fixed spatial and temporal frequencies, which results in small, precise spectral profiles in the Fourier domain. They showed that stimulus motion is manifested as orientation in the Fourier domain; Figure 5B shows the Fourier spectrum for a grating drifting at a fixed velocity. They also demonstrated that applying periodic temporal modulations to a grating creates temporal harmonics of the spectrum, appearing as lower-amplitude copies of the original spectrum at regular intervals along the temporal frequency axis. The modulation applied by Van Santen and Sperling (1985) in this example was temporal subsampling, whereby the grating is periodically replaced with a blank, isoluminant screen. This is shown in Figure

5C. Thus by applying temporal modulations to a stimulus, its spectral range can be manipulated. For a more detailed explanation of the effect of stimulus modulations on the Fourier spectra of regular and irregular gratings, refer to Van Santen and Sperling (1985).

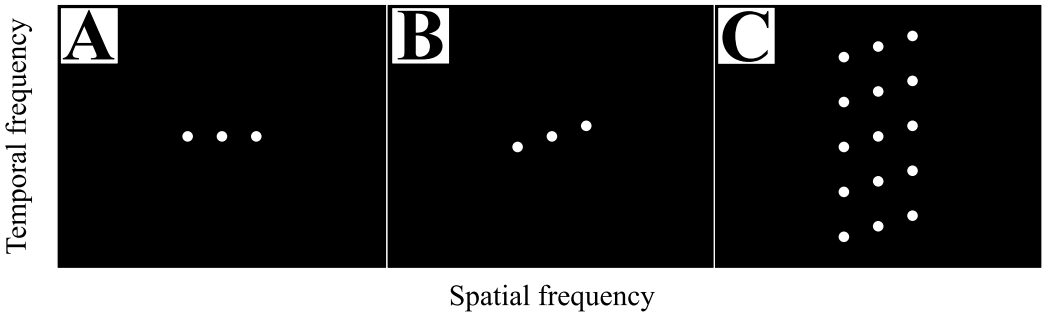

Figure 5: Fourier spectra of sinusoidal gratings in different conditions. The centre of each plot represents zero on both the abscissa and ordinate. (A) The Fourier spectrum of a static sinusoidal grating. (B) The Fourier spectrum of a sinusoidal grating moving at a fixed velocity. Motion results in orientation in the Fourier domain. (C) Fourier spectrum of a sinusoidal grating moving at a fixed velocity, with temporal subsampling. Additional temporal harmonics have appeared above and below the original spectrum. Adapted from Van Santen and Sperling (1985).

Thibos and Anderson (2004) made a link between the Fourier description of a target and its visibility, measured psychophysically. They calculated the difference image of letter pairs using a pixel-by-pixel subtraction, which was transformed into the Fourier domain, creating a difference spectrum for that letter pair. They calculated the spatial dissimilarity of the letters using a normalised comparison of the Fourier components of the individual letters to the difference spectrum. They also psychophysically measured the threshold letter size required to distinguish between the two letters in the pair at 30° eccentricity. By plotting the measure of letter dissimilarity against discriminability, they demonstrated a

strong correlation; the higher the Fourier dissimilarity, the smaller the letters needed to be to be distinguished.

Thus, both visual stimuli and models of visual capacity have been described in the Fourier domain, and analysis of stimuli in the Fourier domain has been used to accurately model visual behaviour.

1.5 Factors affecting acuity

There are many stimulus characteristics that influence the capacity for object resolution. This list includes, but is not limited to, the retinal location at which the target is presented (i.e. its eccentricity; e.g. Battista, Kalloniatis, & Metha, 2005; Brown, 1972a, 1972b), the speed at which it moves (Chung & Bedell, 2003; Levi, 1996), the proximity of irrelevant objects (Chung, 2004; Levi, 2008), the target's luminance (Simpson, Barbeito, & Bedell, 1986), and the luminance contrast between the target and the background (Johnson & Casson, 1995). This thesis will focus mostly on two of these characteristics: target speed and retinal location.

Visual performance is reliant upon the retinal location to which the target object is presented. Target location has a well-documented effect on acuity: as the distance of the target from the centre of the fovea increases (the more eccentric the target), acuity diminishes, i.e. the target must be larger for accurate resolution (e.g. Battista, Kalloniatis, & Metha, 2005; Brown, 1972).

The retinal location of irrelevant objects relative to the target also has a notable effect on visual performance. Targets are generally more difficult to resolve in the presence of other objects in close proximity, a phenomenon referred to as crowding (Bouma, 1970; Levi, 2008). Crowding is detrimental to acuity across

the visual field, but the relative proximity required for performance to deteriorate increases (Falkenberg, Rubin, & Bex, 2007). I.e., the more eccentric the target, the further from it objects must be to avoid impacting its resolution. Crowding can also be limiting to performance in reading tasks when the spacing between consecutive words is too small (Blackmore-Wright, Georgeson, & Anderson, 2013), or if the lines of text in a paragraph are too close (Chung, 2004).

Because acuity is a measure of sensitivity to high spatial frequencies, the loss of acuity with increased eccentricity has been attributed to the observed shift in the range of visible spatial frequencies. As eccentricity increases, both peak sensitivity and the sensitivity limit shift to lower values of spatial frequency (Berkley et al., 1975; Koenderink, Bouman, Bueno de Mesquita, & Slappendel, 1978b). This is demonstrated in Figure 6A.

The same pattern was demonstrated for targets of increasing speed by Burr and Ross (1982): the faster a target moves, the larger it must be for accurate identification. Dynamic visual acuity is a measure of the ability of an observer to discriminate spatial detail in the presence of retinal motion (Brown, 1972a). Investigations of the effects of motion on peripheral acuity are abundant. Studies investigating target speed in the periphery generally support the finding of degraded acuity with faster stimuli (e.g. see Chung & Bedell, 1998; Levi, 1996) compared to the static visual acuity. Brown (1972b) looked closer at the effects of low target velocities over a range of eccentricities. For foveal targets, smooth motion had a consistent degrading effect on resolution thresholds. However, he reported a characteristic decrease in resolution threshold (improvement in performance) for slow, compared to static, peripheral targets. Westheimer and

McKee (1975) on the other hand suggested that target motion does not necessarily improve acuity, but certainly target stasis is not a requirement for good vision in the fovea. This is contrary to Brown (1972a), who indicated that good static acuity appears to be a necessary condition for good dynamic acuity, but that even when observers' resolution of static targets is comparable, measures of dynamic visual acuity are highly variable.

Motion detection occurs for smaller targets than the minimum angle of resolution (MAR) (Thibos, Cheney, et al., 1987). By normalising the detection thresholds at each velocity, Chung, Levi, and Bedell (1996) determined that because thresholds increase with velocity, despite being equally visible, a reduction in stimulus visibility with increasing velocity was not the cause of poorer resolution thresholds for moving targets. They later showed that the limits to letter acuity are spatiotemporal, not just temporal (Chung & Bedell, 2003). By examining the effect of band-pass filters, velocity and contrast on Vernier and letter acuity, they determined that stimuli of higher spatial frequencies became harder to resolve at a lower velocity. This is in support of reduced Vernier and letter acuities resulting from shifts in spatial frequency sensitivity.

Similarly to increasing retinal eccentricity, increasing target speed has been associated with a shift in sensitivity toward lower spatial frequencies (Burr & Ross, 1982), shown in Figure 6B. The loss of acuity at higher target speeds is thus often explained in terms of this shift. An alternative explanation for the observed detrimental effect of increasing smooth target motion is motion smear (Burr, 1980; Burr et al., 1986a). Visual information is summated over time (Cavanagh, Holcombe, & Chou, 2008). Thus, as a target in motion will be presented to

adjacent photoreceptor arrays across time, this leads to a perceptual smearing of the image. Critical details of the target may overlap with other parts of the target throughout the motion trajectory, leading to a blurring of the high frequency image detail (Hammett, Georgeson, & Gorea, 1998).

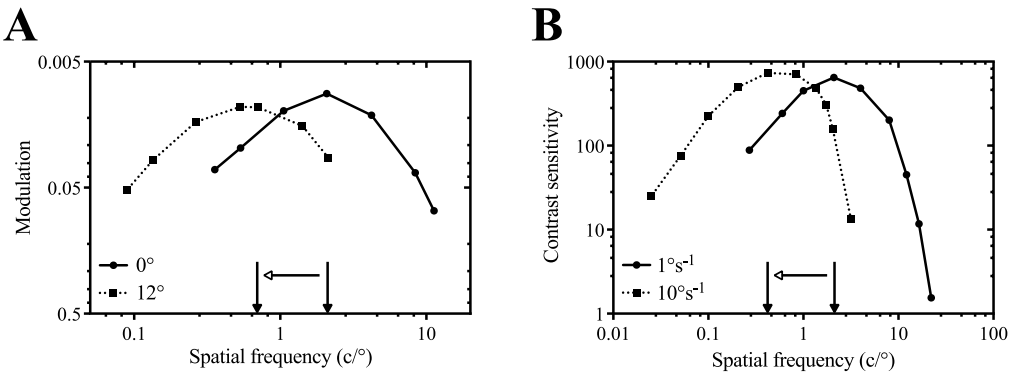

Figure 6: shifts in CSFs, contrast sensitivity to sinusoidally modulated gratings, as a function of spatial frequency. (A) increasing target eccentricity results in the peak sensitivity shifting to lower values of spatial frequency. Data adapted from Kelly (1984). Modulation, on the ordinate, is an inverse measure of contrast sensitivity. (B) increasing target speed also results in a shift in the peak sensitivity towards lower spatial frequencies. Data adapted from Burr and Ross (1982). Filled arrows on the abscissae indicate peak spatial frequencies of the sensitivity curves, and the open arrows show the direction on the shift as the target eccentricity or speed increases.

Thus, with some possible exceptions, smooth target motion is generally detrimental to visual acuity. This has been reported for target trajectories moving across the visual field (Brown, 1972b), and for targets constantly foveated by smooth pursuit eye movements (Brown, 1972a). However, target motion can also be induced by unintentional ocular movement, resulting in a less predictable jittering motion.

1.6 Fixational eye movements

Fixational eye movements (FEMs) are small, natural, involuntary shifts in eye position that occur during normal vision (Collewijn, van der Mark, & Jansen, 1975; Ratliff & Riggs, 1950). This is in contrast to intentional saccades, which are voluntary eye movements intended to foveate or continuously track an intended target. Intentional saccades occur up to five times a second in natural viewing, separated by periods of up to 300ms. FEMs occur during the periods between saccades, or during deliberate periods of fixation (Fischer & Weber, 1993). Three distinct patterns of FEMs have been identified: drifts, microsaccades, and tremors (Martinez-Conde, Macknik, & Hubel, 2004). Drifts are frequent ocular disturbances that shift the retinal image between 3-12 minutes of arc, over a duration of up to 1s (Riggs, Armington, & Ratliff, 1954). This shift is often corrected by a microsaccade, which can return the retinal image to the fovea (Engbert & Mergenthaler, 2006). Microsaccades therefore also shift the image up to around 14 minutes of arc, typically taking up to 25ms to complete, and occurring at a rate of approximately one to three per second (Zuber, Stark, & Cook, 1965). Finally, tremors are very small, very high frequency aperiodic jitters. They can occur at frequencies up to 90Hz, while moving the retinal image between 10-20 seconds of arc (Riggs, Ratliff, Cornsweet, & Cornsweet, 1953). The high frequency and small retinal shift caused by tremors suggests that they have very low impact on visual perception, arising from the tension in opposing ocular muscles (Riggs & Ratliff, 1951).

In this description of FEMs, drifts are erroneously allowing the retinal image to slip away from the fovea, while microsaccades are corrective of this. This

corrective role may extend into binocular oculomotor function. Binocular disparity refers to discordance in fixation between the left and right eye, which is often caused by independent drift (Krauskopf, Cornsweet, & Riggs, 1960). Engbert and Kliegl (2004) demonstrated that disparity was higher directly before a microsaccade than after, again suggesting a corrective function. Aside from correcting erroneous ocular jitter however, there are situations in which FEMs can support visual performance. FEMs have been shown to counteract perceptual fading due to neural adaptation (Riggs et al., 1953). The loss of sensitivity to a static peripheral target is known as Troxler fading (Troxler, 1804). Martinez-Conde, Macknik, Troncoso, and Dyar (2006) demonstrated that the onset of Troxler fading occurred at times when microsaccade rate and amplitude dropped. As targets reappeared, the rate and amplitude increased. Thus, FEMs may have a role in shifting the retinal image in order to prevent neural adaptation to an unchanging stimulus. Other studies have suggested that FEMs play an unimportant role in perception. Kowler and Steinman (1980) argue that they serve no functional purpose, and are instead a result of the artificial environment in which they are measured. They suggest that the habit of inspecting the environment persists during testing. While head motion is restricted, and actively maintaining fixation is encouraged, ordinary saccadic motion is intentionally inhibited, creating unnatural ocular motion.

While the precise function of FEMs is unclear, they undoubtedly shift the visual image across the retina. As discussed previously, reduction in acuity with stimulus motion is well documented (e.g. Brown, 1972b; Burr, Ross, & Morrone, 1986; Chung & Bedell, 2003). Ocular drifts have been reported to have typical speeds between 0.15-0.42°s^{-1} (Martinez-Conde et al., 2004; Yarbus, 1967).

Microsaccades are much faster, with a wide range of reported speeds; Yarbus (1967) suggests they are as slow as $10°s^{-1}$, while Engbert and Kliegl (2003) report them at up to $120°s^{-1}$. Thus, the increased target motion should result in inhibited resolution capacity. However, performance in Vernier acuity, hyperacuity, and crowding are resistant to unstable fixation up to high levels of retinal jitter, which is in contrast to conditions of smooth object motion (Badcock & Wong, 1990; Bex, Dakin, & Simmers, 2003; Falkenberg et al., 2007; Macedo, Crossland, & Rubin, 2011). Resistance to ocular jitter is indicative of a perceptual stabilisation mechanism. Evidence for such a mechanism has been reported by Murakami and Cavanagh (1998). After adapting to dynamic noise, when presented with static noise, the adapted regions appeared stationary while the unadapted regions appeared to jitter. They suggest this indicates a mechanism that is sensitive to the baseline image motion, which it subtracts from the final image leaving only external motion signals. In regular viewing, FEMs are responsible for the baseline image motion. Adapting to dynamic noise interferes with perception of image motion within that region, which creates a new baseline. Thus, the adapted regions appear static, while the unadapted regions maintain an additional motion signal from FEMs. This results in the image motion from FEMs being perceived above the baseline in the unadapted regions. As FEMs are typically responsible for the baseline image motion, retinal image jitter is not usually perceptible.

Thus, while FEMs are an unavoidable and well-documented aspect of visual perception, their effect on visual performance is unclear. Atypical FEMs are often comorbid with other visual defects. For example, central vision loss has been associated with increased FEM amplitude (Macedo, Nascimento, Gomes, & Puga, 2007; Martinez-Conde, 2006b). Kumar and Chung (2014) estimated that FEM

amplitude is exaggerated by a factor of between 2 and 4 in patients with established central vision loss disorders.

1.7 Age-related macular degeneration

Age-related macular degeneration (AMD) is a central vision disorder and is the leading cause of visual impairment in the United Kingdom and most other industrialised nations (Bunce & Wormald, 2006; Evans, Fletcher, & Wormald, 2004; Ghafour, Allan, & Foulds, 1983; Klein et al., 2007). Advanced AMD is characterised by a large central scotoma (blind spot), which reduces visual acuity and contrast sensitivity in the centre of the visual field. Established scotomata cover an average area of 75.17°^{2} (*SD* 56.08°^{2}; Lee & Markowitz, 2010). This results in a region of obscured vision within an average of 4.89° (*SD* 4.22°) of the centre of the visual field. There are two types of AMD. The dry (non-exudative) form is caused by an accumulation of drusen (extracellular debris) behind the retina, causing retinal atrophy and scarring. In the wet (exudative) form, abnormal blood vessels develop behind the retina, causing scarring and exuding blood and fluid into the eye (Coleman, Chan, Ferris, & Chew, 2008; Lim, Mitchell, Seddon, Holz, & Wong, 2012). Although wet AMD is responsible for around 90% of AMD-related blindness, dry AMD accounts for approximately 80% of the incidence of the disease (Mehta, 2015; Velez-Montoya et al., 2014). AMD usually affects one eye more strongly than the other, but the risk of developing AMD in the second eye is as high as 23% three years after initial presentation in the affected eye (Roy & Kaiser-Kupfer, 1990). Treatment for AMD is limited. While there is no treatment for dry AMD, wet AMD is treated with anti-vascular endothelial growth factor (anti-VEGF; Wong, Liew, & Mitchell, 2007). Although

anti-VEGF treatment has been shown to be effective at improving acuity in AMD patients (Rosenfeld et al., 2006), it is often associated with devastating adverse effects such as intraocular inflammation and ocular haemorrhaging (Ghasemi Falavarjani & Nguyen, 2013). Because of these side-effects, and since dry AMD has no cure currently available, patients with AMD often rely on non-invasive coping strategies developed through practice rather than on clinical intervention.

In contrast to many other visual disorders, AMD patients typically maintain peripheral function. This allows for adaptive strategies such as developing a preferred retinal locus (or loci, PRL), a peripheral location consistently used as a substitute fovea for eccentric viewing. Patients with a long-standing, stable scotoma may be expected to more consistently use a single, established PRL while patients with recently developed scotomata are less likely to efficiently use a small, optimum retinal location (Whittaker, Budd, & Cummings, 1988).

The location of the PRL has been extensively studied. Shima, Markowitz, and Reyes (2010) demonstrated that the PRL is not necessarily the retinal location at which visual tasks are best performed. Instead, the PRL is often found at a slightly less eccentric location, although the peripheral eccentricity of the PRL is a poor predictor of visual function. Further, Rees, Kabanarou, Culham, and Rubin (2005) showed that the PRL is often the area of highest visual acuity in patients, but not highest contrast sensitivity. Whittaker et al. (1988) suggested that discrepancy between the PRL and the loci of highest sensitivity to contrast or best visual acuity is partially responsible for the occasional existence of separate PRLs for different visual tasks, i.e. the PRL for facial recognition may not also be so for reading.

Remaining visual performance in AMD patients is thought to rely heavily on the effectiveness of eye movements. Making quick, efficient saccades to the PRL, smoothly and successfully tracking a peripheral object and maintaining relatively stable fixation are all critical to visual capacity (Lee & Markowitz, 2010; Schuchard, 2005). The size of eye movements during fixation are amplified in AMD patients by a factor of 2-4 (Kumar & Chung, 2014), which has been associated with reduced reading speed (Falkenberg et al., 2007). There have been suggestions that exaggerated FEMs may in fact be improving peripheral visual function in patients by maximising the retinal array to which the target is visible (Kumar & Chung, 2014), enhancing visual information processing (Watson et al., 2012), and by preventing retinal fading (Martinez-Conde et al., 2006). Alternatively, Whittaker et al. (1988) and Macedo et al. (2007) suggest amplified retinal jittering from altered fixational patterns imposes limitations on the capacity to maintain an efficient PRL; patients with poorer fixational stability were shown to be more likely to use two or more distinct PRLs.

Due to the uncertainty in the effects of eye movements on peripheral function in patients, and the debilitating and incurable nature of dry AMD, research into alternative viewing strategies for AMD patients is critical. Particularly, investigating the characteristics of a peripheral target that promote or inhibit visibility are useful in determining how visual function may be optimised for everyday tasks such as navigating or reading.

1.8 Visual undersampling

Undersampling of the visual image can lead to perception at a lower resolution than provided by the original image. Neuro-retinal matrix damage (NRMD) refers

to the existence of gaps in the visual field, which can lead to undersampling of the visual image. NRMD can be caused in several ways, including clustered drusen build-up, hyperpigmentation, cellular atrophy or dystrophy, optic neuritis, or injury (Frisén, 2012; Winther & Frisén, 2010). While the gaps in the visual field created by NRMD depend on the specific disorder, anomalies in the retina are generally associated with reduced visual capability. Cone-rod dystrophy, for example, can damage photoreceptor cells throughout the periphery, while creating lesions in the macula (Rabb, Tso, & Fishman, 1986). As in AMD, patients are thus required to perform acuity tasks such as reading in the periphery. Further, in visual fields limited by optic nerve disorders, acuity is directly associated with the number of remaining axons around the optic nerve head (Frisén & Quigley, 1984). The visual undersampling that is characteristic of NRMD is also associated with loss of sensitivity to high spatial frequency (Shah et al., 2016), which is often critical to the identification of the target. Peripheral viewing also limits sensitivity to the high spatial frequency aspects of the stimulus (Berkley et al., 1975). Combined with additional loss of sensitivity due to spatial undersampling (Shah et al., 2016), resolution of targets in the remaining visual field in NRMD can be expected to be far inferior than in healthy eyes, even when eccentricity-matched.

Receptor-level undersampling due to NRMD can affect the entire visual field, but is of course most notable in the fovea where the resolution threshold is proportional to the spatial separation of the cones contributing to the visual image (Frisén & Quigley, 1984). As well as through tissue damage or disease, visual undersampling can occur naturally at the receptor and cortical level. Williams (1986) suggested peripheral undersampling due to sparse photoreceptor mosaics is

possible, contributing to the reduction in performance with increasing retinal eccentricity by lowering the resolution of the image at the retina.

The Nyquist limit defines a constraint on sampling rate, below which a waveform cannot be reconstructed without the occurrence of aliasing (Thibos, Walsh, et al., 1987). If the visual sampling of an image is insufficient to accurately recreate the image, i.e. the Nyquist limit of the image is too high, an artefact can occur as the image is mistakenly recreated at a lower frequency than in the original. This is described in Figure 7.

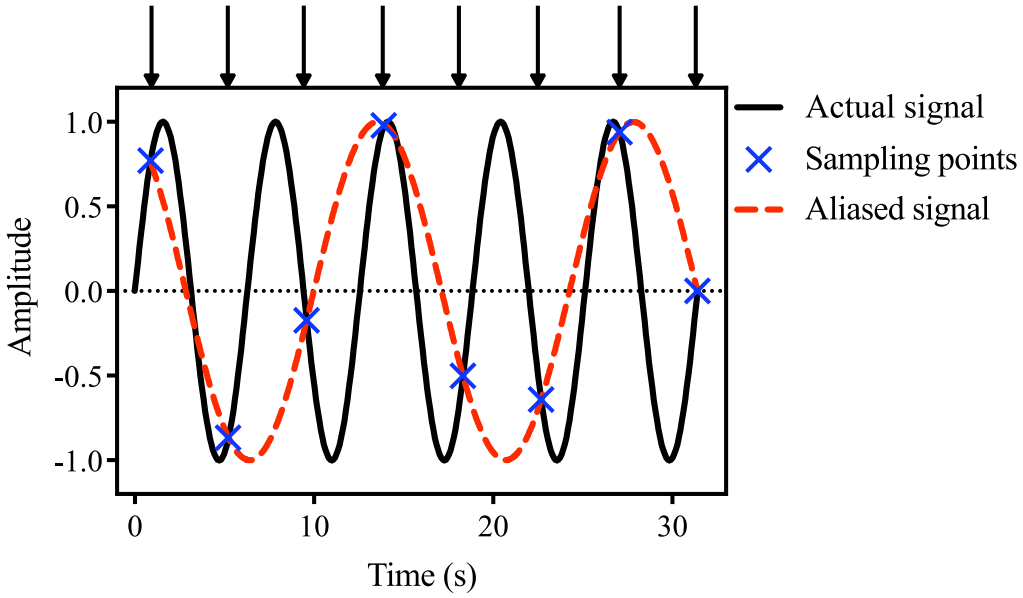

Figure 7: Demonstration of Nyquist aliasing. The actual signal (black, solid line) is sampled at a rate below the Nyquist frequency (shown by the arrows). The amplitude of the actual signal is thus is recorded at points indicated by the blue crosses. When a signal is reconstructed from these points, it results in the aliased signal (red, dashed line), which is at a lower frequency than the actual signal. Nyquist aliasing can occur for waveforms sampled across both time and space.

Nyquist aliasing can occur for waveforms varying in space or in time. Spatial aliasing can occur for spatial frequencies greater than the Nyquist limit. This has

the effect of creating misrepresentation of stimulus features. For stimuli with simple Fourier spectra, such as gratings, this manifests as the grating appearing to have a lower spatial frequency than it actually does (such as in Figure 7). For stimuli with more complex Fourier spectra, such as letter targets, the interaction between super-and sub-Nyquist frequencies is more complicated (Wang, Bradley, & Thibos, 1997a, 1997b).

Peripheral acuity for letter targets is believed to be limited by neural undersampling and the Nyquist limit, which Anderson and Thibos (1999b) suggest has two possible causes. Firstly, as letter size decreases, its spectral range increases into higher spatial frequencies and away from lower spatial frequencies, thus reducing the stimulus energy at frequencies that are detectable by the visual system (the "energy insufficiency hypothesis"). Secondly, higher spatial frequency stimulus information is undersampled and subject to aliasing, which masks the lower spatial frequency information key to letter discrimination (the "masking hypothesis").

Peripheral spatial acuity is better for grating targets than it is for letter targets (Anderson & Thibos, 1999a; Strasburger, Rentschler, & Juettner, 2011). This may suggest that, unlike gratings, peripheral letter acuity is not limited by neural sampling, thus disagreeing with the energy insufficiency hypothesis. However, Bondarko and Danilova (1997) demonstrated that differences in spatial frequency of the Landolt ring due to the gap are maximal at half the spatial frequency of the gap itself, and suggested that this is the critical spatial frequency, used to infer the orientation of the gap. This may suggest that letter acuity can be accounted for in terms of sampling limits, so long as the critical spatial frequencies are considered.

Further, Anderson and Thibos (1999a, 1999b) examined orientation discrimination thresholds for Tumbling E targets. They applied spatial frequency filters to the targets, in order to test whether filtering out low spatial frequency target information will not have a beneficial effect on resolution, in accordance with the energy insufficiency hypothesis. They showed that filtering out the low spatial frequencies hindered peripheral target resolution, which is therefore consistent with the energy insufficiency hypothesis. This indicates that stimulus signal energy below the Nyquist frequency is used in resolution. By reducing the size of the target, the spectral range of the target is extended to higher spatial frequencies, resulting in greater stimulus signal energy appearing at frequencies outside the Nyquist limit.

In support of the masking hypothesis, Wang, et al. (1997b) suggested that by allowing gratings to contain super-Nyquist frequencies, the resolution of the sub-Nyquist information can be impaired. This was shown even for low contrast super-Nyquist frequencies. This suggests that the super-Nyquist signal energy was sufficient to disrupt the perception of the veridical information. However, Wang, et al. (1997a) suggest that the aliasing of the super-Nyquist frequencies of the edges of a letter target is masked by the presence of high-contrast sub-Nyquist frequencies, provided the test target contrast is sufficiently high. As such, the aliased information is rendered invisible by the low-frequency information generated by the bulk of the target. The results of these studies are both consistent with the masking hypothesis. However, Anderson and Thibos (1999b) rejected the masking hypothesis by examining resolution of targets that were filtered to contain only high spatial frequency information. To be consistent with the masking hypothesis, this filtering should improve peripheral letter resolution.

Since they reported the opposite result, this is evidence contrary to the masking hypothesis.

Sampling of a temporal waveform at a rate below the Nyquist limit can also lead to illusory effects. The apparent motion illusion refers to the perception of a sequence of static images as a single, continuously moving object, when they are presented with a sufficient spatial offset and temporal delay (Wertheimer, 1912). Burr, Ross, and Morrone (1986b) demonstrated that the success of the apparent motion illusion is dependent on the object being sampled at a rate above the Nyquist limit. Sampling below this results in the perception of a series of static images. Fahle, Biester, and Morrone (2001) measured the foveal thresholds for discriminating apparent motion from continuous motion as around 40 minutes of arc, but this tolerance diminished with target speed and contrast.

Thus, spatial undersampling misrepresents a spatial signal, leading to altered perception of the actual image. The natural undersampling of the retinal surface in the peripheral retina that occurs as the photoreceptor density drops may lead to a misrepresented signal (Williams, 1986). Further, the exaggerated spatial undersampling that defines NRMD exacerbates this. As in AMD, NRMD is thus very limiting to the capacity of the visual system. Many causes of visual undersampling are irreversible, so NRMD patients would also benefit from research into methods of optimising the remaining visual field.

1.9 Super-resolution

Techniques of overcoming visual undersampling have been established in artificial and natural systems. The ability of digital systems to resolve images

better than the original picture has been well documented (Park, Park, & Kang, 2003). Super-resolution (SR) is a form of image processing in which multiple low-resolution images are merged over time to create a higher-resolution image. While this method of improving resolution is not perfect, it provides an effective improvement without damaging computational costs, making it invaluable in fields such as medical imaging and satellite reconnaissance, wherein low-resolution information can be harmfully unreliable (Yang, Wright, Huang, & Ma, 2010).

For SR to occur, an effective process by which gaps in information can be interpolated must be present. Spatiotemporal interpolation (SI) is a visual mechanism capable of estimating the spatial or temporal information within gaps in the presented information (Fahle & Poggio, 1981). The apparent motion illusion is evidence for the SI mechanism: Fahle and Poggio (1981) described the SI mechanism as a velocity-orientated motion detector, which is activated by objects appearing within its range of sensitive velocity. The receptive field of this detector provides a range of tolerance for spatial and temporal offsets. Morgan and Watt (1983) suggest that the apparent motion illusion fails when the motion signal extends beyond the bandwidth of this tolerance. Kandil and Lappe (2007) provided an alternative description of the SI mechanism. They argue that the monocular description asserted by Fahle and Poggio (1981) does not account for the results of a binocular experiment they conducted. They demonstrated, using dichoptic masking and inter-ocular presentation, that SI is dominated by binocular detectors of form and motion. This description suggests that a partially-occluded object is more effectively interpolated when a coherent surface can be detected, either due to common form or motion characteristics.

Evidence of SI occurring at a cortical level has been reported in neuroimaging studies. Muckli, Kohler, Kriegeskorte, and Singer (2005) investigated primary visual cortex (V1) activations for apparent motion illusions. They demonstrated increased blood oxygenation levels (which is indicative of increased neural function) in cortical locations including those representing spatial regions at which the target was not presented. This is supported by Chong, Familiar, and Shim (2016), who also reported that the cortical locations in V1 associated with spatial regions between target presentations are activated when the apparent motion illusion is present. Further, they showed that this activity is absent when the targets are presented without the temporal delay required to complete the apparent motion illusion. Alternatively, Lin and He (2012) suggest that SI contains higher-level processes, performed by later visual areas that feed back to V1. This suggestion implies that some visual phenomena that rely on SI occur using a range of neural mechanisms. However, this has not been demonstrated using neuroimaging techniques.

The processes resulting in the SI mechanism have thus yet to be determined. However, both the descriptions of SI by Fahle and Poggio (1981) and Kandil and Lappe (2007) indicate that motion is a key aspect of effective SI. This suggests that motion is a potential method of producing the spatial or temporal offsets that occur in SR-based image processing. The ability of biological systems to super-resolve has been previously documented. Land (1969) observed a periodic scanning motion in the retinae of jumping spiders, which appeared to achieve a high spatial acuity for the eye- and brain-size of the predator. It is theorised that this scanning motion provides multiple retinal images of the scene, which may be being merged to create higher-resolution images.

In human vision, beyond the fovea, resolution is naturally degraded due to a number of factors, including heightened photoreceptor sparseness, increased receptive field size, and reduced dedicated cortical areas (Cowey & Rolls, 1974; Thibos, Cheney, et al., 1987). However, there is some evidence that stimulus motion in the periphery does enhance visual acuity (Brown, 1972a, 1972b). Furthermore, there is some suggestion that SR may be implemented by FEMs, in that there is a deterioration in acuity when retinal image movement induced by FEMs is artificially counteracted (Rucci, Iovin, Poletti, & Santini, 2007). This implies that the individual, distinct images made by rapid FEMs are being used in a collective manner.

Artificial under-sampling through overlaying slits or other partially opaque apertures have been used to examine the human capacity for SR. This psychophysical technique is known as dynamic occlusion. Dynamic occlusion has been shown to improve the efficiency of SI; by occluding the gaps between successive target presentations in apparent motion, Scherzer and Ekroll (2012) improved the perceived smoothness of motion. This indicates the visual system accounts for spatially occluded sections between visible sections of the stimulus. Using dynamic occlusion, foveal SR has been demonstrated psychophysically by Frisén (2010). Letter targets were artificially undersampled by superimposed opaque masks. An example of the stimuli used by Frisén (2010) is shown in Figure 8. The final letter is difficult to reconstruct from a static image (one of the images on the top row in Figure 8), but it was demonstrated that the targets were more easily identifiable when they moved behind the masks. This is consistent with a visual system that is capable of merging visible stimulus elements across time to create a more complete image of the target.

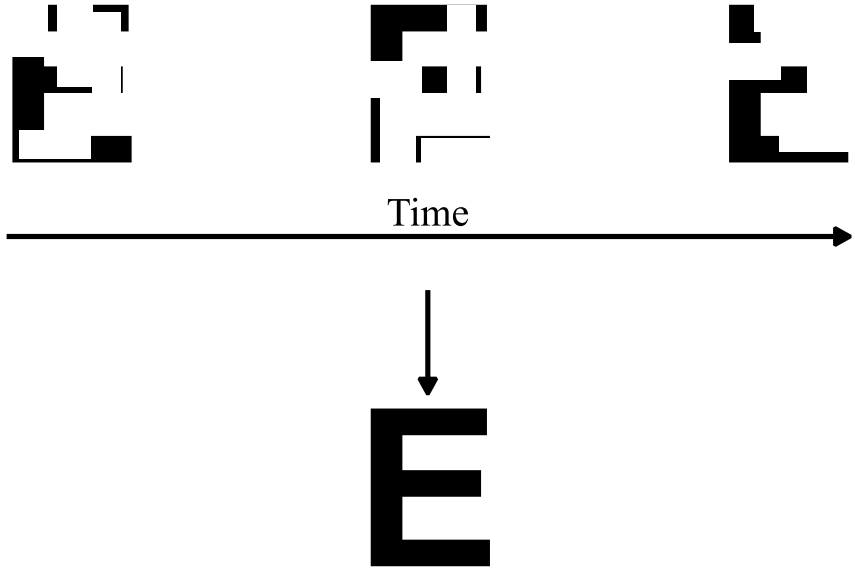

Figure 8: Example stimulus from Frisén (2010). The letter E on the top row is artificially undersampled as it moves behind a static, partially opaque mask. Thus the elements of the E that are visible to the observer change over time. A visual system capable of reconstructing the E from the undersampled images must contain a SR mechanism.

Nishida (2004) compared acuity for letter targets either moving or stationary behind slit arrays. An example stimulus from Nishida (2004) is shown in Figure 9. Moving letters were significantly easier to identify than stationary letters, suggesting that consecutive samples can be merged over time even in the same spatial location. The study controlled for an effect of increasing the number of samples in which the critical detail is visible by randomising the order of the motion sequence, which did not greatly improve acuity compared to static letters. This suggests that increasing the number of samples *per se* is not a sufficient explanation for SR.

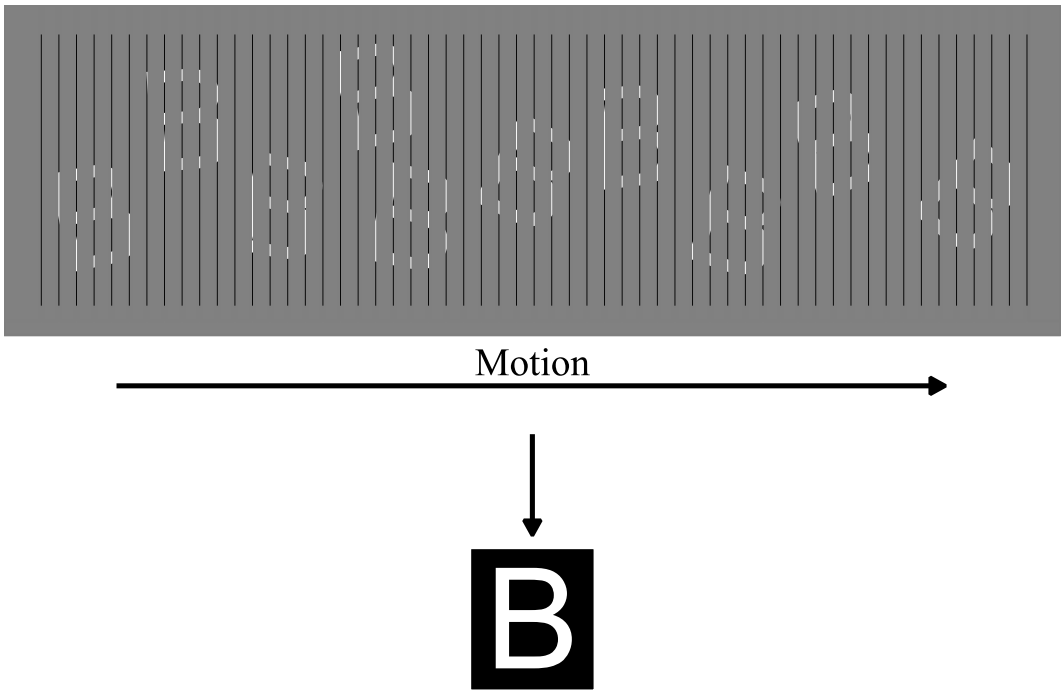

Figure 9: Example stimulus from Nishida (2004). Letter targets were obscured by a slit array. Motion was introduced either by moving the targets or the slits. Similarly to Frisén (2010), an improvement in letter identification accuracy in motion conditions is indicative of a super-resolution mechanism.

Other dynamic occlusion studies have also attempted to investigate the characteristics of successful integration of information across spatial and temporal gaps. Palmer, Kellman, and Shipley (2006) suggest that three simultaneous processes contribute to the formation of the final image: persistence, relatability, and position updating. Persistence, the temporal caching of information, has been demonstrated psychophysically using motion: alternating colours tracking across the retina are merged to the amalgamated colour (e.g. alternating red and green mixes to yellow), even if the individual colours are never presented at the same retinal location (Nishida, Watanabe, Kuriki, & Tokimoto, 2007). The amalgamated colour would not be perceived if the consecutive images were not being merged over time. Relatability is the extent to which the visible target information can be combined into a single object by the visual system.

Relatability can cue from object similarities such as colour (Palmer et al., 2006), motion (Mateeff, Popov, & Hohnsbein, 1993; Scholl & Pylyshyn, 1999) or boundary size (Kanizsa, 1979; Kellman, Yin, & Shipley, 1998). Finally, position updating is the mechanism by which the occluded target is continuously tracked using calculated trajectory information to allow for accurate connection to new target information when it appears. The necessity of position updating in Palmer et al.'s (2006) account suggests, like Frisén (2010), a key importance of target motion. Analysis of an occluded target is more successful with motion in cases of size estimation (Mateeff et al., 1993), contour integration (Palmer et al., 2006), and letter discrimination (Frisén, 2010; Nishida, 2004). Unlike a smoothly moving target behind a static occluding mask, a static target behind a smoothly moving mask does not require position updating, so some models of spatiotemporal summation consider the source of the motion predictive of performance (Palmer et al., 2006). Disrupting position updating has been shown to inhibit visual performance: resolution of a target with unpredictable motion is diminished compared to smooth motion (Mateeff et al., 1993). Dynamic occlusion and SR may thus require predictable motion to adequately reconstruct an image.

Therefore, SR mechanisms may provide the basis for a technique for optimising resolution capacity in situations wherein retinal sparseness results in poor resolution. It is clear that motion is a key aspect of the SR mechanism. However, dynamic occlusion studies have failed to construct a complete description of the conditions under which a SR mechanism functions optimally.

1.10 Overview

This introduction has provided evidence that the visual field is neither homogenous nor isotropic, which provides a difficulty for patients experiencing deterioration of the retinal surface, and subsequent loss in central visual function due to diseases such as AMD or NRMD. Performing visual tasks in the periphery is disadvantageous. Other phenomena of the visual system that have effects on visual performance have been discussed, such as FEMs and visual sampling, dysfunction of which can by symptomatic of central vision loss disorders. Since many of the causes of central vision loss are not easily remedied, developing stimulus-based manipulations that improve peripheral visual performance would be a useful potential alternative to treatment. Evidence for several potential manipulations have been discussed in this introduction. Brown (1972b) reported a potential beneficial effect of target motion on resolution. The importance of motion is also reported in descriptions of SR mechanisms, which utilise the spatial displacement provided by target motion in collating multiple images of the target. Further, Van Santen and Sperling (1985) demonstrated that temporally modulating a stimulus extends its Fourier profile. This suggests that additional temporal modulations may also be able to improve peripheral visual function.

This thesis therefore intends to determine the extent to which non-invasive stimulus manipulations can improve visual function in the healthy periphery and in patients with central vision loss. The first experimental chapter (Chapter 3) investigates the characteristics of peripheral acuity, and how the eccentricity, speed, and location of the target can affect visual performance. The relationship between the retinal position of a target and the capacity to resolve the target is

crucial to patients suffering from central vision loss (due to disorders such as AMD). The influence of target motion is also investigated, examining the suggestion from Brown (1972b) that peripheral acuity can be improved with the introduction of slow, predictable target motion.

The second experimental chapter (Chapter 4) probes the efficacy of SR mechanisms in the periphery using partially obscured Landolt ring targets. A dynamic occlusion technique is used to investigate how visual information is integrated across space and time, as well as the limitations and characteristics of peripheral integration mechanisms. In Chapter 5, additional temporal modulations are applied to static and moving peripheral targets. The modulations are intended to extend the spectral profile of the stimuli. If the extra temporal harmonics created by the additional modulations appear within the spatiotemporal window of visibility, it may aid performance in acuity tasks.

In addition to macular deficits, AMD is also associated with additional symptoms affecting how patients view visual targets. Patients with AMD are reported to have FEMs that are magnified by a factor of 2-4 compared to healthy eyes (Kumar & Chung, 2014). Accordingly, useful stimulus manipulations for improving the remaining visual field in vision loss patients must also be robust to the extra symptoms. Thus, the fourth experimental chapter (Chapter 6) investigates the effect of the additional temporal modulations in conditions of simulated eye disease, both the additional ocular jitter associated with AMD and the undersampled retinal surface characteristic of NRMD.

In Chapter 7, a model is described. The model aims to demonstrate that additional periodic stimulus modulations create additional temporal harmonics in the Fourier

domain. Further, it is examined whether the harmonics increase the spread of the information related to the stimulus within the spatiotemporal window of visibility, and that they are therefore responsible for the effects that the additional modulations have on resolution.

In the final experimental chapter, the modulations found to improve peripheral acuity in the previous chapters are tested in a task more salient in central vision loss: peripheral reading. The effect of the stimulus manipulations on reading speed and accuracy is examined in the healthy periphery and in patients with macular degeneration.

Chapter 2: General Methods

2.1: Apparatus

All experiments utilised a 50.8cm (20”) CRT monitor (LaCie Electron22blueIV, 1152x870 resolution; Seagate technology, Tigard, OR, USA) with a 75Hz refresh rate (giving a frame duration of 13.3ms), unless otherwise indicated. Observers were sat upright at a distance of 100cm, fixed with a chinrest. At this distance, each pixel subtends a visual angle of 0.0175°. Experiments were run using PsychoPy version 1.78-1.83 (Peirce, 2007) on a Mac Mini (Late 2012; Apple Inc., Cupertino, CA, USA). In accordance with the recommendations in Metra, Vingrys, and Badcock (1993) the monitor was switched on for a warm up period of 30-45 minutes prior to testing.

2.2 Monitor calibration

Many of the experiments in this thesis require high temporal precision. The temporal precision of the monitor was tested by recording the duration of each video frame while a temporally varying stimulus was presented. The duration of 500 frames was recorded while a drifting Gabor patch was displayed, which updated on every video frame. The duration of each frame is shown in Figure 10.

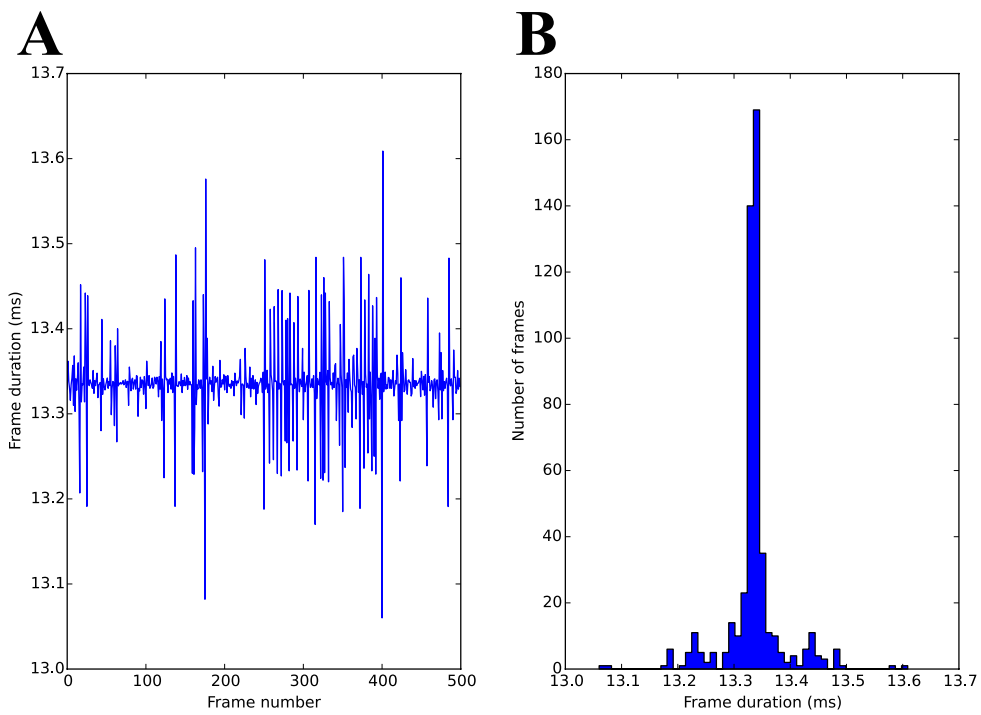

Figure 10: Plots of the duration of each of 500 video frames during presentation of an updating stimulus. (A) The duration of each individual frame, in terms of the deviation from the sample mean. (B) Histogram of all recorded frame durations.

The mean frame duration was 13.33ms (*SD* 0.05ms). The small recorded deviation from the mean signifies that 99% of frame durations fall within 13.21-13.47ms. Figure 10A indicates that no video frames were dropped (i.e. a total screen refresh was completed within each video frame). If a frame is dropped, the screen display remains unchanged for an extra video frame. In an experimental trial, this would result in a frame of twice the duration, and the trial duration extending by the length of one frame. The number of dropped frames was recorded during the development of experiments, such that a coded experiment resulting in dropped frames could be rectified prior to testing. Figure 10B demonstrates that although all frames were not precisely the same duration, the variation is slight, and distributed evenly around the mean.

Typical display monitors do not have a linear relationship between the gun voltage and the output luminance of the gun (Rodieck, 1983). For requested intensity (gun value, between -1 and 1, representing the available range of pixel intensities) V, final luminance value L is typically of the form:

$$L(V) = \alpha + (\beta + \kappa V)^{\gamma} \quad (1)$$

Where α (minimum luminance value), β (DC offset parameter), κ (gain parameter), and γ (gamma) are constants dependent on the monitor (Metra et al., 1993; Pelli & Zhang, 1991). Measuring L for a range of V will fit values to Equation 1. From the values of the parameters in Equation 1, a look-up table (LUT) can be created to give a linear luminance output. From Equation 1, the LUT as a function of V can be generated of the form:

$$LUT(V) = \frac{((1-V)\beta^{\gamma} + V(\beta+\kappa)^{\gamma})^{\frac{1}{\gamma}} - \beta}{\kappa} \quad (2)$$

To calculate the gamma functions for the monitor used in the experiments described in this thesis, a photometer (LS-100 Luminance meter, Konica Minolta, Inc., Japan) was situated 1m from the monitor screen to measure the luminance of a 1152x870 pixel window at 33 incremental, evenly-spaced gun values between -1 and 1. The measured functions of each individual gun and the combined RGB function are shown in Figure 11A. Correcting for the non-linear relationship using Equation 2 gives a linearity between $L(V)$ and V, shown in Figure 11B.

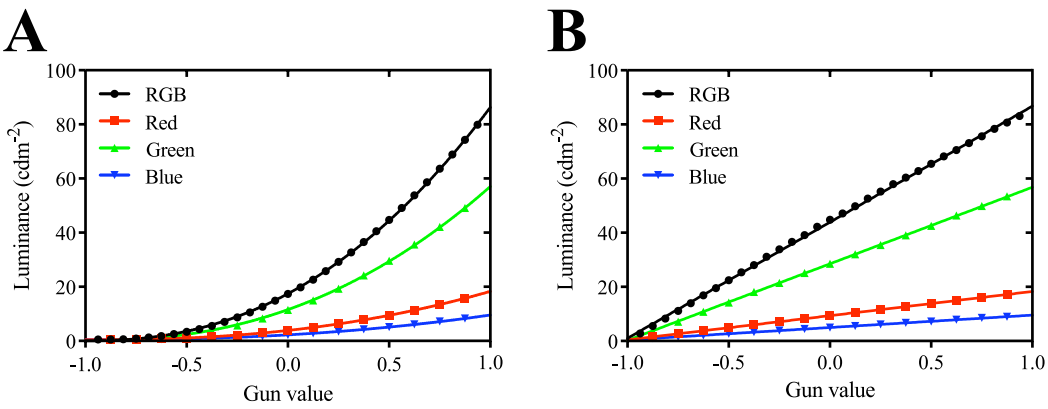

Figure 11: Gamma functions for the experimental monitor. (A) Functions prior to gamma correction for the red, green, and blue guns are shown independently as well as the monochromatic RGB function. (B) Luminance functions after gamma correction was applied to the monitor.

Vision experiments require gamma correction to linearise this relationship such that the difference in luminance of the display between a gun value of 1 (white) and a gun value of 0 (middle grey) will be the same as between a gun value of -1 (black) and a gun value of 0. The monitor used in the experiments described in this thesis used a gamma linearisation value of 2.31. Linear regressions to the corrected functions in Figure 11B indicated $R^2 \geq 0.99$ for all three individual guns and the combined RGB function. The maximum luminance value used in these experiments was 85.0cdm^{-2} (a gun value of 1), around the value at which acuity saturates (Johnson & Casson, 1995; Rabin, 1994).

2.3 Stimulus

The majority of the experiments performed in this thesis concern measurements of acuity. Acuity was assessed using a forced-choice orientation discrimination paradigm using Landolt rings (Sloan, 1959). Landolt rings are a capital letter C drawn in Sloan font (Pelli et al., 1988), shown in Figure 12. Unless otherwise stated, the target was presented at maximum luminance (85.0cdm^{-2}) on a mid-grey

background (44.8cdm^{-2}, Michelson contrast 0.31) in a dark vision laboratory (0.5cdm^{-2}). The task in these acuity experiments was to discern the orientation of the ring, with regard to the position of the gap in the ring (referred to as the critical detail). The Landolt ring could be at one of four possible orientations: 45°, 135°, 225°, or 315° (in polar coordinates). Figure 12 shows a diagram of an example Landolt ring at an angle of 0°.

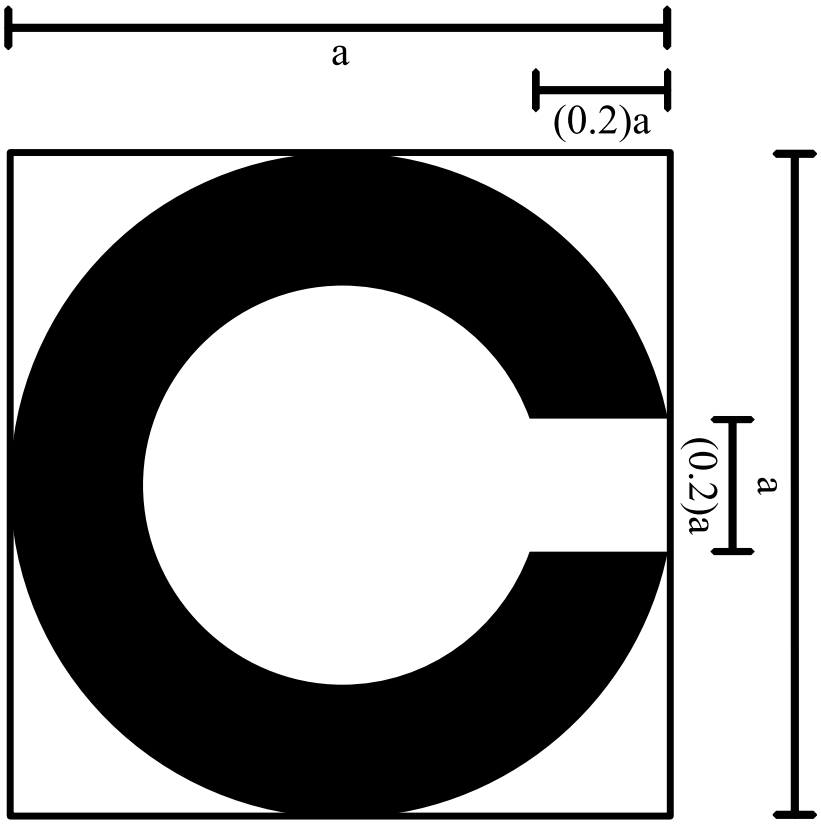

Figure 12: The Landolt ring, a capital letter C in Sloan font (Pelli et al., 1988). The Landolt ring is perfectly circular, with letter thickness maintained at one fifth of the diameter (*a*). The width and height of the critical detail (gap) are also one fifth of the diameter.

2.4 Adaptive staircase procedure

In the experiments in this thesis, threshold performance levels for each given task were typically estimated using an adaptive staircase procedure. In assessments of acuity, threshold target size was estimated with a three-down, one-up staircase procedure (Green, 1990). For each staircase, the target began at 1.5°, at which size its orientation is easily identifiable. If the orientation was correctly identified on three consecutive trials, the target size reduced, increasing task difficulty. For each incorrect response, the target size increased. Before the first reversal, target size decreased in 0.4° intervals. After every second reversal thereafter, the step size halved until the interval reached 0.025° at which it remained for all following reversals. The staircase ended upon reaching the fiftieth trial or the tenth reversal, whichever the later.

2.5 Analysis

2.5.1 Logistic function

From the staircases, the target size and response (correct, 1 or incorrect, 0) from each trial was collected into averaged bins. Each bin represents the average target size and average response (between 0 and 1, representing the proportion correct) of all trials within it. Bins were plotted on a graph with target size on the abscissa and proportion correct on the ordinate, to which a logistic function was fitted. The logistic function provides an estimate of the relationship of target size to proportion correct, and is of the form

$$f(x) = 0.25 + \frac{0.75}{1 + e^{\frac{T-x}{m}}} \quad (3)$$

In which *T* is the point of inflection (at which the second derivative of the logistic function is zero) and *m* represents the spread of the function (Treutwein & Strasburger, 1999). A three-down, one-up staircase procedure estimates the threshold target size for 79% correct responses (Green, 1990). It provides a more accurate indication of sensitivity around this threshold value, and gives less emphasis to sizes too easy or difficult to resolve. Performance in acuity is referred to in this thesis in terms of resolution threshold as calculated by Equation 5: the minimum target size (in degrees of visual angle) possible for the observer to correctly identify the orientation of the target on 79% of trials. Acuity is directly proportional to inverse resolution threshold, so a small value of resolution threshold indicates high acuity. Estimates of threshold values were calculated from logistic functions with data binned from at least five staircase procedures for each condition (at least 250 total trials).

To calculate the target size for which the logistic function estimates 79% of responses are correct, Equation 3 is rearranged to Equation 4 now given in terms of the size of the target, *x*. The threshold target size for 79% successful identification is then calculated using Equation 5.

$$x(f) = T - \left(m \ln\left(\frac{0.75}{f-0.25} - 1\right)\right) \quad (4)$$

$$x(0.79) = T + 0.94m \quad (5)$$

2.5.2 PsychoPy

In most circumstances, psychometric thresholds were calculated using inbuilt PsychoPy analysis functions. In this procedure, the staircase data were sorted in order of target size, then collated into six bins with an equal number of trials in

each. An example of PsychoPy's threshold estimation by a logistic function from an adaptive staircase procedure is shown in Figure 13.

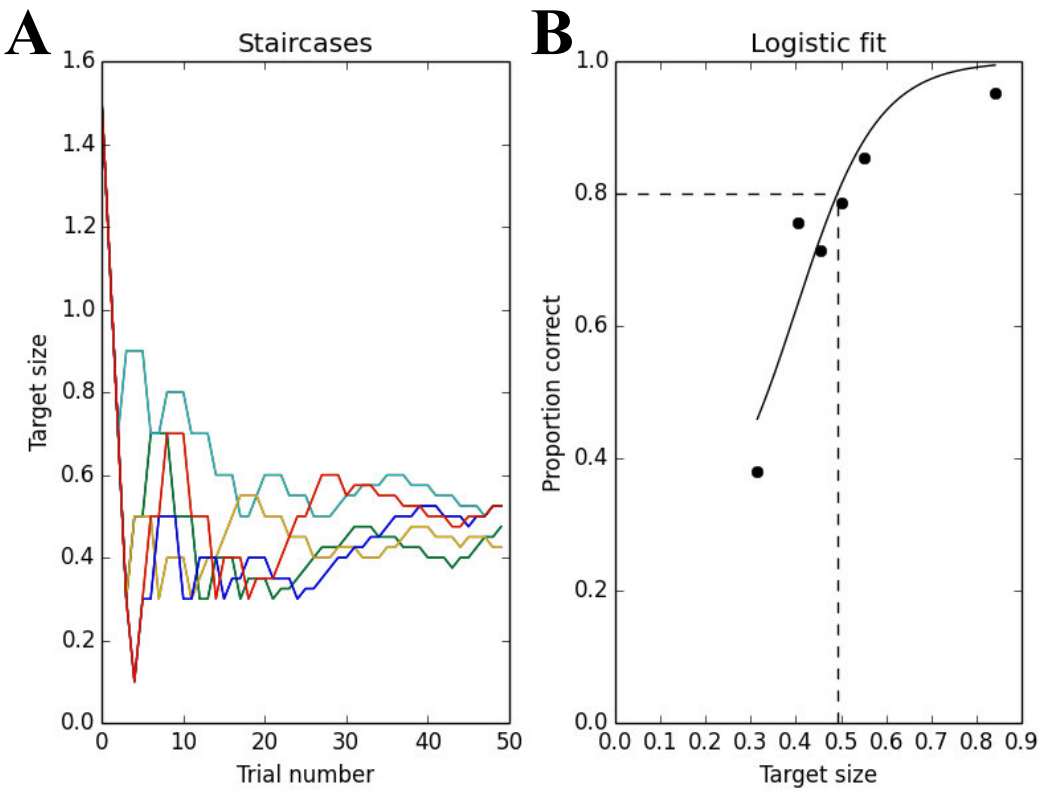

Figure 13: Example analysis of five adaptive staircase procedures. (A) the size of the target on each trial. Different staircases are represented by different colours. (B) The individual trial responses are aggregated into six bins of equal size, to which a logistic function is fit. Using this function, an estimate of threshold size for 79% correct orientation discrimination is estimated (represented by the dashed line).

2.5.3 Prism

In certain situations, the data were decomposed such that no dedicated staircase procedure was performed on that measurement. Such decompositions were performed in RStudio (RStudio, Inc., Boston, MA, USA) and the logistic function in Equation 3 was fit using Prism (version 6.0f for Mac OS X, GraphPad Software, Inc., La Jolla, CA, USA), shown in Figure 14.

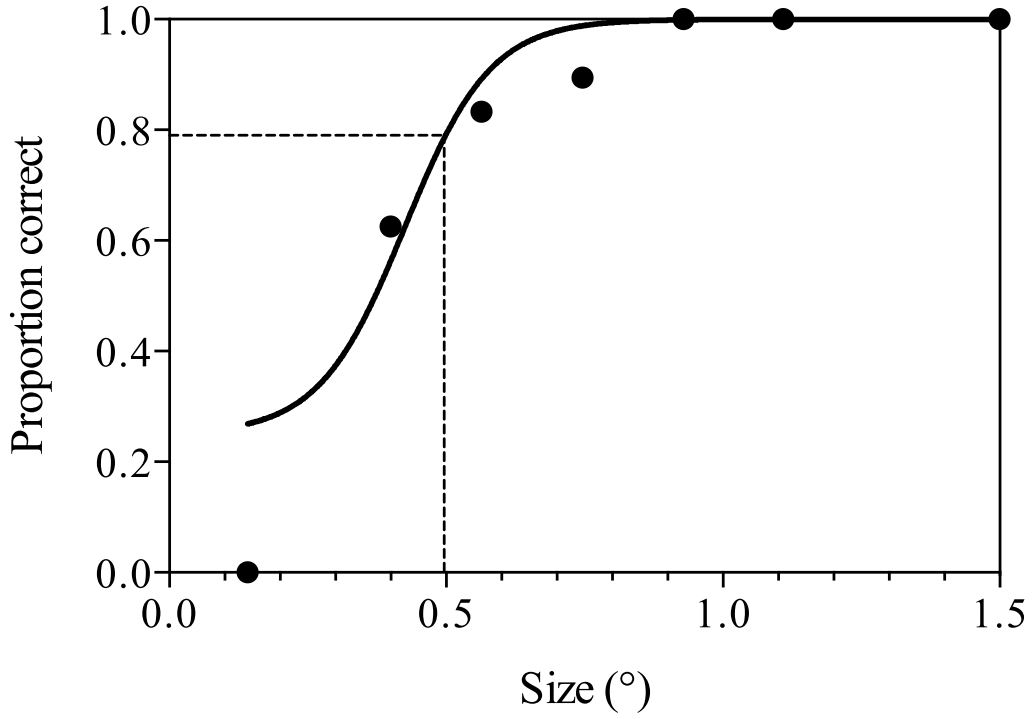

Figure 14: Example logistic fit using Prism software to the staircase data from Figure 13. The estimated threshold size is represented by the dashed line.

The logistic fitting techniques differ between the PsychoPy and RStudio/Prism methods. Unlike PsychoPy, RStudio predefines the bins to encompass a given spread of target sizes, into which the individual trials are sorted (e.g. all trials for which the target size is between 1.1-1.3° are collected into the same bin). The bin is then assigned the size value corresponding to the mean size of the trials aggregated within that bin.

At the number of individual trials used in the experiments described in this thesis (a minimum of 250 for each logistic function), the difference between the fitting techniques should be minimal (Wichmann & Hill, 2001a, 2001b). This was confirmed by analysing the data collected for Experiment 1.1 (for an explanation of the psychophysical procedure, refer to section 3.2) using the two logistic fitting techniques. The normalised root mean square deviation between the two

techniques was calculated as 0.068. The comparison between the analysis techniques is shown in Appendix 1.

Chapter 3: The Characteristics of Acuity in the Peripheral Visual Field

3.1 Introduction

The accuracy of the perception of an image is critically linked to the array of photoreceptors across which it is displayed, a relationship culminating in the Nyquist limit (Hirsch & Curcio, 1989; Williams, 1988; Yellott, 1983). Curcio, Sloan, Packer, Hendrickson, and Kalina (1987; also Curcio, Sloan, Kalina, & Hendrickson, 1990) demonstrated that the distribution of photoreceptor cells on the retina is neither homogeneous nor isotropic. This suggests that the resolving capacity of the visual system is correspondingly variable across the visual field.

Inhomogeneous visual performance, as expected of an inhomogeneous retinal surface, has been observed in several contexts. For example, as the retinal eccentricity of a target increases, threshold size for accurate resolution also rises congruently (Brown, 1972b; Westheimer, 1982). Contrast sensitivity also deteriorates with increased eccentricity (Berkley et al., 1975; Chung et al., 2002), as does Vernier acuity (Westheimer, 1982), visual span (Legge et al., 2001), reading speed (Chung, Mansfield, & Legge, 1998), and line orientation discrimination (Westheimer, 1982). Patients with central vision loss (CVL) are required to perform visual tasks in the periphery, typically at an eccentric pseudo-fovea known as the preferred retinal locus (PRL, Whittaker, Budd, & Cummings, 1988). The inhomogeneity of the visual field therefore makes the PRL a suboptimal location for performing visual tasks.

Anisotropy in visual performance has also been observed; in agreement with the pattern of photoreceptor densities, performance for eccentric targets is improved on the horizontal meridian. This has been shown in measures of contrast sensitivity (Regan & Beverley, 1983; Rovamo et al., 1982), and motion detection (Van De Grind et al., 1993). Other studies have found higher sensitivity in the superior visual field compared to the inferior. These include measures of apparent motion detection (Naito, Sato, & Osaka, 2010) and processing for distant objects (Previc, 2011). Higher sensitivity has been shown in the inferior visual field compared to the superior in measures of attentional resolution (He, Cavanagh, & Intriligator, 1996), contrast sensitivity for low spatial frequencies (Rijsdijk et al., 1980), and reading accuracy (Culham, Fitzke, Timberlake, & Marshall, 1992).

There are several instances where photoreceptor anisotropy does not lead to anisotropy of performance. For example, although Battista and Kalloniatis (2002) found a consistent advantage in word recognition for words presented to the right of fixation, they suggested that the observed asymmetry derives from attentional habits in reading rather than any intrinsic bias. Additionally, Khuu and Kalloniatis (2015) found spatial summation and the rate of change of contrast sensitivity with eccentricity are also independent of spatial meridian. Thus, while visual performance consistently degrades with increasing eccentricity, the effect of the physiological anisotropy is less clear.

As well as the location at which a target is perceived, visual performance also varies with characteristics of the stimulus. Changes to the spatiotemporal characteristics of the stimulus such as the speed (Brown, 1972a; Holcombe, 2009; Kelly, 1985), contrast (Chung & Bedell, 1998; Koenderink, Bouman, Bueno de

Mesquita, & Slappendel, 1978a; Robson, 1966), or the spatial frequency components (Kelly, 1979, 1984) are known to alter resolution capacity. Brown (1972b) described how acuity is affected by the speed of a target at different retinal eccentricities. Increases in both target speed and eccentricity lead to a general reduction in acuity. However, resolution thresholds for peripheral targets were lower for slowly moving targets than for static targets at the same eccentricity. However, no such improvement was evident in the fovea. This suggests that the reduction in acuity for peripheral viewing may be alleviated by introducing target motion. However, Brown (1972b) restricted targets to the horizontal meridian, such that target motion influenced the retinal eccentricity. This interaction between speed and eccentricity may thus have induced the observed improvement in acuity.

As patients with CVL are required to view targets peripherally, the experiments in this chapter investigate the characteristics of peripheral resolution, and provide a more definitive test of whether motion can improve peripheral acuity. In Experiment 1.1, the relationship between target speed, eccentricity and resolution is examined directly in the temporal and nasal visual fields. Unlike in Brown (1972b), targets are restricted to isoeccentric arcs, preventing any interaction between target motion and eccentricity.

To assess any observable biases in performance due to target characteristics, the data from Experiment 1.1 are decomposed according to specific target characteristics and assessed separately in Experiments 1.1.1-1.1.3. In Experiment 1.1.1 the effect of target orientation is investigated. In Experiment 1.1.1.1, the four possible target orientations are assessed separately, then collected into

centripetal and centrifugal orientations in Experiment 1.1.1.2 (facing towards and away from fixation, respectively). Experiment 1.1.1.2 accounts for the additional peripheral eccentricity of the critical detail of the target when facing away from fixation. Experiment 1.1.2 compares the two possible directions of target motion, while Experiment 1.1.3 compares performance for the temporal and nasal visual fields. The influences of target orientation, direction of motion, and location examined in Experiments 1.1.1-1.1.3 are performed using targets at 10° eccentricity. 10° was selected as an appropriate eccentricity to assess the potential benefits of stimulus-based manipulations for patients with CVL. This is sufficiently distant from the fovea that the scope of CVL does not often exceed this eccentricity (Lee & Markowitz, 2010), and not excessively eccentric such that visual performance is unnecessarily degraded. Thus, it is important that Experiments 1.1.1-1.1.3 investigate any potential biases in performance that occur at this eccentricity.

In Experiment 1.2, the effects of target speed and eccentricity on resolution thresholds are assessed for targets presented in the superior visual field. Finally, in Experiment 1.3, resolution thresholds are compared for targets in the horizontal and vertical peripheral visual fields to further examine the influence of the relationship between visual performance and the physiological anisotropy of the retinal surface.

3.2: Resolution of static and moving peripheral targets in the nasal and temporal visual fields (Experiment 1.1)

3.2.1: Methods

3.2.1.1: Participants

Seven observers (mean age 25.14 years, *SD* 2.97 years) with normal or corrected-to-normal visual acuity participated in this study.

3.2.1.2: Apparatus

Observers sat upright with a chinrest 100cm from the centre of the screen. Stimuli were presented monocularly to the right eye, and observers responded on a keyboard positioned outside the visual field. For a detailed description of the experimental setup, see the General Methods chapter.

3.2.1.3: Stimulus

Threshold size for orientation discrimination was obtained for obliquely oriented Landolt ring targets. Targets travelled along isoeccentric paths at four peripheral eccentricities between 2.5-10° (see Figure 15A) at speeds between 0-20°s^{-1} (Figure 15B). The visual field (nasal or temporal) in which the target appeared, the origin of the trajectory (above or below the horizontal meridian), and the orientation of the target were allocated randomly prior to the onset of each trial. For all target speeds, the trajectory was centred on the horizontal meridian.

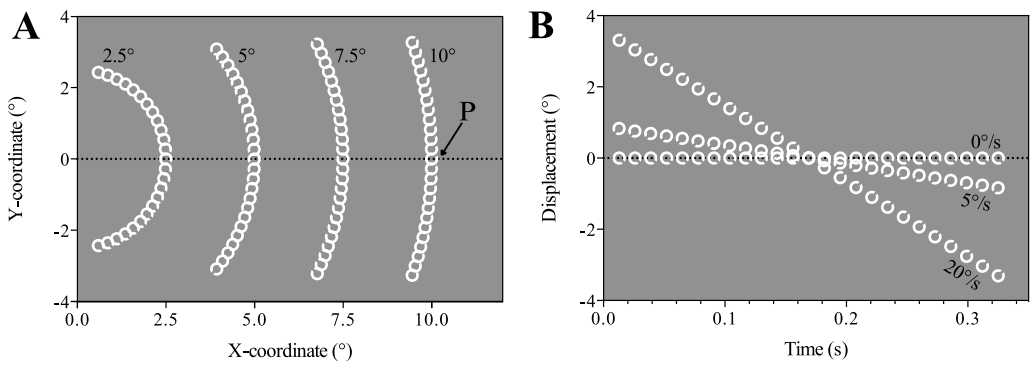

Figure 15: Plots describing the target trajectory in the temporal visual field. (A) Target coordinates for the fastest ($20°s^{-1}$) targets at each eccentricity, highlighting the isoeccentric arcs to which the targets were restricted. (B) For 10° eccentricity, the displacement of the target with respect to screen coordinates [10,0] (marked point P in Figure 15A) across the duration of a trial, for three target speeds. Target coordinates are updated on every video frame, providing the smoothest motion trajectory possible for the display. The black, dotted lines are to represent the horizontal meridian and were not presented along with the stimulus. Target trajectories in the nasal visual field were mirror images of Figure 15A.

3.2.1.4: Procedure

Threshold target size for orientation discrimination was assessed using a three-down, one-up staircase procedure. Staircases were terminated once a minimum of 50 trials and ten staircase reversal had been completed (for a more detailed explanation of the calculation of resolution thresholds, refer to the General Methods chapter). Data were collected across four sessions with each observer, each lasting approximately one hour and occurring on different days. Sessions were broken down into sets of six blocks of trials. Each set examined a preselected target eccentricity; each block within the set consisted of one staircase procedure for each of the six target speeds, in a randomised order. In each trial, observers fixated on a 0.5° cross in the centre of the screen. The Landolt ring target appeared at the preselected eccentricity in either the temporal or nasal

visual field. The field in which the target appeared was allocated at random, to minimise the chances of observers making anticipatory saccades towards the predicted target location. The target travelled at the allocated speed for 25 video frames (0.33s), after which the observer made a response indicating the perceived orientation of the target. Observers received immediate auditory feedback as to the accuracy of their response.

3.2.2: Results

Performance is displayed in terms of the threshold target size required for 79% orientation discrimination accuracy (see General Methods chapter for a detailed explanation of the analysis procedure). Figure 16 shows the effect of target speed and eccentricity on acuity in the horizontal periphery (the temporal and nasal visual fields).

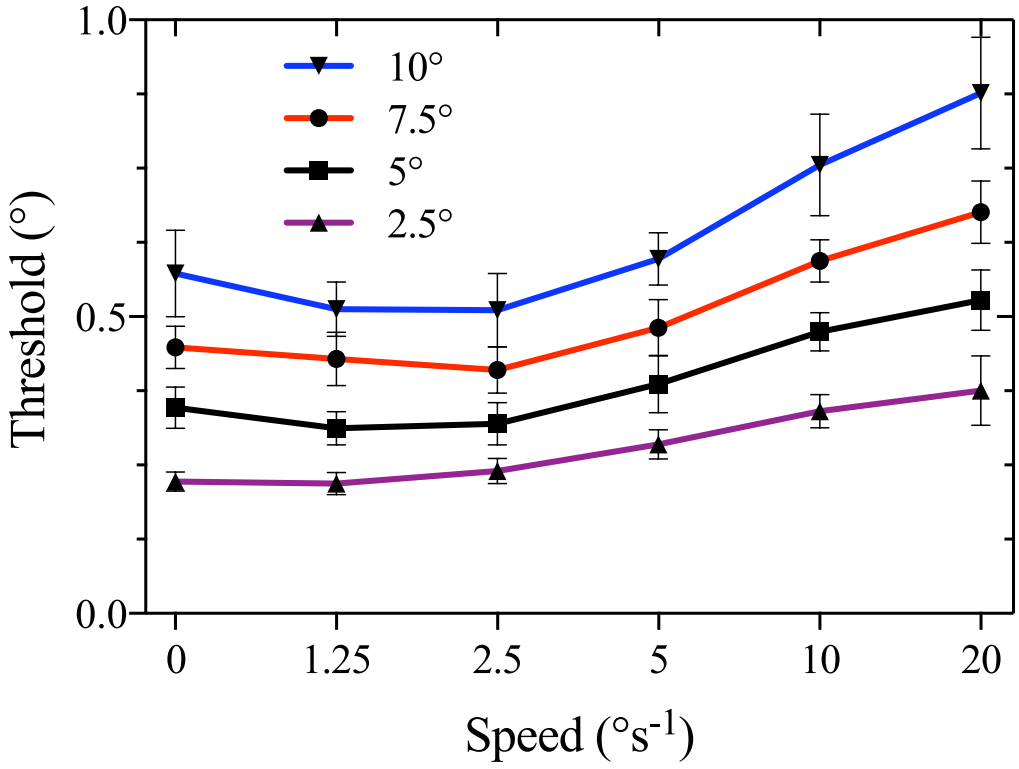

Figure 16: Graph of the effect of target speed and eccentricity on resolution thresholds for targets in the temporal and nasal visual fields. Data points indicate the mean resolution threshold, and error bars are the between-subjects 95% CI.

Figure 16 indicates that as the retinal eccentricity of the target is increased, resolution thresholds rise. Thresholds also rise as the speed of the target is increased. A two-way, repeated measures ANOVA confirmed a significant main effect of both eccentricity ($F(3,18)=250.3$, $p<.0001$) and speed ($F(5,30)=114.8$, $p<.0001$).

A significant interaction between eccentricity and speed was also reported ($F(15,90)=5.6$, $p<.0001$), suggesting that the effect of speed on resolution thresholds depends on the eccentricity of the target. Brown (1972b) reported that although increasing target speed has a generally detrimental effect on resolution thresholds, in the periphery there is a slight improvement in performance for slowly moving over static targets. This improvement is also visible in Figure 16 at

10° eccentricity. To assess whether this improvement is statistically significant, a comparison was made between the resolution threshold for static targets and those for each of the target speeds for which the mean threshold is lower than that. This includes target speeds 1.25°s^{-1} and 2.5°s^{-1}. These comparisons are shown in Figure 17.

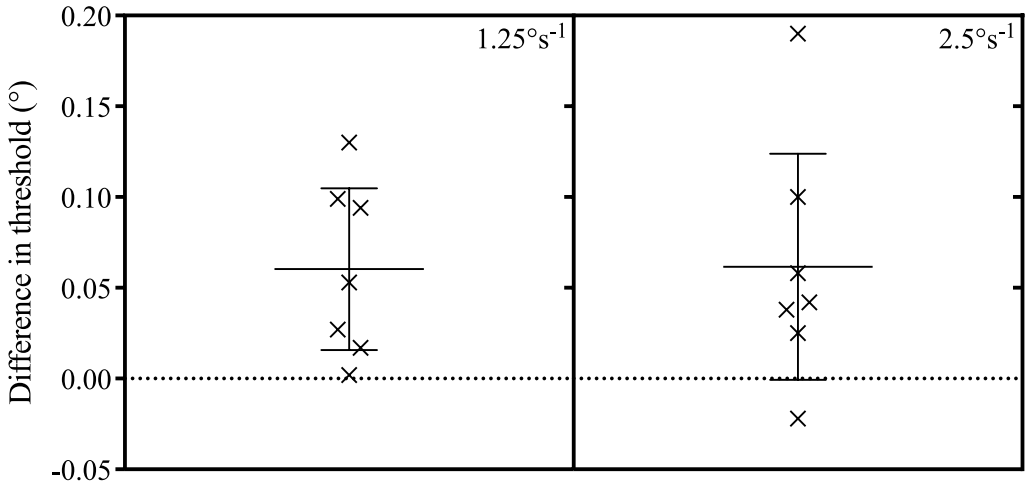

Figure 17: Scatter plot showing the difference in individual observers' resolution thresholds between static and moving targets, for target speeds that provided an average reduction in resolution thresholds. Left: the difference between resolution thresholds for static targets and targets moving at 1.25°s^{-1}. Right: static and 2.5°s^{-1}. Crosses show the difference in thresholds between the speeds for individual observers at 10° eccentricity in the horizontal periphery (see text for explanation). Data points above zero on the abscissa indicate thresholds were lower (performance was better) in the moving condition. Horizontal bars show the mean with between-subjects 95%CI.

A one-tailed, paired samples t-test examined whether resolution thresholds for the 0°s^{-1} (*M* 0.57°, *SD* 0.08°) was significantly higher than each of the moving conditions. As there are five possible comparisons (between static targets and each of the moving target speeds), a Bonferroni correction for the family-wise error is applied. This reduces the α-value to 0.01. The resolution thresholds for targets at 1.25°s^{-1} (*M* 0.51°, *SD* 0.05°) were significantly reduced by motion

(t(6)=3.3, p=.008), however targets at 2.5°s^{-1} were not (*M* 0.51°, *SD* 0.07°, t(6)=2.4, p>.01). This indicates that motion can have a beneficial effect on resolution for targets at 10° eccentricity in the horizontal periphery, but only within a narrow range of speeds.

3.2.3: The effect of target orientation (Experiment 1.1.1)

3.2.3.1: Methods

In Experiment 1.1.1, the data collected for the most eccentric condition in Experiment 1.1 (10°) were separated into their subcategories based on the orientation of the target. Psychometric functions were fit to the data using the technique outlined in section 2.5.3 in the General Methods chapter. Experiment 1.1.1.1 examines all possible target orientations separately, while in Experiment 1.1.1.2 centripetal and centrifugal orientations are compared.

3.2.3.2: Results

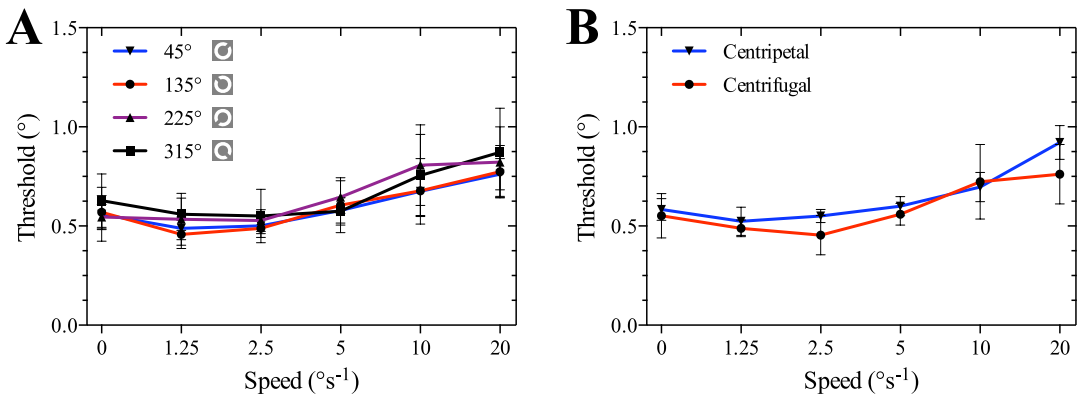

Figure 18: Graph showing resolution thresholds as a function of target speed in the most eccentric condition in Experiment 1.1 (10°), decomposed according to the orientation of the target. (A) Results of Experiment 1.1.1.1, whereby resolution thresholds for the four possible target orientations were assessed individually. (B) In Experiment 1.1.1.2, a comparison was made between centrifugally- and centripetally-orientated targets. Data

points indicate mean resolution thresholds, and error bars represent between subjects 95%CI.

Two-way repeated measures ANOVAs assessed the effects of target orientation on resolution thresholds for static and moving peripheral targets. Experiment 1.1.1.1 indicated that when the data were decomposed into individual orientations, there was no significant difference in thresholds ($F(3,18)=2.07$; $p>.05$), but that the effect of speed remained ($F(5,30)=17.65$; $p<.0001$). There was no significant interaction between target orientation and speed ($F(15,90)=0.63$; $p>.05$). For the centrifugal and centripetal orientations (Experiment 1.1.1.2), there was also no significant effect of orientation ($F(1,6)=3.49$; $p>.05$), but a significant effect of speed ($F(5,30)=27.47$; $p<.0001$). No significant interaction effect was reported ($F(5,30)=1.96$; $p>.05$). This indicates that the orientation of the target does not influence the observers' ability to resolve the target.

3.2.4: The effect of the direction of the stimulus trajectory (Experiment 1.1.2)

3.2.4.1: Methods

Targets in Experiment 1.1 were randomly allocated a direction for each trial: superior or inferior motion (from below fixation travelling up, and from above fixation travelling down, respectively). The data from Experiment 1.1 were decomposed according to the direction of travel. Logistic functions were fit to the data and the 79% target size thresholds calculated, shown in Figure 19.

3.2.4.2: Results

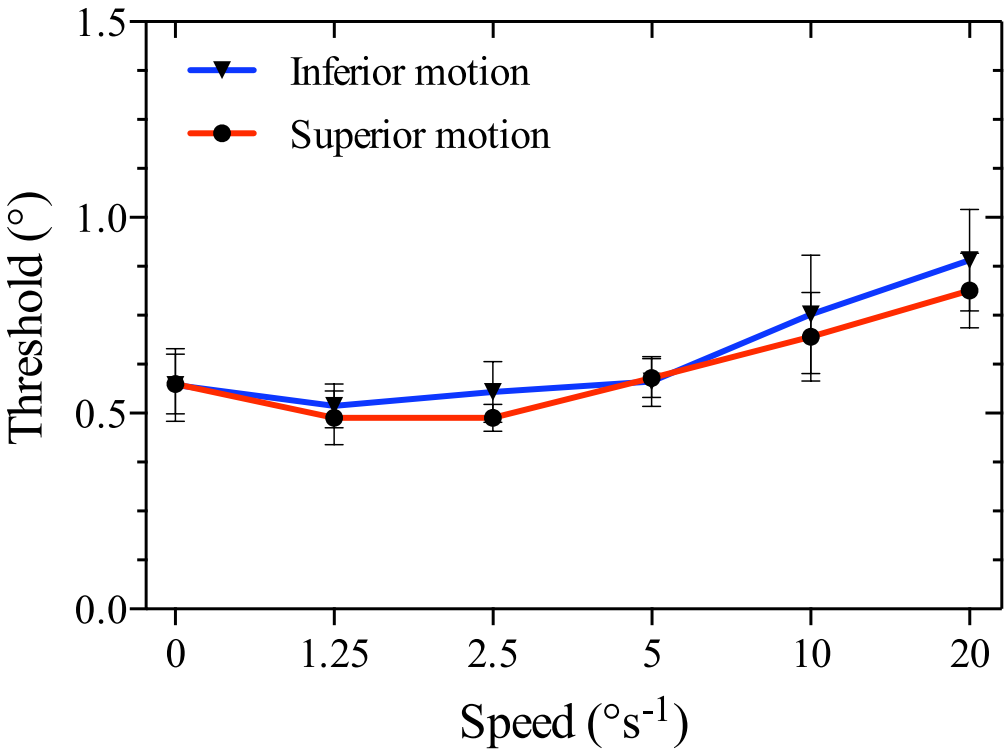

Figure 19: Graph showing resolution thresholds for static and moving targets at 10° eccentricity from Experiment 1.1, decomposed according to the direction of target trajectory. Mean and between-subjects 95%CI.

A two-way, repeated measures ANOVA indicated that target direction had no significant effect on resolution thresholds ($F(1,6)=5.85$; $p>.05$), but the effect of speed on resolution thresholds was still significant ($F(5,30)=24.41$; $p<.0001$). There was no significant interaction between speed and direction ($F(5,30)=0.77$; $p>.05$). Experiment 1.1.2 therefore suggests that the direction in which the target was travelling did not affect the ability of the observers to resolve the target.

3.2.5: Differences between the nasal and temporal visual fields (Experiment 1.1.3)

3.2.5.1: Methods

As photoreceptor densities are anisotropic from the fovea (Curcio et al., 1990), a bias may be observed when comparing the resolution thresholds for the temporal and nasal visual fields. Data were divided into targets that appeared to the left of fixation (nasal field) and right (temporal field), shown in Figure 20.

3.2.5.2: Results

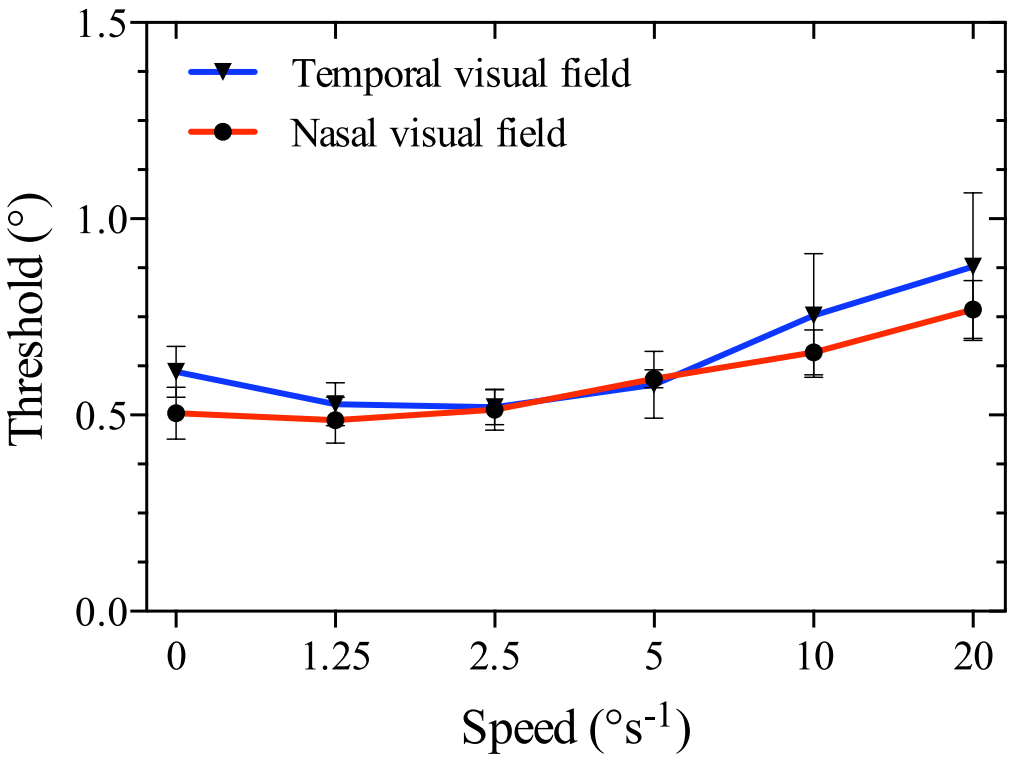

Figure 20: Graph showing resolution thresholds for static and moving targets appearing in the temporal and nasal visual fields separately. Data from 10° eccentricity in Experiment 1.1 decomposed according to visual field. Mean and between-subjects 95%CI.

A two-way, repeated measures ANOVA indicated that the visual field in which the target appeared (temporal or nasal) had no significant effect on resolution thresholds ($F(1,6)=5.02$; $p>.05$). However, target speed still had a significant effect ($F(5,30)=26.58$; $p<.0001$), and no significant interaction was reported ($F(5,30)=1.80$; $p>.05$). Thus, whether the target appeared to the left or right of fixation did not affect target resolution.

3.3: Resolution of static and moving peripheral targets in the superior visual field (Experiment 1.2)

3.3.1: Methods

As demonstrated by Curcio et al. (1987, 1990), the density of photoreceptor cells decreases more sharply in the superior and inferior visual fields than in the temporal and nasal. To examine the effect this has on visual function, acuity for static and moving targets was tested at four eccentricities, shown in Figure 21. Acuity was assessed using the same procedure as in Experiment 1.1. For a detailed description, refer to the General Methods chapter. As in Experiment 1.1, the targets were one of the four oblique orientations, allocated at random for each trial. Target trajectories were either from the left of fixation to the right, or the reverse, centred on the vertical meridian. Due to limitations in monitor screen dimensions, only the superior visual field was examined.

Six of the observers from Experiment 1.1 participated in Experiment 1.2, along with one additional observer (new age *M* 24.29, *SD* 3.50 years).

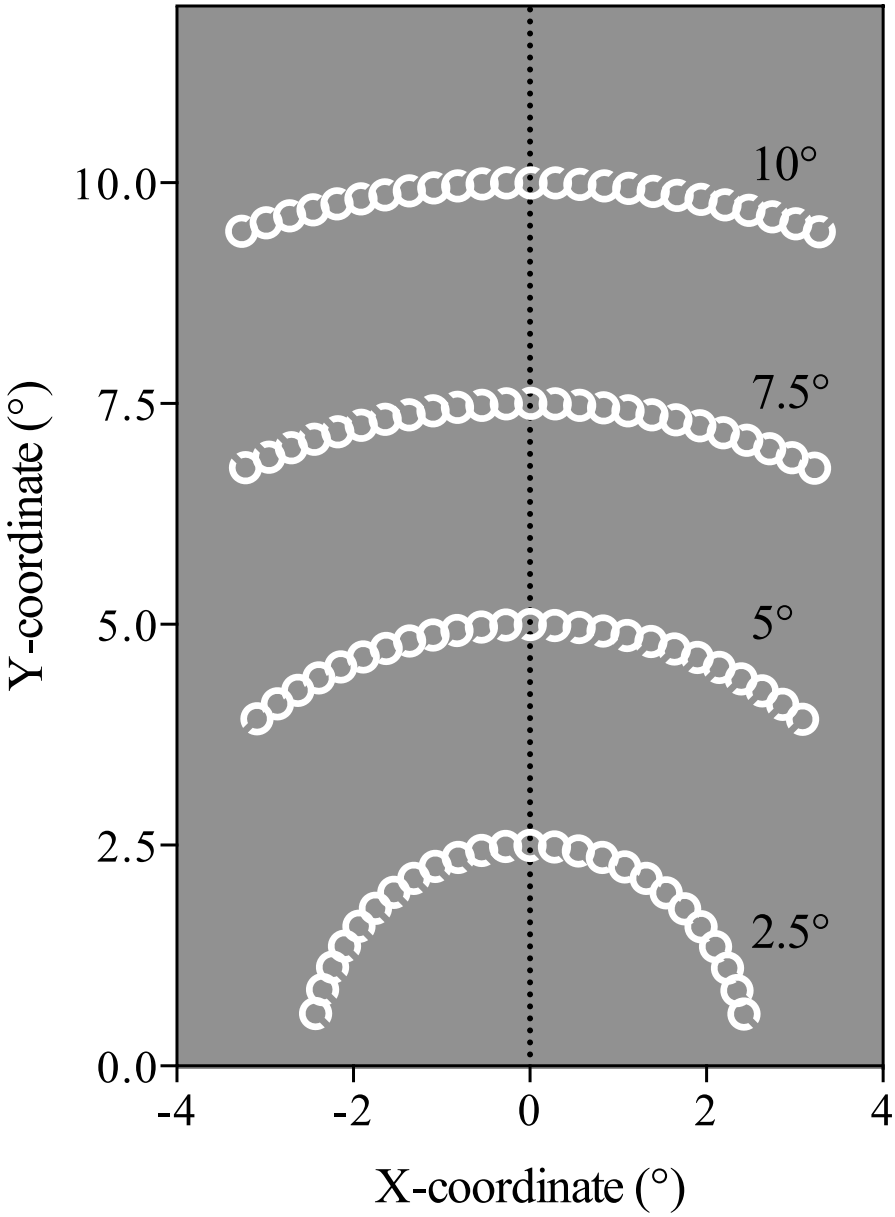

Figure 21: Target coordinates for the fastest condition ($20°s^{-1}$) at each eccentricity in Experiment 1.2. The targets are restricted to isoeccentric arcs centred on the vertical meridian. The black, dotted midline was not visible during stimulus presentation.

3.3.2: Results

Figure 22 shows the effect of target speed and eccentricity on resolution thresholds in the vertical periphery (the superior visual field).

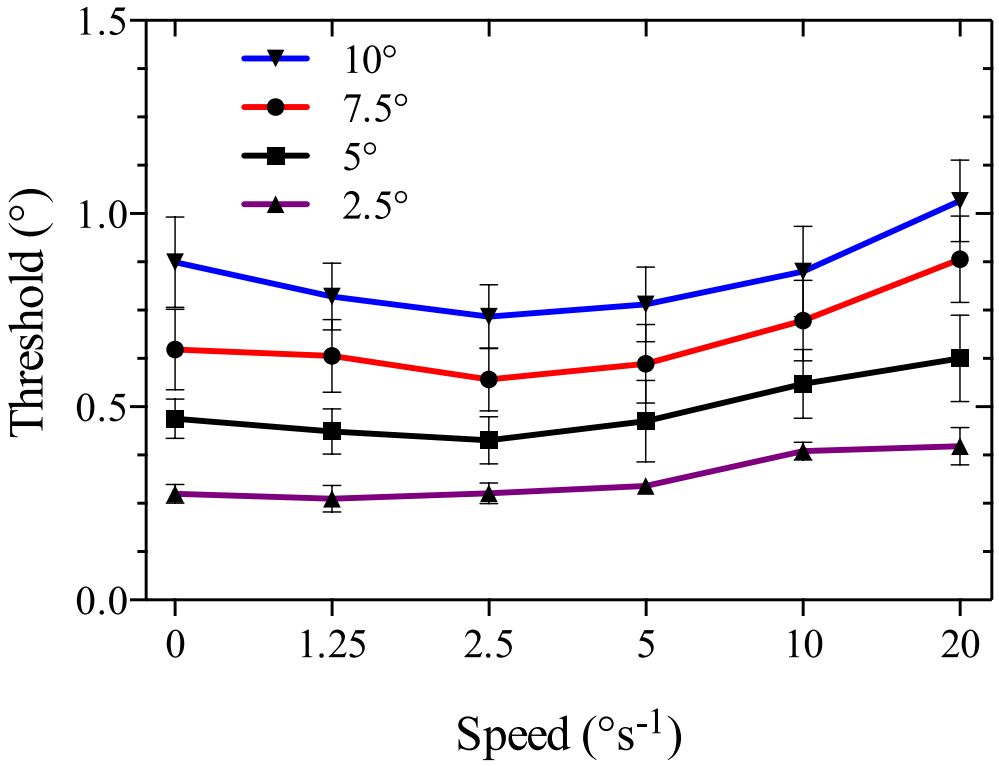

Figure 22: Graph showing the effect of target speed and peripheral eccentricity on resolution thresholds for targets appearing in the superior visual field. Data points indicate the mean resolution threshold, and error bars signify between-subjects 95% CI.

Figure 22 suggests that targets presented further into the superior visual field (away from the fovea) must be larger for accurate resolution. Additionally, within each eccentricity, the speed of the target effects resolution thresholds. At lower eccentricities, increasing speed has a detrimental effect on resolution thresholds, while at 10° target motion provides a benefit to resolution at several speeds. The effects of target speed and eccentricity on resolution threshold were analysed by a two-way, repeated measures ANOVA. There was a significant main effect of both eccentricity ($F(3,18)=133.30$; $p<.0001$) and target speed ($F(5,30)=49.65$; $p<.0001$).

As in Experiment 1.1, there is also a significant interaction effect ($F(15,90)=3.70$; $p<.0001$). To investigate the statistical significance of a potential benefit of slow

target motion, the speeds at which resolution thresholds were lower than in the static condition at 10° eccentricity were analysed. The difference between each observer's resolution thresholds was calculated between static targets and targets moving at 1.25°s^{-1} ,2.5°s^{-1}, 5°s^{-1}, and 10°s^{-1}, illustrated in Figure 23.

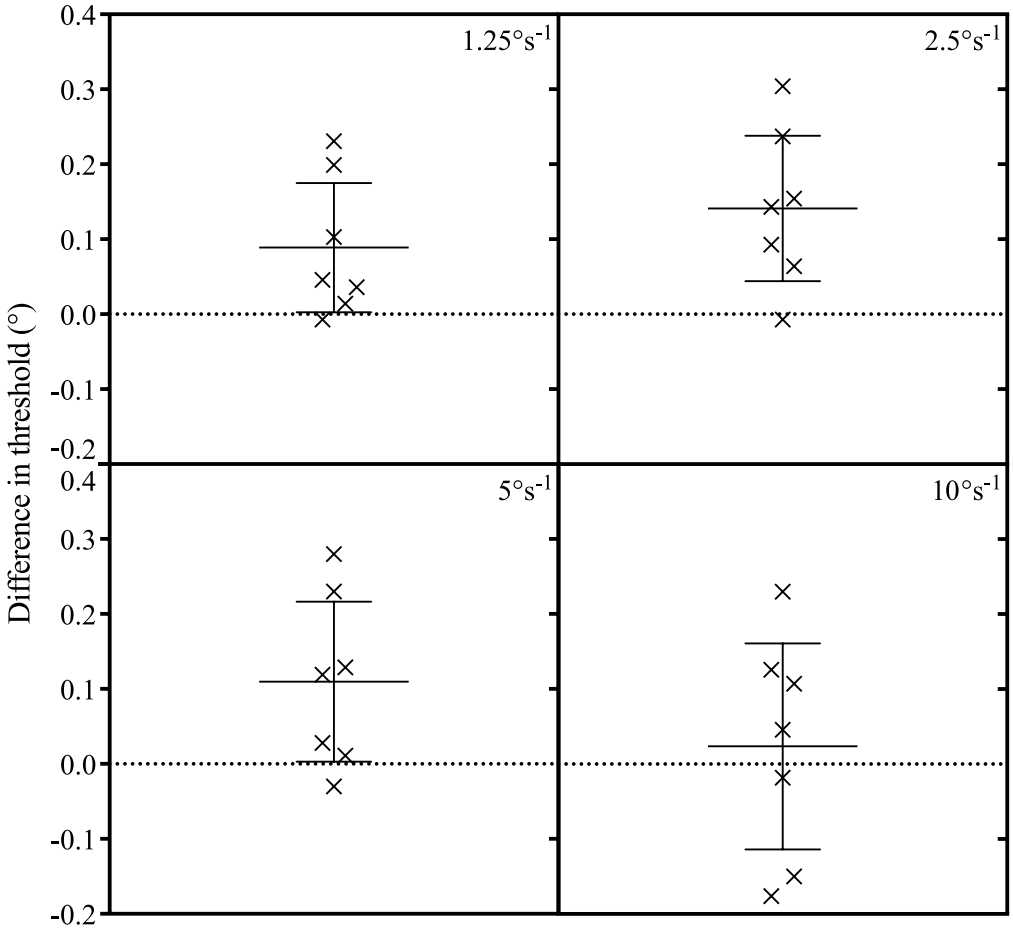

Figure 23: Scatter plots showing the difference in individual observers' resolution thresholds between static and moving targets, for target speeds that provided an average reduction in resolution thresholds. Clockwise from top left: the difference between resolution thresholds for static targets and targets moving at 1.25°s^{-1}, 2.5°s^{-1}, 10°s^{-1}, and 5°s^{-1}. Crosses show the difference in thresholds between the speeds for individual observers at 10° eccentricity in the superior visual field. Data points above zero on the abscissa indicate thresholds were lower in the moving condition. Horizontal bars show the mean with between-subjects 95%CI.

A one-tailed, paired samples t-test examined whether resolution thresholds for the $0°s^{-1}$ (*M* 0.87°, *SD* 0.13°) were significantly higher than each of the moving conditions. A Bonferroni correction was applied to correct for multiple comparisons, reducing the α-value to 0.01.

There was a significant effect of motion for targets at $2.5°s^{-1}$ (*M* 0.73°, *SD* 0.09°), t(6)=3.56; p=.006. However there was no significant reduction in resolution thresholds for any other of the moving conditions, compared to the static targets at 10° eccentricity in the superior visual field: $1.25°s^{-1}$ (*M* 0.79°, *SD* 0.09°), t(6)=2.53; p>.01; $5°s^{-1}$ (*M* 0.76°, *SD* 0.10°), t(6)=2.51; p>.01; $10°s^{-1}$ (*M* 0.85°, *SD* 0.13°), t(6)=0.42; p>.01. Therefore, target motion can improve resolution thresholds for targets within 10° of fixation, within narrow ranges of speed that are influenced by the retinal location of the target. This indicates that the beneficial effect of motion at $5°s^{-1}$ on resolution of peripheral targets suggested by Brown (1972b) is not supported by the experiments in this chapter.

3.4: Comparing the effect of target speed and eccentricity on resolution thresholds between the vertical and horizontal periphery (Experiment 1.3)

3.4.1: Methods

As discussed previously, photoreceptor cell density decreases more sharply in the vertical periphery (superior and inferior retina) than in the horizontal (temporal and nasal) (Curcio et al., 1990). The resolution thresholds calculated in Experiments 1.1 and 1.2 were compared to assess how photoreceptor anisotropy affects acuity. Resolution thresholds are shown for targets at the same eccentricity

in the horizontal (Experiment 1.1) and vertical (Experiment 1.2) visual fields in Figure 24. Only the six participants who took part in both experiments are analysed.

3.4.2: Results

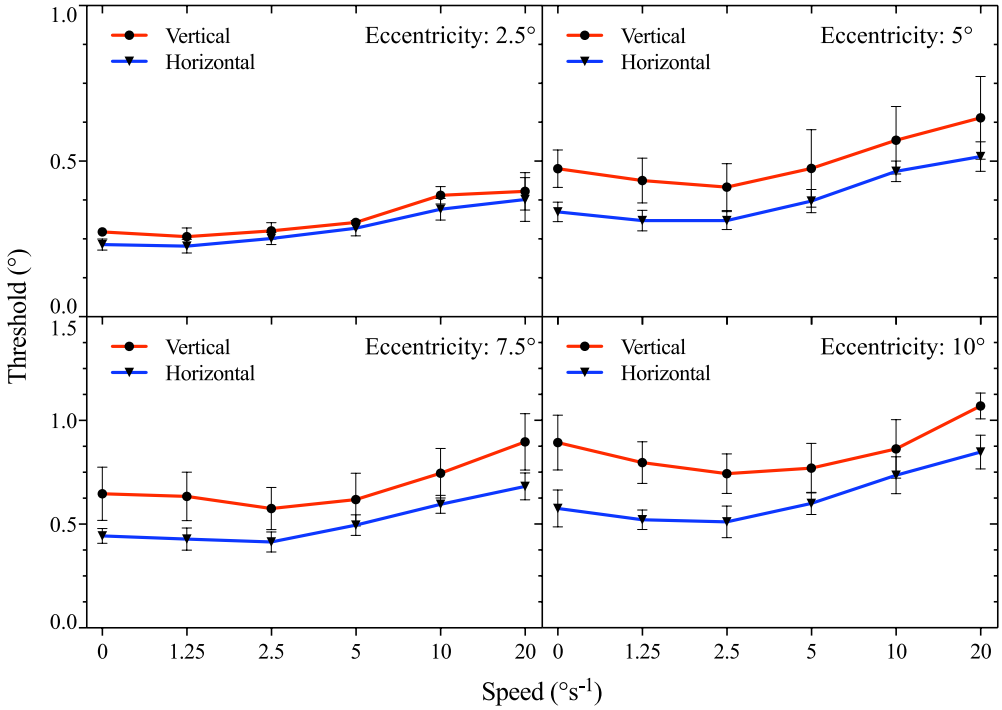

Figure 24: Comparison of resolution thresholds between the horizontal and vertical periphery as a function of target speed. Separate plots compare matched target eccentricity. Data points indicate mean resolution thresholds, and error bars between-subjects 95%CI.

A three-way, repeated measures ANOVA compared the contributions of speed, eccentricity, and visual field to resolution thresholds. As expected, the ANOVA reported significant effects of both speed ($F(5,240)=75.2$; $p<.001$) and eccentricity ($F(3,240)=485.4$; $p<.001$), and also that the visual field (superior or temporal/nasal) has a significant effect on resolution threshold ($F(1,240)=243.2$; $p<.001$). The effect of eccentricity on resolution thresholds is significantly

effected by the visual field in which it is presented ($F(3,240)=22.4$, $p<.001$), but the effect of speed on resolution thresholds is not ($F(5,240)=1.8$, $p>.05$). As in Experiment 1.1 and 1.2, there continues to be a significant interaction between eccentricity and speed ($F(15,240)=2.4$, $p=.003$). The three-way interaction was not significant, however ($F(15,240)=0.6$, $p>.05$). Resolution thresholds were influenced by the visual field in which the target was presented, but the effect of speed on resolution is the same between fields.

3.5: General discussion

Experiment 1.1 demonstrated that increasing target speed and eccentricity both have significant detrimental effects on resolution thresholds. Previous studies have found similar results (e.g. Brown, 1972a, 1972b; Westheimer, 1982). While a slight improvement is visible for some moving targets compared to static targets, this is only a significant difference within narrow ranges of speed. The range of speeds that can improve performance appears to be dependant on the retinal location of the target. This suggests that when eccentricity is controlled, motion alone does not provide a general improvement in acuity within 10° in the temporal and nasal periphery.

The increasingly detrimental effect of target speed is predicted by models of spatiotemporal integration, which suggest that target motion results in a smearing of the neural image (Burr, 1980; Hammett, 1997). Alternatively, the range of visible spatial frequencies has been shown to shift towards lower frequencies as target speed is increased (Burr & Ross, 1982; Burr et al., 1986a). Higher spatial frequencies are responsible for carrying the target information involved in acuity

measurements, so the shift away from these frequencies results in diminished performance in acuity tasks.

In Experiments 1.1.1, 1.1.2, and 1.1.3 acuity was shown to be unaffected by the orientation of the target, the direction in which it is travelling, and whether it appears to the left or right of fixation. In Experiment 1.1.1.1, no significant difference was found in resolution thresholds between the four possible target orientations. Although existing literature suggests the critical details of the target (in this case the gap in the Landolt ring) orientated towards the cardinal axes are more effectively resolved (Appelle, 1972), there is no evidence of a bias between oblique orientations. The critical detail of centrifugally orientated targets in Experiment 1.1.1.2 is more eccentric than the critical detail of centripetally orientated targets by 0.6 target widths, however this difference in eccentricity was not sufficient to elicit a significant difference between resolution thresholds. No significant difference between conditions in Experiments 1.1.1-1.1.3 supports the use of the paradigm used in Experiment 1.1 to assess peripheral resolution in the following chapters.

Experiment 1.2 (Figure 22) indicated that increasing the speed or retinal eccentricity of a target significantly increases resolution thresholds, as in the horizontal periphery in Experiment 1.1. Also in accordance with the horizontal periphery, the significant benefit of motion for eccentric targets was very limited (Figure 23). Thus, motion alone is insufficient to generally improve the resolution of targets viewed eccentrically. At higher eccentricities, whereby the photoreceptor matrix is suitably sparse, motion may provide a broader improvement over static acuity. Although the beneficial effect of summation may

be important to optimising visual performance, a technique designed to maximise the remaining visual function in AMD patients making use of this effect would be limited by the increased retinal eccentricity required for its use. The reduction in performance associated with increased eccentricity would limit the efficacy of the technique. Any developed technique should be for targets at a maximum eccentricity of 10°, to be suitably eccentric to avoid the scotoma but not unnecessarily further. The location of the PRL varies between patients but typically follows this rule; mean scotoma eccentricity has been reported as between 5.6° (*SD* 3.4°) and 7.5° (*SD* 2.5°) (Markowitz & Aleykina, 2010; Shima et al., 2010), and are more often in the horizontal periphery than the vertical (Crossland, Culham, Kabanarou, & Rubin, 2005). Thus, the situations in which motion alone may be sufficient to produce an improvement in peripheral acuity are not suitable for optimising visual performance in AMD patients.

In Experiment 1.3 (Figure 24), resolution thresholds were consistently higher in the vertical periphery than in the horizontal. This is accordance with anatomical data, which suggests that photoreceptor density is a good indicator of peripheral acuity between 2.5° and 10°. However, there was no significant difference between resolution thresholds in the temporal and nasal fields in Figure 20 (Experiment 1.1.3). The anatomical difference between the temporal and nasal fields within 10° of the fovea is much less than for the superior field (Curcio et al., 1990), which defends the lack of a significant difference in performance. This is supported by the interaction effect between eccentricity and field in Experiment 1.3, which suggests that the effect of increasing the eccentricity of the target on resolution thresholds is larger in the vertical periphery than in the horizontal. The significant interactions between the effects of target speed and eccentricity on

thresholds in Experiments 1.1, 1.2, and 1.3 suggests that if any potential benefit of motion on resolution for peripheral targets exists, the speed at which it may occur is dependent on the eccentricity of the target.

The experiments in this chapter have demonstrated that acuity deteriorates as the speed or retinal eccentricity of the target is increased. These results replicate several other reports in the literature (most notably Brown, 1972b), and extend them by using eccentricity-controlled target trajectories, modern psychophysical apparatus, and larger datasets. Analysing the data separately for the different possible target attributes suggested that performance does not differ between the different target orientations, directions of target trajectory, or between the nasal and temporal visual fields. There is a significant difference in resolution thresholds between the horizontal and vertical periphery, which is in line with predictions based on anatomy, and supports models of the retina as being inhomogeneous and anisotropic. Additionally, although there is evidence of slight improvements in resolution thresholds due to target motion, the benefits motion can provide are restricted to specific combinations of target speed and retinal location. Thus, as motion alone is insufficient to provide a general improvement in performance within 10° in the peripheral visual field, the following chapters aim to identify additional stimulus characteristics that could more broadly have a beneficial effect on peripheral acuity.

Chapter 4: Super-Resolution in the Peripheral Retina

4.1: Introduction

Spatially demanding tasks such as reading are, under normal circumstances, performed foveally. The resolution limit of the fovea is well matched to the transfer function of the eye's optical apparatus (Jennings & Charman, 1981; Williams, Artal, Navarro, McMahon, & Brainard, 1996). However, with increasing retinal eccentricity, acuity deteriorates in line with changes to the sampling density of retinal receptors (Curcio et al., 1990; Rossi & Roorda, 2010). External influences, such as ocular disease, can also produce changes in sampling by affecting the properties of the retinal mosaic. Neuro-retinal matrix damage (NRMD) refers to a collection of pathologies that often result in a distributed loss of photoreceptor function. NRMD can be caused in several ways, including clustered drusen build-up, hyperpigmentation, cellular atrophy or dystrophy, optic neuritis, or injury (Frisén, 2010, 2012; Rabb et al., 1986; Winther & Frisén, 2010).

In the peripheral retina, wherein the sampling resolution is limited, spatial frequencies beyond the resolution limit are readily detected, but appear distorted due to aliasing (Thibos, Still, & Bradley, 1996; Thibos, Walsh, et al., 1987). Aliases can also be generated in foveal vision if the blurring properties of the eye's optics are circumvented (Williams, 1985), suggesting that optical factors ultimately limit foveal vision rather than the spatial sampling. In digital imaging systems, sampling limits can be overcome to some extent by super-resolution (SR) techniques that exploit small motion-induced shifts in an image to reconstruct it at a higher resolution (Park et al., 2003). Low-resolution images

obtained at successive points in time are motion-corrected and merged to form a single image with greater spatial detail.

The role of SR processing in biological visual systems is often explored using dynamic occlusion, whereby the resolution and detection capacity is assessed for spatial patterns that are viewed through apertures (Nishida, 2004; Stappers, 1989) or obscured by opaque masks (Frisén, 2010; Kellman et al., 1998; Scholl & Pylyshyn, 1999).

Successful interpretation of dynamically occluded objects requires a functioning spatiotemporal interpolation (SI) mechanism, which allows occluded objects to be perceived as whole, despite their incomplete appearance (Kandil & Lappe, 2007). SI is necessary for illusions such as apparent motion to occur, whereby static images presented with an appropriate temporal and spatial offset can create the perception of a single moving image (Wertheimer, 1912). Fahle and Poggio (1981) suggested that the mechanism behind SI can be described as a monocular motion-energy detector with a velocity-sensitive receptive field, which has a tolerance for spatial or temporal offsets. This description of the SI mechanism implies that there are distinct detectors for different target velocities. Morgan and Watt (1983) examined the limits of the tolerance of the detectors. They showed that SI functions effectively at interpolating spatial offsets within 4 minutes of arc, but becomes gradually less efficient as the spatial interval is increased beyond that. They account for this decline in terms of the bandwidth of the motion detector's receptive field. Further, Hogendoorn, Carlson, and Verstraten (2008) showed that SI can process objects that move unpredictably, provided the spatial offset is within the range of tolerance, but that smooth motion is interpolated more

efficiently. Kandil and Lappe (2007) described an alternative SI mechanism. Using inter-ocular presentation techniques, they found evidence of a binocular mechanism with separate components for identifying object form and motion.

SI is therefore a key feature of the visual system, without which SR cannot efficiently occur. The mechanisms responsible for SI are unclear, but rely on the correct interpretation of visual signals that are separated in space and time. Kandil and Lappe (2007) suggested that successful interpolation requires perception of the global form of the image. This form can be created by providing the target with consistent characteristics such as motion.

There is some evidence to suggest that motion aids the resolvability of occluded spatial patterns. Frisén (2010) simulated NRMD in the fovea using superimposed masks with opaque elements, through which observers viewed letter targets. Whereas static acuity fell systematically with increasing mask density, acuity for moving targets was much less affected. This was interpreted as evidence for SR processing capacity in situations where acuity is sampling limited. However because Frisén employed a static mask, a larger number of independent spatial samples of the target were available in moving, compared to static conditions. As a result, it is difficult to ascertain whether motion-related improvements in acuity reflect *bona fide* SR processing, or simple probability summation.

Similarly, Nishida (2004) demonstrated letter targets viewed through slit apertures were more accurately resolved when moving. Furthermore, when the targets were additionally masked with moving random noise, thresholds were significantly more impaired by noise moving in the same direction as the target than discordant motion. Nishida (2004) also compared letter recognition for targets moving

smoothly with those for which the motion sequence has been randomised (presenting the targets at the same locations between trials, but in a random order). It was reported that letter identification was drastically reduced by randomising the motion sequence. Nishida's (2004) results indicate a component of the SR mechanism that is sensitive to motion. Other descriptions of SR mechanisms also emphasise the influence of motion. Palmer, Kellman, and Shipley (2006) suggest there is a component of the SR mechanism that continuously tracks the position of the target while occluded, such that the new target information can be integrated into the perceived image when it appears. Mateeff, Popov, and Hohnsbein (1993) compared the perceived quality of occluded targets that moved smoothly to targets moving unpredictably. They found that image quality was perceived to be poorer when the motion trajectory was unpredictable, which supports a motion-sensitive component within the SR mechanism. This description of a motion-sensitive component suggests that the source of the motion is predictive of performance; a motion-sensitive tracker would be impaired by a moving mask obscuring a static target.

The studies outlined so far investigate the nature of a foveal SR mechanism, where photoreceptor density (and thus the spatial sampling rate), is at its peak (Curcio et al., 1990). For unobscured targets in the fovea, motion impairs resolution (Brown, 1972b). In the periphery however, there is evidence from Brown (1972b) to suggest that target motion can improve resolution thresholds under particular conditions. The natural relative sparseness of the photoreceptor mosaic in the peripheral retina may provide conditions under which a SR mechanism can operate. This chapter describes a series of experiments examining

the conditions under which motion improves acuity in the peripheral visual field, to provide a more rigorous test of SR processing capacity in human vision.

In Experiment 2.1, resolution thresholds are compared for static and moving peripheral targets presented behind partially-opaque masks. Although Frisén (2010) and other studies have reported evidence of a SR mechanism, it remains unclear whether motion is a critical aspect, or if the motion is only providing extra samples of the target that can be summated to improve performance. Thus, Experiments 2.2 and 2.3 examine the individual contributions of the extra target information and the target motion, respectively. Experiments 2.4-2.7 probe the motion-sensitive component of the SR mechanism. Experiment 2.4 compares resolution thresholds for static targets behind moving tasks with thresholds for moving targets behind static masks to quantify the influence of the source of the motion. Experiments 2.5, 2.6 and 2.7 investigate disruptions to the motion-sensitive mechanism. In Experiment 2.5, resolution of targets moving smoothly and unpredictably are compared, while in Experiment 2.6, smooth and unpredictable mask motion is compared. The motion trajectory is disrupted by randomising the order in which the target appears at the coordinates along its trajectory. The motion-sensitive component, as described by Palmer et al. (2006), Nishida (2004), and Mateeff et al. (1993), predicts that disrupting the motion path should be disruptive to a SR mechanism when the target is the source of the motion. Thus, disrupting the path of a moving mask will have less impact on the motion-sensitive component, allowing for better target resolution than a smoothly moving mask. The method of randomising the motion trajectory used in Experiments 2.5 and 2.6 maintains a consistent retinal displacement between conditions, however the change in target position between frames is variable.

Thus, the target speed is also variable between frames (for a more detailed explanation of this technique, see Experiment 3.1). Therefore, in Experiment 2.7 resolution thresholds are examined for targets with a smooth sinusoidal motion path, with predictable or unpredictable trajectories. This examines how the motion-sensitive component may be influenced by a motion signal which remains smooth and consistent between nodes, but is unpredictable on longer time scales.

4.2: General methods

4.2.1: Participants

Eight observers (mean age 24.5, *SD* 1.4 years) participated in Experiments 2.1-2.6. Six observers (mean age 30.7 years, *SD* 10.4 years) participated in Experiment 2.7. All had normal or corrected-to-normal visual acuity.

4.2.2: Apparatus

Stimuli in Experiments 2.1-2.6 were generated using the apparatus and software described in the General Methods section. Experiment 2.7 was performed using similar apparatus, albeit in a different laboratory and using a different display. The targets in Experiment 2.7 were presented on a gamma-corrected CRT monitor (Sony Triniton Multiscan G520; 1280x1024 resolution; screen width 40cm; Sony Electronics, Inc., San Diego, CA, USA) with 75Hz refresh rate, and the stimuli were generated on a Mac Pro (Apple Inc., Cupertino, CA, USA) using PsychoPy (v1.80.00rc). Observers sat with a chinrest 100cm from the monitor and made responses using an ordinary keyboard. Targets were presented monocularly to the right eye.

4.2.3: Stimuli

Landolt ring targets, centred at 10° from a static fixation cross, were used to quantify resolution thresholds. Opaque masks were superimposed over the targets to reduce the available information. The mask was composed of an array of 5x5 pixel elements. According to the mask density, the corresponding proportion of mask elements were set to be opaque, remaining the same contrast as the background. Three mask densities were examined: the highest was 0.75, whereby 75% of the elements were opaque. For the mask density of 0.5, 50% were opaque, and for the mask density of 0, the mask was completely transparent. Examples of the target behind a mask at each of the three densities are shown in Figure 25.

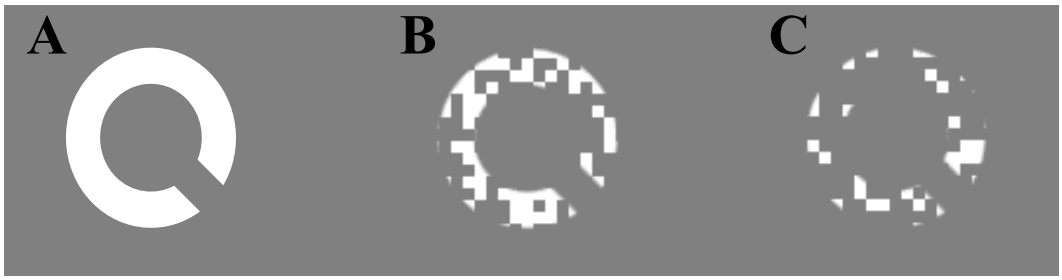

Figure 25: Example images of the target when occluded by the mask. (A) The mask density is set to 0, so the mask is entirely transparent. (B) The mask density is set to 0.5, such that 50% of the mask elements are set to being opaque. (C) The mask density is set to 0.75, such that 75% of the mask is opaque.

The elements to be opaque were chosen at random at the beginning of each trial. Each mask element was a square with sides 5' 53" in length (approximately 2.90μsr) in Experiments 2.1-2.6. In Experiment 2.7 the masks consisted of an array of square elements of side length 5' 17" (approximately 2.36μsr; the difference from Experiments 2.1-2.6 was a result of available screen resolution). Targets were white, with a luminance of 85.0cdm^{-2} presented on a grey

background of 45.0cdm^{-2} (Michelson contrast 0.31) in a dark vision laboratory (0.5cdm^{-2}).

4.2.4: Procedure

Data from ten staircase procedures for each condition were collected for each participant. Resolution thresholds were determined using an orientation discrimination paradigm, detailed in the General Methods chapter (Chapter 2).

4.3: Demonstration of a super-resolution mechanism operating in the peripheral retina (Experiment 2.1)

4.3.1: Methods

Firstly, SR in the peripheral retina was examined directly for increasing levels of artificial stimulus undersampling. Resolution thresholds were compared between static targets, and targets following an isoeccentric arc at 2°s^{-1}. The motion characteristics are shown in Figure 26. Targets were presented behind superimposed, partially opaque masks. The targets were presented on 25 consecutive video frames (0.33s) on each trial.

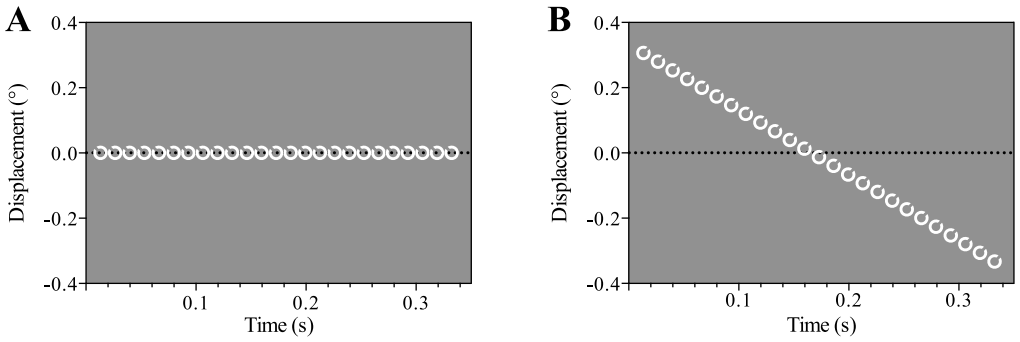

Figure 26: Space-time plots for target trajectories in Experiment 2.1, in terms of absolute displacement from the stimulus origin at 10° to the right of fixation, on the horizontal meridian. (A) Static targets remained at the stimulus origin for the duration of the trial. (B) Targets with smooth motion followed an isoeccentric arc at constant speed ($2°s^{-1}$) for the same duration.

4.3.2: Results

The effect of target motion on orientation discrimination thresholds was examined for three levels of target occlusion to confirm the ability of the peripheral retina to perform image processing akin to SR. In Figure 27 performance is displayed as the average of all observers' resolution thresholds for static and moving peripheral targets, separated by the density of opaque elements in the overlaid mask (left). The relative performance of each individual observer with static and moving targets is also compared (right): data points below the dotted line indicate more accurate discrimination of moving targets.

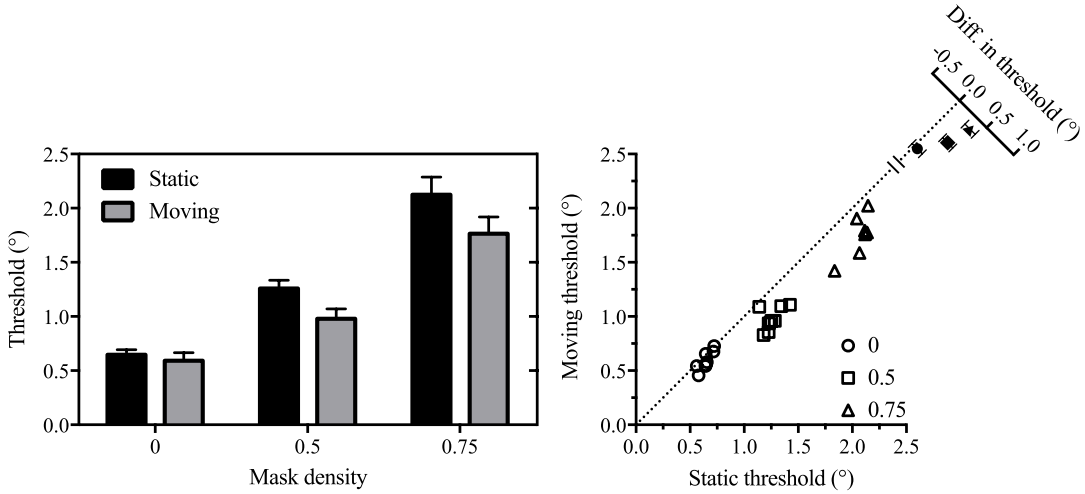

Figure 27: Results from Experiment 2.1 comparing resolution thresholds for static and moving peripheral targets occluded by superimposed opaque masks of varying density. Left, mean threshold critical detail width for static (black) and moving (grey) targets as a function of mask density. Error bars show 95% confidence intervals. Right, open symbols show data of individual observers separated by mask density; closed symbols show average difference in threshold between motion conditions at each mask density, plotted on an oblique axis.

Figure 27 indicates that as mask density increases, the mean resolution thresholds steadily increase. Further, there is little difference in the mean resolution threshold for static and moving targets at a mask density of 0. However, at the higher mask densities, thresholds are clearly lower for moving targets than for static targets. A two way, repeated measures analysis of variance (ANOVA) indicated that increasing mask density significantly diminished accuracy ($F(2,14)=660.5$, $p<.0001$), but performance was significantly improved by introducing target motion ($F(1,7)=85.3$, $p<.0001$). There was also a significant interaction ($F(2,14)=13.1$, $p=.0006$). Analysis of the simple effects using Fisher's least significant difference (LSD) test, corrected for multiple comparisons using a Bonferroni correction, suggests the effect of motion was significant for mask

densities of 0.5 ($t(14)=6.37$, $p<.0001$) and 0.75 ($t(14)=8.21$, $p<.0001$) but not 0 ($t(14)=1.23$, $p>.017$).

The results here show that resolution thresholds for artificially undersampled peripheral targets were progressively impaired as the mask density was increased. For the artificially undersampled targets, motion significantly reduced resolution thresholds. However, resolution for unmasked targets (0 mask density) was not improved by target motion. This shows further that the beneficial effect of speed noted under certain conditions in Chapter 3 is very limited.

4.4: Contribution of additional stimulus information (Experiment 2.2)

4.4.1: Methods

When opaque masks are overlaid on targets (Experiment 2.1), a proportion of the motion-related improvement in acuity may be due to the provision of additional spatial samples of the target rather than by motion *per se*. To control for the spatial extent of the visible target, resolution thresholds were compared for static targets presented behind either a static or randomly updating mask. For the latter, the locations of the opaque elements were randomly allocated and updated at the beginning of each video frame, thus 25 unique masks obscured the target during each trial.

Although the extent of the target visible on each frame was unchanged, by updating the locations of the opaque elements on each frame, more of the target is uncovered throughout the trial.

4.4.2: Results

Figure 28 shows mean resolution thresholds (left) for static targets behind static, unchanging masks, and masks with the opaque element locations updating on every frame. Resolution thresholds for individual observers and the overall mean thresholds for each mask density are also compared between conditions (right). Data points below the diagonal indicate improved resolution for the updating mask condition.

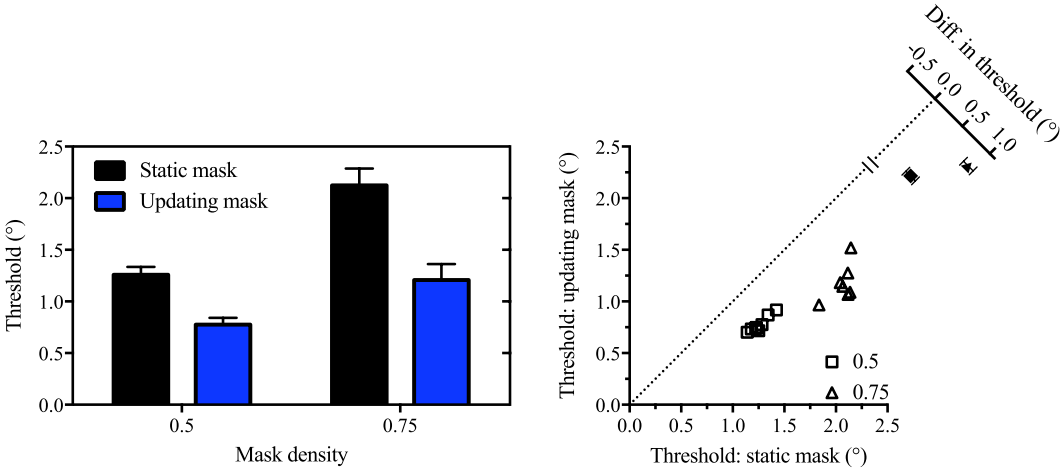

Figure 28: Results from Experiment 2.2 comparing resolution thresholds for static targets occluded by static or randomly updating opaque masks (black and blue bars, respectively). Left, the mean resolution thresholds across participants. Right, the threshold for each observer (open symbols) is compared between conditions, and the group mean difference in thresholds (closed symbols) is shown on an oblique axis. Error bars indicate between-subjects 95%CI.

A two-way, repeated measures ANOVA revealed resolution performance to be significantly improved by the addition of the extra target information in the updating mask condition ($F(1,7)=518.5$, $p<.0001$). It also indicated thresholds were significantly higher for the denser mask ($F(1,7)=308.7$, $p<.0001$) and that a

significant interaction exists between mask update condition and mask density ($F(1,7)=69.21$, $p<.0001$): analysis of the simple effects using Fisher's LSD, corrected for multiple comparisons by a Bonferroni correction showed resolution thresholds for the randomly updating mask were significantly lower than the static mask for both mask densities (0.5: $t(7)=13.09$, $p<.0001$; 0.75: $t(7)=24.85$, $p<.0001$).

The results of this experiment indicate that updating the locations of the mask elements on each video frame significantly improves resolution of the obscured Landolt ring target. This suggests that extra spatial samples of the target can be integrated across time without a coherent motion signal.

4.5: Isolating the contribution of motion (Experiment 2.3)

4.5.1: Methods

To test whether motion provides any benefit beyond merely increasing the information content of the stimulus sequence, resolution thresholds were compared for static and moving targets in the presence of randomly updated masks (see Experiment 2.2). This ensured that the number of independent target samples was matched in the two conditions and that any differences in performance could be directly attributed to motion of the target. Target motion is described in Figure 26.

4.5.2: Results

Figure 29 shows the mean resolution thresholds (left) for static and moving peripheral targets, obscured by masks with opaque elements, the locations of

which are updated on each video frame. Right, the resolution thresholds of each observer are compared for the static and moving conditions. The group mean relative difference is also compared between conditions on the oblique axis. Data points below the diagonal indicate resolution thresholds were lower for moving targets.

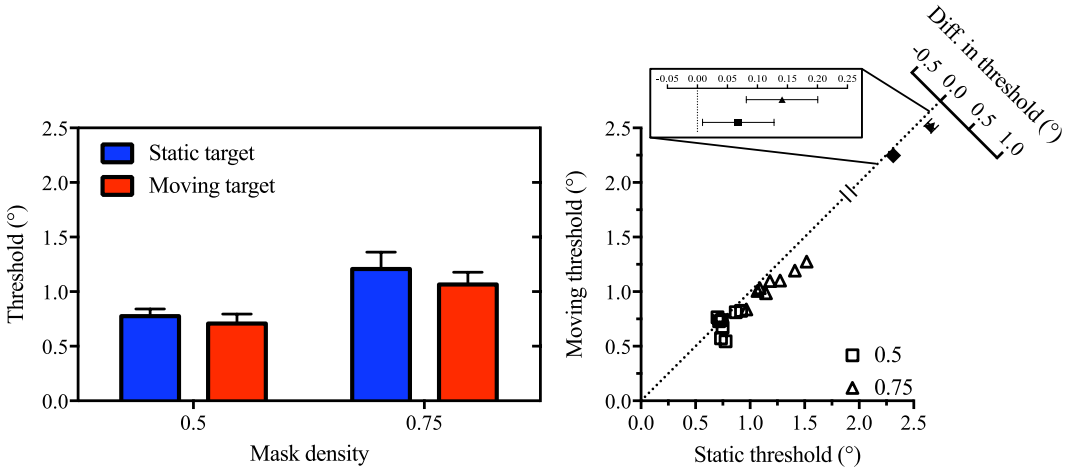

Figure 29: Results of Experiment 2.3, comparing orientation discrimination thresholds for static and moving peripheral targets behind masks with randomly updating element locations. Left, the mean between-subjects threshold for static (blue bar) and moving (red bar) targets, for each mask density. Right, the relative performance of individual observers (open symbols), and the group mean difference in threshold (closed symbols) between conditions. The inset provides a zoomed-in indication of the relative performance, whereby positive values indicate lower thresholds for moving targets. Error bars indicate between-subjects 95%CI.

A two-way, repeated measures ANOVA confirmed statistically significant reductions in resolution thresholds from the additional target motion ($F(1,7)=19.43$, $p=.0031$) as well as the increase in thresholds associated with increasing mask density ($F(1,7)=104.2$, $p<.0001$), while the interaction was not significant ($F(1,7)=4.182$, $p>.05$).

The results of Experiment 2.3 suggest that resolution thresholds were significantly lower for moving targets. Thus, while a portion of the beneficial effect of motion seen in Experiment 2.1 can be accounted for by the increase in the spatial extent of the target that is visible across the trial, a residual beneficial effect of motion remains. Since the interaction was not significant, the beneficial effect of motion persists across mask densities.

4.6: Effect of the source of motion (Experiment 2.4)

The motion-sensitive component of the SR mechanism (detailed by Palmer et al., 2006) may be disrupted by a source of motion that does not originate within the target. It is unclear from the results in the previous experiments in this chapter whether the motion-sensitive component is perceptive to target motion across the retina, or whether it can operate so long as there is target motion relative to the mask. These two possibilities are dissociated in Experiment 2.4 by comparing resolution thresholds for moving targets behind static masks, with thresholds for static targets behind moving masks.

4.6.1: Methods

A comparison was made between resolution thresholds for targets moving along isoeccentric arcs behind static masks (Figure 26B) and thresholds for static targets behind masks moving along the same trajectory at the same speed, i.e. it was examined whether it matters if the target or the mask moves. Unlike in the randomly updating mask conditions, the mask in Experiment 2.4 maintained a coherent global form; the coordinates of the centre of the mask were updated on

each video frame but the opacity of the elements within the array was chosen at the beginning of each trial and was unchanged for the duration of the trial.

4.6.2: Results

Figure 30 compares resolution thresholds for moving targets behind static masks with thresholds for static targets behind moving masks. Left, the mean thresholds are compared between motion conditions across the two mask densities. Right, individual observers' thresholds are compared, and the mean difference in thresholds is plotted on an oblique axis. Data points above the dotted line indicate resolution thresholds were lower for the moving target behind the static mask.

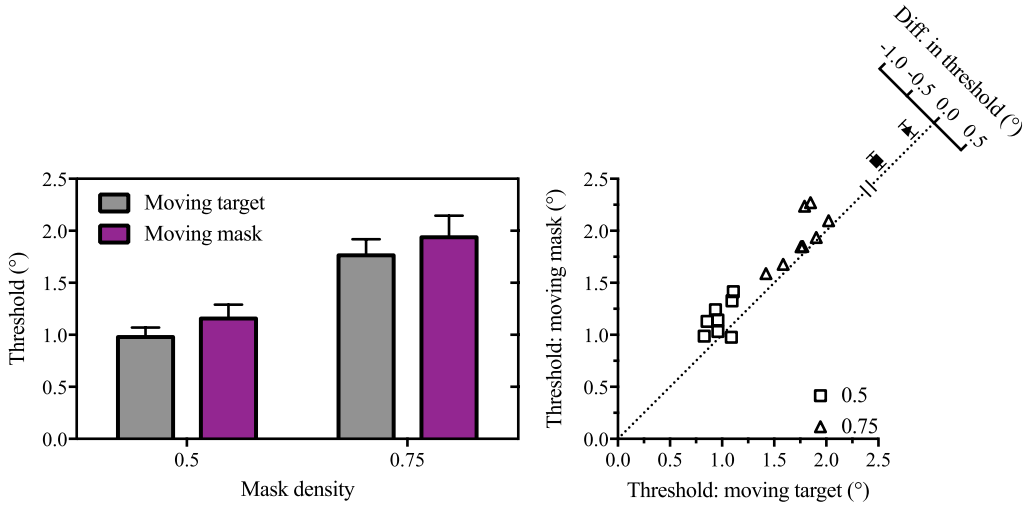

Figure 30: Results of Experiment 2.4, comparing peripheral orientation discrimination thresholds for moving targets behind static masks to those for static targets behind moving masks. Left, the mean thresholds across observers. The moving target, static mask condition is shown in grey; static target, moving mask in purple. Right, the individual observers' thresholds are compared between motion conditions for both mask densities separately (open symbols). The between-subjects mean difference in threshold (closed symbols) is plotted on the oblique axis. Error bars indicate between-subjects 95%CI.

Thresholds were significantly lower for target motion than mask motion ($F(1,7)=17.23$, $p=.0043$), indicating that summation is more successful when the source of the motion is the object to be resolved. The ANOVA also indicated increasing mask density deteriorated thresholds ($F(1,7)=264.7$, $p<.0001$), and that no interaction was present ($F(1,7)=0.003$, $p>.05$).

Since resolution thresholds were significantly lower for the moving target, static mask condition, the results of Experiment 2.4 indicate that the peripheral SR mechanism contains a component sensitive specifically to target motion across the retinal surface. By introducing motion to a source other than the target, this motion-sensitive component is disrupted.

4.7: Effect of predictability of target motion (Experiment 2.5)

4.7.1: Methods

To further examine the characteristics of the motion-sensitive component, resolution thresholds were assessed for smooth and disrupted motion trajectories. Resolution thresholds were compared for targets moving along the trajectory in a sequential order behind a static mask with targets following the same trajectory but appearing at each point in its sequence in a random order (Figure 31).

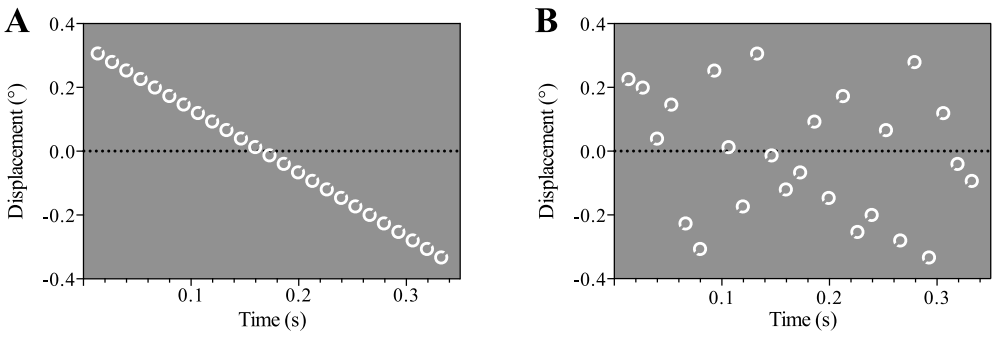

Figure 31: Space-time plots for target trajectories in Experiment 2.5, in terms of absolute displacement from the stimulus origin at 10° to the right of fixation, on the horizontal meridian. (A) Targets with smooth motion were presented at coordinates along an isoeccentric arc with constant distance between successive presentations. (B) Targets in the unpredictable motion condition appeared at the same coordinates, but in an unpredictable order.

4.7.2: Results

In Figure 32, resolution thresholds are compared for targets moving either smoothly or in an unpredictable order. The group mean resolution thresholds are compared on the left. Right, the relative performance between motion conditions is shown for individual observers, and the group mean. Data points above the dotted oblique line indicate relative performance was better for smooth motion than for unpredictable motion.

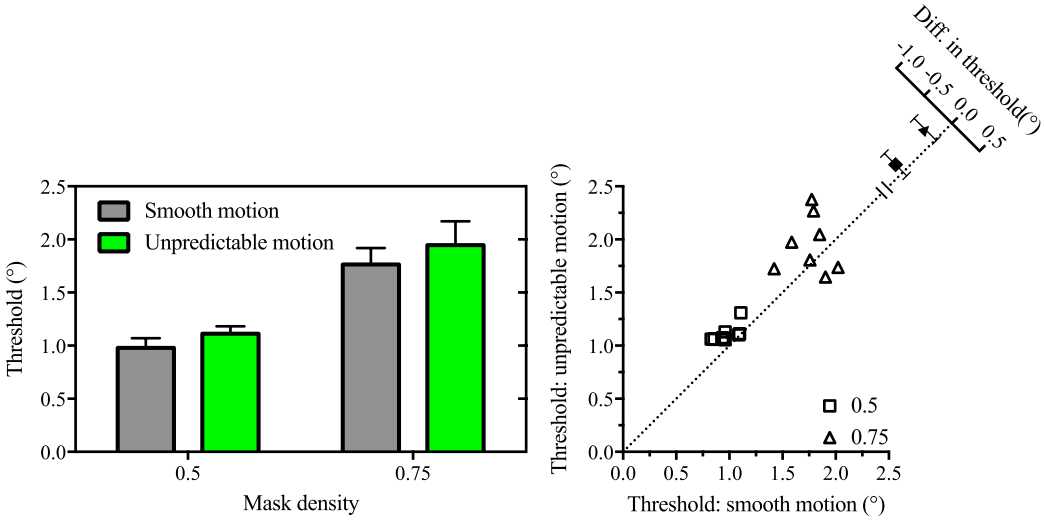

Figure 32: Results of Experiment 2.5, comparing resolution thresholds for targets moving smoothly and unpredictably behind static masks. Left, between-subjects average resolution thresholds for smooth (grey) and unpredictable (green) motion conditions are compared for each of the mask densities. Right, the difference in performance between the motion conditions is shown for individual observers (open symbols) and the group mean (closed symbols), plotted on the oblique axis.

A two-way, repeated measures ANOVA indicated that randomising the order of the motion path increased thresholds ($F(1,7)=7.075$, $p=.033$); increased mask density also deteriorated performance ($F(1,7)=212.8$, $p<.0001$) and no interaction was indicated ($F(1,7)=0.17$, $p>.05$). This supports a peripheral SR mechanism that contains a motion-sensitive component, since performance was impaired by interference with the smooth motion path.

4.8: Effect of predictability of mask motion (Experiment 2.6)

The results of Experiments 2.4 and 2.5 support a description of a peripheral SR mechanism that contains a component that is sensitive to target motion. Experiment 2.4 demonstrated that resolution thresholds were relatively impaired when the motion source did not originate in the target, while Experiment 2.5

showed that disrupting the smooth motion signal was disruptive to performance. Thus, in Experiment 2.6, further evidence of the motion-sensitive component is investigated by disrupting the smooth motion signal of mask motion.

4.8.1: Methods

Resolution thresholds for static targets were compared for occluding masks moving sequentially (following the coordinates in Figure 31A) or in a random order (Figure 31B). The masks maintained coherent global form throughout the trial. A significant reduction in resolution thresholds for unpredictable mask motion compared to smooth mask motion would further support the motion-sensitive component of the peripheral SR mechanism.

4.8.2: Results

Resolution thresholds for Landolt ring targets obscured by either smoothly moving or unpredictably moving masks are shown in Figure 33. Left, the average resolution threshold across observers, separated by mask density. Right, the relative performance is compared for each observer, and the average difference in threshold between conditions is plotted on the dotted oblique axis. Points below the oblique axis indicate observers' resolution thresholds were lower in the unpredictable mask motion condition.

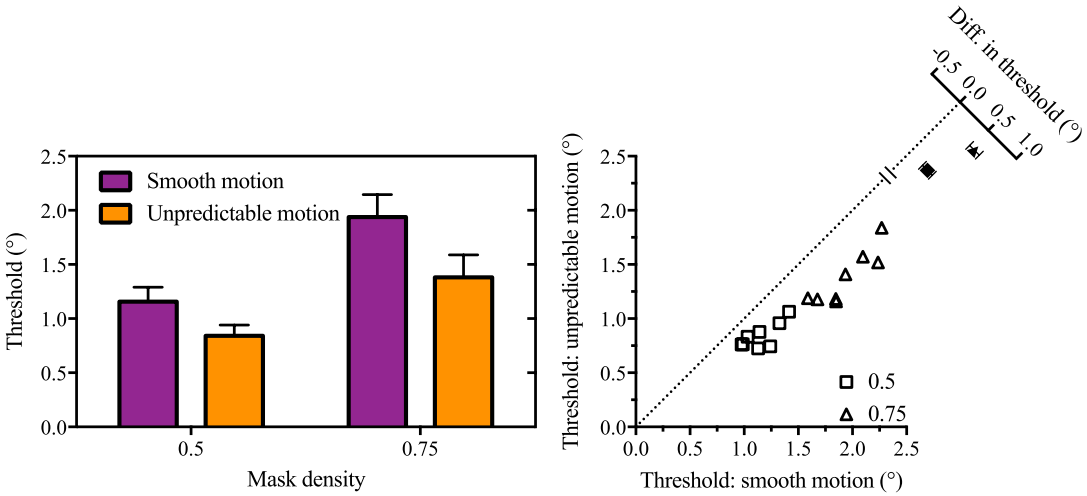

Figure 33: Results of Experiment 2.6, comparing resolution thresholds for peripheral targets behind smoothly and unpredictably moving opaque masks. Left, bars show the mean between-subjects resolution thresholds for Landolt ring targets behind either smoothly moving (purple) or unpredictably moving (orange) masks. Right, the relative performance of individual observers (open symbols) is compared between conditions. The average difference in resolution thresholds (closed symbols) for each of the mask densities is plotted on an oblique axis. Error bars indicate between-subjects 95%CI.

A two-way, repeated measures ANOVA indicated that unlike unpredictable target motion, irregularity in the motion of a moving mask improved performance ($F(1,7)=203.1$, $p<.0001$), while increasing mask density was detrimental to resolution thresholds ($F(1,7)=180.4$, $p<.0001$). A significant interaction was also reported ($F(1,7)=21.60$, $p=.0023$). Analysis of the simple effect using Fisher's LSD indicated a significant effect of motion predictability at both mask densities (0.5: $t(7)=8.64$, $p<.0001$; 0.75: $t(7)=15.22$, $p<.0001$).

The results of Experiment 2.6 further support a peripheral SR mechanism with a motion tracking component. By introducing motion from a source other than the target (Experiment 2.4), the motion-sensitive component was disrupted.

Interrupting this motion source by interfering with the coherent motion signal of the mask prevents the disruption to the motion-sensitive component.

4.9: Effect of predictability in smooth target motion (Experiment 2.7)

4.9.1: Methods

In Experiment 2.5, a comparison was made between targets that move smoothly in a sequential order along the motion trajectory, and targets appearing at the same locations but in a randomised order. It was shown that randomising the motion sequence was detrimental to resolution thresholds. This result was explained in terms of a disruption to the motion-sensitive component of the peripheral SR mechanism. The paradigm created disruption in the motion sequence at the cost of smooth motion. In Experiment 2.7 it was examined whether the motion-sensitive component is capable of tracking smooth, unpredictable target motion, and is thus disrupted only by disjointed motion. Resolution thresholds for partially-obscured targets were compared between regular, sinusoidal motion trajectories and trajectories with unpredictable changes in direction and speed.

The targets in this experiment were Landolt rings centred at 10° in the periphery, and similar to the previous experiments, were either static or moving. However, unlike in the previous experiments, the motion trajectory was not isoeccentric but instead varied sinusoidally. There were two motion conditions, described by Equation 6.

$$R(\theta) = 10 + A\sin(F\theta) \qquad (6)$$

Where R is the eccentricity of the target in degrees at polar angle θ, and A and F are the amplitude and frequency of the sinusoidal modulation, respectively. A was set to 0.5. This value was a good compromise of noticeable sinusoidal variation in eccentricity, and number of complete cycles that could be completed. A higher value of A resulted in higher amplitude jitter, but fewer complete cycles were possible with a reasonable target speed, i.e. fewer nodes at which unpredictability could be introduced. A lower value of A did not produce adequate variation in eccentricity to be sufficiently noticeable at 10° in the periphery. For the predictable motion condition, sinusoid frequency F was selected at random from the set of possible frequencies (1.25, 1.85, 2.36 and 3.09cycles/°; equivalent temporal frequencies: 1.11, 1.65, 2.19, 2.75cycles/s) and did not change throughout the trial. For the unpredictable condition, each time the target eccentricity reached 10° (i.e. at each node), F was reselected at random and the direction of the sinusoidal displacement was also reselected. A comparison of the predictable and unpredictable conditions is shown in Figure 34.

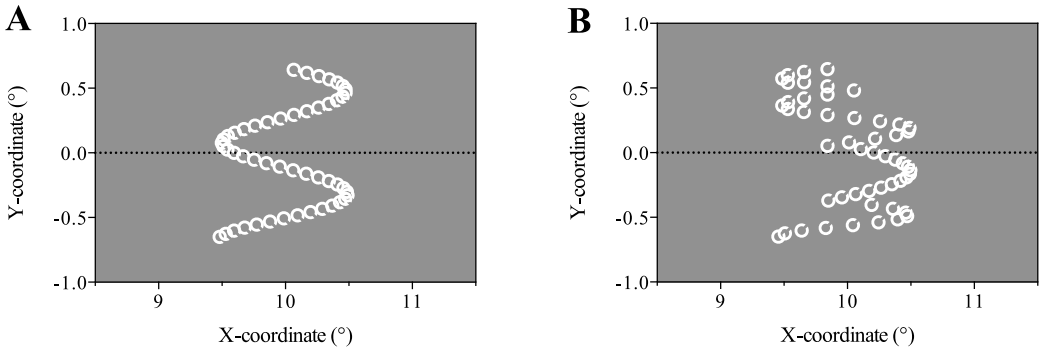

Figure 34: Plots showing example target progression over time for the motion conditions in Experiment 2.7. The plots here have been converted to Cartesian coordinates. (A) an example of target coordinates in the predictable motion condition, here with the minimum frequency of 1.25 cycles/°. (B) example of unpredictable motion, whereby at each node the sinusoid frequency (F) and direction (towards or away from fixation) is reselected at random.

As in the previous experiments in this chapter, the targets were partially obscured by superimposed opaque masks. Unlike Experiments 2.1-2.6, targets were displayed for 0.66s (50 video frames) in each trial. Target duration was extended to increase the number of occasions on which uncertainty was introduced. The procedure otherwise matched the previous experiments in this chapter.

4.9.2: Results

Figure 35 presents resolution thresholds for static targets, targets moving along an unchanging sinusoidal path, and targets moving along a path with unpredictable changes in direction and velocity.

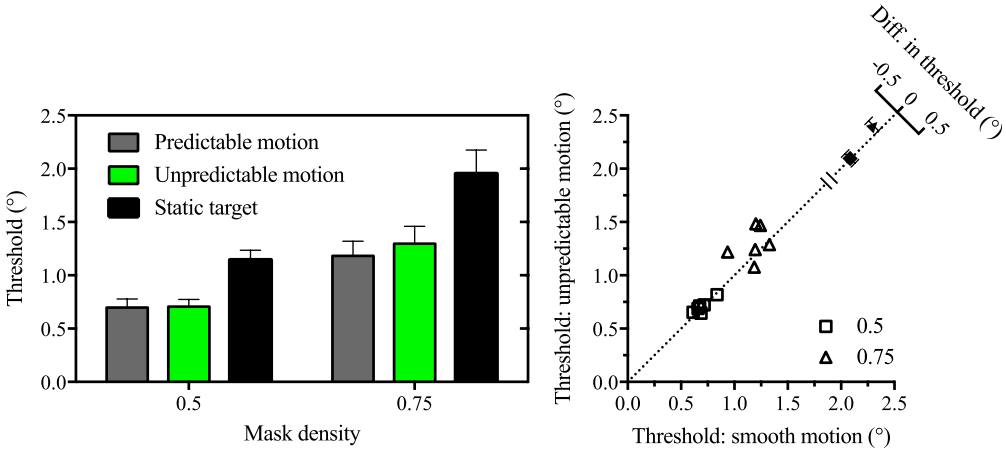

Figure 35: Resolution thresholds for static targets, and targets with predictable or unpredictable sinusoidal motion paths. Left, the mean between-subjects resolution thresholds for static targets (black), targets moving along an unchanging path (grey), and targets moving along an unpredictable path (green). Right, relative performance between predictable and unpredictable motion conditions is compared for individual observers (open symbols), and the group mean difference in threshold between conditions is plotted on the oblique axis. Error bars indicate between-subjects 95%CI.

Figure 35 indicates a large decrease in resolution thresholds for moving targets, compared to the static condition, similar to data presented in Figure 27. Resolution thresholds for static targets were not included in the analysis. A comparison of the predictable and unpredictable motion conditions was performed using a two-way, repeated measures ANOVA. The results indicated that increasing the mask density raised resolution thresholds ($F(1,5)=300.8$, $p<.0001$). However, no effect on performance due to motion predictability was identified ($F(1,5)=2.42$, $p>.05$), and no interaction was indicated ($F(1,5)=2.82$, $p>.05$).

Varying the spatial frequency of the sinusoidal variation affects the speed of the target. To ensure the target speed had no significant effect on resolution thresholds, the data from the predictable motion condition were decomposed according to the frequency of the sinusoid (*F*). For a detailed description of the procedure for this analysis technique, see the general methods chapter. A comparison of resolution thresholds for each of the sinusoid frequencies is shown for both mask densities in Figure 36.

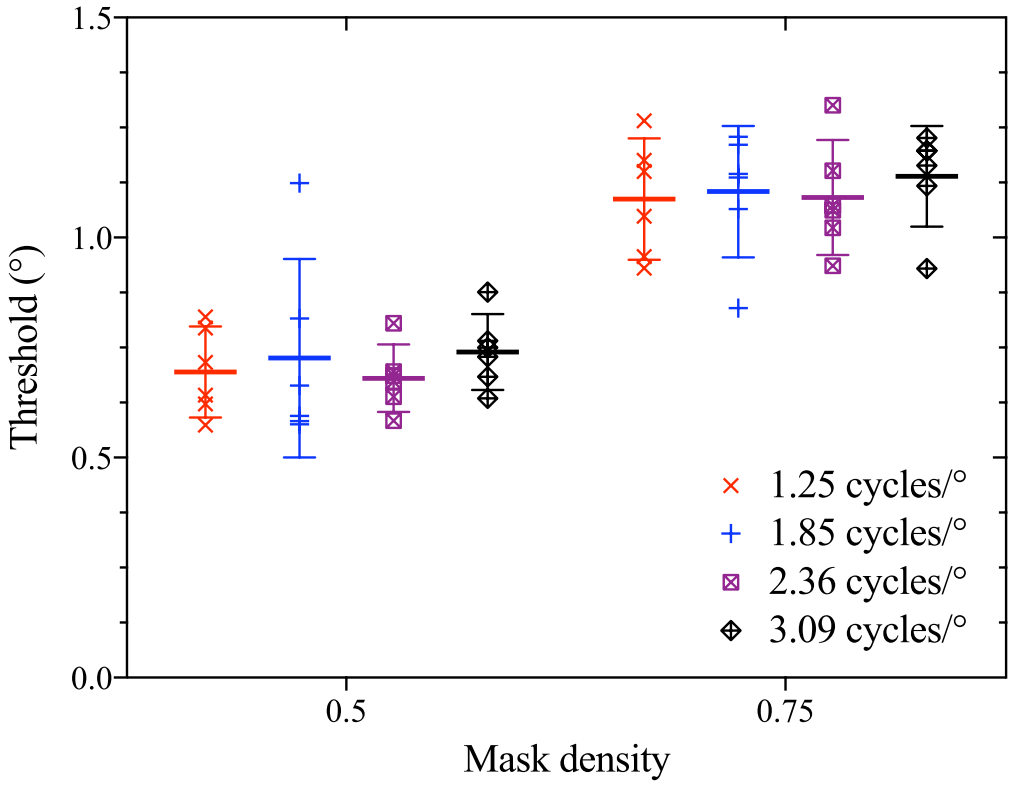

Figure 36: Resolution thresholds for targets traversing predictable sinusoidal trajectories, decomposed according to the sinusoid frequency (*F*). Individual points are thresholds for each observer; solid horizontal lines indicate the mean, and error bars indicate 95%CI.

Figure 36 shows clear separation of resolution thresholds according to mask density, but little variation between sinusoid frequencies. This is supported by a two-way, repeated measures ANOVA, which indicated that there was a significant difference between mask densities ($F(1,5)=148.8$, $p<.0001$), but no significant effect of sinusoid frequency ($F(3,15)=0.63$, $p>.05$). No significant interaction effect was reported ($F(3,15)=0.07$, $p>.05$). Thus, any effects of motion path unpredictability was not influenced by the sinusoid frequencies at which the target was presented throughout the trial. Additionally, that there was no significant difference between target resolution for all the tested sinusoid frequencies justifies analysing the predictable path thresholds together, regardless of frequency, as in Figure 35.

4.10: General discussion

In this chapter, the characteristics of a super-resolution mechanism in the human periphery were investigated. Experiment 2.1 showed a statistically significant improvement in resolution thresholds for moving targets compared to static targets, behind static, opaque masks. This observation is consistent with a system that summates visual signals over time. This is in agreement with previous foveal studies of dynamic occlusion (Mateeff et al., 1993; Palmer et al., 2006; Shipley & Cunningham, 2001; Stevenson, Cormack, & Schor, 1989), and is a direct extension of Frisén's (2010) results from the fovea into the periphery.

While these benefits are consistent with the operation of a SR mechanism that integrates target information across space and time, it is important to note that when a target moves behind a static mask, more independent samples of the target are available in the stimulus sequence. Experiment 2.2 therefore examined whether resolution is improved by providing extra samples of the target, without additional target motion. Resolution thresholds were lower for targets behind masks with updating element locations than targets behind static masks. This indicates temporal information summation is possible without spatial displacement. Accordingly, at least some of the effect of motion in Experiment 2.1, and the foveal demonstration in Frisén (2010) may be explained by the additional information conveyed in motion sequences, without the need for any dedicated SR mechanism that synthesises samples over space and time. However, the updating mask has no analogous biological function (the retinal mosaic cannot change in a similar manner), so for the principles of SR to be beneficial to patients with NRMD, a spatial displacement is necessary. Target motion across the retina,

or movement of the retinal array, may provide extra spatial information by displaying the target in multiple locations.

Experiment 2.3 examined the effect of motion while the extent of visible target information was controlled. A significant residual motion-related benefit remained, which suggests a peripheral SR mechanism contains a motion-sensitive component. Although the motion-related benefit is dominated by the amount of information content available, such a mechanism can evidently enhance visual capabilities in undersampled conditions. However, there was no significant motion-based improvement for unmasked targets in Experiment 2.1. Thus, the natural retinal sparseness at 10° in the (healthy) nasal periphery causes insufficient undersampling for a SR mechanism to operate. This replicates and extends the results from Experiment 1.1 to include a target speed of $2°s^{-1}$. Alternatively, the natural drift of the image across the retinal surface due to fixational eye movements may mediate performance for unmasked stimuli by providing the necessary spatial variability (Martinez-Conde, 2006a; Martinez-Conde et al., 2004).

Experiment 2.3 thus supports a motion-sensitive component within the peripheral SR mechanism. Experiments 2.4-2.7 investigated the characteristics of the motion-sensitive component. Shipley and Cunningham (2001) predict that having an image stable on the retina (at least at the fovea) should not affect performance when dynamically occluded, i.e. integration should be possible for an object being tracked or static at fixation. Conversely, Experiment 2.4 suggests performance is enhanced by a mechanism that is sensitive to the source of the motion. Resolution thresholds were significantly higher when the source of motion was the mask

rather than the target. This is consistent with a model of SR containing a dedicated motion-sensitive component, which is disrupted in the mask motion condition. Furthermore, when disrupting this component in Experiment 2.5 by disordering the trajectory of the target, resolution thresholds were significantly impaired. Similarly, when Mateeff et al. (1993) asked observers to rate the quality of an image with dynamically occluded smooth or unpredictable motion, they found a significant preference when the image moved smoothly. Nishida (2004) also demonstrated that letter identification was hindered by interrupting smooth target motion. Experiment 2.5 extends these findings further into the periphery. The failure of the visual system to account for the unpredictable motion may stem from the limits of the receptive field of the velocity-orientated motion detector that Fahle and Poggio (1981) suggested is responsible for SI. By randomising the motion sequence, the average spatial offset between successive target presentations is increased, which Morgan and Watt (1983) proposed causes decline in the efficiency of SI. Since SR is reliant upon effective SI, the SR mechanism is therefore also affected.

Experiment 2.6 further supports the motion-sensitive component within the SR mechanism. As suggested by Experiment 2.4, this component is hindered when the source of motion does not originate in the object critical to the task. In Experiment 2.6, target resolution thresholds were compared for static targets behind masks that were either moving smoothly or unpredictably. It was shown that thresholds were improved when the mask trajectory was disordered. This may be explained by the motion-sensitive component no longer being diverted by the mask in the disordered mask motion condition.

Randomising the order in which the target appears (as described in Figure 31) creates unpredictability at the cost of smooth target motion. In Experiment 2.7, a sinusoidal motion path with unpredictable changes in target speed and direction was used to examine whether the motion-sensitive component is disrupted by these unpredictable changes, or whether it is capable of tracking targets as they progress along their trajectory so long as the motion is smooth. The unpredictability was not sufficient to significantly disrupt resolution, suggesting that the motion-sensitive component may operate within very short time-scales (between 8 and 19 video frames, or 106.4 to 252.7ms), such that it has facilitated resolution within one half cycle, while the trajectory is predictable. Alternatively, the component can adapt very quickly to the new trajectory, such that changes in trajectory or direction provide minimal disturbance to the whole integration procedure.

The unpredictable paths in Experiments 2.4 and 2.7 both alter the target speed across the trial. Increased target speed is known to reduce resolution (e.g. Brown, 1972b), thus the inflated inter-frame target speed may be impeding resolution. This could be tested using an alternative motion trajectory. For example, setting the target location on each video frame as a predetermined distance from the location of the target on the previous frame, with the direction along the trajectory being reallocated at random on each frame. Fixing the inter-frame distance controls for changes in target speed, while maintaining an unpredictable path. Such a trajectory also reduces the duration for which the target path is predictable compared to Experiment 2.7.

The finding that motion can improve peripheral performance suggests that the periphery is capable of processing images using SR. The unpredictable motion provided by fixational eye movements may not be sufficient to improve performance, as smooth motion has been shown to be more effective. Adding small, predictable motion sequences to peripheral targets such as words may however improve reading ability in patients with neuroretinal matrix disorders. Relative performance is consistent across the two mask densities, suggesting that such a technique could be used in patients across range of vision loss severity.

The experiments in this chapter have demonstrated that the human periphery can summate over space and time to develop a more robust image from which it can extract crucial spatial details. Further, both the additional spatial target information that provided by target motion, and the motion itself, were shown to contribute to effective SR. Investigating the characteristics of a motion-sensitive component within the SR mechanism has shown that SR is most effective when the source of motion is the target and not the overlying mask, and when the motion is smooth and predictable, whereby SI is most effective (Hogendoorn et al., 2008). These results support Palmer et al. (2006) and Frisén (2010). Since the descriptions of the SI mechanisms by Fahle and Poggio (1981), and by Kandil and Lappe (2007) both involve a motion-sensitive component, the evidence of such a component reported in this chapter is complicit with both descriptions of SI.

This chapter has shown that smooth, predictable motion can improve resolution of the critical detail in peripheral acuity tasks in conditions of spatial undersampling. This may have applications in optimising the remaining visual function of patients with some forms of NRMD, such as cone-rod dystrophy (Rabb et al., 1986).

Chapter 5: Improving visibility of targets with smooth object motion

5.1: Introduction

Patients with central vision loss are forced to perform high acuity tasks in the peripheral visual field. As Chapter 3 and existing literature (e.g. Brown, 1972a, 1972b; Legge et al., 2008; Westheimer, 1982) illustrate, this is suboptimal for visual performance. Chapter 3 further demonstrated performance gets progressively poorer as the speed of smooth target motion increases. Peripheral targets are often dynamic, either due to ocular motion, vection, or motion of the object itself (Westheimer & McKee, 1975). The previous chapter indicated that the peripheral retina at 10° eccentricity is insufficiently sparse for super-resolution mechanisms to operate efficiently, thus preventing motion alone from enhancing visual performance. As such, it is important to investigate characteristics of peripheral targets that have the potential to alleviate this degradation.

There are several possible explanations for the detrimental effect of motion. A perceptual blurring, referred to as motion smear (Burr, 1980), is often attributed to temporal summation of the target across retinal loci (Hammett, 1997; Hammett et al., 1998), with the suggestion that active deblurring mechanisms are insufficient when not tracking the object. Alternatively, loss of performance with increasing speed is attributed to a loss of sensitivity to high spatial frequencies, which are responsible for the target attributes important in acuity (Burr & Ross, 1982; Burr et al., 1986a).

Adding temporal modulations to visual targets creates extra harmonics in the Fourier domain (Van Santen & Sperling, 1985; Watson & Ahumada, 2005; Watson et al., 1986). Manipulating the stimuli to exploit such characteristics may extend their frequency range, presenting extra information about the target to be available at frequencies to which the observer may be sensitive. Temporal modulations have been shown to improve visual performance under certain conditions. Adelstein, Kaiser, Beutter, McCann, and Anderson (2013) examined reading ability in observers experiencing vibration. By temporally subsampling the display at a rate matching the vibration frequency, the error rate in reading the display was decreased compared to the unmodulated presentation. Further, Bauer and Cavonius (1980) assessed character recognition accuracy when rapidly switching viewing between separate displays. They demonstrated that the number of errors was reduced by presenting the different displays at opposing contrast polarities.

In this chapter, we investigate target manipulations to establish conditions for improving the visibility of a moving peripheral target. First, the effect of removing motion smear by presenting the target at the same locations, but not in a sequential order is investigated. Then, the effects of adding additional temporal characteristics to the target are assessed.

Impaired performance for resolution of moving targets is often attributed to motion smear (Burr, 1980; Hammett, 1997; Hammett et al., 1998). Randomising the motion sequence interferes with the summation procedure by increasing the average gap between successive target locations, which Morgan and Watt (1983) suggest results in a reduction in the efficiency of spatiotemporal interpolation.

Also, randomising the sequence introduces changes in the direction of apparent target motion. By interfering with the summation procedure, Experiment 3.1 investigates the extent of the effect of motion smear on resolution for moving targets. By reducing motion smear, it may be possible to improve the resolution of moving targets. In order to improve peripheral acuity for both static and moving targets, the effect of adding temporal modulations to the target is then examined.

The effect of subsampling the target is examined in Experiment 3.2 by increasing the spatial and temporal interval between stimulus presentations. This procedure provides the extra temporal modulations, but at the cost of reducing the overall time-averaged contrast of the trial. Therefore in Experiment 3.3 the effect of reversing the contrast polarity of the target is investigated. This manipulation preserves the absolute target contrast.

It is hypothesised that by reducing motion smear, the threshold target size for accurate resolution can be reduced for moving targets. Further, by adding temporal modulations to the target, it is expected that resolution thresholds can be improved across a range of target speeds.

5.2: General methods

In this chapter, the effects of manipulations to the trajectory on resolution thresholds for static and moving peripheral targets were investigated. Thresholds were calculated using a monocular orientation discrimination task. The threshold Landolt ring size required for 79% correct orientation identification was estimated for each condition by the combined analysis of five staircase procedures for each participant, as outlined in the General Methods chapter (Chapter 2).

The Landolt ring targets in these experiments was fixed at 10° eccentricity for all conditions. The target appeared either statically or travelling at one of five speeds, up to 20°s^{-1} (evenly spaced logarithmically), along an isoeccentric arc for 25 video frames (332.5ms). The target appeared in the temporal or nasal peripheral visual field, and travelled from above to below the horizontal meridian or the reverse.

5.3: Examining the effect of motion smear (Experiment 3.1)

5.3.1: Methods

To investigate the importance of sequential or predictable motion to the resolution of moving objects, the effect of random object motion was examined. Resolution thresholds were calculated and compared for Landolt rings traversing a smooth path and an unpredictable (random) path. Target coordinates between the smooth and random motion conditions were identical, but the order in which the target was presented at the coordinates was randomised at the start of each trial in the random motion condition. Example target trajectories from the two motion conditions are represented in Figure 37.

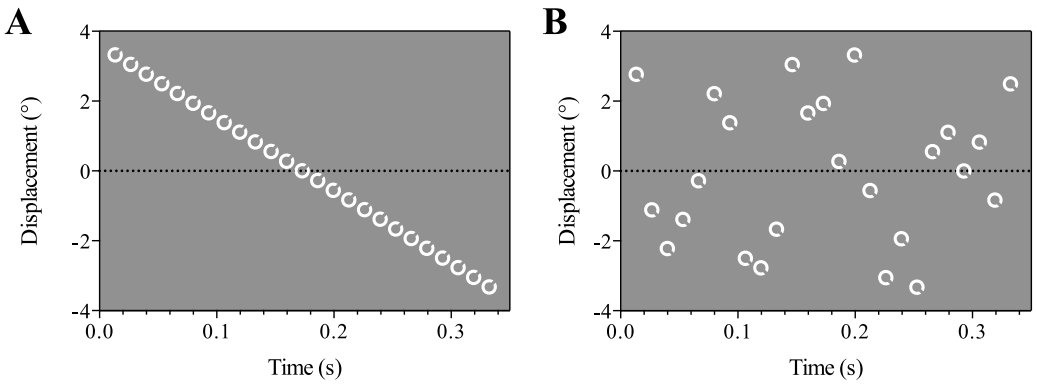

Figure 37: Space-time plots of the different conditions in Experiment 3.1 for a target speed of 20°s^{-1}. (A) showing target progression with smooth motion. (B) with randomised path order. The targets in the randomised condition visit the same locations, but in an unpredictable order.

Six smooth motion target speeds between 0-20°s^{-1} and corresponding random motion conditions were examined. For each trial, the target orientation and the visual field in which it appears (temporal or nasal) was randomly allocated. For the smooth motion condition, the target direction (superior to inferior, or the reverse) was also allocated at random, and for the random motion condition the target coordinates for each video frame were randomised prior to trial onset.

5.3.2: Actual target speed

Randomising the order of the target coordinates stimulates an identical retinal surface area, but shifts the actual target speed between frames from a constant (given by the condition) to a distribution, the minimum value of which is the corresponding smooth motion speed. This distribution is discrete, as for each target coordinate there is a fixed, finite number of possible target coordinates for the following video frame. An example of this distribution is shown in Figure 38.

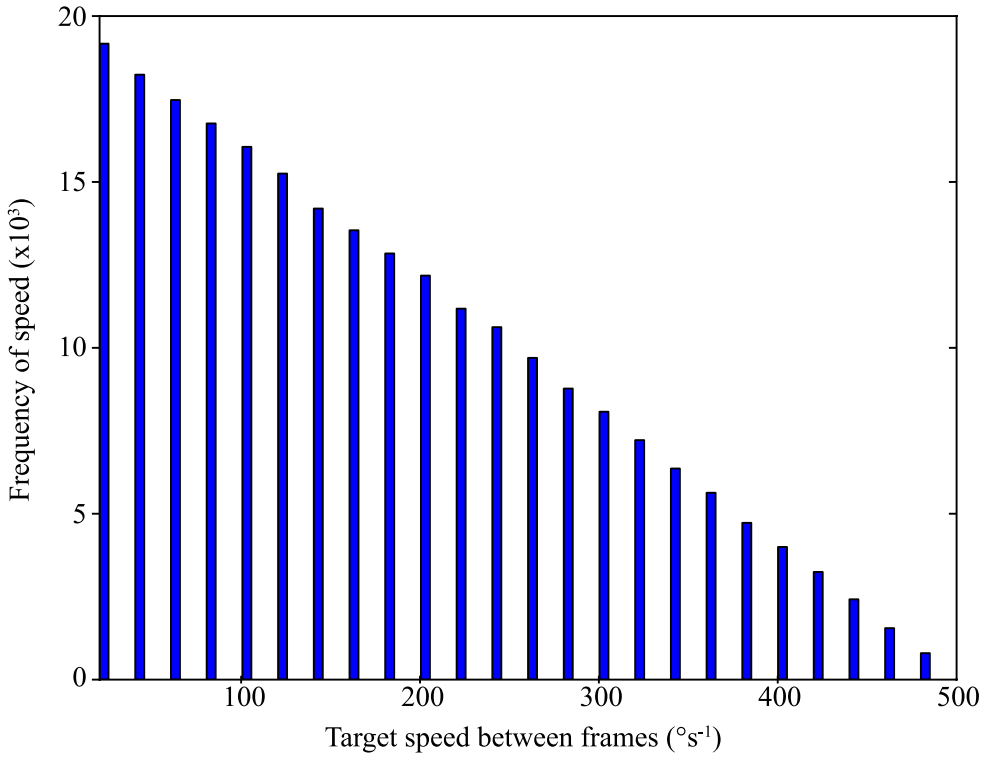

Figure 38: Histogram showing the target speeds between successive frames in the random motion condition. The corresponding smooth motion target speed in this example is 20°s^{-1}. Target speeds were calculated as the quotient of the distance between successive target presentations and the frame duration of 13.3ms, across 10000 simulated trials (240000 different motion instances).

For each random motion condition, the modal target speed was at the distribution minimum, and therefore the corresponding smooth motion speed. This is because in the smooth motion condition, the target proceeds to the closest step along the trajectory, i.e. it does not skip points along the motion path. The median target speed for each random motion condition is represented in Table 1. Median speeds were estimated using 10000 simulated iterations of randomised target sequences.

Table 1: Actual target speeds for the random motion conditions in relation to the corresponding smooth motion target speeds.

Corresponding smooth motion target speed ($°s^{-1}$)	Median actual target speed ($°s^{-1}$)	Inter-quartile range ($°s^{-1}$)
0	0	0
1.25	10.42	11.72
2.5	20.83	23.44
5	41.67	46.86
10	83.33	93.75
20	166.67	187.50

For both conditions, the targets were presented for 0.33ms (25 video frames), with a new position on each screen refresh (every 13.3ms). Although the paradigm for the smooth motion condition matches the 10° eccentricity condition in Experiment 1.1, the data were recollected.

Nine participants (mean age 24.00 years, *SD* 2.74 years) with normal or corrected-to-normal vision participated in this experiment.

5.3.3: Results

The effect of randomising the sequence of steps along the motion path on resolution threshold was investigated for the range of smooth motion speeds from 0-20°s^{-1}. The results are shown in Figure 39.

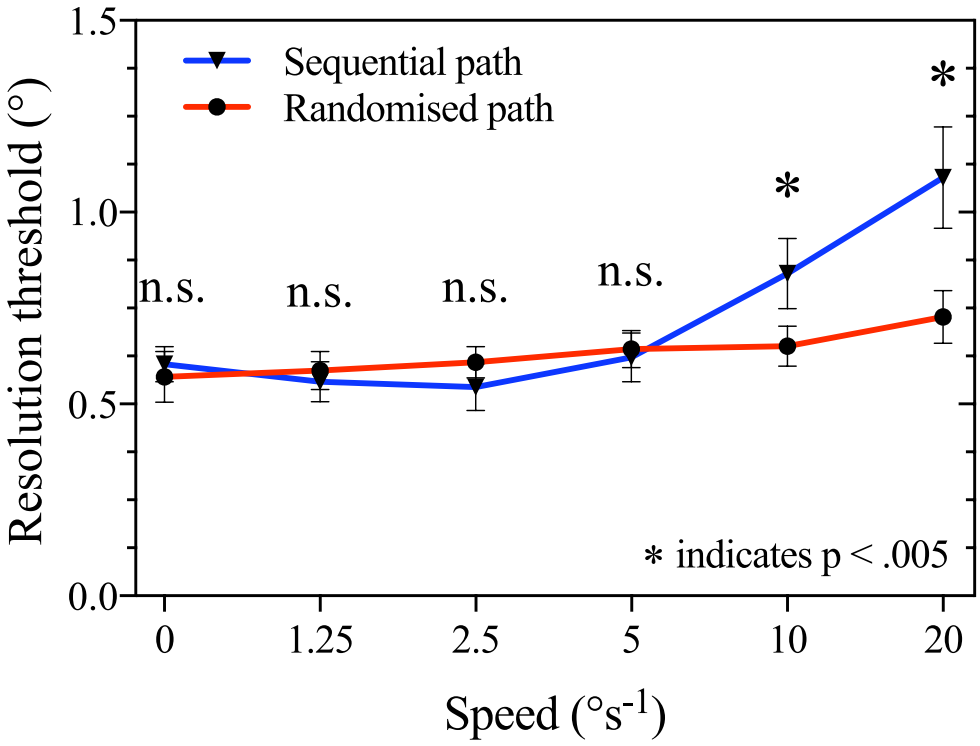

Figure 39: Effect of motion path sequence on resolution thresholds. Peripheral targets either followed a smooth trajectory along an isoeccentric arc (sequential path), or were presented at the same locations in an unpredictable order (randomised path), such that subsequent target coordinates were not necessarily the closest possible location to the preceding coordinates. See text for detailed explanation. Data points indicate the mean resolution threshold between subjects, and error bars show the between-subjects 95%CI.

Figure 39 suggests that the loss of sensitivity to targets at speeds above 5°s^{-1} for smooth motion is negated by disordering the motion sequence. As in Chapter 3, slow target speeds in the smooth motion condition demonstrate a slight reduction in resolution thresholds, followed by a sharp rise above speeds of 5°s^{-1}. For the randomised path, these effects are replaced by a more gentle rise in resolution thresholds. While the increase in resolution threshold between static and the fastest moving targets (20°s^{-1}) for the smooth motion condition was 0.486° (*SE* 0.051°), an increase of 80.3%, thresholds in the randomised path condition rose only by 0.156° (*SE* 0.034°) or 27.4%. The statistical difference between the two

conditions was assessed using the Holm-Sidak method for multiple t-tests (one per speed). Each speed was analysed individually, without assuming homoscedasticity, and adjusted for multiple comparisons. No significant difference was found between smooth (sequential) and randomised for target speeds of 0-5°s^{-1} (0°s^{-1}: $t(16)=0.96$, $p>.05$; 1.25°s^{-1}: $t(16)=0.96$, $p>.05$; 2.5°s^{-1}: $t(16)=2.01$, $p>.05$; 5°s^{-1}: $t(16)=0.60$, $p>.05$). However, at higher speeds thresholds for smooth object motion rose progressively higher than randomised path thresholds (10°s^{-1}: $t(16)=4.15$, $p=.0038$; 20°s^{-1}: $t(16)=5.59$, $p=.0002$).

5.3.4: Discussion

By randomising the order of the motion path, resolution thresholds were protected from the deterioration in performance associated with increased target speeds in smooth motion. By interfering with the order of appearance across the motion path, the likelihood of temporally consecutive targets spatially overlapping is reduced. This may reduce motion smear by reducing temporal summation of target information in the region of the critical detail; the chance of the gap in the Landolt ring being covered by an overlapping portion of the target on subsequent video frames, close enough in time for the luminance difference in the critical detail to be at risk of being averaged out, is reduced. Due to uncertainty in the actual target speed, it is difficult to comment on how spatial frequency sensitivity may be changing in this condition. However, the actual speed is far higher than the corresponding smooth motion speed, so a corresponding reduction in sensitivity to higher spatial frequencies may be expected, yet resolution thresholds did not diminish (as would be expected from a shift away from higher spatial

frequencies). Thus, spatial frequency sensitivity with jittering targets does not appear to behave in the same way as with smooth motion.

Experiment 2.5 indicated that, at the speed examined ($2°s^{-1}$), resolution thresholds were significantly lower for partially occluded targets with smooth motion than for a randomised trajectory. The discrepancy between this and the results of this experiment indicate that different mechanisms are supporting resolution when the target is occluded to when it is not. The super-resolution mechanism that is considered to be driving performance in the dynamic occlusion experiments in Chapter 4 contains a component sensitive to smooth motion. While this mechanism may be in operation without spatial undersampling (as in this experiment), occlusion enhances the spatial range of the motion-sensitive component (Scherzer & Ekroll, 2012).

Resilience to target jitter is indicative of a mechanism designed to counteract the effects of irregular motion, perhaps from fixational eye movements. This is in alignment with previous research. For example, Badcock and Wong (1990) demonstrated that Vernier acuity is unaffected by large amounts of positional jitter, which is in contrast to the detrimental effect smooth motion has on Vernier acuity (Fahle & Poggio, 1981; Wertheimer, 1912). Additionally, Falkenberg, Rubin, and Bex (2007) demonstrated that letter acuity is stable to target jitter. Presenting the targets in such a way to eliminate motion smear has eliminated the detrimental effect of increasing smooth object motion on resolution thresholds. However as predicted, performance for static and slow targets is largely unaffected.

5.4: Examining the effect of temporal subsampling on resolution (Experiment 3.2)

5.4.1: Methods

Removing motion smear has been shown to reduce speed-related acuity loss in the periphery. While improving performance for specific circumstances is important to optimise usage of the remaining visual field in patients with central vision loss, a technique that enhances spatial vision for static and moving targets would have more practical applications. Therefore, Experiment 3.2 investigates a procedure that both reduces motion blur and provides additional temporal harmonics in order to enhance performance for static and slowly-moving targets as well as preserving spatial vision at higher speeds.

The effect of subsampling the motion path on resolution thresholds is investigated in Experiment 3.2.1. Subsampling is a procedure whereby the target is presented with interspersed blank frames.

The target appeared at one of five different subsampling rates. In the smoothest (least subsampled) condition the target appeared on every video frame across the trial. As sample rate decreased, the number of frames on which the target appeared was reduced, to every sixth video frame in the most subsampled condition. Figure 40 shows space-time plots of the extreme conditions, from which it can be seen that the target travels across the same retinal distance in the same length of time, differing only in number of samples presented.

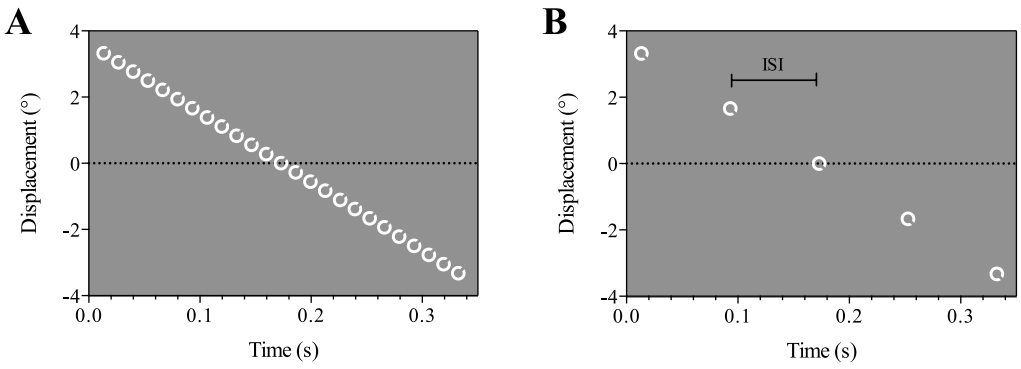

Figure 40: Space-time plots showing the different sampling conditions in Experiment 3.2. The ordinate value is the screen distance of the target from a point on the horizontal meridian, 10° from fixation. Targets travelled along isoeccentric trajectories. The examples in this figure are at the maximum speed of $20°s^{-1}$. (A) the least subsampled condition (unmodulated, 0ms ISI); the target was displayed on every video frame. (B) the most subsampled condition (66.7ms ISI); the target was displayed only on every sixth video frame.

Eight observers (mean age 22.75 years, *SD* 2.31 years) with normal or corrected-to-normal vision participated in Experiment 3.2.1.

One side effect of temporal subsampling is a reduction in the time-averaged contrast of the trial in the more subsampled conditions. Therefore, in Experiment 3.2.2, this is controlled. The contrast of the target was reduced in less subsampled conditions, such that the time-averaged contrast of the trial was equated across conditions. This is shown in Figure 41.

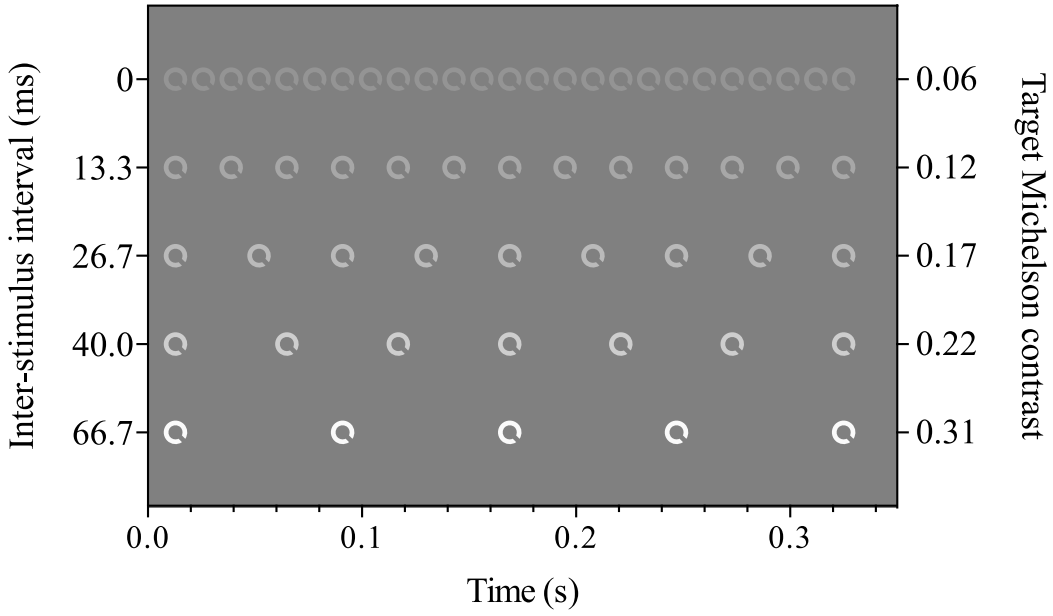

Figure 41: Graphical depiction of the contrast modulation in Experiment 3.2.2. The least subsampled condition (0ms ISI, in which the target is shown on every video frame) is presented at a lower contrast than the more subsampled conditions, such that the time-averaged Michelson contrast is equated between subsampling conditions.

The targets were presented at the luminance required for the Michelson contrast for that condition, as shown in Figure 41. The background was mid-grey (44.8cdm^{-2}). The luminance of the target in the 0ms ISI condition was 50.6cdm^{-2}. In the 13.3ms ISI condition, the luminance was 56.8cdm^{-2}. In the 26.7ms ISI condition, it was 63.4cdm^{-2}; in the 40.0ms ISI condition, it was 70.3cdm^{-2}; and in the 66.7ms ISI condition, it was 85.0cdm^{-2}. Four observers (mean age 24.50 years, *SD* 1.91 years) participated in Experiment 3.2.2.

5.4.2: Results

Figure 42 shows the results of Experiment 3.2.1, showing the effect of subsampling the motion trajectory on resolution threshold. All of the targets in

Experiment 3.2.1 were shown at maximum luminance (85.0cdm^{-2}) on a mid-grey background (44.8cdm^{-2}) throughout the trial.

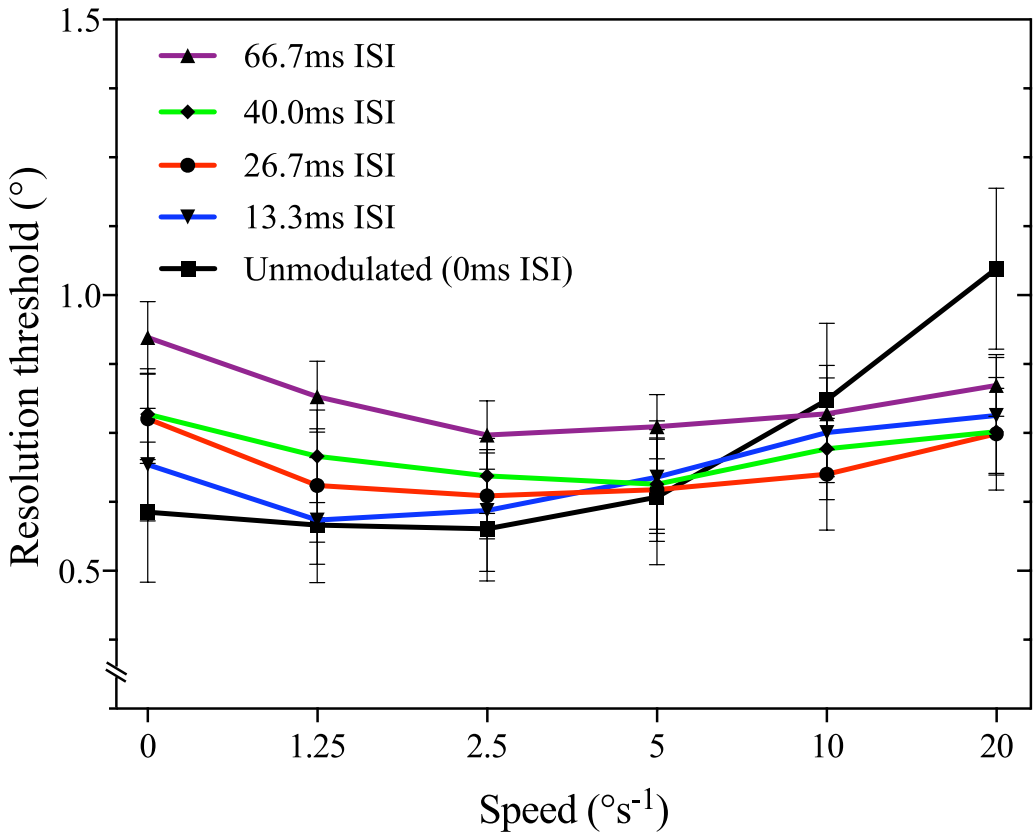

Figure 42: Graph of the results of Experiment 3.2.1, showing threshold target size as a function of target speed across a range of subsampling conditions. Data points show the mean resolution threshold, and error bars show the between-subjects 95%CI.

The data presented in Figure 42 shows that resolution thresholds for static targets rise as the ISI is increased. However for subsampled stimuli, the detrimental effect of increasing target speed, that is observed in the 0ms ISI condition (as well as in Chapter 3), is drastically reduced. At speeds above 5°s^{-1} thresholds are lower for subsampled targets than targets that are presented on every video frame. In contrast, when the targets are static, subsampling has the opposite effect. As samples are removed, resolution thresholds steadily increase. This is most likely explained by changes in the time-averaged contrast across sampling conditions.

Subsampling in this manner has the side effect of reducing the time-averaged contrast of the stimulus, which may be driving the detrimental effect of subsampling for low speeds. This is investigated in Experiment 3.2.2 by repeating the experimental paradigm with stimulus modulated to equate the time-averaged contrast across all conditions.

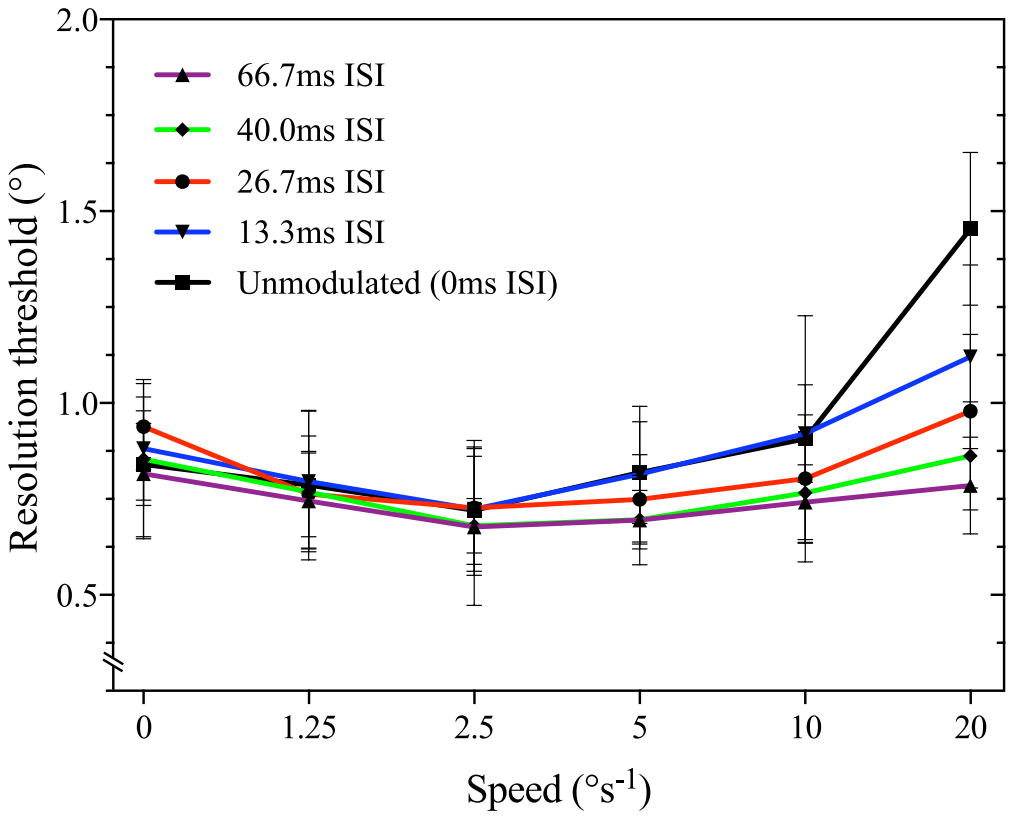

Figure 43: Graph of Experiment 3.2.2, showing resolution thresholds for subsampled stimuli, with contrast modulated to be equal across each trial (see Figure 41). Data points show the mean resolution threshold of all subjects, and error bars indicate the between-subjects 95%CI.

When stimulus contrast is time-averaged, thresholds converge for static and low speeds, as seen in Figure 43. Although equating the time-averaged contrast removes the detrimental effect for static and slowly moving targets, the preservation of thresholds for sampled stimuli at higher speeds is still present. The

detrimental effect of increasing speed remains for the 0ms condition (presented on every video frame), for the largest ISI thresholds are essentially invariant of speed.

5.4.3: Discussion

In Experiment 3.2.1, subsampling the stimulus reduced the speed-related impairment in resolution thresholds seen in the 0ms ISI condition (without additional temporal modulation). However, thresholds for subsampled targets were increasingly higher at low speeds as sampling rate was decreased. The detrimental effect of subsampling seen at low speeds is eliminated by equating stimulus contrast energy in Experiment 3.2.2. The order of most to least beneficial subsampling rates at higher speeds differs between Figure 42 (Experiment 3.2.1) and Figure 43 (Experiment 3.2.2). For contrast-equated stimuli, the most subsampled condition (66.7ms ISI) is the optimum condition, whereas for targets at maximum luminance the 26.7ms ISI condition provided lowest resolution thresholds. This indicates a trade-off between the beneficial effect of subsampling and the detrimental effect of reducing contrast energy, which is optimum at 0ms ISI for static targets and 26.7ms ISI for moving targets.

Controlling for the loss of contrast (Experiment 3.2.2) mediates the associated loss of performance, resulting in similar performance between conditions at low speeds. The reduction in the detrimental effect of smooth target motion is maintained, however; at higher speeds, the increase in resolution thresholds is progressively reduced as the ISI increases.

The results of Experiment 3.2.1 aligns with the description of motion smear (Burr, 1980). By increasing the spatial distance between consecutive presentations of the target, the spatial overlap is reduced. Thus, the rise in resolution thresholds as target speed increases is restricted. Further, it was hypothesised that the additional temporal harmonics that periodic temporal modulations create in the Fourier domain (Van Santen & Sperling, 1985) would provide extra stimulus information at frequencies to which the visual system is sensitive. In turn, it was expected that this would improve resolution of static and slowly moving targets. However, this is not observed. The reduction in the time-averaged stimulus contrast limits the potential benefit from the additional information provided by the temporal modulations. Reducing target luminance reduces sensitivity to high spatial and temporal frequencies (de Lange, 1958; Rabin, 1994). Thus, sensitivity to the additional temporal harmonics may be restricted for subsampled stimuli.

5.5: Examining the effect of reversing target contrast polarity on resolution (Experiment 3.3)

Experiment 3.2 demonstrated that subsampling the target reduces the speed-related rise in resolution thresholds seen in smooth object motion. As in Experiment 3.1, this may be attributed to a reduction in motion blur. However, this is at the cost of performance at low target speeds. The increasing rise in thresholds at lower speeds is attributable to the reduction in the time-averaged contrast of the trial, as demonstrated in Experiment 3.2.2. Accordingly, in Experiment 3.3 the effect of reversing the contrast polarity of the target on resolution thresholds is investigated. This manipulation provides additional

temporal modulations without reducing the absolute time-averaged contrast of the stimulus.

5.5.1: Methods

In Experiment 3.3.1, the contrast polarity of the target was reversed from black ($0.5cdm^{-2}$) to white ($85.0cdm^{-2}$) or the reverse on the mid-grey background. Target polarity was reversed after periods ranging from 13.3ms to 173.3ms (alternating on each video frame, to staying the same luminance polarity for 13 sequential frames), alongside a control condition with no reversal. In Experiment 3.2.1 the maximum contrast difference is between the target and background, while polarity reversal doubles the effective contrast of the stimulus. Thus, similarly to Experiment 3.2.2, in Experiment 3.3.2 the target contrast was equated between conditions. Targets in Experiment 3.3.2 were reversed between $63.72cdm^{-2}$ and $21.22cdm^{-2}$. Michelson contrast for Experiment 3.3.1 and 3.3.2 were therefore 0.99 and 0.50, respectively. Example stimulus sequences for targets in Experiments 3.3.1 and 3.3.2 are shown in Figure 44.

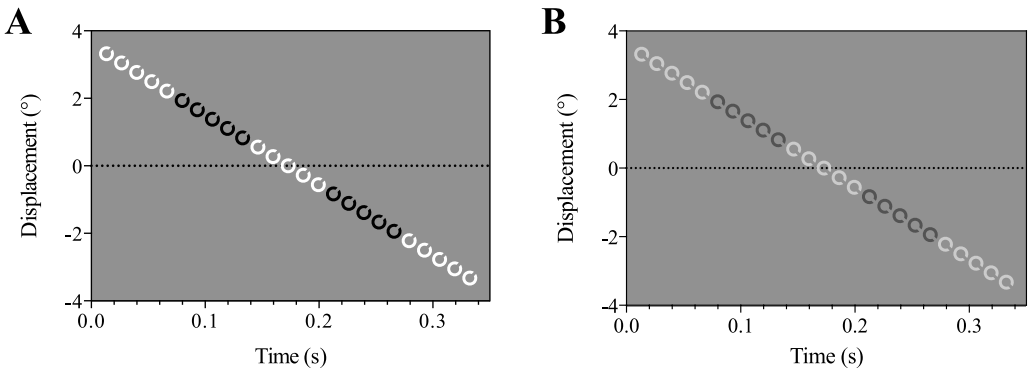

Figure 44: Space-time plots showing examples of the conditions in Experiment 3.3 for a contrast polarity reversal period of 66.7ms (reversal on every sixth video frame). (A) Stimulus progression in Experiment 3.3.1, in which targets reverse between the maximum and minimum luminance values (85.0cdm^{-2} and 0.5cdm^{-2}, respectively). (B) Stimulus progression in Experiment 3.3.2, in which target contrast is halved (target luminances 63.72cdm^{-2} and 21.22cdm^{-2}).

Resolution thresholds for target speeds between 0-20°s^{-1} were compared across a set of seven different reversal periods. Targets were presented on every video frame across the trial duration of 0.33s (25 video frames), moving along isoeccentric arcs at 10° in the temporal or nasal visual fields. Eight participants (mean age 24.00 years, *SD* 2.93 years) with normal or corrected-to-normal vision participated in Experiment 3.3.

5.5.2: Results

Figure 45 shows the effect of contrast polarity reversal on resolution.

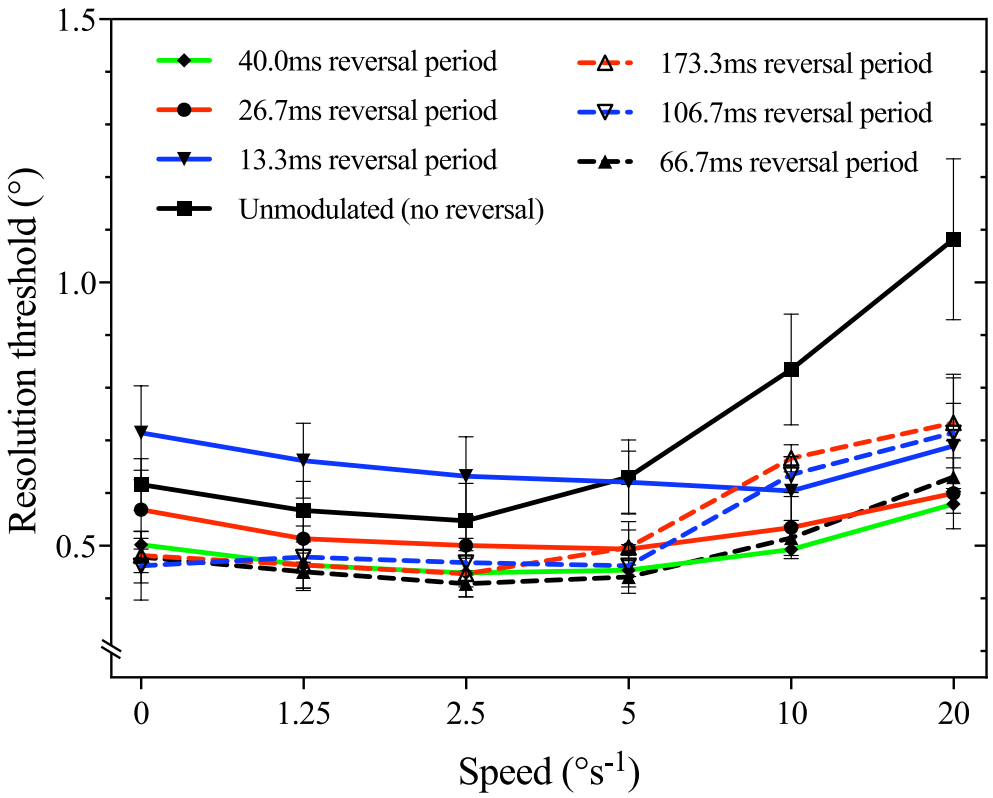

Figure 45: Graph of Experiment 3.3.1, showing the effect of reversing contrast polarity of the target at a range of intervals on resolution thresholds for static and moving targets. Contrast polarity reversal in Experiment 3.3.1 utilised the maximum possible range of target luminance. Data points indicate the between-subjects mean resolution thresholds, and error bars show between-subjects 95%CI.

The effect of contrast polarity reversal on resolution thresholds at low speeds is very similar for a wide range of reversal rates. Figure 45 suggests that the optimum reversal rate at low target speeds is between 65.7-106.7ms reversal (reversal after every five to every eight video frames).

Figure 46 shows the results of Experiment 3.3.2, investigating the effect of target contrast in contrast polarity reversal by comparing resolution thresholds for targets reversing contrast polarity between a luminance of 0.5cdm^{-2} (black) to 85.0cdm^{-2} (white) against targets reversing between 63.72cdm^{-2} (light grey) and

21.22cdm^{-2} (dark grey). The Michelson contrasts were therefore 0.99 and 0.50, respectively.

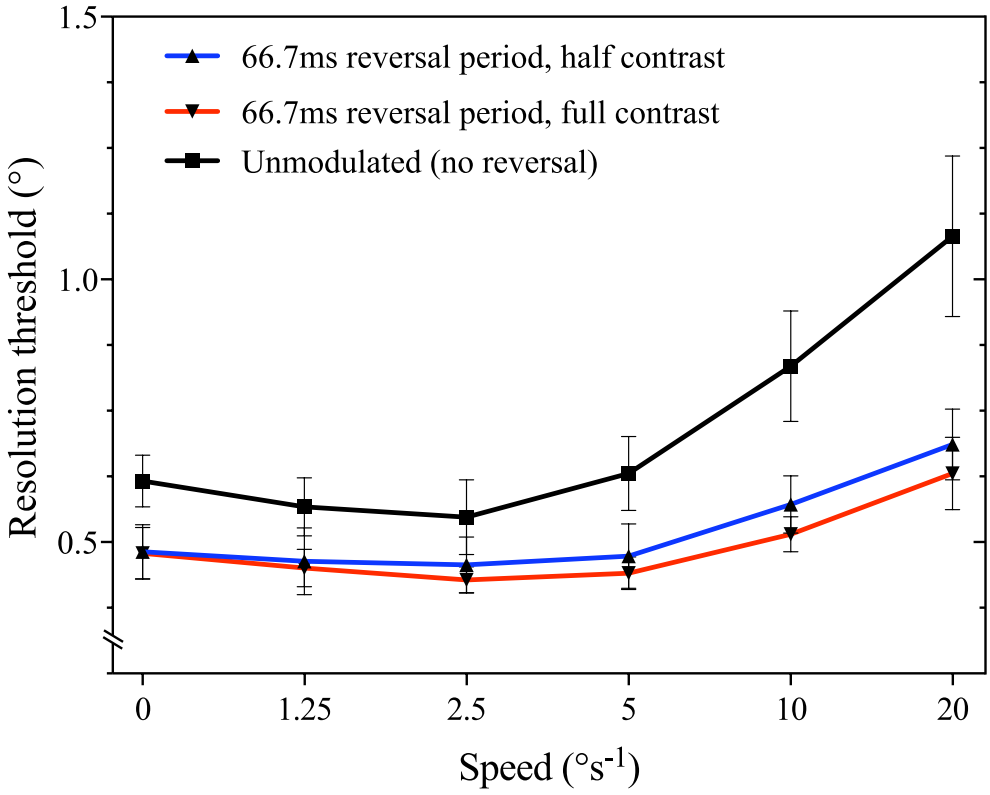

Figure 46: Graph of Experiment 3.3.2, comparing resolution thresholds for contrast polarity reversal between a target luminance of 0.5cdm^{-2} to 85.0cdm^{-2}, a Michelson contrast of 0.99 (red line) with reversal between 63.72cdm^{-2} and 21.22cdm^{-2}, a Michelson contrast of 0.50 (blue line). The control condition with no additional temporal modulation is also shown. Both contrast polarity reversal conditions were 66.7ms reversal (after every fifth video frame). Data points show the mean resolution threshold of all subjects, and the error bars indicate between-subjects 95%CI.

Figure 46 indicates that the depth of contrast has very limited effect on resolution thresholds for targets with reversing contrast polarity. The statistical difference between the two conditions was assessed using the Holm-Sidak method for multiple t-tests (one per speed), adjusted for multiple comparisons. No significant difference was found between full- and half-contrast contrast polarity reversal for any individual target speed (0°s^{-1}: $t(14)=0.09$, $p>.05$; 1.25°s^{-1}: $t(14)=0.41$, $p>.05$;

$2.5°s^{-1}$: $t(14)=1.17$, $p>.05$; $5°s^{-1}$: $t(14)=1.09$, $p>.05$); $10°s^{-1}$: $t(14)=2.10$, $p>.05$; $20°s^{-1}$: $t(14)=1.36$, $p>.05$). These results demonstrate that the beneficial effect of contrast polarity reversal on resolution thresholds persists when the luminance range of the target is equated between conditions.

5.5.3: Discussion

Similarly to Experiments 3.1 and 3.2, the addition of contrast polarity reversal has reduced the detrimental effect of increasing smooth object motion speed (e.g. Brown, 1972b). However, unlike temporal subsampling (Experiment 3.2.1), there is also a visible improvement in resolution thresholds at low speeds for some reversal rates.

The detriment to performance at low speeds and short reversal period (13.3ms) shown in Figure 45 is consistent with a system with non-immediate adjustment of sensitivity with changes in luminance. The onset of a stimulus within the receptive field of a photoreceptor initiates a electrical response from the photoreceptor (Swanson, Ueno, Smith, & Pokorny, 1987). The amplitude of this response is related to the duration and the luminous intensity of the stimulus, but the time delay between the onset of the stimulus and the beginning of the photoreceptor response is a fixed property of the photoreceptor (Land, 1999). This response is known as the temporal response function (TRF).

At the luminance tested, the response functions of rod and cone cells peak at approximately 50ms (Cao, Zele, & Pokorny, 2007; Swanson et al., 1987; Zele, Cao, & Pokorny, 2008). This implies that stimuli appearing within the receptive field of the photoreceptor for a shorter time than this will not initiate the

maximum temporal response. This has been connected with motion smear (Land, 1999): the intensity of a target that is moving too quickly to allow for the maximum temporal response of the photoreceptor will not be accurately signalled, resulting in a blurring of the image. Similarly, if a stimulus switches from one contrast polarity to the other, at a rate too fast for the maximum temporal response to occur, this also results in inaccurate signalling, and consequently a rise in resolution thresholds. By reversing the contrast polarity of the target at a rate suitable for allowing the maximal temporal response, both on- and off-channels of retinal ganglion cells can be stimulated to their maximal output, thus helping to improve resolution (Schiller, Sandell, & Maunsell, 1986).

At the lowest target speeds, the optimum reversal period is 66.7ms, which provides the highest rate of additional temporal modulation while remaining sufficiently slow for maximum cellular response. As target speed increases, the optimum reversal period lowers to 40.0ms reversal at $20°s^{-1}$, suggesting the optimum reversal period depends on the target speed. The optimum reversal period is higher for targets with insufficient speed to avoid stimulating the same retinal area. This may be because the temporal response of the photoreceptor cells must return to the baseline response amplitude before the response of the opposing contrast polarity can be initiated. At higher speeds, target motion reduces the overlap between stimulated retinal locations, such that the opposing contrast polarities can stimulate different receptive fields.

In Experiment 3.3.2 there was no significant difference in resolution thresholds between the high and low Michelson contrast conditions. The results of Experiment 3.3.2 therefore suggest that the higher Michelson contrast in the

contrast polarity reversal condition (Experiment 3.3.1), compared to the control condition without temporal modulations, is not entirely responsible for the reduction in thresholds at low speeds in Figure 45 and Figure 46. With reduced stimulus contrast, the TRF reaches the maximum output faster, suggesting the optimum reversal period may not be the same for both contrast conditions. However, resolution thresholds were not examined for a range of reversal periods in the reduced contrast condition.

The results of Experiments 3.3.1 and 3.3.2 therefore suggest that reversing the contrast polarity of a peripheral target can improve resolution across the tested range of target speeds. Since Experiment 3.3.2 confirmed that the increased Michelson contrast of the stimulus cannot account for the improvement in resolution, this supports the view that the temporal harmonics created by the additional temporal modulations in the Fourier domain are providing extra stimulus information that is being utilised by the visual system. Experiment 3.3.1 indicated that the optimum reversal period for targets moving at up to $5°s^{-1}$ is after 66.7ms, which is accounted for by the description of the photoreceptor response to stimuli (Land, 1999; Swanson et al., 1987).

5.6: General discussion

Visual performance deteriorates as the speed and retinal eccentricity of a target increases. Patients with foveal scotomas are forced to rely on peripheral vision to perform routine tasks. Accordingly, this chapter investigated stimulus presentation techniques designed to optimise peripheral resolution.

The deterioration of visual thresholds with increasing target speed is often associated with motion smear, a detrimental by-product of temporal summation over neighbouring retinal regions brought about by the temporal response properties of peripheral retinal receptors (Burr, 1980). It was hypothesised in Experiment 3.1 that interfering with motion smear by disrupting the smooth motion path would reduce the detrimental effect of increasing smooth motion. In Experiment 3.1 (Figure 39) it was shown that thresholds for a randomised path did not rise as the target speed increased, in spite of the increase in the actual target speed between frames. This suggests that randomising the path order, thus reducing the probability of consecutive targets being displayed with a spatial overlap, can limit the effect of motion smear. Alternatively, randomising the path order may prevent the shift in spatial frequency sensitivity associated with increasing smooth motion. The effect of randomising the motion trajectory on spatial frequency sensitivity was not examined directly. This could be investigated in a contrast detection task, by using Gabor patch targets instead of Landolt ring targets. The effect of randomising the motion trajectory on resolution thresholds is also not fully explained in terms of the TRF. Land's (1999) description of the TRF suggests that static target presentation initiates the maximum photoreceptor output, while presenting the target for brief durations at large spatial offsets is not optimal. This suggests that resolution thresholds should not be independent of target speed. The results of Experiment 3.1 therefore do not allow for a definitive explanation of the mechanism driving the loss of performance with increasing smooth motion speed, and the protection against it resulting from randomising the motion trajectory.

While randomising the motion path prevented the well-documented decrease in performance at high target speeds, it had no effect on slowly moving targets. Thus, in Experiments 3.2 and 3.3 additional temporal modulations were added to the stimulus. It was hypothesised, in accordance with van Santen and Sperling (1985), that the temporal harmonics of the stimulus in the Fourier domain created by the additional modulations would provide more stimulus information at frequencies to which the visual system is sensitive. As such harmonics would appear for stimuli of all speeds, additional temporal modulations should show a reduction in thresholds for static and moving peripheral targets.

Temporal subsampling in Experiments 3.2.1 and 3.2.2 was shown to have a similar beneficial effect on resolution thresholds at high speeds (as was seen in Experiment 3.1). However in Experiment 3.2.1 (Figure 42), subsampling had a negative effect for static and slowly moving targets. It was demonstrated in Experiment 3.2.2 (Figure 43) that this is strongly mediated by the reduction in overall stimulus contrast energy. In Experiment 3.3.1, contrast polarity reversal was shown to produce reductions in resolution thresholds across target speeds, for reversal rates of 26.7ms or higher. Contrast polarity reversal offers twice the overall luminance range than does temporal subsampling. In Experiment 3.3.2 the luminance range of contrast polarity reversal was lowered to 63.72cdm^{-2} and 21.22cdm^{-2}, thus matching the luminance range of the unmodulated condition. Figure 46 indicates that the beneficial effects of contrast polarity reversal persist.

The mechanism underlying the effects that additional temporal stimulus modulations have on resolution is unclear. One possible explanation is in terms of the temporal harmonics created in the Fourier domain by applying periodic

temporal modulations to the stimuli. A second possible explanation is in terms of the TRF of photoreceptor cells.

In the unmodulated condition (with no additional temporal modulation), the luminous intensity is fixed, so the magnitude of the TRF depends on the speed of the target; the target must being slow enough for the TRF to peak before the target leaves the receptive field of the photoreceptor. If the target exceeds this speed, this provides a suboptimal response from the photoreceptor. Thus, as target speed increases, resolution of the target decreases. Alternatively, introducing motion to a stimulus has the effect of orienting the Fourier spectrum of the stimulus: the higher spatial frequency information is presented at higher temporal frequencies (Van Santen & Sperling, 1985). Thus, target motion without additional temporal modulation has the effect of shifting the critical target information to frequencies for which sensitivity is lower. Further increasing target speed exaggerates this effect, thus increasing target speed is expected to deteriorate target resolution.

Similarly, the results of the temporal subsampling experiment (Experiments 3.2.1 and 3.2.2) can also be explained in terms of both the TRF and additional temporal harmonics. The time taken for the TRF of photoreceptor cells to peak at this luminance is approximately 50ms (Cao et al., 2007; Zele et al., 2008). In the temporally subsampled conditions, the target was displayed for a single frame (13.3ms) at a time. Since this is not sufficient for the TRF to peak, the response from the photoreceptor is limited. Increasing spatial and temporal offsets between subsequent target presentations as the ISI increases prevent the target from being presented within a single receptive field. This results in resolution thresholds becoming independent of target velocity. Reducing the luminous intensity of the

target (Experiment 3.2.2) reduces the maximum magnitude of the response from the photoreceptor. However, whether multiple subsequent target presentations are within the same receptive field is driven by the ISI. Thus, while resolution thresholds are expected to be influenced by the luminous intensity of the targets (thresholds are expected to reduce as the luminous intensity is reduced), the effect of speed on resolution thresholds is not. This aligns with the observed results. Alternatively, subsampling the stimulus reduces the time-averaged stimulus contrast, but creates additional temporal harmonics. The higher the ISI, the broader the temporal range across which the harmonics appear. The additional harmonics result in stimulus information remaining within the spatiotemporal window of visibility even at even high speeds, provided the ISI is sufficiently large for distinct harmonics to appear. Thus, the effect target speed has on the extent to which the frequency content of the target is within the window of visibility is negated at high ISI. The amplitude of these harmonics is influenced by the time-averaged contrast: lower contrast results in lower amplitude in the Fourier domain. This explains the effect of increasing the ISI at low target speeds in Experiment 3.2.1. Further, since the luminous intensity (and therefore contrast) of the stimulus only affects the amplitude and not the spacing of the harmonics, the results of Experiment 3.2.1 can also be explained in terms of additional temporal harmonics.

By reversing the contrast polarity of the target, both on- and off-channels of retinal ganglion cells can be stimulated to their maximal output, thus helping to improve resolution (Schiller et al., 1986). However, the reversal period must be sufficiently long for the TRF to reach maximum output before switching. Reversing the polarity of a static or slowly-moving target thus improves

resolution by increasing the retinal signals initiated by the stimulus compared to signals produced by only on- or off-channels. Relative performance for the different reversal rates in Experiment 3 are consistent with the TRFs of photoreceptor cells as estimated by Cao et al. (2007), Zele et al. (2008), and Swanson et al. (1987), suggesting an optimum reversal rate of approximately 66.7ms (Figure 45). However, the TRF of photoreceptor cells does not account for the reduction of the detrimental effect of increasing target speed. If the target moves too quickly for the maximal TRF response, the output will be suboptimal. Also, since the target is not presented with an ISI, the spatial and temporal offset between subsequent target presentations is insufficient for the presentations to be perceived separately. Similarly to temporal subsampling, reversing the contrast polarity increases the temporal frequency content of the stimulus by creating additional temporal harmonics. As with temporal subsampling therefore, the influence of target speed is negated by the additional harmonics maintaining information within the window of visibility. Further, unlike subsampling, contrast polarity reversal does not influence the time-averaged contrast of the stimulus. Thus, resolution thresholds are less influenced by the reversal period of contrast polarity reversal than by the ISI in subsampling. This is provided the harmonics are suitably separated; Figure 45 suggests that at the longest reversal periods, the separation between harmonics has extended such that at high speeds, the amount of information within the window of visibility has dropped, resulting in higher resolution thresholds. Thus, the observed phenomenon that contrast polarity reversal reduces the detrimental effect of increasing target speed can be explained in terms of the additional harmonics, but not in terms of the TRF.

Reducing the contrast of the stimulus (Experiment 3.3.2) should limit the maximum TRF magnitude, resulting in diminished resolution (similarly to Experiment 3.2.2). No significant difference was seen between contrast conditions in Experiment 3.3.2. Thus, these results do not align with descriptions of the TRF. Similarly, the reduction in time-averaged stimulus contrast is expected to reduce the amplitude of the Fourier spectrum of the stimulus, resulting in diminished resolution. The results of Experiment 3.3.2 therefore suggest that contrast mediates benefits of temporal modulations with low luminance range, but this effect saturates with a broader range (at higher contrasts).

Thus, the results of the experiments in this chapter support additional temporal harmonics created by the temporal modulations driving the observed effects they have on resolution thresholds. However, the TRF can account for many of the observed phenomena. A more comprehensive explanation of the effects of additional temporal modulations on resolution thresholds for peripheral targets may therefore rely on a combination of both mechanisms, or perhaps also post-receptoral cortical mechanisms.

The results of the experiments in this chapter therefore suggest that resolution thresholds are protected from deteriorating with increasing target speed by almost any modulation of the motion path, but only polarity reversal is seen to improve performance at low speeds, or for static targets. Experiment 3.3.2 suggests that maintaining high luminance ranges (as in Experiment 3.3.1) may be unnecessary for testing contrast polarity reversal. Although black targets on a white background may be common in tasks such as reading, this is not always the case. Many road signs or posters, or indeed other (non-text) objects of interest in the

visual field may be presented on dark or coloured backgrounds. However, for contrast polarity reversal to be a useful tool in optimising the use of the remaining visual field in patients with restricted central vision, there are other tasks it must withstand. For example, exaggerated ocular motion is commonly associated with AMD and related foveal disorders (Crossland, Culham, & Rubin, 2004; Kumar & Chung, 2014; Martinez-Conde, 2006b; Rubin & Feely, 2009), so a technique designed to aid visual performance in such patients must be resilient to target jitter. Additionally, it must extend to more salient tasks, such as sentence reading.

Thus, the experiments in this chapter show that for targets in the near periphery, the known detrimental effect of increasing smooth object motion speed can be ameliorated by introducing temporal stimulus manipulations. However, for slowly moving targets, manipulations that interfere with motion smear alone are insufficient. Visual performance for static targets as well as across a wide range of speeds can be improved by adding temporal modulations to the stimulus, but the precise mechanism driving the improvement is unclear. Contrast polarity reversal at reversal rates between 66.7-106.7ms was demonstrated to be optimal for peripheral acuity.

Chapter 6: Use of additional temporal stimulus modulations in simulated conditions of eye disease

6.1: Introduction

Patients that have lost central visual function are often forced to perform typical visual tasks in suboptimal conditions. For example, reduced oculomotor control is a symptom that commonly occurs alongside central vision disorders such as AMD (Crossland et al., 2004; Rubin & Feely, 2009). This reduced oculomotor control manifests as fixational eye movements (FEMs) that are exaggerated by a factor of 2-4 in patients with AMD (Crossland et al., 2004; Kumar & Chung, 2014; Martinez-Conde, 2006b).

Typically FEMs are small, involuntary changes in the position of the eye in the socket. They have been extensively studied since the advent of accurate eye-tracking software and hardware (Bellmann, Feely, Crossland, Kabanarou, & Rubin, 2004; Bullimore & Bailey, 1995; Hennig & Wörgötter, 2003; Martinez-Conde et al., 2004; Rucci et al., 2007). While the functional role of saccades is to foveate peripheral stimuli, the role of the smaller, more frequent microsaccades is less well understood.

Although associations have been made between fixational instability and poor visual performance, some aspects of visual perception appear to be less influenced by increased ocular jitter. The findings are mixed with regards to decreased performance in reading tasks. Bullimore and Bailey (1995) examined the oculomotor behaviour of AMD patients while reading, and suggested that reading

performance was more dependent on the number of letters covered by the observer in each forward saccade (the perceptual span), than it was on the fixational stability of the observer. Additionally, Rubin and Feely (2009) did not find fixational instability to be a significant predictor of reading speed in AMD patients. Seiple, Szlyk, McMahon, Pulido, and Fishman (2005), however, reported that reading performance could be improved by training AMD patients in controlling ocular motion, suggesting a link between fixation stability and reading performance in AMD.

Badcock and Wong (1990) demonstrated that foveal Vernier line-width judgements were resistant to high levels of positional noise. Further, Falkenberg, Rubin, and Bex (2007) demonstrated with Landolt ring targets that crowding and resolution are also unaffected by increased retinal jitter. On the other hand, Watson et al. (2012) suggest that image jitter can improve word recognition speed, facial emotion recognition, and contrast sensitivity in AMD patients only at low jitter frequencies. At frequencies more typical of oculomotor instability, the positional jitter can actively impair performance. This is in contrast to Macedo, Crossland, and Rubin (2011), who examined resolution thresholds for Landolt ring targets in AMD patients. The target motion in their experiment either compensated or exaggerated the ocular jitter. Thus, while the amplitude of the jitter varied between conditions, the jitter had the same temporal frequencies. They demonstrated that compensating for oculomotor jitter had no effect on resolution thresholds, but that thresholds were significantly worse when the jitter was amplified. So although reduced oculomotor control commonly occurs alongside AMD, at present it is unclear whether improving oculomotor function will improve target resolution in patients.

Neuroretinal matrix damage (NRMD) refers to any interference from damage or disease leading to visual undersampling at retinal or cortical level. High frequency information is more vulnerable to loss as a result of the visual undersampling that is characteristic of NRMD (Shah et al., 2016). Notably, this loss is associated with a reduction in acuity (Frisén & Quigley, 1984). Some forms of NRMD such as cone-rod dystrophy can lead to macular lesions as well as clustered peripheral photoreceptor loss (Rabb et al., 1986). They are associated with decreased acuity across the visual field, as well as reduced reading speed (Hamel, 2007). Visual prognosis in such diseases is often poor, and there is currently no clinical treatment for disorders such as cone-rod dystrophy. Thus, patients may benefit from a stimulus manipulation that can improve resolution for peripheral targets.

The results of Chapter 5 indicated that increasing the spectral content of the stimulus by applying additional temporal modulations can improve resolution thresholds for peripheral targets. The experiments in this chapter are designed to investigate whether additional temporal stimulus modulations can continue to provide beneficial effects on resolution thresholds in the presence of two common visual defects simulated in healthy observers: increased oculomotor instability, and undersampling of the visual image.

In Experiment 4.1, fixational instability is simulated in healthy observers by recording natural ocular motion during fixation and applying the time-varying changes in position to otherwise static targets. Two additional separate temporal modulations are applied to the stimulus. One manipulation is a temporal subsampling of the stimulus (see Experiment 3.2.1), in which the target is displayed with an increased temporal interval between presentations. The other

manipulation reverses the contrast polarity of the stimulus from white to black throughout the trial (Experiment 3.3.1). Periodically-modulated presentation is believed to create harmonics in the temporal domain of the stimulus, increasing the range of temporal frequency information available (Van Santen & Sperling, 1985). The nature of subsampled presentation effectively reduces the absolute contrast of the stimulus, while reversing the contrast polarity has a similar temporal activation, but maintains the absolute contrast of the stimulus. Although the previous chapter indicated that resolution thresholds for subsampled targets were often higher than for unmodulated targets, Kaiser et al. (2014) suggested that subsampled presentation can improve visual performance in observers experiencing vibration. Since jittering the object is a similar percept to vibration, the effect of subsampling on resolution thresholds was examined despite the contraindication from the previous chapter.

The natural eye movements of observers while fixating on a small foveal cross were recorded prior to testing. The positional displacement of fixation from the centre of the cross was quantified and applied to peripheral Landolt ring targets. The amplitude of the jitter imposed on the target was multiplied by a gain factor to simulate deteriorating fixational stability. In Experiment 4.1.1 both the X- and Y-coordinates of the target are drawn from the pre-recorded fixation data. The displacement of the target due to the FEMs occur in every direction, so the applied ocular jitter influences the retinal eccentricity of the target. Retinal eccentricity has a robust, predictable effect on resolution thresholds: the further a target appears from the centre of the fovea, the larger it must be for accurate identification (Brown, 1972b). Therefore, in order to account for variation in target eccentricity, in Experiment 4.1.2 only the Y-coordinate reflected the

observers' ocular motion while the X-coordinate was calculated to restrict the target to 10° from fixation. Increasing target speed along isoeccentric paths is known to impair acuity (Experiment 1.1; Brown, 1972a, 1972b), yet acuity is resistant to increasing retinal jitter in spite of the effective increase in target speed (Experiment 3.1; Badcock & Wong, 1990; Falkenberg et al., 2007). Accordingly, it is expected that resolution thresholds in Experiment 4.1 will be robust to increasing jitter amplitude.

In Experiment 4.2, NRMD was simulated in healthy observers by superimposing partially opaque masks onto Landolt ring targets. Obscuring irregular, unpredictable patches of the target simulates the undersampling associated with NRMD. Resolution thresholds were compared for partially obscured targets with and without reversing contrast polarity. The comparison is made for both static and moving peripheral targets. This is in order to assess whether additional temporal modulations such as contrast polarity reversal have the potential to improve resolution of peripheral targets in undersampled conditions. The experiments in Chapter 4 demonstrated that superimposing a partially opaque mask impairs resolution, and that the extent of the impairment was influenced by the density of the mask. Further, it was demonstrated that by introducing a target motion, resolution could be improved. Thus, patients with undersampled retinae may rely on target motion in order to optimise resolution. However, it remains to be seen whether additional stimulus modulations can further enhance perception in undersampled conditions, as Experiment 3.3 demonstrated it can for unobscured peripheral targets.

6.2: The effect of temporal modulations applied to targets in simulated conditions of oculomotor instability (Experiment 4.1)

6.2.1: Methods

6.2.1.1: Participants

Six observers participated in all experimental conditions (mean age 25.2 years, *SD* 2.8 years). All observers had normal or corrected-to-normal visual acuity and no reported signs or symptoms of eye disease.

6.2.1.2: Apparatus

The FEM characteristics of each observer were recorded with an EyeLink 1000 eye tracker (SR Research, Ltd., Mississauga, Ontario, Canada), with a 500Hz sampling rate and 0.5° average accuracy. A nine-point calibration paradigm was performed at the beginning of each run. Stimuli were generated and displayed using the techniques outlined in the General Methods chapter (Chapter 2).

6.2.1.3: Stimulus

Resolution thresholds were calculated for peripheral Landolt ring targets, using an orientation discrimination paradigm outlined in the General methods chapter. Targets appeared for 0.33s (25 video frames) at one of three temporal modulation conditions: temporally subsampled, with reversing contrast polarity, and with no additional modulation. Examples of these conditions are shown in Figure 47.

Figure 47A and B illustrate the control condition with no additional temporal modulation, whereby the target was presented on every available video frame.

The target presented was white (85.0cdm^{-2}) for the duration of the trial. Figure 47C shows the temporal subsampling condition, whereby the number of frames on which the target was displayed was reduced. The inter-stimulus interval (ISI) was increased from 0ms to 66.7ms, such that the target was displayed only on every fifth video frame. In Figure 47D the contrast polarity of the target is reversed from white (85.0cdm^{-2}) to black (0.5cdm^{-2}) or the reverse at 66.7ms intervals (after every fifth video frame).

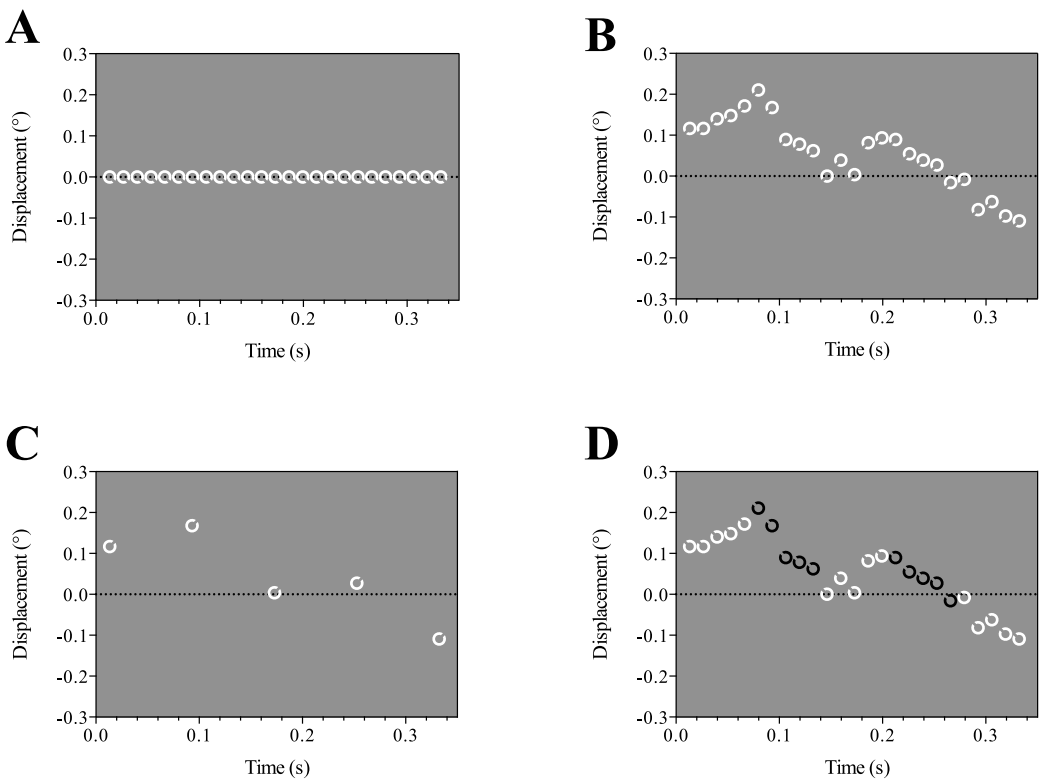

Figure 47: Evolution of the target in space-time for the different experimental conditions, in terms of the displacement of the target from the stimulus origin at screen coordinates (10,0). Observers fixated on a 0.5° cross 10° to the left of the stimulus origin, at screen coordinates (0,0). (A) Space-time plot for a static target displayed on every video frame (no additional modulation). (B) Stimulus progression for a target with positional jitter, in the control condition with no additional temporal modulation, from the example in Figure 48A. The amplitude of the positional jitter in these examples has a gain factor of 1, thus representing the amplitude of the natural eye movements of an observer. (C) Progression of the target with the same positional jitter, in the 66.7ms ISI (temporally subsampled)

condition. (D) Progression of the target with the same positional jitter, in the 66.7ms reversal condition (contrast polarity reversal after every fifth video frame).

6.2.1.4: Procedure

Ocular jitter was simulated using pre-recorded fixation data from each of the observers. Prior to the experimental phase, the observers fixated on a 0.5° cross for three blocks of 10s while eye position data were recorded at 500Hz. Data were extracted by filtering eye positions from the recording rate to match the 75Hz refresh rate of the display monitor. Coordinates of eye positions were normalised to the median location, such that fluctuations centred on a common point.

Deviations from the median position were applied to the stimulus, multiplied by a gain factor of between 0-8. A gain factor of 0 produced a static target, 10° in the periphery in the temporal visual field. A gain factor of 1 represents a jitter matching the natural eye movements of the observer, while other gain factors multiplied the deviation in the position of the stimulus due to eye movements by that factor, exaggerating the retinal jitter.

In the experimental phase, a random time point from the eye-tracking data was chosen at the start of each trial, and the frame position of the stimulus was modified by the frame position of fixation at that time point. The XY-positions of the subsequent 24 time points we used for the remaining trial frames, such that the stimulus jitter followed the pattern of eye movements over the course of that duration during the fixation task.

In Experiment 4.1.1, the target X- and Y-coordinates were both drawn from the fixation data. An example stimulus trajectory over the course of one trial for a

gain factor of 1 is shown in Figure 48A and a gain factor of 8 in Figure 48B. However, as FEMs naturally occur in every direction, jittering the target in this way allows the absolute distance of the target from fixation to vary. This may spuriously affect resolution capacity as the target appears closer to, or further from, the fovea (Brown, 1972b). Thus, this was controlled for in Experiment 4.1.2 with an alternative trajectory, whereby only the Y-coordinate of the target was controlled by the fixation data from the observers. The X-coordinate for each target presentation was calculated such that it maintained a fixed 10° eccentricity. An example of this manipulation with a gain factor of 1 is shown in Figure 48C, and a gain factor of 8 in Figure 48D.

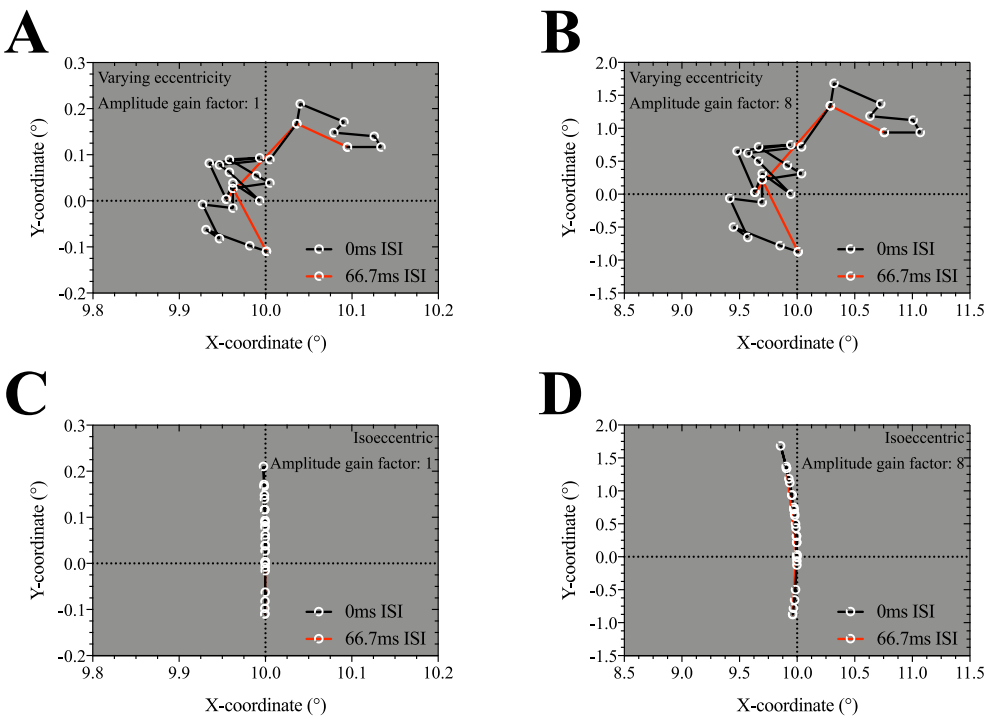

Figure 48: Example target coordinates for the ocular motion conditions in Experiment 4.1. The black trace shows target coordinates in the unmodulated and the contrast polarity reversal condition (in both of which the target is displayed on every video frame). The red trace shows the subsampled condition, which appears at fewer locations interspersed with the blank background. Observers fixated on a cross at screen coordinates (0,0), not visible in these figures. (A) In Experiment 4.1.1, the X- and Y-coordinates were updated

according to the eye-movement data of the participant. The retinal eccentricity of the target is therefore able to vary during each trial. The amplitude gain factor in this example is 1, such that the size of the displacement of the stimulus from coordinates (10,0) reflects the typical size of eye movements of the participant during fixation. (B) An example target trajectory from Experiment 4.1.1 with the maximum amplitude gain factor of 8. (C) In Experiment 4.1.2 the Y-coordinate was updated on each frame according to the eye-movement data of the participant, and the X-coordinate was calculated to maintain a target eccentricity of 10°. The amplitude gain factor in this example is 1. (D) An example target trajectory from Experiment 4.1.2 with the maximum amplitude gain factor of 8. The isoeccentric curve is more visible due to the increased Y-coordinate range.

Five staircase procedures of each of the six experimental conditions (two motion conditions and three temporal modulations) were completed by each observer. For a detailed description of the staircase analysis procedure, refer to Chapter 2.4.

6.2.3: Results

Figure 49 shows the results of Experiment 4.1.1, examining the effect of jittering both X- and Y-coordinates according to participants' FEM data on resolution thresholds for Landolt rings.

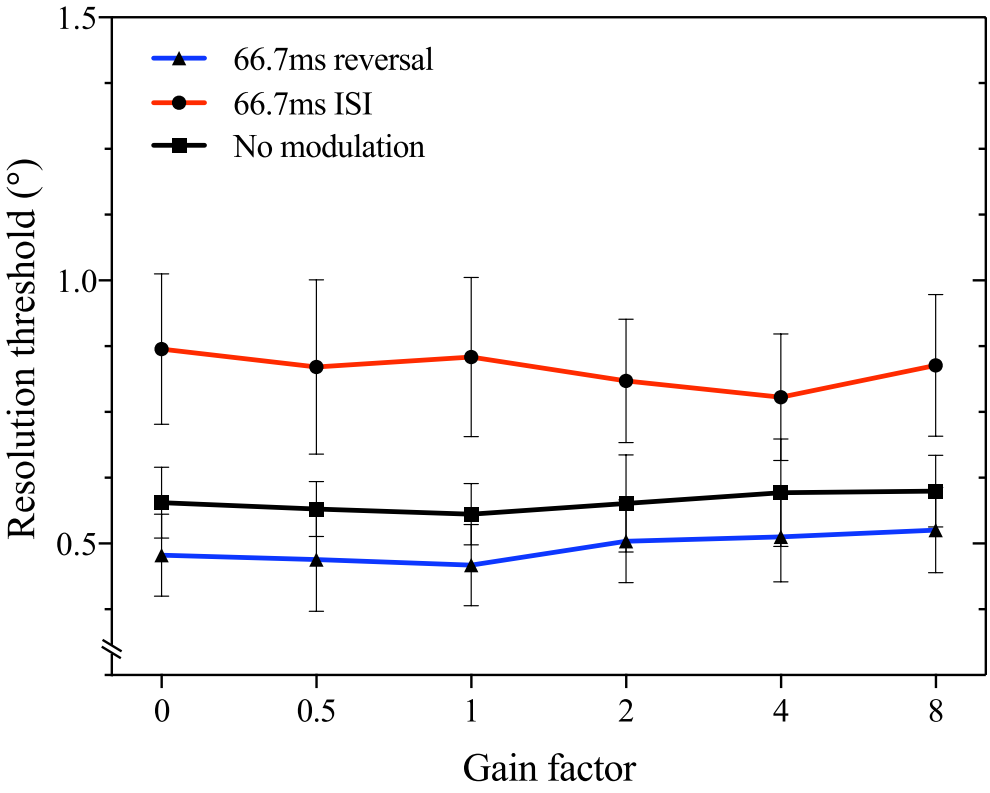

Figure 49: Results of Experiment 4.1.1, showing the effect of simulated retinal instability on resolution thresholds for three temporal modulation conditions: 66.7ms reversal, whereby the target reversed contrast polarity between black and white after every fifth video frame (blue line); 66.7ms ISI, whereby the target was presented with interspersed blank intervals (red line); and without additional temporal modulation (black line). Both X- and Y-coordinates were set based on participants' eye movement data. The median target position was along the horizontal meridian at 10° in the periphery. Data points represent the mean resolution threshold of all observers, and the error bars indicate between-subjects 95%CI.

In Experiment 4.1.1 (Figure 49), a two-way, repeated measures analysis of variance indicated there was a significant effect of temporal modulation on resolution thresholds ($F(2,10)=116.9$, $p<.0001$), however the effect of gain factor was not statistically significant ($F(5,25)=1.6$, $p>.05$). A significant interaction between gain factor and temporal modulation was reported ($F(10,50)=2.8$, $p=.008$). Post hoc comparisons were completed using the Tukey HSD test. This test was used to compare between all mean values individually and between

motion conditions. Due to the number of comparisons being made, the Bonferroni correction is an excessively conservative measure (Perneger, 1998). The Tukey test suggested that mean scores were significantly different between all temporal modulation conditions: No modulation (*M*=0.58, *SD*=0.02); subsampled (*M*=0.83, *SD*=0.03); contrast polarity reversal (*M*=0.49, *SD*=0.03).

Figure 50 shows the results of Experiment 4.1.2, examining the effect of jittering the Y-coordinate and fixing the X-coordinate to maintain a stimulus eccentricity of 10°.

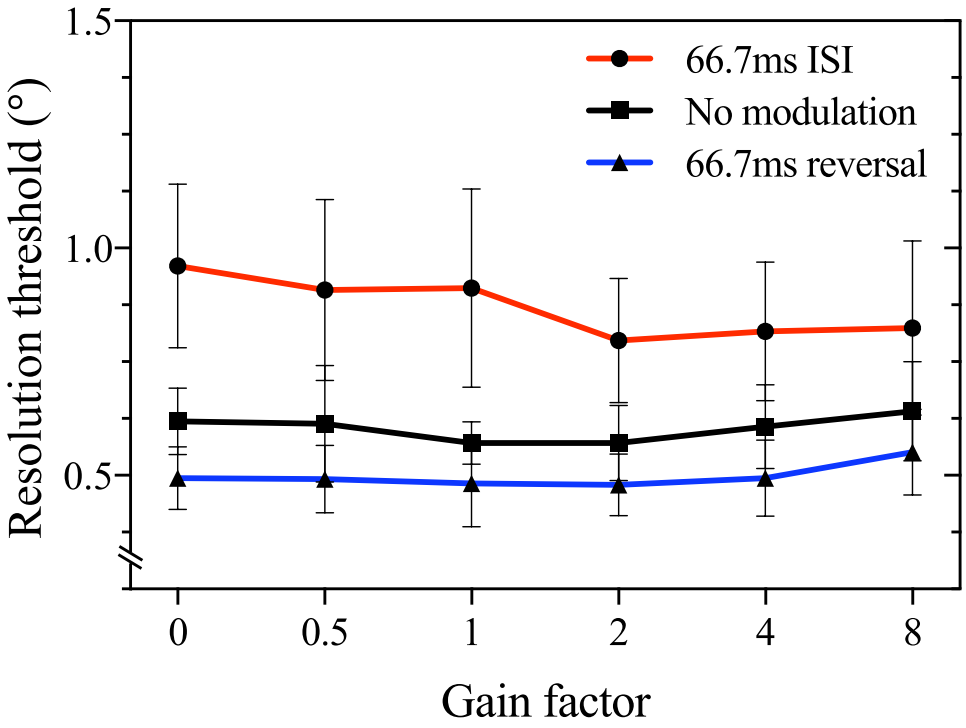

Figure 50: Results of Experiment 4.1.2, showing the effect of simulated retinal instability on resolution thresholds for three temporal modulation conditions: contrast polarity reversal (blue line), temporal subsampling (red line), and without additional temporal modulation (black line). The Y-coordinate was based on participants' eye movement data and the X-coordinate was calculated to maintain a constant eccentricity of 10°. Data points represent the mean of the observers' resolution thresholds, and error bars represent between-subjects 95%CI.

Experiment 4.1.2 (Figure 50) showed a significant effect of temporal modulation ($F(2,10)=55.8$, $p<.0001$) as well as a significant effect of gain factor ($F(5,25)=4.6$, $p=.004$). A significant interaction between gain factor and temporal modulation condition was also present ($F(10,50)=5.1$, $p<.0001$). Post hoc analysis using Tukey's test revealed the effect of gain factor and the interaction effect was driven by a significant drop in resolution thresholds between low and high gain factors in the temporal subsampling condition. Table 2 reports all the conditions between which differences in the mean resolution thresholds were significant.

Table 2: List of conditions in Experiment 4.1.2 between which the mean difference in resolution thresholds was significant.

Modulation condition	Amplitude gain factor, threshold 1	Amplitude gain factor, threshold 2	Mean difference in resolution thresholds (°)	Significance of difference
66.7ms ISI	0	2	0.16	***
66.7ms ISI	0	4	0.14	***
66.7ms ISI	0	8	0.14	***
66.7ms ISI	0.5	2	0.11	**
66.7ms ISI	0.5	4	0.09	*
66.7ms ISI	0.5	8	0.08	*
66.7ms ISI	1	2	0.12	**
66.7ms ISI	1	4	0.10	**
66.7ms ISI	1	8	0.09	*
*** indicates p < .001; ** indicates p < .01; * indicates p < .05				

No significant differences in resolution thresholds were reported between any other conditions. Similarly to Experiment 4.1.1, mean scores were significantly different between all three temporal modulation conditions: No modulation (M=0.60, SD=0.03); subsampled (M=0.87, SD=0.07); contrast polarity reversal (M=0.50, SD=0.03).

Both Experiment 4.1.1 and 4.1.2 suggest that temporal subsampling has a consistently detrimental effect on resolution thresholds for jittering targets, while

contrast polarity reversal significantly improves resolution. This effect is evident for targets with both varying and constant eccentricity.

Experiment 4.1.1 indicates acuity is resistant to high levels of retinal instability when eccentricity is not controlled. For isoeccentric targets in Experiment 4.1.2, the increased jitter had no effect on targets in the contrast polarity reversal condition and the condition with no additional modulation. However, the detrimental effect of temporal subsampling was alleviated at high levels of isoeccentric jitter.

6.2.4: Discussion

Experiment 4.1 aimed to determine whether adding temporal modulations to an eccentric stimulus could improve its discriminability under conditions of stimulus jitter in healthy participants. Resolution thresholds were unaffected by the increased retinal jitter in Experiment 4.1.1 (Figure 49). This result aligns with the findings from Falkenberg et al. (2007) and Badcock and Wong (1990), in which performance was found to be resistant to retinal instability. Watson et al. (2012) suggested that retinal jitter has a positive or negative effect on performance depending on the temporal frequency of the jitter. They suggested that if the jitter frequency is within the range of sensitive temporal frequencies at that retinal area, the jitter can improve performance. If the jitter frequency falls outside this range, it is detrimental. The targets in Experiment 4.1 have two important temporal frequencies: the frequency of the jitter, and the frequency of the additional temporal modulation (if one is applied). Since the jitter frequency does not change as the amplitude gain factor increases (above 0), this could be the reason that thresholds are unaffected by the increased retinal jitter. The findings of this

experiment are not in agreement with Macedo et al. (2011), who demonstrated that amplifying retinal jitter is detrimental to Landolt ring resolution. However, Macedo et al. used a gaze-contingent target positioning paradigm, i.e. the location of the target was based on the fixation stability of the observer at the time of the task. This is in contrast to this experiment, whereby the target position was drawn from pre-recorded fixation data. Thus, in Macedo et al.'s study, the effect the positional jitter has on oculomotor behaviour was linked back to the positional jitter. The rate of the observers' FEMs in Macedo et al.'s study were shown to depend on the positional jitter. Thus, this may be the cause of the dissimilarity between the results of this experiment and that in Macedo et al. (2011). Alternatively, the amplitude gain factor applied by Macedo et al. was 10, such that the amplitude of the positional jitter was an order of magnitude higher than the amplitude of the fixational jitter in AMD patients. The equivalent amplitude gain factor in this experiment would therefore be 20-40, since AMD patients typically demonstrate oculomotor jitter exaggerated by a factor of 2-4 compared to healthy participants (Kumar & Chung, 2014). Therefore there may be a limited tolerance to image jitter that was not reached in this experiment. This tolerance could be related to the size of the receptive fields of the photoreceptors in the retinal location to which the target is presented.

Experiment 4.1.1 also demonstrated a significant effect of additional temporal modulation on resolution thresholds. Across the range of examined gain factors, subsampled targets were resolved more poorly than targets with no additional temporal modulation, while contrast polarity reversal improved resolution. This is consistent with Land's (1999) description of the temporal response function (TRF). Presenting the target within the receptive field of a photoreceptor initiates

an electrical response from that photoreceptor. The time taken for the response to reach maximal output is a property of the photoreceptor. At the luminance tested, the response functions of rod and cone cells peak at approximately 50ms (Cao et al., 2007; Swanson et al., 1987; Zele et al., 2008). Thus, the subsampled condition, wherein the target is presented for 13.3ms at a time, does not allow the photoreceptor to reach the maximal output. By reversing the contrast polarity of the target at a rate greater than this, both on- and off-channels of retinal ganglion cells can be stimulated to their maximal output, thus helping to improve resolution (Schiller et al., 1986).

Experiment 4.1.2 (Figure 50) indicated that for temporally subsampled stimuli, increasing the amplitude of the ocular jitter improves resolution. This result cannot be explained in terms of an increase in the amplitude of the Fourier spectrum of the stimulus at frequencies to which the visual system is sensitive. The direction of the jitter trajectory does not influence the Fourier spectrum, so restraining the target to an isoeccentric arc would not alter the spectrum compared to the unrestrained condition (Experiment 4.1.1). An explanation involving the Fourier spectra would therefore predict an improvement in resolution thresholds for subsampled stimuli as gain is increased in Experiment 4.1.1, which is not observed.

For the results of Experiment 4.1.2 to be compatible with an explanation involving the TRF, this would suggest that the difference in position between frames affects how accurately the target is resolved. A potential explanation is that presenting subsequent targets outside the receptive field of the same photoreceptor results in reduced interference, and thus better performance.

Restraining the target to an isoeccentric arc reduces the average difference in target position between video frames, compared to the unrestrained condition (Experiment 4.1.1). However, subsampling the target increases the average difference in position, since presenting the target with temporal intervals allows the eye to travel further between presentations. Therefore, if the difference in position at the higher gain factors in the unmodulated condition is sufficiently large in Experiment 4.1.1, this should also influence target resolution. However, when comparing resolution thresholds against the size of the difference in position between target presentations, it emerged that the modulation condition (unmodulated or subsampled) has a stronger effect on resolution thresholds than the difference in position. This investigation can be seen in Appendix 3. This indicates that presenting targets with larger spatial intervals between them is not contributing to the improvement in resolution thresholds for subsampled targets in Experiment 4.1.2. This effect is therefore also not well explained in terms of the TRF. Post-receptoral cortical mechanisms may therefore also be sensitive to the additional temporal modulations, and could contribute to the observed effects on resolution thresholds.

The gain-independence demonstrated in Figure 49 may be due to the appearance of the target at eccentricities lower than 10° for brief periods. The higher the gain factor, the closer to fixation the target was able to appear. However, in patients with central scotomas (a symptom of AMD), the target is imperceptible at locations closer to the fovea, so although acuity was unaffected by image instability in healthy participants, improving fixational stability in patients may still benefit AMD patients. Falkenberg et al. (2007) noted that unlike acuity, reading speed was reduced by instability, so correcting for unstable fixation may

be a source of improvement for visual capabilities of patients with central vision loss. The resilience to retinal jittering under controlled eccentricity shown in these experiments supports previous findings in several visual tasks such as acuity, crowding, and hyperacuity (Badcock & Wong, 1990; Bex et al., 2003).

Observers' FEMs during the experimental phase were not accounted for, so retinal jitter may still have influenced the static conditions in Experiment 4.1. While perfect fixation is associated with a perceptual (Troxler) fading, the peak onset for Troxler fading is outside the duration of a trial (Martinez-Conde et al., 2006). Thus, if a target were presented perfectly to a constant photoreceptor array, the presentation duration would not be sufficient for Troxler fading to inflate resolution thresholds. It is therefore a possibility that contrast polarity reversal could be a useful technique for improving the peripheral visual capabilities of AMD patients.

6.3: Additional temporal stimulus modulations in simulated retinal matrix damage (Experiment 4.2)

Patients with NRMD often suffer from macular deficits, as well as distributed peripheral insensitivity (Rabb et al., 1986). The visual undersampling that is characteristic of NRMD is also associated with loss of sensitivity to high spatial frequency (Shah et al., 2016), which is often critical to the identification of the target. Since the additional temporal modulations have been shown to create harmonics of the stimulus in the Fourier domain, the lower spatial frequency content is repeated at higher temporal frequencies. Contrast polarity reversal may therefore also provide improvements in resolution for visually undersampled peripheral targets. In order to examine whether addition stimulus modulations

could provide an improvement in resolution in such patients, in Experiment 4.2, contrast polarity reversal is applied to targets behind partially opaque masks, simulating the visual undersampling associated with NRMD.

6.3.1: Methods

6.3.1.1: Participants

Six participants (mean age 30.5 years, *SD* 10.8 years) with normal or corrected-to-normal monocular acuity participated in Experiment 4.2.

6.3.1.2: Apparatus

Experiment 4.2 was performed on a gamma-corrected CRT monitor (Sony Triniton Multiscan G520; 1280x1024 resolution; screen width 40cm; Sony Electronics, Inc., San Diego, CA, USA) with 75Hz refresh rate (13.3ms frame duration). Stimuli were generated using PsychoPy (v1.80.00rc) on a Mac Pro (Apple Inc., Cupertino, CA, USA). Observers sat with a chinrest 100cm from the monitor and made responses using a keyboard. Targets were presented monocularly to the right eye.

6.3.1.3: Stimulus

Landolt ring targets were presented in the temporal visual field, 10° from a 0.5° fixation cross. Targets were either static on the horizontal meridian or moving along an isoeccentric arc at $2°s^{-1}$ for the trial duration of 0.33s (25 video frames). The direction of target motion was allocated at random at the beginning of each trial. Targets were partially obscured by a static overlaid mask. The mask consisted of an array of square elements of side length 5’ 17” (approximately

2.36μsr). The experiment was undertaken with mask densities 0.5 and 0.75 (obscuring 50% and 75% of the total surface area, respectively), examples of which are shown in Figure 25 (Chapter 4). Targets were presented at two modulation conditions. In the contrast polarity reversal condition, the target luminance polarity was switched from black (a luminance of 0.5cdm^{-2}) to white (85.0cdm^{-2}) or the reverse after every fifth video frame (every 66.7ms). In the condition without additional temporal modulation, the target remained white for the duration of the trial. Targets were presented on a grey background (44.8cdm^{-2}) in a dark vision laboratory (0.5cdm^{-2}).

6.3.1.4: Procedure

Resolution thresholds were assessed using for correctly identifying the orientation of Landolt ring targets from four possible (oblique) orientations, as outlined in the General Methods chapter. Each observer completed ten staircase procedures for each target speed (0°s^{-1} and 2°s^{-1}) and condition (with contrast polarity reversal and with no additional temporal modulation). Experiment 4.2.1 examined the effect of additional temporal modulations on resolution thresholds for static targets. In Experiment 4.2.2 the comparison was made for targets moving at 2°s^{-1}.

6.3.2: Results

Resolution thresholds for partially obscured Landolt rings were compared between targets without additional modulation, and targets with periodically reversing contrast polarity. The results of Experiment 4.2.1, in which the targets appeared statically on the horizontal meridian, are shown in Figure 51. The results

of Experiment 4.2.2, in which targets moved isoeccentrically at $2°s^{-1}$, are shown in Figure 52.

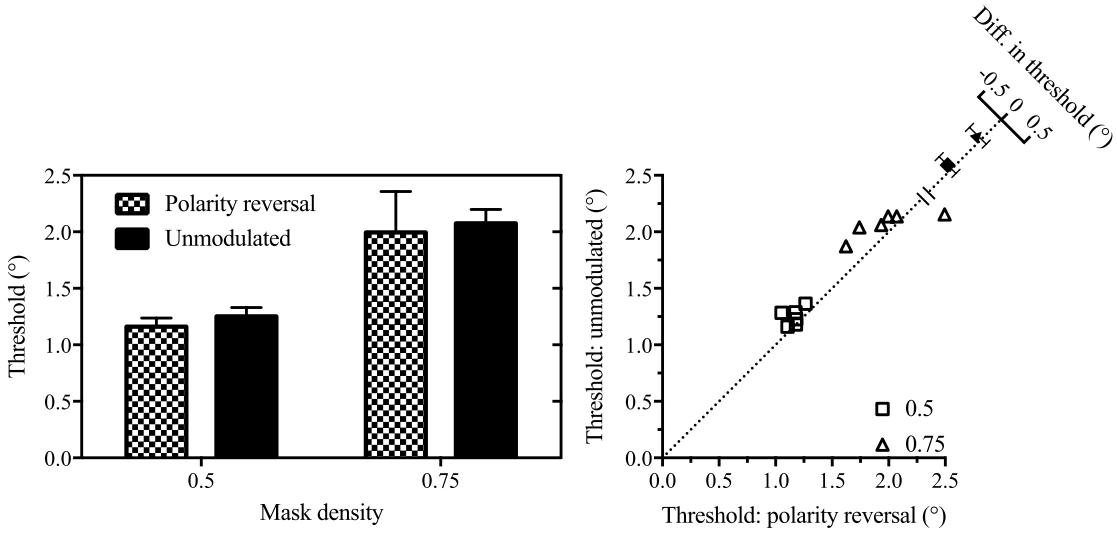

Figure 51: Results of Experiment 4.2.1, comparing resolution thresholds for static targets with and without additional temporal modulation. Left: bars indicate the mean target resolution threshold across all observers, and error bars indicate the between-subjects 95%CI. Modulated (black checked pattern) and unmodulated (solid black) targets are separated by mask density. Right: resolution thresholds for unmodulated targets as a function of resolution thresholds for targets with reversing contrast polarity. Open symbols indicate individual observers' relative performance. Closed symbols on an oblique axis indicate mean difference in threshold between conditions.

Analysis of variance indicated that for static targets in Experiment 4.2.1, mask density had a significant effect on resolution thresholds ($F(1,5)=146.6$, $p<.0001$), however there was no significant effect of contrast polarity reversal ($F(1,5)=2.3$, $p>.05$), or interaction ($F(1,5)=0.1$, $p>.05$). This indicates that contrast polarity reversal does not significantly reduce resolution thresholds for static peripheral Landolt ring targets when they are obscured by partially opaque masks.

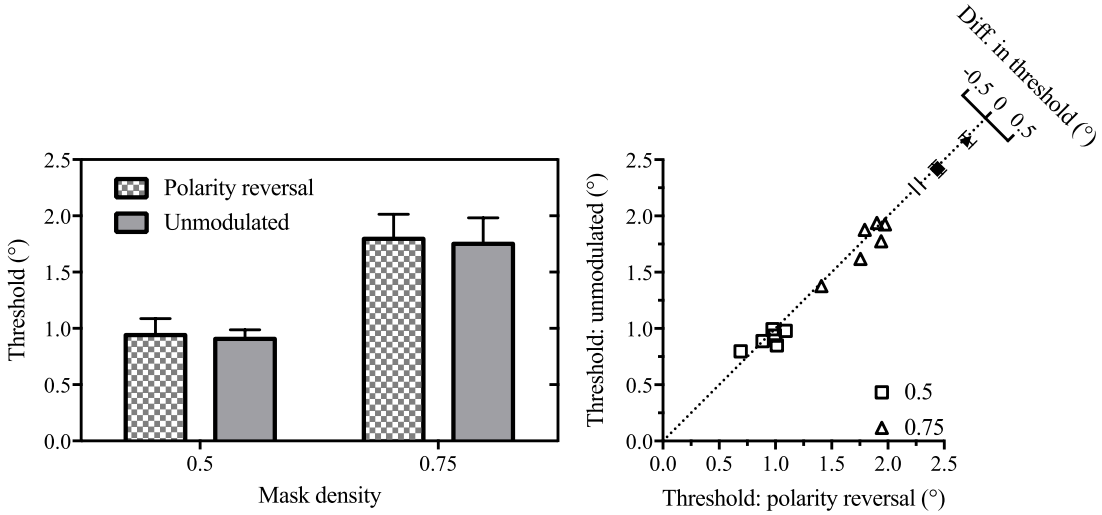

Figure 52: Results of Experiment 4.2.2 comparing resolution thresholds for targets moving at $2°s^{-1}$, with and without additional temporal modulation. Left: bars indicate the mean resolution thresholds for all observers, and error bars indicate between-subjects 95%CI for modulated (grey checked pattern) and unmodulated (solid grey) targets, separated by mask density. Right: Open symbols indicate the relative performance of each individual observer. Closed symbols indicate mean difference in threshold between conditions, plotted on an oblique axis.

In Experiment 4.2.2, resolution thresholds for moving targets were compared with and without contrast polarity reversal. Analysis of variance reported a significant effect of mask density ($F(1,5)=206.5$, $p<.0001$), but not modulation condition ($F(1,5)=2.8$, $p>.05$). No significant interaction between mask density and polarity was reported ($F(1,5)=0.1$, $p>.05$). This indicates that resolution thresholds for slowly moving peripheral targets are not improved by contrast polarity reversal when the targets are partially obscured by opaque mask elements.

6.3.3: Discussion

Experiments 4.2.1 and 4.2.2 suggest that applying extra temporal harmonics to a partially obscured target does not improve resolution. Expanding the spectral

range of the stimulus is thus an inappropriate technique for optimising the use of the remaining visual field in NRMD patients. Partially obscuring the targets with mask elements that have clear edges (i.e. there is, for example, no Gaussian transition to the elements) increases the high spatial frequency content of the stimulus, and reduces the low spatial frequency content. The temporal harmonics created by the additional temporal modulations all have the same spatial frequency content (Van Santen & Sperling, 1985). Thus, even though contrast polarity reversal may increase the temporal frequency range of the stimulus, the disruption to the lower spatial frequencies that is caused by the mask elements may not be providing additional information at frequencies key to the resolution of the target. The spatial undersampling therefore may be responsible for preventing contrast polarity reversal from reducing peripheral resolution thresholds. However, the fovea is sensitive to higher spatial frequencies than the periphery (Johnson et al., 1978; Rijsdijk et al., 1980). Thus, foveal targets that are spatially undersampled (such as the paradigm in Frisén, 2010) may benefit from introducing contrast polarity reversal to the stimulus.

The results of Experiment 4.2 are not compatible with the TRF of photoreceptors driving the effects of additional temporal modulations on resolution. The only difference between the retinal input between conditions is the reversal of contrast polarity, at a rate that has been shown to be beneficial to peripheral resolution. Thus, since this would allow both on- and off-channels to be stimulated (Schiller et al., 1986), it would be expected that resolution would be better in the reversing contrast polarity condition. Since this is not the case, this supports the increased spectral stimulus content driving the effects that additional temporal modulations have on resolution.

The experiments in Chapter 4 described a super-resolution mechanism reliant on additional information being made available across time. Thus, resolution thresholds for obscured targets relied heavily on mask density and the extent of the target visible across the trial. While adding contrast polarity reversal to the obscured target did not lead to an improvement in resolution thresholds, the effect of mask density and target motion described in Chapter 4 have not changed; increasing mask density still resulted in a significant rise in resolution thresholds.

6.4: General discussion

The experiments in this chapter investigated how adding temporal modulations to a target can affect acuity in simulated conditions of eye disease. For targets jittering in accordance with eye motion, simulating the oculomotor instability associated with certain visual impairments, resolution thresholds were robust to increasing levels of jitter in most situations. No detrimental effects of increased ocular jitter were reported in Experiment 4.1, even when controlling for changes in target eccentricity. These results agree with the findings in Experiment 3.1, and with the existing literature on jittering targets (e.g. Badcock & Wong, 1990; Falkenberg et al., 2007). However, Macedo et al. (2011) demonstrated that peripheral resolution is diminished by positional jitter of amplitudes far greater than those examined here. This suggests a limitation on the tolerance to image jitter, that may be related to the size of the receptive field of the photoreceptors responsible for resolving the target. This hypothesis could be tested by examining the tolerance to positional jitter at a range of peripheral eccentricities. It would be expected that resolution would begin to diminish at a lower amplitude of

positional jitter in more foveal locations, whereby the receptive fields of the photoreceptors are smaller (Ransom-Hogg & Spillmann, 1980).

The pattern of results in Figure 49 and Figure 50 suggests the ocular jitter functions as an additional temporal modulation; resolution thresholds independent of frame-to-frame target displacement was shown in Chapter 5 to be characteristic of modulated stimuli. The results of Experiment 4.1 are also consistent with a link between the time-averaged stimulus contrast and performance. As discussed previously, subsampling reduces the time-averaged contrast, while contrast polarity reversal has an effective doubling of target contrast between frames. This coincides with the relative detriment and improvement in resolution thresholds seen in Experiment 4.1.

For targets artificially undersampled by superimposed opaque masks in Experiment 4.2, reversing the contrast polarity of the target did not have any significant effect on resolution thresholds. This suggests that extending the spectral profile of an undersampled stimulus using contrast polarity reversal is not suitable for improving resolution thresholds. The spatial undersampling was achieved using square mask elements. The elements' sharply-defined edges add higher spatial frequencies to the stimulus. In the peripheral visual field, sensitivity to high spatial frequencies is lost (Rijsdijk et al., 1980). This suggests that the temporal harmonics created by contrast polarity reversal are not increasing the spatiotemporal information within the visible range of frequencies.

Contrast polarity reversal has been shown to improve resolution thresholds for static, smoothly moving, and jittering peripheral targets, but only in situations whereby the target appears unobscured. Accordingly, this supports the possibility

that the contrast polarity reversal technique could be used to improve the performance in salient tasks in AMD patients, such as peripheral reading. However, Experiment 4.2 does not suggest contrast polarity reversal could be used as part of a technique aiming to improve visual performance in NRMD patients.

Chapter 7: Examining the contribution of temporal harmonics to stimulus perception using a model of theoretical performance

7.1: Introduction

The previous chapters have demonstrated that adding temporal modulations to a stimulus can affect on an observer's ability to resolve its spatial form. The temporal modulations applied to the stimuli were subsampling, whereby the target was displayed with interspersed blank intervals, and contrast polarity reversal, whereby the target luminance was alternated between black and white on the grey background at regular intervals. Temporal subsampling is reported in terms of the duration of the blank interval (the inter-stimulus interval, ISI), and contrast polarity reversal in terms of the duration for which the target was presented at each contrast before reversing.

Resolution thresholds for static and smoothly moving peripheral targets were assessed with and without temporal modulations in Chapter 5. For smooth object motion, the well-known detrimental effect of increasing target speed (Brown, 1972b) was drastically reduced by both temporal subsampling and contrast polarity reversal. However, these two forms of temporal modulations had differing effects on spatial resolution thresholds at low speeds. For subsampled stimuli, resolution thresholds rose as the ISI increased, whereas contrast polarity reversal provided a reduction in thresholds compared to the condition with no additional temporal modulations (the unmodulated condition). In Chapter 6, targets with positional jitter were examined. For jittering targets however, temporal subsampling increased resolution thresholds compared to the

unmodulated condition across the range of jitter intensities. Contrast polarity reversal maintained a reduction in thresholds, suggesting it is a robust technique for improving acuity for peripheral targets.

Van Santen and Sperling (1985) explored the spatiotemporal characteristics of stimuli with and without additional temporal modulations. They demonstrated that by subsampling the stimulus, additional harmonics of the stimulus are created in the Fourier domain. This can be visualised as spatiotemporal replicas of the stimulus information appearing periodically on the temporal frequency axis. These additional harmonics extend the range of spectral information across the temporal frequency axis. If the extra information is provided within the range of frequencies to which the visual system is sensitive, this may be the contributing to the effect temporal modulations have on resolution. The disparity in resolution thresholds between the modulation conditions was attributed (in Experiment 3.2.1) in part to the absolute, time-averaged contrast of the stimulus; as the subsampling ISI is increased, the time-averaged contrast of each trial decreases. The reduction in contrast was accompanied with a rise in thresholds. When contrast was controlled, the thresholds converged at low speeds. The minimum time-averaged contrast in the contrast polarity reversal conditions in Experiment 3.3 were the same as the unmodulated condition or higher. Thus, the contrast of the stimulus may also be a critical factor in the magnitude of the effect of temporal modulations on acuity.

It is therefore hypothesised that the interaction between temporal modulations and resolution thresholds can be accounted for in terms of the time-averaged stimulus contrast, and the increased spectral range of the stimulus when modulated. To

support this hypothesis, a model is described here, whereby a theoretical relative measure of how easily resolved a stimulus should be is calculated using the spectral content of the stimulus.

The model is based on existing models of visual capacity. Variation of contrast sensitivity across spatial and temporal frequency is well documented, and is usually measured in terms of the lowest contrast at which a target is still detectable (de Lange, 1958; Robson, 1966; Van Nes & Bouman, 1967; Van Nes, Koenderink, Nas, & Bouman, 1967). Much research has been performed looking into the effect of stimulus characteristics such as target eccentricity (Kelly, 1984; Rees et al., 2005; Rijsdijk et al., 1980) and speed (Burr & Ross, 1982) on contrast sensitivity. Kelly (1979) developed mathematical formulae to model contrast sensitivity as a function of spatial and temporal frequencies and used this to calculate a 3D spatiotemporal sensitivity surface, displaying contrast sensitivity as a function of spatial and temporal frequency. This has been extended and developed into a description of the spatiotemporal 'window of visibility' (WOV, for a comprehensive explanation see Watson, 2013). The WOV describes the region of the Fourier domain to which an observer is sensitive, and defined as the boundaries of contrast sensitivity as a function of spatial and temporal frequency. Several factors affect the size and shape of the WOV. For example, increasing stimulus contrast increases the spatial and temporal limits of the WOV, and reducing stimulus contrast restricts the boundaries of the WOV. Similarly, increasing the retinal eccentricity of the target also shrinks the limits.

The spatiotemporal characteristics of stimuli are often considered in terms of difference spectra when analysing a discrimination task. Difference spectra are

calculated as the difference between the spatiotemporal fingerprints of stimuli with targets at orthogonal orientations. Difference spectra have previously been used to estimate the visibility of visual stimuli; Thibos and Anderson (2004) and Vol, Pavlovskaja, and Bondarko (1990) calculated the relative amplitudes of difference spectra created from opposing letter stimuli, and other objects. They demonstrated a clear link between the amplitude of the difference spectra and discriminability, measured psychophysically. Additionally, Bondarko and Danilova (1997) calculated the difference spectra of two orthogonally-orientated Landolt rings. The spatial frequencies at which they observed the highest amplitude differences were at lower frequencies than those matching the size of the gap. They linked this to psychophysical evidence that observers were able to discriminate the orientation of Landolt rings in situations in which the size of the gap was sufficiently small that spatial frequencies pertaining to it were beyond the observers' resolution limit (Bondarko & Danilova, 1995). They concluded that the spatial frequency most critical to identifying the orientation is 1.3 times the spatial frequency of a sinusoid, the period of which matches the size of the Landolt ring target (N.B. the gap is at 2.5 times this frequency). Thus, the difference spectra of orthogonal Landolt rings are a good indicator of relative resolvability.

This model evaluates the difference spectra of the stimuli in the different temporal modulation conditions, and assesses the extent to which the stimulus information is generated at frequencies within the WOV. The calculated difference spectra are discrete arrays with each cell describing the amplitude at each combination of spatial and temporal frequency. The WOV used in the model is adapted from the spatiotemporal sensitivity surface described mathematically by Kelly (1979). In order to estimate the visibility of each stimulus, the difference spectra are

combined with the spatiotemporal sensitivity surface, providing an estimate of the spatiotemporal information of the stimulus normalised according to the visibility of visual input at that combination of spatial and temporal frequency. The sum of this range is calculated, giving a relative estimate of the amount of target information appearing at visible frequencies. This is a proxy measure of relative target resolvability.

The resolvability indication was calculated for targets with smooth and ocular motion (Experiments 3.2.1, 3.3, and 4.1.1, respectively). The relative effects of both temporal subsampling, contrast polarity reversal, and the unmodulated conditions were calculated by the model, and compared to the observer data from the previous chapters.

7.2: Methods

7.2.1: Stimulus

As in the experimental chapters, the stimuli used in modelling were Landolt rings (Sloan, 1959) drawn in Sloan font (Pelli et al., 1988). The target size was set to the largest threshold for unmodulated targets. Thus for smooth motion, target size was set to 1.0° and for ocular motion, 0.6°. For these target sizes, critical spatial frequencies are 1.30 and 2.17 cycles per degree, respectively. The experimental conditions were rendered as a 3D MATLAB array, consisting of a series of 2D drawings of the stimulus. A 2D sheet was created for each video frame of the stimulus during a 25-frame trial.

For both smooth and ocular motion, three modulation conditions were modelled: temporal subsampling, contrast polarity reversal, and unmodulated. Visibility was

assessed for targets with smooth motion between speeds of 0-20°s^{-1}, and ocular motion between gain factors of 0-8.

7.2.2: Difference spectra

The model was created using MATLAB (version 2013b; MathWorks, Inc., Natick, MA, USA). The process of creating difference spectra is described in Figure 53, using as an example a static, constantly presented target. Images of the target in its two orientations are shown in Figure 53A and Figure 53B. 3D fast Fourier transforms (FFTs) of the stimuli were calculated. One of these is shown in Figure 53C, plotted in terms of its two spatial dimensions. The temporal frequency component of the stimulus is shown in Figure 53D. The spatial components of the difference spectra (Figure 53E) were calculated by a pixel-wise subtraction of the spatial components of orthogonally-orientated targets (Figure 53C). This provides an indication of the spatial frequency components of the stimulus containing information pertaining to the orientation of the target. The temporal frequency component is exempt from the subtraction procedure, as the differences between orientations are exclusively spatial factors. The temporal frequency spectrum is combined with one of the spatial dimensions from Figure 53E to create the final spatiotemporal difference spectrum in Figure 53F. The two spatial frequency axes were collapsed into one, such that the difference spectra could be represented in only two frequency dimensions, to parallel the spatiotemporal frequency surface.

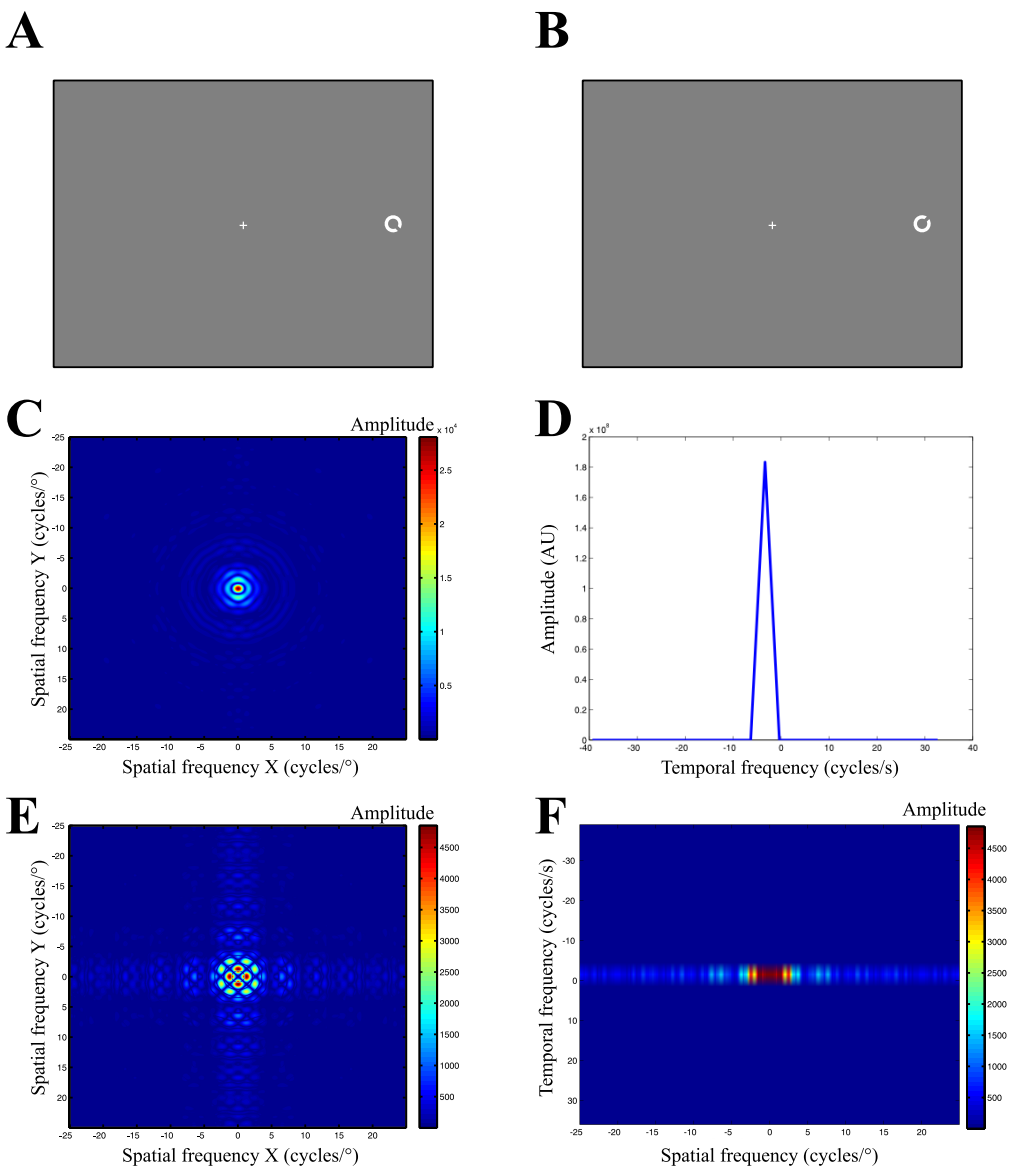

Figure 53: Process of obtaining difference spectra, using an example static, constantly presented Landolt ring target. A FFT is performed on the stimulus in two orthogonal orientations (A, B), each resulting in Fourier spectra in two spatial dimensions of the target (C) and one temporal dimension (D). The spatial frequency components of the FFTs of the two targets are subtracted element-wise from one another to create a spatial frequency difference spectrum (E). The difference spectrum plotted as one spatial and one temporal dimension (F).

7.2.3: Spatiotemporal sensitivity surface

Calculating the theoretical visibility of targets under the varying conditions required an indication of the window of visibility in the Fourier domain. A spatiotemporal sensitivity surface was created using formulae adapted from Kelly (1979). The surface represents the contrast sensitivity to a given combination of spatial and temporal frequency (x, w, respectively), $S(x,w)$.

$$S(x,w) = \left[6.1 + \left(7.3 \left|\log\left(\frac{w}{3x}\right)\right|^3\right)\right] wx\, e^{\left(\frac{-2x\left(\frac{w}{x}+3\right)}{45.9}\right)} \quad (7)$$

$$S(x,w) = \left[5.89 + \left(0.66 \left|\log\left(\frac{w}{3x}\right)\right|^{2.9}\right)\right] wx\, e^{\left(\frac{-2x\left(\frac{w}{x}+2\right)}{45.9}\right)} \quad (8)$$

The function for modelling the spatiotemporal sensitivity surface from Kelly (1979) is shown in Equation 7. The parameters were optimised for Equation 7 by refitting contrast sensitivity functions to data in Kelly (1979) using computational software unavailable at the time, allowing for more accurate plot fitting. The spatiotemporal sensitivity surface generated by Equation 8 is shown in Figure 54, indicating the relative sensitivity to the combinations of temporal and spatial frequencies.

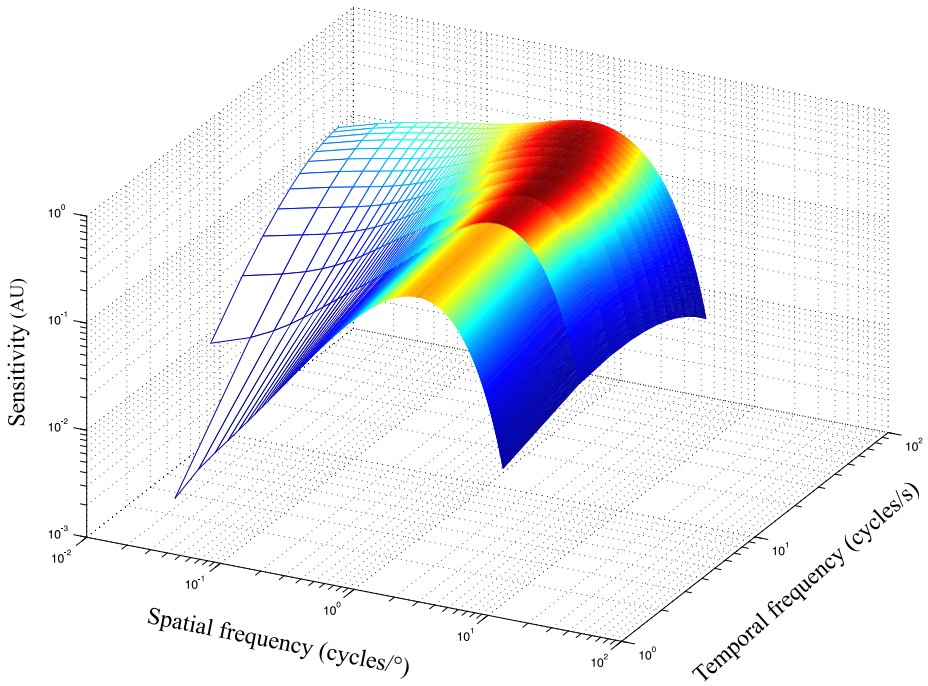

Figure 54: Spatiotemporal sensitivity surface generated by Equation 5, adapted from Kelly (1979).

The spatiotemporal frequency surface was normalised using Equation 9, such that its values were in the range 0-1.

$$S_{norm}(x,w) = \frac{S(x,w)-S_{min}}{S_{max}-S_{min}} \quad (9)$$

Whereby $S_{norm}(x,w)$ represents the normalised contrast sensitivity at spatial frequency x and temporal frequency w, and S_{max} and S_{min} are the maximum and minimum contrast sensitivity values of the unnormalised surface. Although the surface is designed to represent foveal contrast sensitivity, temporal frequency sensitivity decreases linearly with increasing eccentricity, and the shape of the functions is unchanged (Koenderink, Bouman, de Mesquita, et al., 1978). Peak spatial frequency sensitivity shifts to lower values of spatial frequency as eccentricity is increased (Rijsdijk et al., 1980). Although the shift in spatial

frequency is not directly included in the model, since the assessment is a relative measure of estimated resolvability, its exclusion is not expected to have an effect on the model's output.

7.2.4: Resolvability estimation

For each condition, the calculated difference spectrum is combined with the spatiotemporal sensitivity surface using an element-wise multiplication (a Hadamard product). The resulting array represents the Fourier amplitude of stimulus information at each combination of temporal and spatial frequency, normalised by visual sensitivity to targets of those frequencies. The sum of all values in this array was used as an estimate of stimulus resolvability for that condition.

Since the model's estimate of resolvability is calculated in arbitrary units, the resolvability is compared in relative resolvability. The measure of resolvability is compared to the relative resolution thresholds in the observers' data. For smooth motion, the observers' resolution thresholds for subsampled targets are from Experiment 3.2.1, while the thresholds for contrast polarity reversal and unmodulated stimuli are from Experiment 3.3. The two experiments from which data were collated were completed by different groups of observers. Both groups, however, collected data for the unmodulated condition. Their resolution thresholds in the unmodulated condition were not significantly different between groups (this analysis can be seen in Appendix 2). Thus, it is reasonable to consider the relative observer performance for subsampled, contrast polarity reversing, and unmodulated targets together.

Since the resolvability estimation calculated by the model is a relative measure in arbitrary units, a statistical comparison between the model output and the observer data is not appropriate.

7.3: Results

7.3.1: Smooth object motion

The difference spectra for targets with smooth object motion are shown in Figure 55.

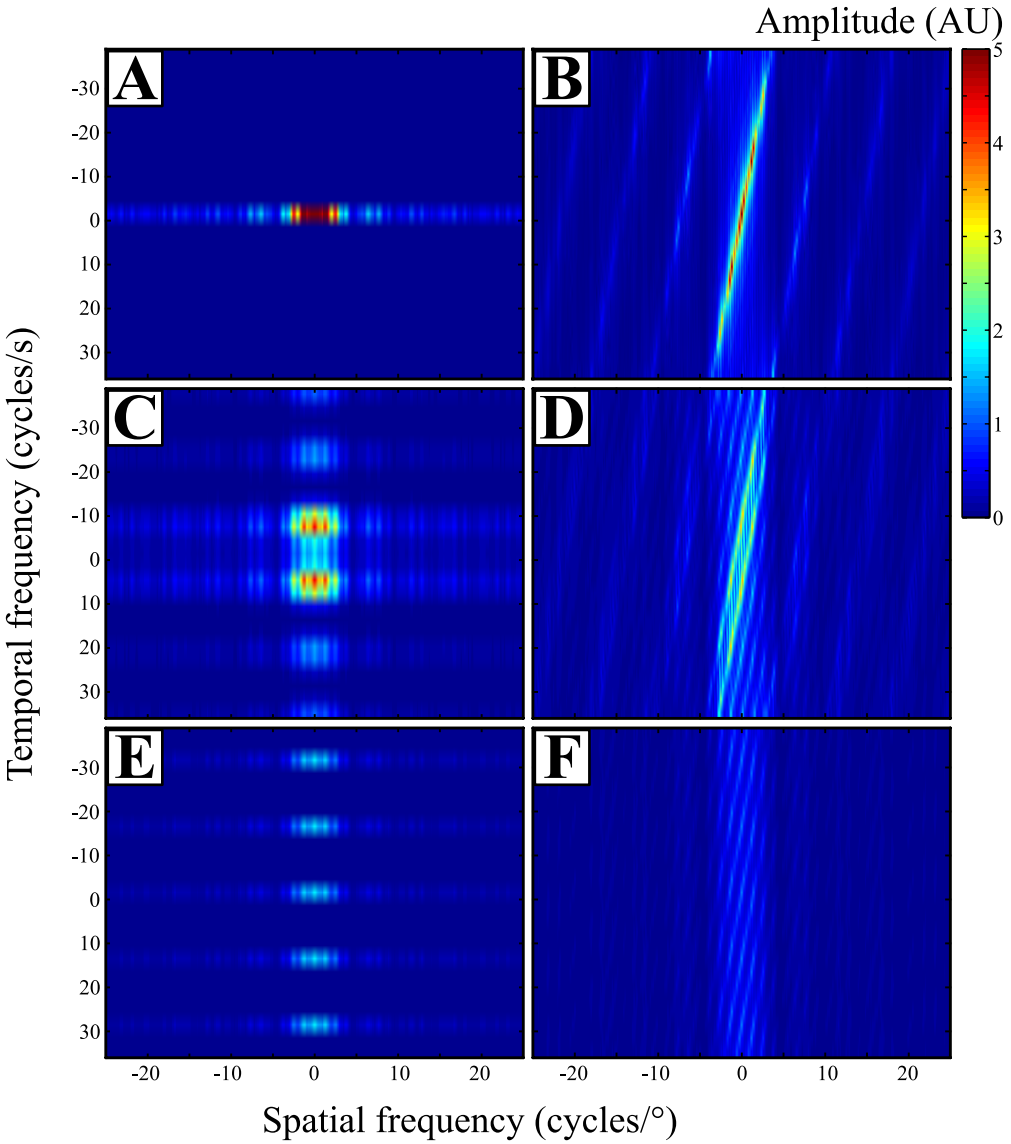

Figure 55: Difference spectra for targets with smooth object motion. Targets in A, C, and E are static; B, D, and F are moving smoothly along an isoeccentric arc at 20°s^{-1}. Targets in A and B have no additional temporal modulations; targets in C and D are reversing their contrast polarity; E and F are subsampled.

The difference spectrum for a static Landolt ring target with no additional modulations in Figure 55A shows a limited temporal frequency range, while the combination of spatial frequencies required to make a Landolt ring target is demonstrated in the spread of power across the abscissa. By adding smooth motion to the target in Figure 55B, the stimulus in the spatiotemporal Fourier

domain obtains orientation. The additional temporal modulations in C, D, E and F have created harmonics of the stimulus in the temporal frequency axis, but the amplitude of the spectra is reduced in comparison to the unmodulated targets in A and B.

The relative measures of stimulus resolvability are shown in Figure 56. For comparison, the observers' resolution thresholds for the same conditions are also shown.

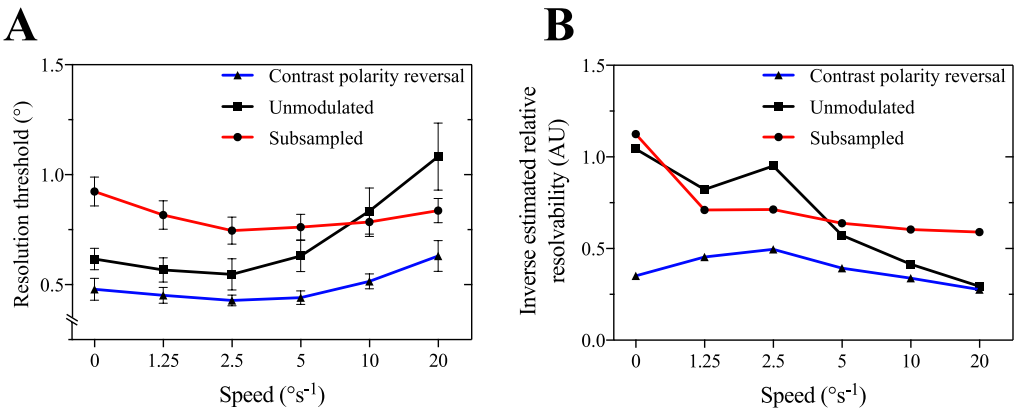

Figure 56: Comparison of the estimation of resolvability according to the model with observer data. (A) Observer data, showing the effect of the three temporal modulation conditions on resolution thresholds for targets moving smoothly at speeds from 0-20°s^{-1}. The subsampled data are the mean resolution thresholds and between-subjects 95%CI for subsampling with 66.7ms ISI from Experiment 3.2.1, and the unmodulated and contrast polarity reversal data are the mean resolution thresholds and between-subjects 95%CI from Experiment 3.3. In the contrast polarity reversal condition, reversal was after every 66.7ms. (B) model estimates of relative target resolvability in the corresponding conditions. Inverse measures are shown, such that a low value on the ordinate reflects high estimated resolvability.

Figure 56 indicates that the model correctly identifies that stimuli with additional temporal modulations do not show a consistent elevation in resolution thresholds as target speed is increased. It is also shown that resolution thresholds are lower for contrast polarity reversal than for temporal subsampling. However, the

elevation in thresholds in the unmodulated condition is not accurately modelled. Only at low target speeds does the modelled relative performance between the three modulation conditions reflect the observer data.

7.3.2: Ocular motion

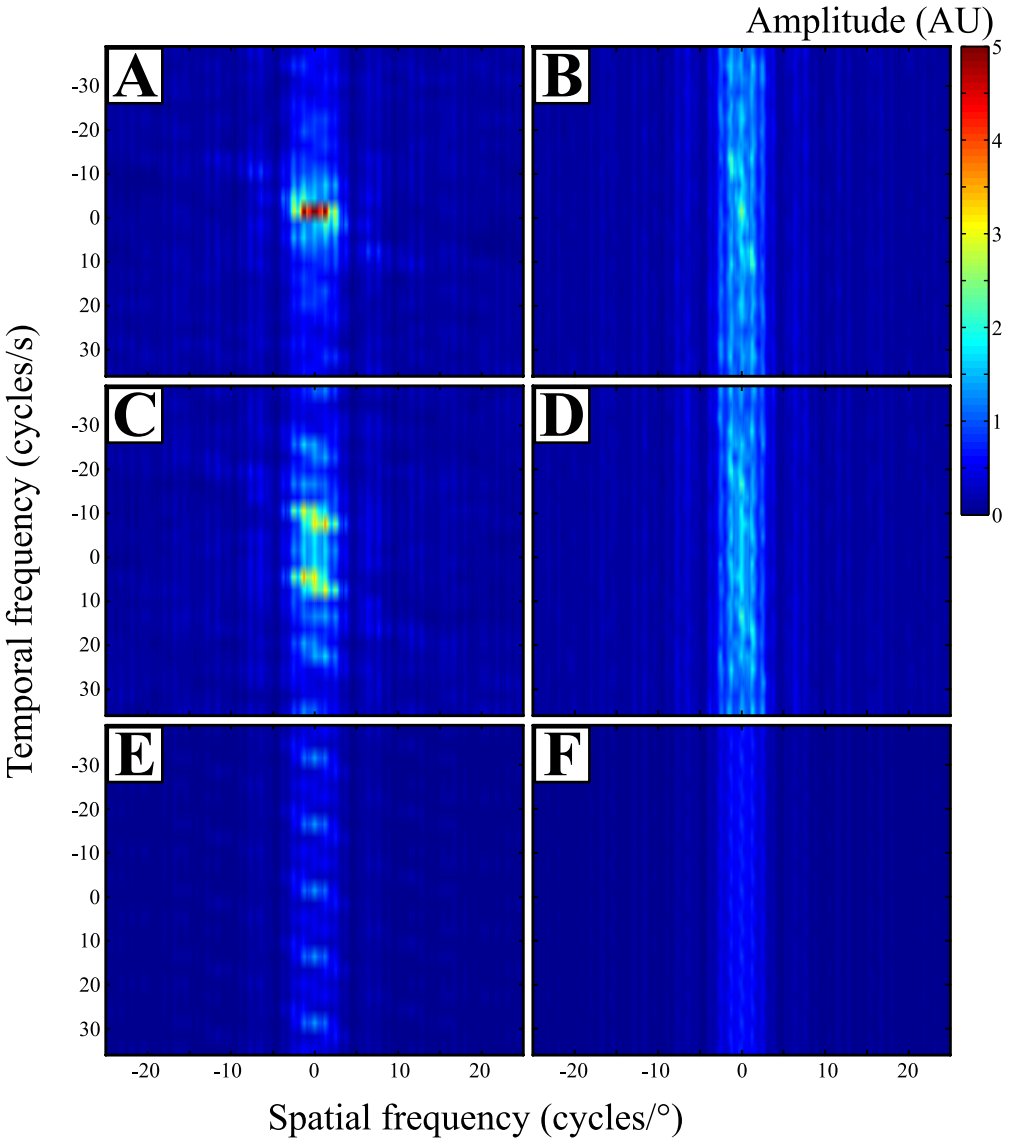

Figure 57: Difference spectra for targets with ocular motion. A, C and E are at a gain factor of 1 (the size of natural eye movements from healthy eyes); B, D and F are at the maximum gain factor of 8. The stimuli in A and B have no additional temporal modulations; C and D periodically reverse target contrast; E and F are temporally subsampled.

Similarly to Figure 55, the additional temporal modulations in Figure 57C, D, E, and F have created harmonics in the temporal frequency axes, but the relative amplitude is comparatively lower than in A and B.

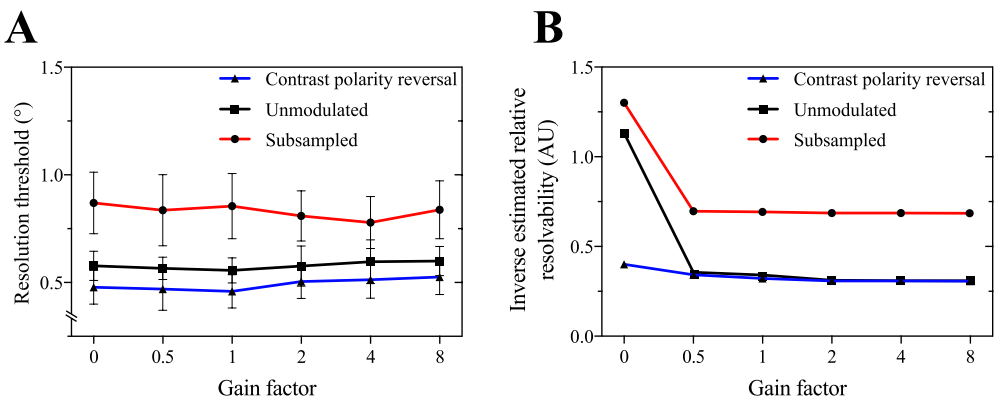

Figure 58: Comparison of the estimation of target resolvability from the model with observer data. (A) The observer data, showing the effect of the three temporal modulation conditions on resolution thresholds for targets jittering with ocular motion at gain factors in the range 0-8. The observer data are mean resolution thresholds and between-subjects 95%CI error bars from Experiment 4.1.1. The subsampled targets were presented with blank intervals of 66.7ms between presentations. In the contrast polarity reversal condition, targets reversed between black ($0.5cdm^{-2}$) and white ($85.0cdm^{-2}$) after every 66.7ms. (B) the estimates of relative target resolvability calculated by the model for the same conditions.

Figure 58 suggests that as in the observers' data, the model indicates that gain factor has minimal effect on resolution thresholds, with the exception of static targets. Additionally, the model suggests that subsampling is detrimental to performance, but it does not predict that any further improvement due to contrast polarity reversal should be possible beyond targets with no additional temporal modulation.

7.4: Discussion

In this chapter a model was designed to illustrate the spatiotemporal characteristics of stimuli used in this thesis, and estimate theoretical performance based on predictions of stimulus visibility. In previous chapters, temporal modulations were applied to peripheral stimuli, and it was demonstrated that these modulations had notable effects on observers' resolution of the targets. For targets following smooth isoeccentric paths, increasing the speed of the target produces a predictable impairment of resolution thresholds. Both temporal subsampling and contrast polarity reversal negate this loss, instead providing resolution mechanisms with resilience to changes in target speed. However, temporal subsampling elevated thresholds compared to static, unmodulated targets, whereas contrast polarity reversal reduced thresholds across the range of target speeds. For targets jittering in accordance with exaggerated oculomotor instability, resolution thresholds for targets with and without temporal modulations are resilient to the additional motion. However, thresholds were consistently higher for subsampled targets, and lower for targets with reversing contrast polarity.

The model first assessed the spatiotemporal characteristics of the stimuli using FFTs. As expected, static targets had no orientation in the spatiotemporal Fourier domain. Orientation was introduced by increasing the target speed along a smooth trajectory. Ocular jitter had the effect of spreading the spectral information across a wide range of spatial and temporal frequencies. The additional temporal modulations in Figure 55 and Figure 57 provide the extra harmonics on the temporal frequency axis, as predicted by Van Santen and Sperling (1985). However, the peak power amplitude is reduced for contrast polarity reversal

compared to situations with no additional modulations, and reduced further still for subsampled stimuli. This reduction in amplitude may explain the relatively higher resolution thresholds for subsampled targets in Experiment 3.2.1 and Experiment 4.1.1. The increase in absolute contrast that is provided by contrast polarity reversal was not reflected in the amplitude of the difference spectra. This implies that an explanation of the benefit of contrast polarity reversal on resolution thresholds is not completely explained by this contrast increase. The increased spectral range of the stimulus must therefore be utilised by the visual system in resolving the target.

Target resolvability was estimated by combining the difference spectrum of the stimulus in each condition with the spatiotemporal sensitivity surface (Kelly, 1979). The values in the resulting array were summed across to give a scalar representative of the resolvability of the stimulus. The model accurately predicted some important aspects of the observer data. For smooth motion, estimated thresholds in the temporal modulation conditions did not rise with increasing target speed, in accordance with the observer data. However, the consistent, predictable rise was also not visible in the unmodulated condition, which is a well observed and robust phenomenon (e.g. Brown, 1972; Burr, Ross, & Morrone, 1986). This inaccuracy may be a result of the model failing to take temporal summation effects into account. As discussed in previous chapters, motion smear is a predictable outcome of temporal summation that is detrimental to resolution. Since the model does not account for motion smear, but does account for the effect of motion on spatiotemporal sensitivity, this supports motion smear as an explanation of the rise in thresholds with increasing target speed. Additionally, the

relative estimated thresholds were lowest for the contrast polarity reversal condition, accurately reflecting the observer data.

For ocular motion, resolution thresholds that were independent of gain factor were accurately modelled for moving targets, although the model predicts elevated thresholds for static targets, which does not occur in the observer data. Additionally, while temporal subsampling was correctly shown to increase thresholds compared to the other modulation conditions, the relative reduction in thresholds for contrast polarity reversal is not captured.

Thus, while the model predicts several aspects of the observer data, there are also features of the estimated performance that are not accurate. There are several drawbacks to the model in its current form, which may underlie the deviations between the model and the observer data.

The contrast sensitivity surface created by Kelly (1979) was created using foveal measurements. The effect of eccentricity on contrast sensitivity was not directly included in the model. Experiment 1.1 (investigating the effect of target speed and eccentricity on resolution thresholds) reported a significant interaction effect, i.e. the effect of target speed on resolution is affected by the eccentricity of the target. The model does not explicitly account for this. Future iterations of the model must therefore correct for eccentricity.

The contrast sensitivity surface was estimated based on observations of visual sensitivity to Gabor patches (Kelly, 1979). Detection is possible for targets with components of frequencies beyond the resolution limit (Thibos, Walsh, et al., 1987), thus a model designed on detection ability may not be appropriate for a

resolution task. However, the relationship between contrast sensitivity and acuity is fixed, thus the normalisation procedure negates the necessity of scaling accordingly. Watson (2013) reported that eye motion has a shearing effect on the WOV; the limits of temporal frequency sensitivity are increased, while spatial frequency sensitivity is unaffected. This has the effect of increasing the extent of the spectral range of a tracked target (i.e. a target being followed by gaze such that it remains within the fovea) that appears within the WOV. Targets that are not being tracked are displaced from fixation, and are thus subject to the shrinking effect that eccentricity has on the WOV. Since the model is not considering tracked targets, it is not expected that including the effects of eye motion on the WOV would improve the accuracy of the model.

Additionally, Equation 7 (for creating the spatiotemporal sensitivity surface) is unsuitable for modelling static targets. This due to the logarithm: the ratio of temporal and spatial frequency is speed. As the speed approaches zero, the logarithm of speed approaches negative infinity. This may be the cause of the relatively inflated thresholds for static targets in the ocular motion conditions. Excluding the static targets results in more accurate predictions in the ocular motion condition, but does not correct for the inaccurate predictions in the unmodulated, smooth motion condition.

The model considers only the amplitude spectrum of the stimulus in the Fourier domain; phase information from the stimulus is discarded. The Fourier phase spectrum has some important influences on perception. Burr, Morrone, and Spinelli (1989) reported evidence for two classes of visual detectors: one with a Fourier phase spectrum of 0°, which is sensitive to lines and another with a phase

spectrum of 90°, which is sensitive to edges. The stimuli used by this model are orthogonal Landolt rings, which differ considerably in the phase spectrum (Thibos & Anderson, 2004). Thus, future iterations of the model should consider the discriminability of Landolt rings using a method that includes the phase spectrum, such as Thibos and Anderson (2004) and Vol, Pavlovskaja, and Bondarko (1990). However, Badcock (1984) suggested that observers do not use phase in making judgements, but rather make use of local differences in stimulus luminance. Thus, while including phase may contribute to a more accurate simulation of performance, it would not be expected to influence predicted performance differently for any of the modelled conditions.

The rise in thresholds with increasing target speed in the unmodulated condition is seen at all eccentricities in observer data (see Chapter 3), as well as foveally in Brown (1972b), but not in the model. This may indicate that the mechanism driving the rise in thresholds with increasing target speed is related to the temporal response function (TRF) of the photoreceptors (Land, 1999; Swanson et al., 1987). The TRF refers to the magnitude of the electrical signal created by a stimulated photoreceptor, and how it changes with time after the onset of the stimulus. A photoreceptor cell requires approximately 50ms to reach the maximum output signal magnitude (Cao et al., 2007; Zele et al., 2008). Thus, if a target is present within the receptive field of the photoreceptor for less than this duration, the output is suboptimal, and can result in motion smear (Burr, 1980).

For smooth object motion, the relative effects of temporal subsampling and contrast polarity reversal predicted by the model largely align with the observers' data. Both of the additional temporal modulations were predicted to be mostly

unaffected by the target speed, which is in agreement with the observers' thresholds. Further, contrast polarity reversal was accurately described as providing better target resolvability than temporal subsampling. For ocular motion, the model does not predict that contrast polarity reversal provides any additional benefit to resolution thresholds compared to unmodulated stimuli, but does suggest that subsampling is relatively detrimental to performance. This indicates that the ocular jitter is providing sufficient spread of information across the temporal frequency range that it functions similarly to an additional temporal modulation. Thus, perhaps adding an extra modulation was ineffective; positional jitter may provide sufficient spectral expansion to mask the additional harmonics created by the additional temporal modulations. Positional jitter may also interfere with the magnitude of the TRF. However, the beneficial effect of contrast polarity reversal on resolution in the ocular motion condition is compatible with the a mechanism that originates at the TRF. The target in the ocular motion condition was able to move in all directions, and could be presented within the same receptive fields on multiple occasions throughout its trajectory. Thus, both on- and off-channels could be stimulated within receptive fields, enhancing the overall retinal signal initiated by the stimulus.

By adding temporal modulations to the stimuli, it has been demonstrated that harmonics are created in the Fourier domain. The spread of information across the temporal frequency axis may be exploited by the visual system in creating an accurate image of the target. Figure 55 and Figure 57 indicate that the additional harmonics are associated with a general decrease in the relative amplitudes of the spectra, which may be limiting the visual benefits of temporal modulations. However, a model designed to estimate the amplitude of target information

appearing within the WOV succeeded in accurately predicting only some aspects of the observer data. In order to fully describe the observers' data, the model must account for physiological aspects such as eccentricity, and the behaviour of photoreceptor cells in response to stimulation.

The model was designed to account for the effects of additional temporal stimulus modulations only in terms of the temporal harmonics they create. However, some aspects of the observers' data are only explained when the retinal response to the stimuli is included. This chapter therefore suggests that a complete description of the mechanism responsible for the effects of additional temporal modulations includes a combination of the retinal response to the stimulus input, and the sensitivity of the visual system to the stimulus characteristics.

Chapter 8: The effect of contrast polarity reversal on reading performance in central vision loss and in the normal periphery

8.1: Introduction

Visual disorders such as age-related macular degeneration (AMD) make performing daily tasks such as reading extremely challenging. The loss of central visual function forces patients to position visual targets they wish to view at more peripheral locations (usually at a preferred retinal locus, PRL; Fletcher & Schuchard, 1997). Performance in many tasks associated with reading becomes poorer with increasing peripheral eccentricity. This includes visual span (Legge et al., 2001), word recognition (Latham & Whitaker, 1996), acuity (Brown, 1972a, 1972b), and crowding (Hussain, Webb, Astle, & McGraw, 2012; Levi, 2008; Toet & Levi, 1992).

Chung, Mansfield, and Legge (1998) assessed and plotted reading speed as a function of print size for sentences viewed at a range of peripheral eccentricities. They demonstrated that the function describing the relationship shifted as retinal eccentricity increased, i.e. reading speed was slowed and the target print size required for a specific reading speed increased. However, the general shape of the function remained the same; as print size increases, the reading speed increases linearly until it reaches a plateau. The print size at which reading speed plateaus is known as the critical print size (CPS). Thus, as the eccentricity at which a sentence is read is increased, the CPS also increases, and reading speed is slowed.

The deficit in reading speed in macular disease has also been attributed to the increased fixational instability that accompanies foveal scotomas. Crossland,

Culham, and Rubin (2004) suggest that reading speed is proportional to fixational stability throughout the progression of AMD. Existing techniques for improving reading performance in AMD have attempted to reduce the influence of eye movements by presenting target sentences one word at a time; This rapid serial visual presentation (RSVP) technique prevents unnecessary slowing from eye movements (Rubin & Turano, 1992). RSVP increases reading speed compared to traditional page reading both in healthy eyes and in AMD, however the improvement is smaller in AMD (Rubin & Turano, 1994). As AMD patients have exaggerated eye movement patterns compared to those in healthy eyes (Kumar & Chung, 2014), this suggests the improved reading speed in RSVP over page reading is not completely explained by oculomotor behaviour. Alternatively, the source of increased accuracy from RSVP may be because crowding is eliminated, as presenting target sentences one word at a time reduces crowding by the previous and subsequent words in the sentence (Pelli et al., 2007). Crowding can be reduced for page reading by increasing the line spacing, both in the healthy periphery (Chung, 2004), and in AMD (Blackmore-Wright et al., 2013). However, this was shown to be ineffective in AMD patients (Chung, Jarvis, Woo, Hanson, & Jose, 2008). Similarly, increasing letter spacing did not improve reading speed in AMD (Chung, 2012).

Scrolling text paradigms have been shown to improve reading speed relative to performance in RSVP paradigms in visually impaired patients (Fine & Peli, 1995), for text sizes within eight times the acuity limit (Fine & Peli, 1998). Scrolling text has also been shown to reduce reading error rates, compared to static text (Walker, Bryan, Harvey, Riazi, & Anderson, 2016). Text scrolling allows fixation to be maintained, thus removing any detriment to reading from

abnormal oculomotor control. Another alternative to RSVP is elicited serial presentation (ESP; Arditi, 1999). Similar to RSVP, the text appears one word at a time in a predetermined location, however in ESP word onset is triggered by the observer. ESP gave superior performance over RSVP in low vision patients; reading latency was reduced by approximately half. This suggests that reading in low vision is enhanced by observer-directed progression through the sentence.

Haberthy and Yu (2016) have previously reported on the effects of adding temporal modulations to peripheral word targets. They compared reading performance for unmodulated single word targets to temporally subsampled targets, i.e. targets that periodically disappeared and reappeared. They found temporal subsampling was of limited benefit for peripheral reading in healthy observers. However, as discussed in Chapters 5 and 6, temporal subsampling may not be the optimal method of providing extra temporal modulations. Contrast polarity reversal however was shown to improve acuity for static targets, as well as for targets with smooth motion and exaggerated target jitter. Thus, while it is clear that reading speed is diminished in AMD, the cause of the reduction is unclear. Additionally, several reading techniques have been proposed, but the characteristics of the optimal technique for improving performance remains elusive.

In previous chapters, the resolution of peripheral targets was shown to improve when the contrast polarity of the target was reversed at periodic intervals. The experiments in this chapter extend these findings by examining how contrast polarity reversal influences performance in a peripheral reading task. The effect of contrast polarity reversal on reading speed and accuracy for scrolling text is

investigated in the periphery of observers with normal vision and in patients with macular degeneration. Scrolling text was chosen because it was shown to be superior to RSVP in patients with central vision loss (Fine & Peli, 1995). Additionally, the rate at which the text scrolled across the screen is controlled by the observer, to further optimise performance as suggested by Arditi (1999). While it has been suggested that upper case text is better for reading speed (Arditi & Cho, 2007), using mixed-case is more salient to real-world situations. Reading speed has been shown to be faster for target fonts that are fixed width (as opposed to proportionally-spaced) (Mansfield, Legge, & Bane, 1996) and serif (as opposed to sans-serif) (Arditi & Cho, 2005; Beymer, Russell, & Orton, 2008). Accordingly for this experiment, Courier font was selected, as it has of both of these beneficial characteristics.

In Chapter 6 it was demonstrated that the effects of contrast polarity reversal are robust to target jitter, thus unstable fixation in the patient population is not expected to interfere with performance. For healthy observers, reading speed and accuracy is examined at 6° in the upper visual field. This eccentricity is close to estimates of average PRL eccentricity (Markowitz & Aleykina, 2010; Shima et al., 2010). Performance is assessed for four temporal modulation conditions: three contrast polarity reversal conditions, and a control condition with no additional temporal modulation. A reversal every 66.7ms was shown in Chapter 5 to be the optimum reversal rate for slowly moving peripheral targets. This reversal rate aligns with photoreceptor temporal response functions at the examined luminance (Cao et al., 2007; Swanson et al., 1987). Accordingly, one of the reversal conditions examined here was 70.6ms reversal, the closest available to 66.7ms reversal. As the temporal dynamics of photoreceptor function are slowed in AMD

patients (Jackson, Owsley, & Curcio, 2002), a second, slower reversal rate of 129.4ms reversal was included. This reversal rate is within the range of rates that gave a beneficial effect on resolution thresholds in Chapter 3. As previously discussed, contrast polarity reversal doubles the effective stimulus contrast compared to the control condition. Accordingly, the 129.4ms reversal condition was conducted at both full and half contrast values. For the full contrast condition, target luminance reversed from 85.0cdm^{-2} (white) to 0.5cdm^{-2} (black), a Michelson contrast of 0.99. For the half contrast condition, target luminance reversed between 63.7cdm^{-2} (light grey) and 21.2cdm^{-2} (dark grey), a Michelson contrast of 0.50. The background luminance was 44.8cdm^{-2}. In the unmodulated control condition the target sentence was allocated a positive or negative stimulus contrast (a luminance of 85.0cdm^{-2} or 0.5cdm^{-2}) at random, which it remained for the duration of the trial. Culham, Fitzke, Timberlake, and Marshall (1992), and Legge, Rubin, Pelli, and Schleske (1985) suggest that observers read positive and negative contrast equally well. However, in order to identify any potential bias from stimulus contrast polarity, the reading speed and accuracy of observers in the positive and negative contrast unmodulated trials were separated and compared.

Reading performance in AMD patients was assessed using the same paradigm. However, instead of maintaining a set peripheral target location, patients were encouraged to use a PRL to perform the task. Gaze position was not monitored, as foveating the target would be detrimental to resolution. The reading speed and accuracy was examined for three temporal modulation conditions in patients. Target sentences were presented with contrast polarity reversal every 66.7ms or 133.3ms (after every fifth or tenth video frame), or with no additional temporal modulation. Patients were presented target sentences at maximum contrast (white

targets were presented at 85.0cdm^{-2}; black targets at 0.5cdm^{-2}. The target Michelson contrast was therefore 0.99).

It is expected that the effects on reading speed of the additional temporal modulations will be maximal for target print sizes around the CPS. Thus, the ratio of the target print size and the CPS was calculated, and the relationship between the effect of contrast polarity on reading speed and this ratio was examined.

8.2: Methods

8.2.1: Healthy observers

8.2.1.1: Participants

Six participants took part in this experiment (age *M* 24.00 years, *SD* 2.37 years), all native English speakers. Participant reading ability was assessed with the test of word reading efficiency (TOWRE, Torgesen, Wagner, & Rashotte, 1999). All participants were required to achieve a standardised total word reading efficiency score of "average" or higher (≥80) to participate.

8.2.1.2: Apparatus

This experiment was performed on a gamma-corrected 50.8cm CRT monitor (Iiyama Vision Master Pro 514, Iiyama Corporation, Hoofddorp, Netherlands), with screen resolution 1280x1024 pixels and 85Hz refresh rate (giving a frame duration of 11.8ms) using a Mac Pro (Mid 2010; Apple Inc., Cupertino, CA, USA). Observers were sat with a chin and forehead rest at a screen distance of 75cm. At this distance, a pixel subtends 1.79x1.79arcmin. Fixation was monitored using an EyeLink 1000 eye tracker (SR Research, Ltd., Mississauga, Ontario,

Canada) at a sampling rate of 250Hz. Typical foveating saccades of 6° occur at durations of the order of 50ms, an order of magnitude above the sample rate (Whittaker & Cummings, 1990), so the eye tracker was capable of recording any foveations of the target during each trial.

8.2.1.3: Stimulus

Full sentences were presented at 6° in the superior visual field. Sentences were chosen at random from a set of 401 sentences from the IURead collection (Xu & Bradley, 2015). These are complete sentences with a mean length of 60.06 (*SD* 0.74) characters including spaces, containing an average of 12.00 (*SD* 1.14) words at 10-year-old reading level. Chung et al. (1998) reported that at 5° eccentricity, healthy observers had a CPS around 0.7°. Thus, the maximum letter height in this experiment was 1° (such that it had a lower-case x-height of 0.75°). An example stimulus is shown in Figure 59.

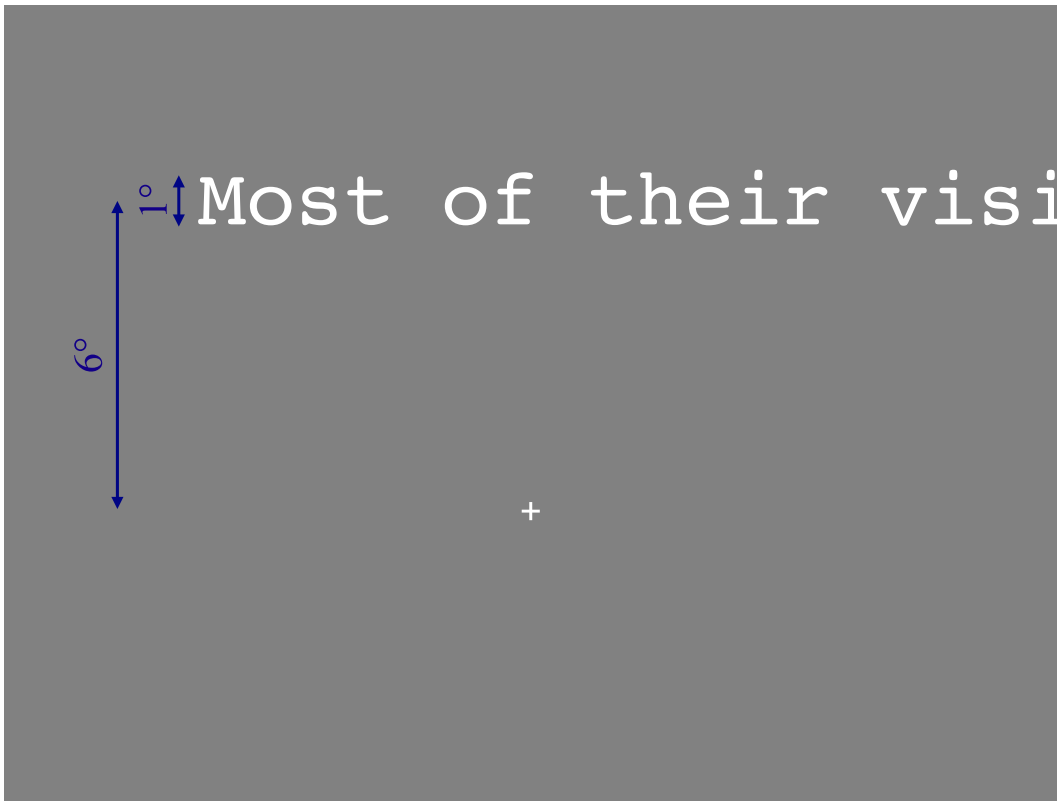

Figure 59: Example stimulus for the main experiment. Participants fixated on the cross while moving the sentence across the screen with the mouse. The blue arrows were not visible during the experiment.

Experiment 3.3 demonstrated improvements in acuity for peripheral targets with contrast polarity reversal rates between 39.9-106.4ms at low speeds. However, photoreceptor recovery is slower in eyes with AMD (Dimitrov, Guymer, Zele, Anderson, & Vingrys, 2008), so alongside the reversal rate identified as optimal in previous studies (66.7ms), a longer reversal rate was also selected. Due to the higher screen refresh rate of the screen used in this experiment, the precise reversal rates used in Experiment 3.3 and when testing the patient group were unavailable. Accordingly, the reversal rates examined in this experiment were 0ms, 70.6ms, and 129.4ms (no reversal, and reversal every 6 and 11 video frames, respectively).

The participants were recorded during testing, and after each session the number of errors and rereads was counted. Using the example sentence from Figure 59:

Most of their visit was spent in the hospital emergency room

possible errors included omission, e.g. *Most of their visit was in the hospital emergency room*;

addition, e.g. *Most of their visit here was spent in the hospital emergency room*;

or misreading of words, e.g. *Most of the visit was spent in the hospital emergency room*.

8.2.1.4: Procedure

At the beginning of each trial, the first word of the sentence appeared above the fixation cross. The participant was instructed to use the mouse to scroll the text across the screen by moving the mouse laterally, thus giving participants control over text speed, location of the target word in the visual field, and allowed them to reverse the direction of the motion as desired. Prior to the test phase, the participants were given twelve practice trials to allow them to practice moving the sentence as required and suppressing target foveations.

Each trial began with an auditory cue (a brief tone), after which participants read the sentences aloud as quickly and accurately as possible. Sentences were chosen at random and presented in blocks of 44 trials (11 of each condition in a randomised order), after which the participant could rest. At the beginning of each

block, a nine-point eye tracker calibration procedure was undertaken. Each session lasted 45 minutes to one hour, in which the participants completed three to five blocks, depending on reading speed and fatigue. Data collection required two to four sessions from each participant, usually on different days. Collection was completed when the participant reached 75 useful trials (in which no saccades were made towards the target) for each condition. A trial was discarded as invalid if a saccade was detected in which the gaze position was 3° above fixation at any point in the trial.

8.2.2: Patients with central vision loss

8.2.2.1: Participants

Four patients with bilateral AMD, and one with bilateral myopic macular degeneration participated in this study (age *M* 73.2, *SD* 10.7 years). Their visual characteristics are shown in Table 3.

Table 3: Visual characteristics of the five observers with macular degeneration.

Observer	Gender	Age	Form	Years since onset	Reading acuity (logMAR)	CPS* (logMAR/°)	Max. RS^ (wpm)	PRL OS (°)$^{+}$	PRL OD (°)$^{+}$
1	M	81	Dry	7	1.18	1.3/1.18	48	14.29	7.28
2	F	84	Wet	17	1.12	1.2/1.02	35	19.01	7.68
3	F	75	Wet	13	0.28	0.7/0.42	125	1.84	2.18
4	F	57	Wet	3	0.20	0.5/0.26	85	1.88	1.78
5	M	69	Myopic	33	0.72	0.9/0.63	26	12.49	4.34

*Critical print size. ^Reading speed. $^{+}$Absolute PRL eccentricity, relative to the centre of the anatomical fovea.

The location of the PRL was evaluated with microperimetry using the CenterVue Macular Integrity Assessment (CenterVue Inc., Fremont, CA, USA). Other measures of patient visual ability was assessed prior to testing using the

MNREAD continuous reading acuity charts (Mansfield, Ahn, Legge, & Luebker, 1993).

8.2.2.2: MNREAD

For each patient, the reading time was recorded for short sentences. Patients read binocularly using corrective lenses, at a distance of 40cm. Each time a sentence was read successfully, the print size was reduced until it became too small for the patient to read. Reading acuity is calculated according to the minimum print size the observer could read, corrected for accuracy of reading. To calculate the CPS and maximum reading speed, reading time was plotted for each sentence as a function of the print size on log-log axes. An example of this plot is shown in Figure 60. The observer whose data is plotted is a typical example of reading performance without any visual defects.

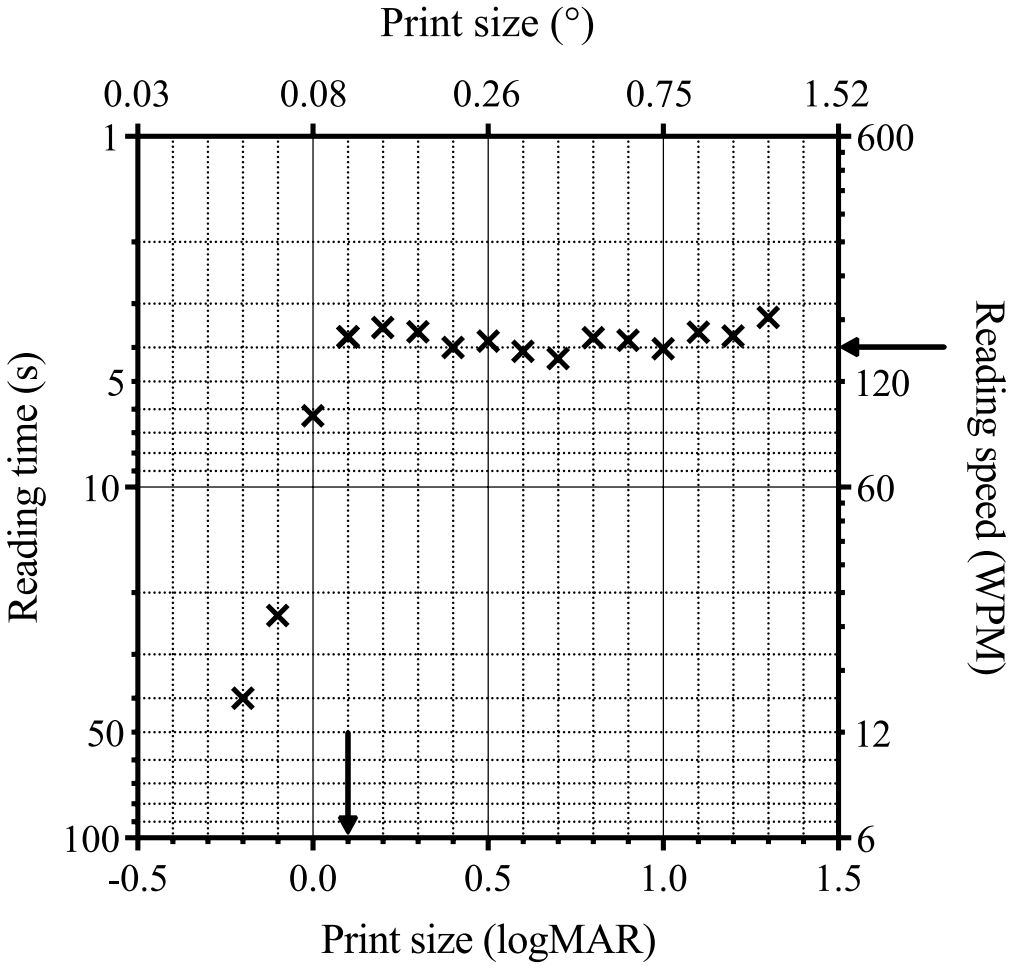

Figure 60: Example MNREAD graph for a typical observer with no visual defects. Reading time for short sentences is plotted as a function of the print size of the sentence. Arrows on the ordinate and abscissa represent the observer's maximum reading speed and critical print size, respectively; see text for details.

The reading time reduces as print size is increased up to a plateau. The reading speed of this plateau represents the maximum reading speed of the observer. The print size at which the reading time plateaus is the CPS. These measures are highlighted with arrows on the right y-axis and on the x-axis, respectively. The observer in Figure 60 was assessed for foveal reading. The patients in this study must necessarily read the target sentences in the periphery. The MNREAD remains suitable for testing outside the fovea; the scaling hypothesis predicts that

the plot of reading time as a function of print size shifts horizontally as peripheral eccentricity is increased (Chung et al., 1998). Accordingly, the CPS will be increased in patients viewing at more eccentric PRLs, but the shape of the plot and the maximum reading speed will remain relatively constant.

8.2.2.3: Apparatus

For patients with foveal scotomas, foveating the target is naturally detrimental to performance. Thus, the experiment was performed without eye tracking. Stimuli were presented on the experimental apparatus described in the General Methods chapter. Patients were seated at a screen distance of 100cm. Patients wore full aperture lenses during testing that corrected the refractive error and included an appropriate addition for reading at this distance. This ensures that reading during the examination was not limited by optical blurring.

8.2.2.4: Stimulus

The stimulus was modified for use with patients. The fixation cross was replaced with vertical lines to aid peripheral localising. The same list of sentences was used in presentation to patients. Letter size was based on the severity of vision loss in each patient. Patients with a CPS smaller than 1° were presented with targets at a lower-case x height of 0.75° (thus a maximum target height of 1°), while for patients with a CPS greater than 1° the target height was doubled to a lower-case x height of 1.5° (maximum height of 2°). An example stimulus is shown in Figure 61 for both target sizes.

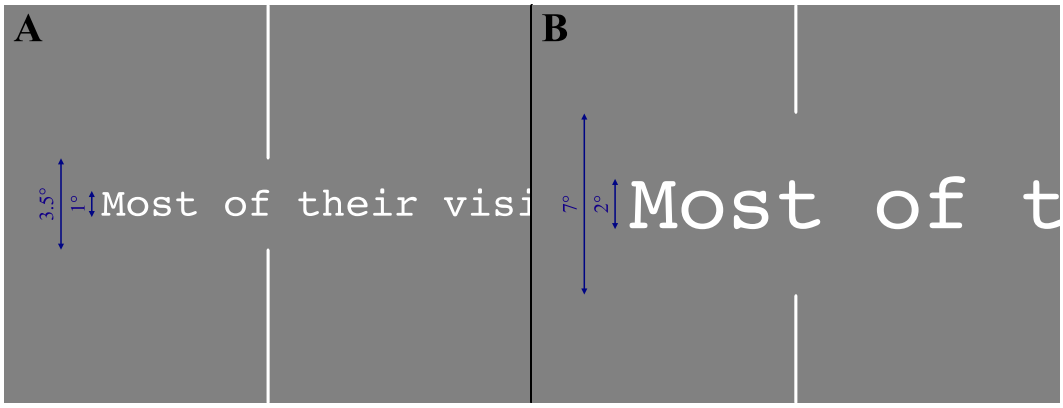

Figure 61: Example stimulus for testing in central visual loss patients. Patients were free to fixate in a location suitable to present the stimulus in their preferred retinal locus while moving the sentence with the mouse. Two different target sizes were used for different levels of vision loss severity; (A) target text with a lower-case x-height of 0.75°, as was presented to patients with a CPS smaller than 1°. (B) Target text with a lower-case x-height of 1.5°, as was presented to patients with a CPS greater than 1°. Blue arrows and text were not visible during the experiment.

Three modulation conditions were examined with patients: no modulation (no contrast polarity reversal), 66.7ms reversal (contrast polarity reversal after every fifth video frame), and 133.3ms reversal (reversal after every tenth video frame). These reversal rates differ because the patient and healthy participant groups were examined using different monitors with different screen update rates. Stimuli were presented at the extreme luminance values (85.0cdm^{-2} and 0.5cdm^{-2}).

8.2.2.5: Procedure

Similarly to healthy observers, patients completed 12 practice trials (four of each condition) to become accustomed to the procedure. Both a visual and an auditory cue (a flicker of the fixation lines and a brief tone, occurring simultaneously) indicated trial onset. The first word of the target sentence appeared within the fixation lines. Patients were instructed to read the sentence as quickly and accurately as possible, moving the mouse to scroll the sentence as desired.

Sentences were presented in blocks of 30 (10 of each condition), with a break after each block. Patients completed one practice block and five test blocks (150 total test trials, 50 of each condition) in a single session.

8.3: Results

8.3.1: Healthy observers

8.3.1.1: Reading speed

The participants' reading speed S in words per minute was calculated for each sentence using Equation 10.

$$S = \frac{L \times 60}{T} \tag{10}$$

In which L is number of words in the sentence, and T the time taken by the observer to read the sentence (in seconds), from the initial stimulus presentation until the last word was finished aloud. Figure 62 shows the average reading speed for the contrast polarity reversal conditions for each participant (on the y-axis), as a function of the reading speed without contrast polarity reversal (on the x-axis). The dotted line represents equal reading speed between conditions.

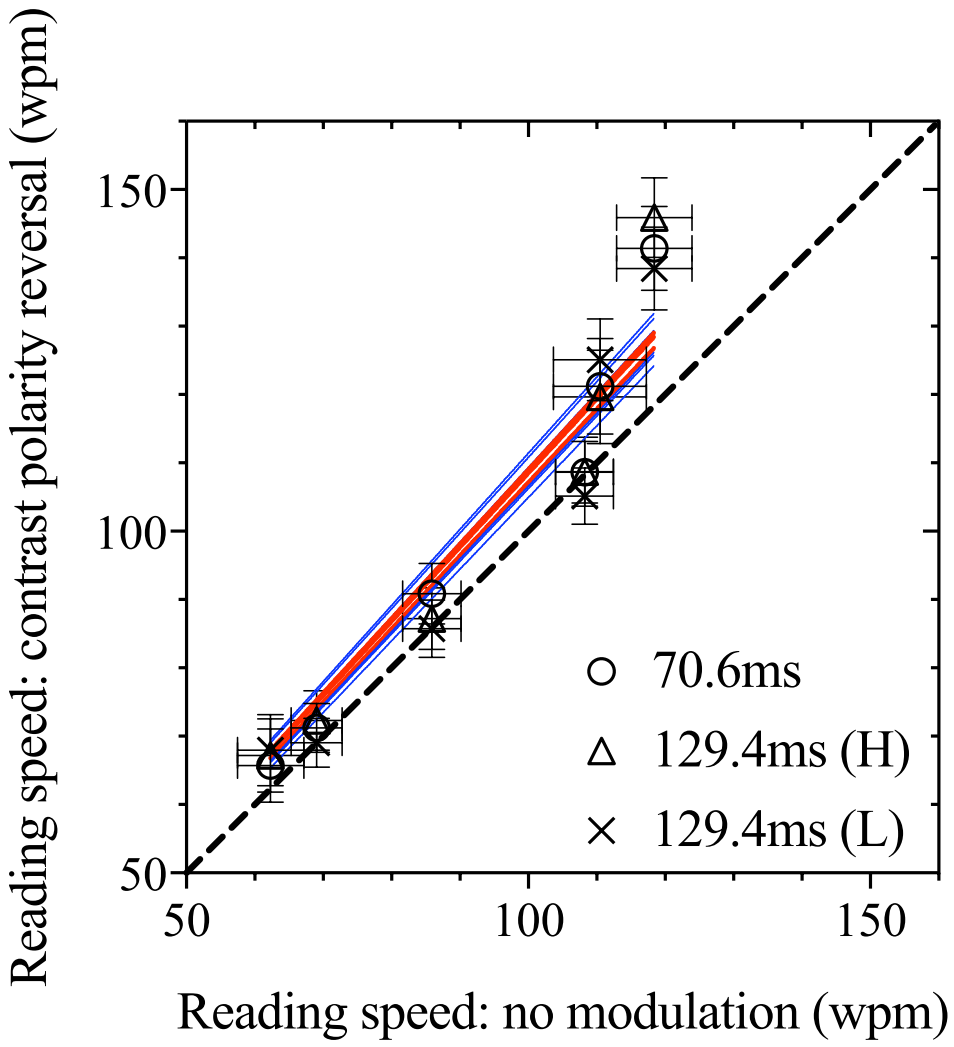

Figure 62: Reading speed for sentences with reversing contrast polarity as a function of the corresponding reading speed for sentences without temporal modulation (in words per minute). Data points are the average and 95%CI for each observer. Circles show reading speed for contrast polarity reversal every 70.6ms (after every sixth video frame). Triangles and crosses are reading speeds for reversal every 129.4ms, at high (H) contrast difference (reversal between target luminance of 85.0cdm^{-2} and 0.5cdm^{-2}), and low (L) contrast difference (between 63.7cdm^{-2} and 21.2cdm^{-2}), respectively. The dashed line represents equal reading speed for modulated and unmodulated conditions, thus data points above the diagonal represent a contrast polarity reversal condition whereby reading speed was faster than the corresponding unmodulated condition. Regression lines (red, 95%CI in blue) are fit to each condition separately, across participants.

Regression lines were fit to the three contrast polarity reversal conditions separately, constrained to intercept the y-axis at the origin. This restriction does

not allow for simple additive benefits to be quantified, and negates the potential for the effect to switch from beneficial to detrimental or the reverse. However, it is a more conservative measure of the general effect of contrast polarity reversal on reading performance. This is appropriate for identifying stimulus modulations that provide benefits across the range of patient visual ability. The slope of the regression lines represents the magnitude of the effect of contrast polarity reversal. A value of the slope between zero and one would indicate contrast polarity reversal has a detrimental effect on reading speed, while a value above one would indicate a beneficial effect. Thus, the best-fit values of the regression line slopes were calculated, and extra sum-of-squares F tests were used to examine whether they were statistically distinguishable from unity (representing no effect).

The slope of the linear regressions for all three modulation conditions suggested a significant improvement in reading speed compared to the unmodulated condition. The best-fit slope value for the 70.6ms reversal condition was calculated as 1.09 (*SE* 0.012), which was significantly different from unity ($F(1,507) = 53.3$, $p<.0001$). For the 129.4ms, higher contrast reversal condition, the slope was also calculated as 1.09 (*SE* = 0.012), and accordingly also significantly different from unity ($F(1,498) = 53.7$, $p<.0001$). For the 129.4ms, lower contrast reversal condition, the slope was 1.07 (*SE* = 0.011), also significantly different to unity ($F(1,507) = 40.9$, $p<.0001$).

8.3.1.2: Reading accuracy

The number of errors (as defined above) was counted on each trial. Figure 63A shows the absolute number of errors made by each participant across testing,

whereas Figure 63B shows the percentage of trials on which errors were made, thus controlling for the number of successful trials. As in Figure 62, the error counts for each of the contrast polarity reversal conditions are shown as a function of the error count for the condition without reversal. Data points below the diagonal suggest fewer errors were made by that observer in the applicable contrast polarity reversal condition than in the no modulation condition.

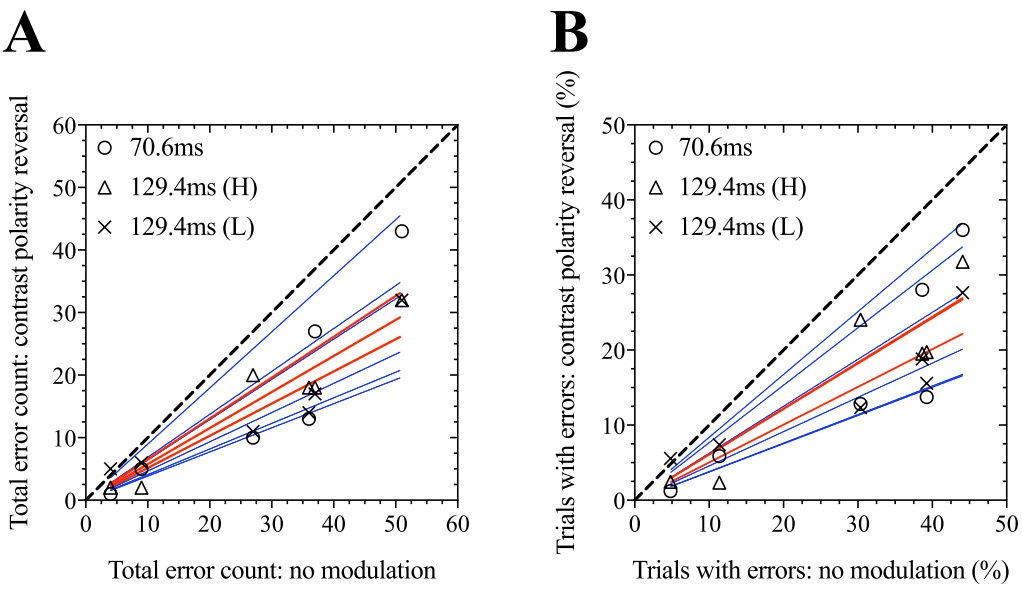

Figure 63: Graph showing the errors in reading made by healthy observers during testing. H and L indicate that the target was in the high or low contrast difference condition, respectively. (A) Record of the total number of errors made (including multiple errors within a single trial). (B) The percentage of trials on which an error was made. Regression lines for each contrast polarity reversal condition in red, 95%CI in blue.

Figure 63 shows that generally more errors were made when reading sentences without contrast polarity reversal. This is supported by the regressions in Figure 63A, which were all calculated to be significantly distinguishable from a line with unity slope (70.6ms reversal: best fit slope value 0.65 (*SE* 0.09), $F(1,5) = 13.37$, $p=.02$; 129.4ms, high contrast: slope 0.58 (*SE* 0.04), $F(1,5) = 98.70$, $p=.0002$; 129.4ms, low contrast: slope 0.51 (*SE* 0.05), $F(1,5) = 93.54$, $p=.0002$). Similarly

in Figure 63B, controlling for differences in the number of successful trials, the regressions were also all calculated to be significantly distinguishable from unity (70.6ms reversal: best fit slope value 0.61 (*SE* 0.09), F(1,5) = 19.24, p=.007; 129.4ms, high contrast: slope 0.61 (*SE* 0.06), F(1,5) = 41.82, p=.001; 129.4ms, low contrast: slope 0.50 (*SE* 0.05), F(1,5) = 108.50, p=.0001).

8.3.1.3: Difference between black and white stimulus presentation

As the stimulus alternated between black and white in the contrast polarity reversal conditions, the condition without modulation was presented in either black or white for the duration of the trial. A bias towards one polarity may thus influence results. Average reading speeds were therefore compared for black and white stimulus presentation separately (without modulation), shown in Figure 64, and the total number of errors in Figure 65.

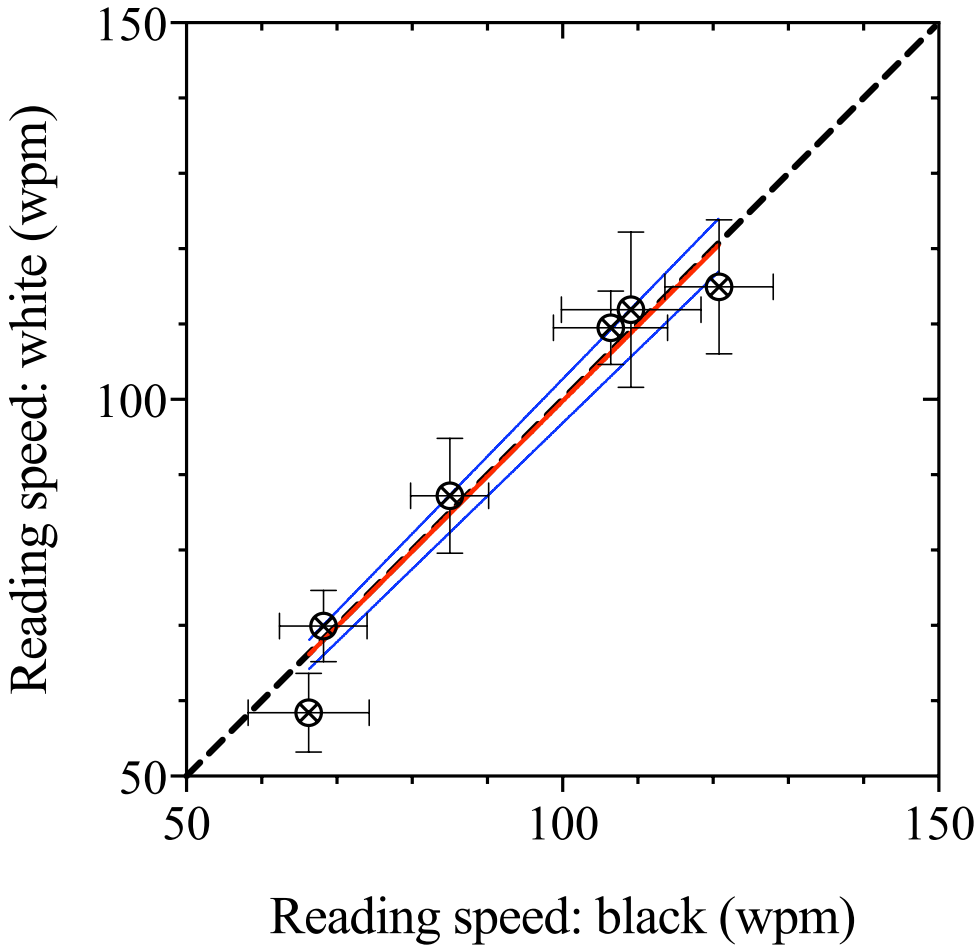

Figure 64: Graph comparing healthy observers' peripheral reading speed (in words per minute) for sentences presented black (target luminance 0.5cdm^{-2}) and white (target luminance 85.0cdm^{-2}), without additional temporal modulation. Reading speed for black and white presentations are shown on the abscissa and ordinate, respectively. The regression line is shown in red (95%CI in blue). Equal reading speed for black and white presentations is shown with the black dashed line.

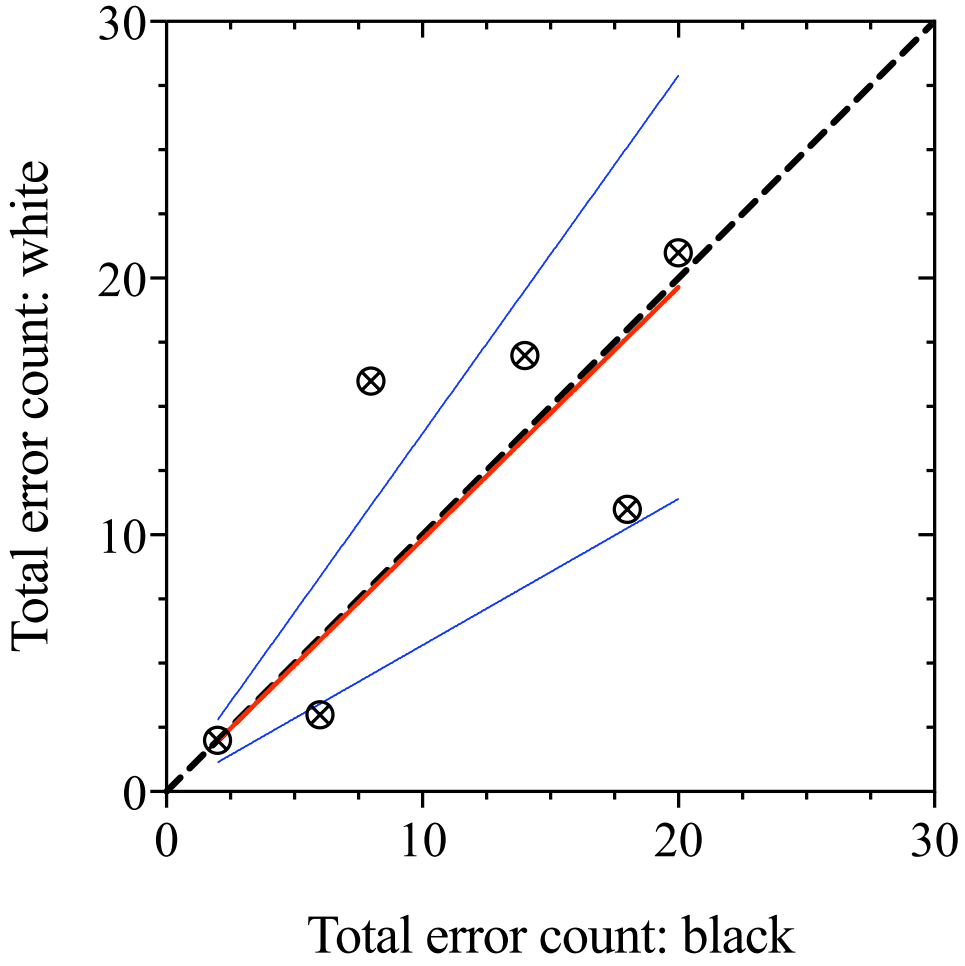

Figure 65: Total number of errors made by each of the healthy observers in the unmodulated condition. Counts for black (target luminance 0.5cdm^{-2}) and white (target luminance 85.0cdm^{-2}) presentations are shown on the abscissa and ordinate, respectively. Regression lines in red (95%CI in blue).

The best-fit value of the slope of the regression line in Figure 64 was calculated as 0.998 (*SE* 0.015), a value not significantly different from the diagonal ($F(1,231) = 0.02$, $p>.05$). Similarly, the slopes of the regression line in Figure 65 was 0.982 (*SE* 0.160), which was not significantly distinguishable from unity ($F(1,5) = 0.01$, $p>.05$). Thus, reading speed and accuracy were not affected by the contrast polarity of the presented sentence, but rather by the modulation itself.

8.3.2: Patients with central vision loss

8.3.2.1: Reading speed

Reading speed was calculated for each patient using Equation 10. Figure 66 compares average reading speed for the contrast polarity reversal conditions for each of the patients (on the y-axis), as a function of the reading speed without contrast polarity reversal (on the x-axis). The dotted line represents equal reading speed between conditions.

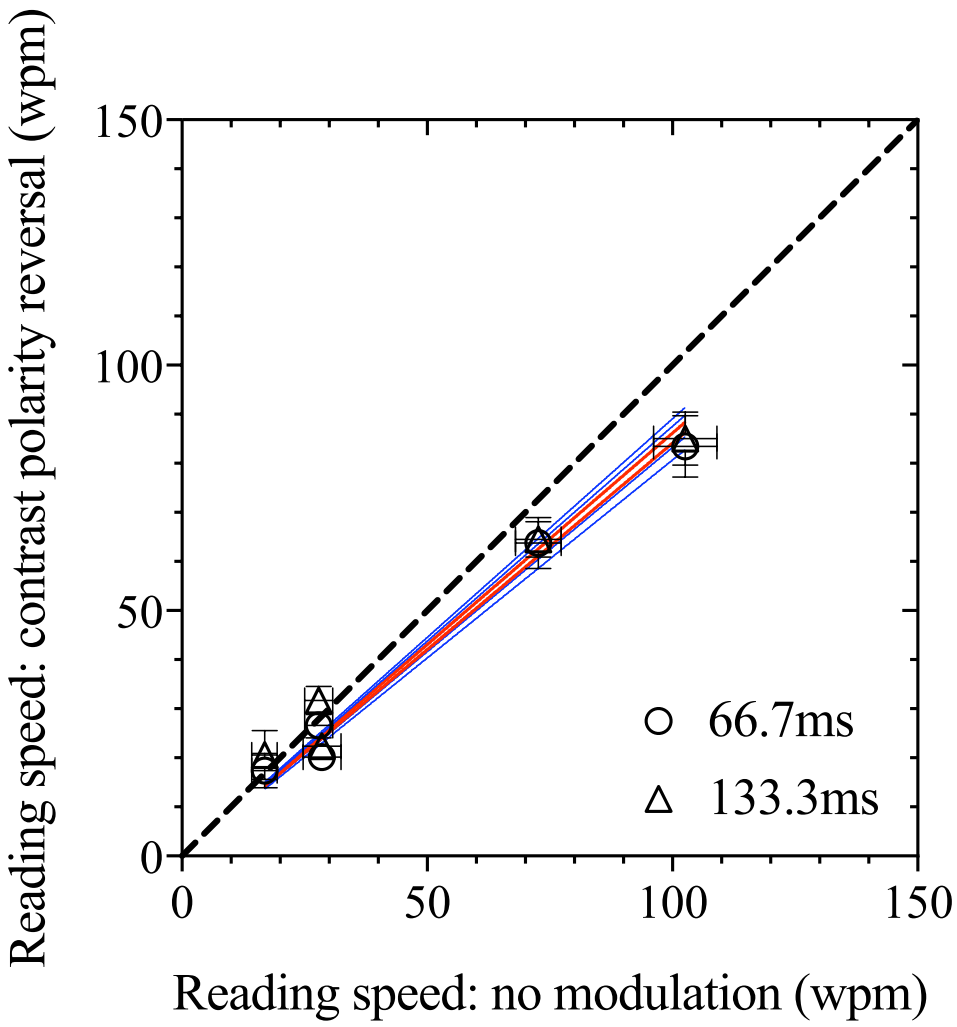

Figure 66: Reading speed for sentences with reversing contrast polarity as a function of the corresponding reading speed for sentences without temporal modulation (in words per minute) for four patients with bilateral AMD and one with myopic macular degeneration. The dashed line represents equal reading speed for modulated and unmodulated conditions. Regression lines (red, 95%CI in blue) are fit to each condition separately, across patients.

The regression lines in Figure 66 are fit to the two temporal modulation conditions separately, and confined to the origin. The slope of the linear regressions for both modulation conditions suggested that contrast polarity reversal was detrimental to reading speed compared to the unmodulated condition. The best-fit slope value for the 66.7ms reversal condition was calculated as 0.84 (*SE* 0.017), which was significantly different from unity ($F(1,96) = 84.5$,

p<.0001). For the 133.3ms reversal condition, the slope was calculated as 0.86 (*SE* = 0.015), also significantly different from unity (F(1,106) = 88.1, p<.0001).

8.3.2.2: Errors in reading

The accuracy of reading was assessed as outlined above. The error counts for the contrast polarity reversal conditions is plotted for each patients against the corresponding error count for the unmodulated condition in Figure 67. Figure 67A shows the absolute number of errors across all trials, while Figure 67B shows the proportion of trials on which errors were made.

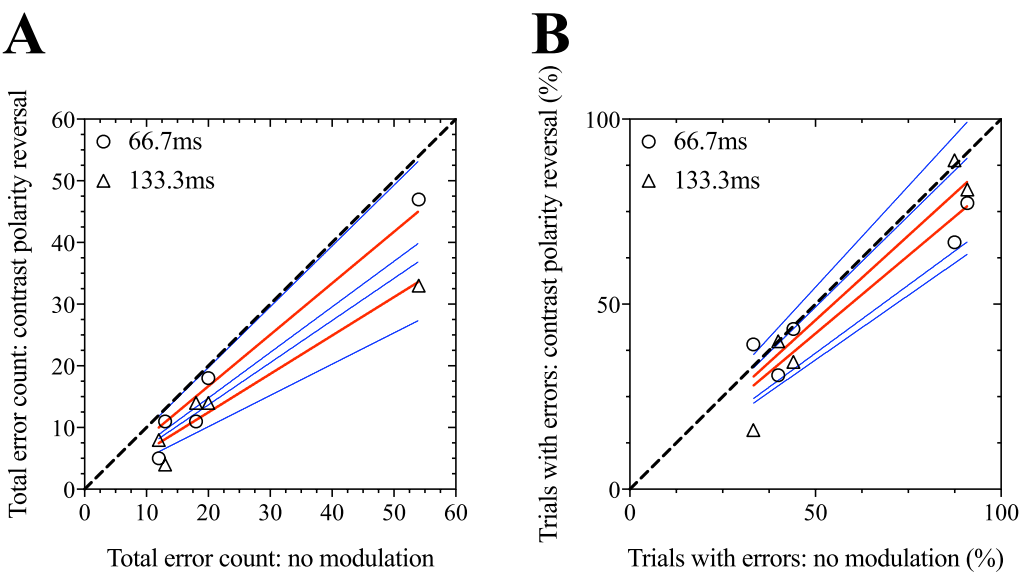

Figure 67: The accuracy of patients during reading as a function of modulation condition. (A) The total number of errors made, including multiple errors within a single trial. (B) The percentage of trials on which an error was made. Regression lines (in red, 95%CI in blue) are fit for each contrast polarity reversal condition separately, constrained to the origin.

Figure 67 indicates that in general patients read more accurately in the contrast polarity reversal conditions. For the total number of errors made during all trials of each condition in Figure 67A, the slope coefficients for both modulation

conditions were significantly below unity, suggesting fewer errors were made than in the corresponding unmodulated condition (66.7ms reversal: slope coefficient 0.83, *SE* 0.054; F(1,4) = 9.2. p=.038. 133ms reversal: slope coefficient 0.62, *SE* 0.042; F(1,4) = 81.4, p=.0008). Figure 67B controls for differences in the number of completed trials in each condition by assessing error rate in terms of the percentage of trials on which at least one error was made. Patients made significantly fewer errors in the 66.7ms reversal condition than the unmodulated condition (slope coefficient 0.84, *SE* 0.051; F(1,4) = 9.5, p=.037). However, the proportion of trials in which errors were made in 133.3ms reversal condition was not significantly different from the unmodulated condition (slope coefficient 0.91, *SE* 0.064; F(1,4) = 1.8, p>.05).

8.3.2.3: Relationship with CPS

Legge, Rubin, and Luebker (1987) examined the effect of contrast on reading rate. They demonstrated that reading rate is most dependent on contrast when letter size is below the CPS. Thus, the effect that contrast polarity reversal has on sentence reading is expected to be maximal at print sizes lower than, or at least close to the CPS. To investigate this, for each observer the difference in reading speed for each of the modulated conditions and the unmodulated control condition was calculated. This is plotted in Figure 68 as a function of the ratio of the print size of the target sentences presented to the observer and that observer's CPS.

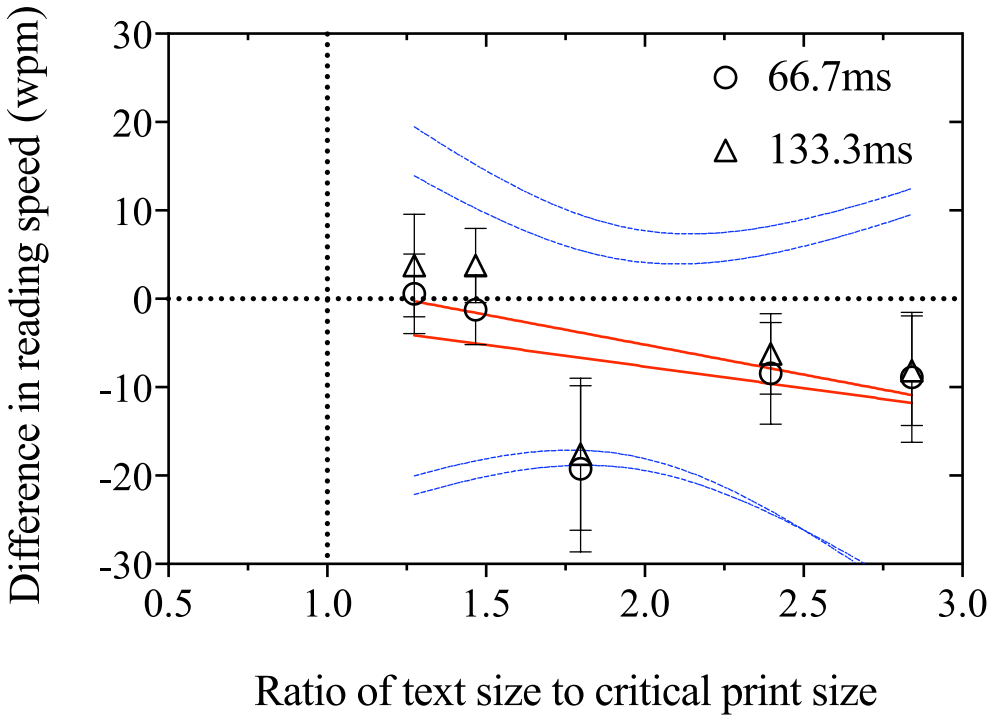

Figure 68: Plot of the difference in reading speed between modulated and unmodulated conditions, as a function of the ratio of the print size to the CPS. Values above zero on the ordinate indicate an observer's reading speed was faster in the modulated condition than in the unmodulated condition. Values above unity on the abscissa indicate the target print size was greater than the observer's CPS, i.e. a value of two on the abscissa indicates the target print size was twice that observer's CPS. Regression lines (in red, 95%CI in blue) are fit to each condition separately.

As the ratio of text size to CPS increases above unity in Figure 68, the effect of contrast polarity reversal on reading speed goes from an improvement to a detriment. The regression lines indicate a negative correlation, suggesting that the beneficial effect of contrast polarity reversal occurs only when the print size is very close to the CPS, as predicted. To further demonstrate this, in Figure 69 the effect of contrast polarity reversal on reading speed is examined for print sizes within and without one and a half times the CPS (ratios below 1.5 and above 1.5, respectively) separately. Patients for whom the print size was within 1.5 times the

CPS and patients for whom the print size was greater than 1.5 times the CPS are shown in in Figure 69A and B, respectively.

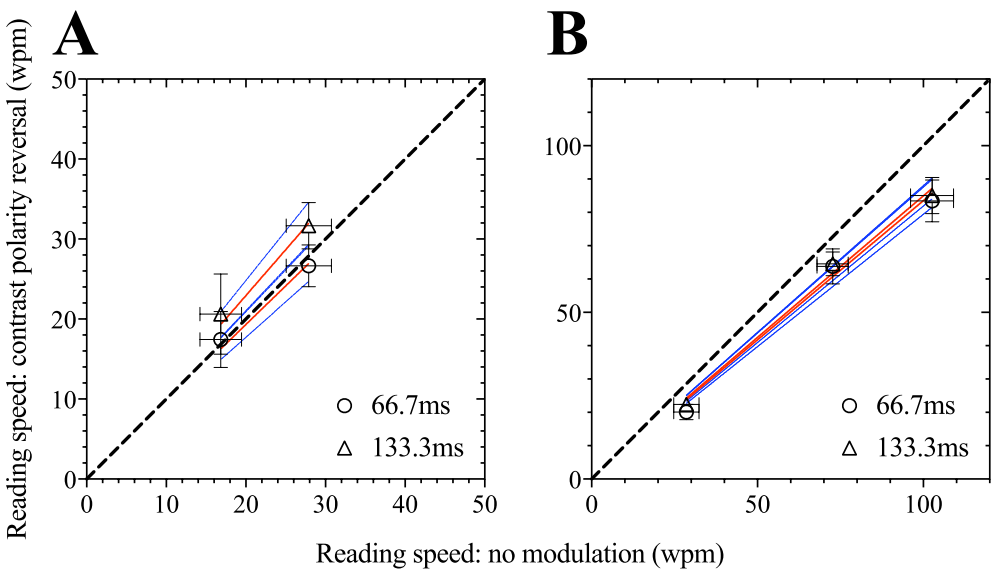

Figure 69: Reading speed for sentences with reversing contrast polarity as a function of the corresponding reading speed for sentences without temporal modulation. Patients are separated by the ratio between the print size at which the target sentences were presented, and their individual calculated CPS. (A) Patients for whom this ratio was below 1.5 (patients 1 and 2 in Table 3). (B) Patients for whom this ratio was above 1.5 (patients 3, 4, and 5 in Table 3). Regression lines (red, 95%CI in blue) are fit to each condition separately, across patients.

Figure 69 indicates that the effect of reversing the contrast polarity is most beneficial at print sizes close to the CPS. Patients for whom the target text height was within 1.5 times the CPS (Figure 69A) read significantly faster in the 133.3ms reversal condition than in the unmodulated condition. The slope coefficient was 1.15 (*SE* 0.046), significantly above unity ($F(1,29) = 10.1$, $p=.0035$). The 66.7ms reversal condition showed no significant effect on reading speed (slope coefficient 0.97, *SE* 0.039; $F(1,30) = 0.8$, $p>.05$). However, reading speeds in patients presented with target sentences larger than 1.5 times the CPS (Figure 69B) were significantly slowed by contrast polarity reversal. The best-fit

slope value for the 66.7ms reversal condition was calculated as 0.84 (*SE* 0.023), which was significantly different from unity ($F(1,52) = 50.3$, $p<.0001$). For the 133.3ms reversal condition, the slope was calculated as 0.85 (*SE* = 0.018), and was also significantly different from unity ($F(1,56) = 69.6$, $p<.0001$).

8.4: Discussion

Experiments in previous chapters demonstrated that resolution thresholds for peripheral targets can be reduced by periodically reversing the contrast polarity of the target. In this chapter this modulation was applied to peripherally viewed sentences. Observers with normal visual function read sentences at 6° in the superior visual field, and patients with macular degeneration read at the field location chosen by them. Healthy observers read temporally modulated sentences faster and more accurately than unmodulated sentences. This effect was observed across two reversal rates and two contrast ranges. In the patient group however, although fewer errors were made in the modulated conditions, reading speed was reduced by contrast polarity reversal. However, the proximity of the target print size to the patients' CPS was shown to influence the effect of contrast polarity reversal on patients' reading speed. Patients who read the target sentences at text heights close to their CPS were shown to have improved reading speeds in the 133.3ms contrast polarity reversal condition compared with the unmodulated condition. However, patients reading at larger text sizes were markedly slowed by the contrast polarity reversal. The TRF of photoreceptors in macular disease takes longer to peak than it does in healthy eyes (Jackson et al., 2002). This may be the reason that the 66.7ms reversal rate condition was less effective at increasing reading speed than the 133.3ms reversal condition.

These results suggest that contrast polarity reversal may benefit peripheral reading in patients with restricted foveal vision. However, the benefit appears to be restricted to text sizes close to the CPS of the observer. Text size in typical publications is at a lower-case x-height of approximately 0.20-0.26° (Legge & Bigelow, 2011). Thus, the usage of contrast polarity reversal may be limited to magnified digital text. So far however only two patients have been examined with target print sizes close to their CPS. Thus, more extensive examination is required to reach firm conclusions about the effects of contrast polarity reversal on reading speed in macular disease patients. The experiments in this chapter provide a basis for an in-depth study of the use of temporal modulations in improving function in useful visual field locations in patients with macular disease. While these experiments do suggest a potential improvement, a future study is necessary to establish the situations in which contrast polarity reversal may be a suitable technique. The healthy observers that participated in this experiment were far younger than the patient group. Photoreceptor density has been shown to reduce with typical aging (Curcio, 2001; Curcio, Millican, Allen, & Kalina, 1993), and aging can also affect the opacity of the ocular media (Ruddock, 1965), resulting in potential glare from the contrast polarity reversal conditions. An age-matched group is therefore a more appropriate control. Alternatively, the use of contrast polarity reversal could be examined in central vision loss disorders not associated with aging, such as Stargardt's disease (Fishman, Farber, Patel, & Derlacki, 1987).

In the patient assessment, eye position data were not collected. Thus, it is not possible to confirm whether the patients were viewing sentences using their PRL. By assessing patients using a scanning laser ophthalmoscope (SLO), the precise

retinal location of the target can be monitored. Timberlake, Peli, Essock, and Augliere (1987) examined reading in the PRL and other locations in the visual field in AMD patients, and found that the PRL was not necessarily the location at which reading was fastest. Examining performance with a SLO will support evaluation of the optimum technique for peripheral reading with contrast polarity reversal, and patients could be trained in positioning targets accordingly.

Chapter 9: General discussion

9.1: Summary of findings

9.1.1: Peripheral visual acuity for moving targets

It is well observed that many aspects of visual performance degrade as the eccentricity of a target increases (for reviews, see Battista, Kalloniatis, and Metha, 2005, and Strasburger, Rentschler, and Jüttner, 2011). Patients with age-related macular degeneration (AMD) and other visual disorders are often forced to view objects in the periphery. As a result, performance in acuity, reading, and other important tasks is impaired (e.g. Latham & Whitaker, 1996; Legge, Mansfield, & Chung, 2001). In most cases, there is no cure for the central vision loss associated with AMD. Thus, the aim of this thesis was to establish stimulus manipulation techniques designed to optimise peripheral visual function.

Brown (1972b) observed a slight improvement in peripheral visual acuity when targets moved slowly along predictable trajectories, compared to acuity for static targets, suggesting motion may be such a manipulation. Thus, in Chapter 3 resolution thresholds were calculated for targets at a range of speeds and peripheral eccentricities. There is a strong, significant general degradation in resolution thresholds as both target speed and eccentricity are increased. Although slight improvements in acuity were observed for slowly moving targets presented within 10° in the horizontal or vertical periphery, these improvements were not statistically significant. Therefore motion alone is not necessarily sufficient to improve peripheral visual acuity.

The data were decomposed according to the orientation and direction of travel of the target, and the visual field in which it was presented. It was demonstrated that there was no significant effect of target orientation or the direction of motion on resolution thresholds. However, although there was no significant difference in resolution thresholds between the nasal and temporal visual fields, thresholds in the superior visual field were significantly worse at the same eccentricity. Thus the experiments in Chapter 3 demonstrate that the visual field is neither homogeneous nor isotropic, and that motion does not provide a significant improvement, at least within the eccentricity range examined. This condemns those who have lost central vision to suboptimal visual performance, as peripheral visual acuity is consistently worse than in the fovea. Although a beneficial effect of motion may emerge at higher eccentricities than those examined, the detrimental effect of eccentricity on resolution thresholds suggests that overall performance suffers. Since AMD patients typically demonstrate foveal scotomas covering an average 4.89° diameter (*SD* 4.22°, Lee & Markowitz, 2010), presenting at eccentricities in excess of 10° is unnecessary when attempting to establish a technique to improve maximum acuity in AMD patients.

9.1.2: Super-resolution in the peripheral retina

When viewing objects peripherally, the retinal image can be spatially undersampled. This can occur at the photoreceptor level, due to the sparseness of the photoreceptor array outside the fovea, or postreceptorally, due to damage or disease (Anderson & Thibos, 1999; Anderson & Hess, 1990). This can be exaggerated by neuro-retinal matrix damage (NRMD, Frisén, 2010; Rabb, Tso, & Fishman, 1986). Disorders resulting in clustered loss of peripheral photoreceptors

are rare, so methods of improving performance in these conditions have limited potential clinical use. However, there is a clear theoretical motivation for investigating how dynamically occluded targets are perceived. The reconstruction of undersampled images is achieved in digital systems using super-resolution (SR; Park, Park, & Kang, 2003). SR is a mechanism whereby multiple low-resolution images are merged together over time to produce a higher-resolution image. The previous chapter demonstrated that motion is not necessarily sufficient to improve peripheral acuity in the healthy eye. This may be because the retinal surface is not sufficiently sparse for a SR mechanism to operate efficiently. Thus, the use of SR mechanisms in techniques that may have the potential for improving peripheral vision in NRMD patients was investigated. The principles of peripheral SR were examined psychophysically in healthy observers by introducing artificial undersampling to peripheral stimuli.

It was verified that, when artificially undersampled, smoothly moving peripheral targets are more accurately resolved than static targets. This is consistent with a peripheral SR mechanism. Frisén (2010) demonstrated that foveal letter targets that were partially obscured by overlaid masks were more accurately identified when the targets were moving. This study therefore aligns with Frisén (2010), and extends the demonstration of an SR mechanism into the periphery. However, both Frisén (2010) and this experiment do not account for the increase in the total spatial extent of stimulus information that is available across one trial. By introducing motion, more independent samples of the target are available to the observer. Experiments 2.2 and 2.3 used an updating mask technique that controls for the amount of the stimulus presented during each trial. It was demonstrated that although a substantial amount of the observed benefit in the previous

experiment results from the additional available target information, a residual benefit of motion remains. This suggests that motion is a key aspect of effective peripheral SR. This has yet to be demonstrated in the fovea, wherein spatiotemporal summation mechanisms may differ.

Since motion was shown to be an integral feature of peripheral SR, the effect of motion source characteristics were then investigated. It was demonstrated that target resolution thresholds were lower for moving targets behind static masks than for static targets behind moving masks. Thus the SR mechanism operates more optimally when the motion signal comes from the target rather than the mask. The motion path was further investigated by interfering with the smooth, predictable motion trajectory. The targets were presented at trajectory positions in a random order, rather than consecutively. Resolution thresholds were higher when the trajectory was fragmented, suggesting that the peripheral SR mechanism contains a tracking mechanism, which hinders resolution of the target when disrupted. Similarly, Mateeff, Popov, and Hohnsbein (1993) asked observers to rate their perception of an occluded target in smooth and disjointed motion conditions. The observers indicated that their perception of the target was better when the motion was smooth. This finding is thus confirmed using an objective measure of performance, and extended into the periphery. Conversely, when disrupting the trajectory of mask motion, the opposite was found; target resolution thresholds were higher when mask motion was smooth compared to disjointed. These results support the existence of a dedicated tracking mechanism, whereby a motion source originating in the mask distracts the tracking mechanism by supporting perception of the mask rather than the target. When the tracking

mechanism is disrupted by disjointed motion, the hindrance to target resolution is removed.

Randomising the order of the motion path introduces variability in the distance between the target locations on successive video frames. Therefore, the speed of the target is also variable within a trial. Thus, an experiment was conducted in which the trajectory of the target was unpredictable, but the variability in target speed was reduced. This was achieved using a sinusoidal trajectory, the frequency and phase of which was reallocated at random at each node. Variability in target speed was thus restricted to a more constrained range. No significant difference was found between predictable and unpredictable sinusoidal motion. There are several possible reasons for this: it may indicate that that the tracking mechanism functions on a timescale of hundreds of milliseconds, such that the short durations between nodes during which the motion was predictable, but not on a single video frame. Alternatively, the extended stimulus presentation duration used in this condition (the target was displayed for 50 video frames, rather than the 25 in previous conditions) may have allowed performance to saturate.

Thus, the experiments in Chapter 4 confirmed the existence of an SR mechanism capable of combining spatial target information across time. Further, it was demonstrated that it functions most effectively in situations of smooth, predictable target motion. Although at 10° in a healthy peripheral retina motion alone is not enough to improve performance, in conditions whereby the retina is sufficiently sparse for an SR mechanism to operate (such as in NRMD), smooth, predictable motion can be beneficial to acuity.

9.1.3: Disrupting smooth motion

No significant benefit of motion was reported without artificial undersampling in Experiment 1.1 or in Experiment 2.1. The described SR mechanism therefore appears to operate only when in situations whereby the image is spatially undersampled, such as in NRMD. Natural retinal sparseness may also provide the necessary undersampling for the SR mechanism to operate, but not within 10° eccentricity, the maximum examined in this thesis. Making use of the SR mechanism is thus unsuitable as a technique for improving peripheral performance in the healthy periphery or in AMD patients, whose peripheral retinal surface is often not atypical. Accordingly, the experiments in Chapter 5 investigated stimulus manipulations that may improve peripheral performance without artificial undersampling.

The first experiment investigated the nature of the detrimental effect of increasing smooth motion by disrupting the motion path. As in Experiments 2.5 and 2.6 in Chapter 4, the target was presented at the same 25 locations as in the corresponding smooth motion condition, but in a randomised order. Resolution thresholds for targets in the disjointed condition did not rise as the corresponding smooth motion speed was increased. This occurred in spite of the sharp rise in the median inter-frame speed that accompanies randomising the presentation sequence. Previous studies have also indicated that visual performance can be resilient to jittering targets (Badcock & Wong, 1990). This experiment demonstrates that this resilience persists into the periphery. Additionally, this finding suggests that the loss of acuity with increasing target speed is not completely explained in terms of a shift in spatial frequency sensitivity.

It is well documented that sensitivity to high spatial frequencies is lost as target speed increases (e.g. Burr & Ross, 1982). Thus, since the median target velocity in the randomised path condition is increased compared to the smooth motion condition, it would be expected to result in further reduction in acuity. This was not observed, suggesting that an explanation based on shifts in spatial frequency sensitivity cannot account for the speed-related acuity loss, perhaps because it is inadequate for stimuli with complex Fourier spectra. An alternative explanation for the loss of performance with increasing smooth motion is motion smear (Burr, 1980), whereby temporal summation over consecutive stimulus presentations results in a perceptual blurring of the fine details of the target. By disordering the presentation sequence, the likelihood of consecutive video frames presenting targets that spatially overlap drops. Since resolution thresholds at high speeds were lowered by the disjointed motion sequence, and not raised as would be predicted by shifts in spatial frequency sensitivity, Experiment 3.1 indicates that the loss of target resolution with increasing speed is at least in part explained by a perceptual smearing.

The results of Experiment 3.1 are also consistent with an SR mechanism with an integral tracking mechanism. Experiment 2.5 demonstrated that targets with motion were more accurately perceived than those with a disjointed motion sequence. Experiment 3.1 demonstrated that outside undersampled conditions, wherein an SR mechanism does not efficiently operate, there was no significant difference between smooth and disjointed motion at low speeds. Thus, efficient SR requires the target location to be tracked using a mechanism that has been shown to not operate outside SR conditions.

9.1.4: Stimulus-based modulations in smooth target motion

For stimuli with complex Fourier spectra, interrupting the motion sequence may improve peripheral acuity. However, randomising the motion sequence had no significant effect at low speeds or for static targets, rendering it insufficient as a method of optimising peripheral vision. Thus, in Experiments 3.2 and 3.3 a regular temporal modulation was added to the target. Van Santen and Sperling (1985) suggested that additional temporal modulations can extend the temporal frequency spectrum of the stimulus, potentially providing more stimulus information within the range of frequencies visible to the observer.

In Experiment 3.2 the stimulus was temporally subsampled: the target was displayed with interleaved blank intervals. Subsampling the stimulus was shown to reduce resolution thresholds at high target speeds, but had a detrimental effect at low speeds and for static targets. The loss of performance at low speeds was eliminated by correcting for the reduction in time-averaged stimulus contrast that occurs as a result of subsampling. This suggests that subsampling has no effect on static or slowly moving targets beyond reducing the stimulus contrast, which raises resolution thresholds. The threshold reduction at high speeds may therefore be a result of eliminating motion smear in the same way as randomising the motion path. Temporal subsampling is thus an unsuitable modulation for optimising peripheral visual function, in spite of the additional harmonics it provides.

The temporal modulation in Experiment 3.3 was contrast polarity reversal, whereby the target colour alternated between black and white (on a mid-grey background) at regular intervals during the trial. Similarly to temporal

subsampling, contrast polarity reversal drastically reduced the motion-related loss of acuity observed in unmodulated smooth target motion. However, contrast polarity reversal also resulted in reduced thresholds for static and slowly moving targets. Since the improvement occurred across the range of target speeds, an explanation of the effect involving the counteracting of motion smear is insufficient. Additionally, the beneficial effect of contrast polarity reversal persisted when the overall Michelson contrast was equated to that of the unmodulated condition. Thus an explanation concerning the increase in overall absolute stimulus contrast is also insufficient. It was therefore concluded that contrast polarity reversal may be useful in the optimisation of peripheral function.

9.1.5: Stimulus-based modulations in simulated ocular disease

Certain temporal modulations have thus been shown to improve acuity for static and moving peripheral targets in the healthy periphery. In Chapter 6 this is extended to simulated conditions of eye disease in healthy observers, in order to examine the potential benefit to patients with central vision loss. Because fixation instability is a common symptom in central vision loss, often resulting in oculomotor jitter being larger in patients by a factor of 2-4 (Kumar & Chung, 2014; Martinez-Conde, 2006b), fixational instability was simulated in healthy observers, and the effect of temporal modulations on acuity was examined.

Exaggerated ocular jitter was simulated by recording the natural fixational eye movements (FEMs) of healthy observers prior to testing. The deviations in fixation were then applied to the target during testing, multiplied by a gain factor, whereby a factor of 0 resulted in a static target, and a factor of 1 represented the observer's own eye motion behaviour. Since ocular motion naturally occurs in all

directions, the target jitter often resulted in the target eccentricity varying throughout each trial. As target eccentricity was shown in Chapter 3 to have a significant effect on resolution thresholds, a second experiment was conducted in which the target was restrained to an isoeccentric arc, 10° from fixation. The ocular motion was therefore applied only to the vertical axis, while the horizontal coordinate was adjusted to maintain the fixed eccentricity. Although temporal subsampling was shown to have a generally detrimental effect on resolution thresholds for smoothly moving objects in Chapter 5, Kaiser et al. (2014) suggest that in conditions resulting in ocular vibration, temporally subsampled presentation can improve foveal visual performance. Thus, resolution thresholds were examined for both temporal subsampling and contrast polarity reversal, alongside the control unmodulated condition.

For both the unrestricted and isoeccentric target experiments, resolution thresholds were not significantly effected by increasing the gain factor. This supports the findings of Falkenberg, Rubin, and Bex (2007), and Badcock and Wong (1990), and demonstrates that resilience to target jitter extends into the periphery. This pattern was common to all three modulation conditions. However, the modulation condition did have a significant effect on resolution thresholds: temporal subsampling consistently raised thresholds compared to the unmodulated condition, whereas contrast polarity reversal showed an improvement. Contrast polarity reversal has therefore been shown to improve acuity for peripheral targets across a range of motion conditions.

Experiment 4.2 extended the investigation of contrast polarity reversal as an optimisation technique into simulated conditions of NRMD. Disorders such as

cone-rod dystrophy can damage photoreceptor cells throughout the periphery, while creating lesions in the macula (Rabb et al., 1986). Peripheral retinal undersampling was simulated using the partially-opaque masks described in Chapter 4. Resolution thresholds were therefore compared between peripheral targets, which were unmodulated or had reversing contrast polarity. Thresholds were compared between modulation conditions for static targets, and for targets moving smoothly along isoeccentric paths at $2°s^{-1}$. Contrast polarity reversal did not result in a significant improvement in resolution thresholds, suggesting it is not a suitable technique for optimising the remaining visual function in disorders causing visual undersampling. Interrupting a low spatial frequency signal with small, discrete edges (which therefore have high spatial frequencies) increases the amount of high spatial frequency information in the stimulus, and diminishes low spatial frequency information (Van Santen & Sperling, 1985). Therefore, the spatial undersampling caused by small opaque patches may have had this effect on the spectral content of the stimulus. The additional harmonics introduced by the temporal modulation may thus be providing extra stimulus information at insensitive frequencies.

9.1.6: Estimating theoretical resolution for temporally modulated stimuli

It has thus been demonstrated psychophysically that applying periodic temporal modulations to peripheral targets can have beneficial effects on acuity. Van Santen and Sperling (1985) suggested that additional temporal stimulus modulations provide temporal harmonics of the stimulus in the spatiotemporal Fourier domain. In Chapter 7, the spatiotemporal characteristics of the stimuli

were assessed in order to examine whether the additional harmonics may be responsible for the effects temporal modulations have on resolution thresholds. This was achieved by analysing the stimulus in the spatiotemporal Fourier domain.

A spatiotemporal difference spectrum of the stimulus was calculated as the element-wise difference of Fourier transforms of the stimulus with orthogonally-orientated targets. The difference spectrum was used as an indicator of the spatiotemporal characteristics of the target details critical to identifying the orientation. The difference spectra of targets in the smooth motion and ocular motion conditions were examined, with contrast polarity reversal, subsampling, and without temporal modulation.

Analysis of the spatiotemporal Fourier spectra of the stimuli with temporal modulations confirmed the appearance of additional temporal harmonics of the stimulus. These manifested as copies of the unmodulated spectra appearing at higher temporal frequencies. However, the maximum amplitude of the difference spectra in the modulated conditions was reduced in comparison to the unmodulated conditions. The observers' resolution thresholds in the subsampled condition were shown to be strongly influenced by the overall time-averaged stimulus contrast. The reduction in amplitude in the difference spectra of the subsampled condition supports this explanation of the observer data. However, the concurrent reduction in the amplitude in the contrast polarity reversal condition visible in the spectral analysis does not alone predict the observer data. This suggests that the contrast of the stimulus is not a complete explanation for the effect of temporal modulations on resolution thresholds. Perhaps a more

detailed explanation may include the receptor-level response to the stimuli. By reversing the contrast polarity of the target at a suitable frequency, both on- and off-channels can be stimulated to the maximum response, increasing the output signal magnitude from the retina (Schiller et al., 1986).

A model was developed in order to measure the contribution the additional harmonics may be making to the perception of the target. The extent to which the difference spectra of the stimulus appears at visible frequencies was analysed. This was achieved by modelling the window of visibility, the sensitivity of the visual system as a function of temporal and spatial frequency (Watson et al., 1986). The window was created based on the model created by Kelly (1979). An estimate of the resolvability of the stimulus was generated by calculating the element-wise multiplication (Hadamard product) of the difference spectrum and the spatiotemporal sensitivity surface, and taking the sum of all elements within the resulting spectrum. This gives a relative estimate of resolvability between conditions. This estimate was compared to the observer data for the three modulation conditions for smooth and ocular motion.

The model accurately reproduced the effect of additional temporal modulations on smooth motion in that it predicted that subsampling, while providing the extra harmonics, has a generally detrimental effect on resolution thresholds. It also predicted that contrast polarity reversal can improve thresholds. However, it did not accurately model the increase in thresholds as smooth motion is increased without temporal modulations. This result is in support of factors other than the spectral content of the stimulus contributing to the visibility of the target. It may be a result of the model failing to include temporal summation features, which

indirectly supports the contribution of temporal smear to the loss of sensitivity with increasing speed. The model includes estimates of how contrast sensitivity is affected by speed, and the rise in thresholds is not seen. This is an indication that spatial frequency sensitivity is an inadequate predictor of acuity for targets with complex spectra.

For ocular motion, the model accurately estimates that target resolution is unaffected by increased target jitter. The model again predicts that subsampling a stimulus has a detrimental effect on resolvability. However, it does not suggest that contrast polarity reversal can provide any additional benefit to resolution thresholds. This may be due to the ocular jitter providing an increase in the spectral range of the stimulus, such that the extra harmonics did not provide additional information. This suggests that the model is not accounting for a physiological mechanism that corrects for ocular motion, which is masking the benefit of temporal modulations. A mechanism that prevents the sensation of ocular jitter has previously been described by Murakami and Cavanagh (1998). Future iterations of the model that account for this stabilisation mechanism may more accurately represent the beneficial effect of contrast polarity reversal.

The estimates of relative performance calculated by the model are compatible with explanations of the effects previously discussed: the effects the additional temporal modulations have on resolution thresholds have been discussed in terms of the response of photoreceptor receptive fields to the stimuli, and in terms of the amplitude of the Fourier spectra of the stimuli that appears within the WOV. The model examined only the effect that the increased spectral range of the stimuli has on stimulus visibility. Thus, the predictions made by the model support a

description of the visual analysis of presented targets that includes a combination of mechanisms, perhaps including post-receptoral cortical processes that have not been examined here.

9.1.7: Stimulus-based modulations in a peripheral reading task

Contrast polarity reversal has been shown to improve peripheral visual acuity for static and moving targets, and also in simulated conditions of unstable fixation. This supports the use of contrast polarity reversal as a technique for optimising the use of the remaining visual field in AMD patients. To test this, Chapter 8 examined the use of contrast polarity reversal in a more critical everyday task: peripheral sentence reading. Reading speed and accuracy were tested in healthy observers, viewing peripherally, and in macular degeneration patients viewing naturally. Full sentences of between 10-12 words (from the IURead collection; Xu & Bradley, 2015) were read aloud by the participants, who were in control of the scrolling speed during the stimulus presentation.

In healthy observers viewing at 6° in the superior visual field, reading speed and accuracy was analysed for four modulation conditions. An unmodulated control condition was included whereby the target appeared either black or white, remaining that shade for the entire trial. Two different contrast polarity reversal periods were examined: reversal after intervals of 70.6ms and 129.4ms. Since the contrast polarity reversal paradigm, as discussed previously, doubles the Michelson contrast of the stimulus, a contrast polarity reversal condition was included whereby the Michelson contrast was equated to the unmodulated condition. The reversal period in the half contrast condition was 129.4ms. The healthy observers read significantly faster, and made significantly fewer reading

errors in all three modulated conditions, compared to the unmodulated condition. Contrast polarity reversal therefore can improve performance on reading tasks in the healthy periphery.

The macular degeneration patients selected for the study had established, binocular scotomata. They performed the same reading task as the healthy observers. No direction was given to the patients on the retinal location in which they performed the task; instead they were encouraged to use the location they felt most appropriate. The reading speed and accuracy were recorded for three modulation conditions: unmodulated, and with reversal periods of 66.7ms and 133.3ms. The target was at maximum contrast throughout presentation. Unlike the healthy observers, when analysed as a group the patients did not show an improvement in reading speed in the contrast polarity reversal conditions. However, the patients who were presented with targets at a print size close to their critical print size (CPS) were shown to read faster. The patients for whom the print size was at least 150% of the CPS were significantly slowed by contrast polarity reversal. This patient subgroup, however, contains only two participants; in order to strengthen conclusions as to the nature of the effect, a larger study is required.

The observed dichotomy may be a result of the relationship between reading speed and print size. As print size is increased, reading speed increases up to a saturating point. The reading speed at saturation is the observer's maximum reading speed, and the print size at the saturating point is the CPS. Targets at print sizes far larger than the CPS are more likely to be possible to read at the maximum reading speed, and thus there is less room for improvement. However,

the patients' CPS was measured using static target sentences. A more appropriate CPS value would be calculated by measuring a CPS for scrolling text. The difference in reading method between measuring the CPS with the MNRead and examining reading speed may be the reason that a benefit is visible for patients with the targets closer to the CPS. The CPS for moving text at a screen distance of 100cm may be at a larger print size than for static text at 40cm. Thus, reading speed may not have saturated, allowing for room for improvement. The relationship between the size of the effect of contrast polarity reversal and the value of the ratio of stimulus print size to CPS is a negative linear trend. However, since several other symptoms such as increased PRL eccentricity and reduced reading acuity are comorbid with increased CPS, the magnitude of the benefit of contrast polarity reversal on reading speed for peripheral sentences may therefore alternatively be because of one of the other symptoms of AMD. Although in patients reading speed was only improved by contrast polarity reversal in certain situations, reading accuracy was consistently improved by it. This provides evidence that stimulus modulations can improve performance across a range of visual tasks performed in the periphery.

9.2: Future directions

9.2.1: Additional potential tasks that may benefit from additional temporal modulations

This thesis has demonstrated that, in a range of circumstances, contrast polarity reversal can improve peripheral visual function. Other potential avenues for the use of contrast polarity reversal could be explored in the future. The use of contrast polarity reversal in examining complex visual scenes could be examined,

as it remains to be confirmed whether the accuracy of perception of objects within a scene could be improved by stimulus modulations. An examination of accuracy of scene identification could be performed using a study in which a cinematic display with reversing contrast polarity is viewed peripherally. The observers would identify their perception of what is occurring within the scene, and their performance would be compared to an unmodulated scene. If contrast polarity reversal improves accuracy, it may be a useful display technique for AMD patients.

Further, it remains to be tested in cinematic displays whether the whole scene can be given a temporal manipulation or the intended target must have a unique profile. A target with a unique profile within the scene (either with contrast polarity reversal at a different phase, or appearing in an unmodulated scene) would likely be more easily attended due to pop-out effects (Nothdurft, 1991; Treisman & Gelade, 1980). Modulating an entire scene may also have detrimental effects on perception of motion within the scene. Illusory apparent motion effects have been demonstrated using additional temporal modulations in scene viewing. Shioiri and Cavanagh (1990) demonstrated that a spatial displacement between frames in a temporally subsampled scene resulted in the appearance of motion in the opposite direction to the spatial displacement, i.e. an illusory reversal of motion. Further, Anstis and Rogers (1986) demonstrated that the periodic reversal of contrast polarity also instigates illusory reverse motion in scene viewing. However, examining feature identification performance in modulated scenes has not been directly compared.

9.2.2: The nature of the beneficial effect of contrast polarity reversal

The mechanism underlying the effects that additional temporal stimulus modulations have on resolution is unclear. One possible explanation is in terms of the TRF of photoreceptor cells. When a target appears within the receptive field of a photoreceptor, it stimulates the photoreceptor, which initiates the production of an electric signal (Swanson et al., 1987). The magnitude of this response is related to the luminous intensity of the stimulus, and the duration for which it appears within the receptive field of the photoreceptor. The maximum magnitude of the response, and the stimulus duration required to reach it, are properties of the photoreceptor, known as the TRF. A second possible explanation is in terms of the temporal harmonics created in the Fourier domain by applying periodic temporal modulations to the stimuli. When additional temporal modulations are applied, the spectral replicas of the stimulus appear at higher and lower temporal frequencies in the Fourier domain (Van Santen & Sperling, 1985). If the extra stimulus information is being produced at frequencies to which the visual system is sensitive, this may result in improved perception of the stimulus. Further investigation of these mechanisms could provide a more comprehensive view of their contributions to visual perception.

It was hypothesised that temporal harmonics created by the stimulus modulations are extending the available stimulus information within the window of visibility, which may be contributing to the improved peripheral resolution. In Chapter 7 the spatiotemporal characteristics of the stimuli were investigated, and a model was constructed aiming to reproduce the experimental results. While the analysis demonstrated that the harmonics are being created by the modulations, the model

failed to predict key aspects of the observer results. For example, the model did not demonstrate that for unmodulated targets, resolution becomes impaired as target speed is increased.

There are several drawbacks to the model in its current form, which could be corrected in future iterations of the model. The model does not account for certain features of the visual system, such as temporal summation, and the receptor-level response to temporally-modulated input. A notable result of these factors is motion smear (Burr, 1980), which has a consistently detrimental effect on resolution thresholds at high target speeds. Thus by incorporating a temporal summation feature, the model may more accurately reflect the observer data. This could be achieved by calculating the maximum duration across which summation can occur at 10° eccentricity. The input stimulus in the model could then remain at each frame location for that duration after initial presentation. This would create a smeared stimulus input to the model. Further, including non-immediate sensitivity to polarity reversal may more accurately reflect the observer data.

The model does not account for the mechanism that stabilises the visual image during ocular jitter (Murakami & Cavanagh, 1998). By including this mechanism, the model may more accurately predict the beneficial effect of contrast polarity reversal on resolution thresholds in exaggerated ocular motion. This could inform on the receptor response to contrast polarity reversal, and the contribution it has on the beneficial effect on resolution thresholds. When the image stabilisation mechanism is included, if the model then predicts a benefit of contrast polarity reversal, this would suggest that the increased TRF response is responsible for the beneficial effect of contrast polarity reversal. The spectral content of the stimulus

would not have changed, thus a description based on stimulus frequencies appearing within the WOV would not predict an improvement.

9.2.3: The effect of contrast polarity reversal in optimising peripheral reading

The final patient study demonstrated that the beneficial effect of contrast polarity reversal on reading speed is observed only in certain conditions. The primary source of the beneficial effect is unclear; the magnitude of the effect may depend on the size of the target in relation to the CPS of the observer. Alternatively, it may co-vary with the eccentricity at which the target is viewed, or depend on the relationship between print size and the reading acuity of the observer. A future study could separate out these factors to determine the conditions under which contrast polarity reversal could be most useful. A limit to the conclusions of the study as reported is the limited sample size; a larger dataset is required in order to strengthen any conclusions.

Extending the patient experiment in Chapter 8 to include target print sizes close to the CPS may be useful to confirm the relationship whether the beneficial effect of contrast polarity reversal is only available to targets around the CPS. Further, the CPS itself requires closer examination; a CPS for scrolling sentences with the same typographic characteristics as the target sentences would provide a more accurate baseline measure of performance. Additionally, the CPS could be measured at the same eccentricity as the target sentences in the healthy observers to further illuminate the relationship between the magnitude of the effect and the CPS/print size ratio.

A tracking scanning laser ophthalmoscope (TSLO; Hammer et al., 2003) can be used to maintain fixed stimulus position on the retina during presentation. By presenting targets at fixed retinal location, a more accurate analysis of performance with respect to the PRL of the observer can be performed. Since the PRL is not necessarily the optimum location for peripheral reading (Shima et al., 2010), establishing the location that is the optimum would serve as a basis for developing a training procedure to maximise the beneficial effect of contrast polarity reversal and thus enhance the speed at which patients can read.

9.3: Concluding remarks

The experiments in this thesis have investigated peripheral visual function in healthy observers and in AMD patients. It has been shown that motion alone is insufficient to improve peripheral acuity in the healthy periphery. However, this thesis has shown that a peripheral SR mechanism operates in undersampled conditions. Further, it has been shown that this mechanism contains a tracking feature, such that it operates optimally in smooth, predictable motion.

It was also demonstrated that stimulus-based temporal modulations can optimise peripheral visual function in certain circumstances. Specifically, the technique of periodically reversing the contrast polarity of the target has been shown to improve acuity for static and moving peripheral targets, for targets in conditions of unstable fixation. Further, peripheral reading speed and accuracy was improved by contrast polarity reversal. By modelling these conditions, it was suggested that a feature of contrast polarity reversal that heavily contributes to improved performance is the increase it provides in the temporal frequency range of the stimulus, and not, as might be expected, the increased time-averaged, absolute

contrast. However, not all observed phenomena were compatible with this explanation. This suggests a more complete description may include contribution from several factors, perhaps including both photoreceptor behaviour and spatiotemporal summation mechanisms.

This provides a strong basis for the development of simple presentation techniques that could improve performance in important visual tasks in patients with limited central vision.

References

Adelstein, B. D., Kaiser, M. K., Beutter, B. R., McCann, R. S., & Anderson, M. R. (2013). Display strobing: An effective countermeasure against visual blur from whole-body vibration. *Acta Astronautica*, *92*(1), 53–64. http://doi.org/10.1016/j.actaastro.2012.07.003

Altpeter, E., Mackeben, M., & Trauzettel-Klosinski, S. (2000). The importance of sustained attention for patients with maculopathies. *Vision Research*, *40*(10), 1539–1547. http://doi.org/10.1016/S0042-6989(00)00059-6

Anderson, R. S., & Thibos, L. N. (1999a). Relationship between acuity for gratings and for tumbling-E letters in peripheral vision. *Journal of the Optical Society of America A*, *16*(10), 2321–2333.

Anderson, R. S., & Thibos, L. N. (1999b). Sampling limits and critical bandwidth for letter discrimination in peripheral vision. *Journal of the Optical Society of America A*, *16*(10), 2334–2342.

Anderson, S. J., & Hess, R. F. (1990). Post-receptoral undersampling in normal human peripheral vision. *Vision Research*, *30*(10), 1507–1515.

Anstis, S. M., & Rogers, B. J. (1986). Illusory continuous motion from oscillating positive-negative patterns: implications for motion perception. *Perception*, *15*(5), 627–640. http://doi.org/10.1068/p150627

Appelle, S. (1972). Perception and discrimination as a function of stimulus orientation: the "oblique effect" in man and animals. *Psychological Bulletin*, *78*(4), 266–278. http://doi.org/10.1037/h0033117

Arditi, A. (1999). Elicited sequential presentation for low vision reading. *Vision Research*, *39*(26), 4412–4418. http://doi.org/10.1016/S0042-6989(99)00154-6

Arditi, A., & Cho, J. (2005). Serifs and font legibility. *Vision Research*, *45*(23), 2926–2933. http://doi.org/10.1016/j.visres.2005.06.013

Badcock, D. R. (1984). Spatial phase or luminance profile discrimination? *Vision Research*, *24*(6), 613–623. http://doi.org/10.1016/0042-6989(84)90116-0

Badcock, D. R., & Wong, T. L. (1990). Resistance to positional noise in human vision. *Nature*, *343*(6258), 554–5. http://doi.org/10.1038/343554a0

Battista, J., & Kalloniatis, M. (2002). Left–right word recognition asymmetries in central and peripheral vision. *Vision Research*, *42*(12), 1583–1592. http://doi.org/10.1016/S0042-6989(02)00075-5

Battista, J., Kalloniatis, M., & Metha, A. (2005). Visual function: The problem with eccentricity. *Clinical and Experimental Optometry*, *88*(5), 313–321. http://doi.org/10.1111/j.1444-0938.2005.tb06715.x

Bauer, D., & Cavonius, C. R. (1980). Improving the legibility of visual display units through contrast reversal. In E. Grandjean & E. Vigliani (Eds.), *Ergonomic aspects of visual display terminals* (pp. 137–142). London: Taylor & Francis.

Bellmann, C., Feely, M., Crossland, M. D., Kabanarou, S. A., & Rubin, G. S. (2004). Fixation stability using central and pericentral fixation targets in patients with age-related macular degeneration. *Ophthalmology*, *111*, 2265–2270. http://doi.org/10.1016/j.ophtha.2004.06.019

Berkley, M. A., Kitterle, F., & Watkins, D. W. (1975). Grating visibility as a function of orientation and retinal eccentricity. *Vision Research*, *15*(2), 239–244.

http://doi.org/10.1016/0042-6989(75)90213-8

Bex, P. J., Dakin, S. C., & Simmers, A. J. (2003). The Shape and Size of Crowding for Moving Targets. *Vision Research*, *43*(27), 2895–2904.

Beymer, D., Russell, D., & Orton, P. (2008). An eye tracking study of how font size and type influence online reading. *Proceedings of the 22nd British HCI Group Annual Conference on People and Computers: Culture, Creativity, Interaction*, *2*, 15–18.

Blackmore-Wright, S., Georgeson, M. A., & Anderson, S. J. (2013). Enhanced Text Spacing Improves Reading Performance in Individuals with Macular Disease. *PLoS ONE*, *8*(11), e80325. http://doi.org/10.1371/journal.pone.0080325

Bondarko, V. M., & Danilova, M. V. (1995). Crowding-effect: different surroundings and different sizes of test stimuli. *Perception*, *24*, 124.

Bondarko, V. M., & Danilova, M. V. (1997). What spatial frequency do we use to detect the orientation of a Landolt C? *Vision Research*, *37*(15), 2153–2156.

Bouma, H. (1970). Interaction effects in parafoveal letter recognition. *Nature*, *226*, 177–178.

Brown, B. (1972a). Dynamic visual acuity, eye movements and peripheral acuity for moving targets. *Vision Research*, *12*(2), 305–321.

Brown, B. (1972b). Resolution Thresholds for Moving Targets at the Fovea and in the Peripheral Retina. *Vision Research*, *12*(2), 293–304.

Bullimore, M. A., & Bailey, I. L. (1995). Reading and Eye Movements in Age-Related Maculopathy. *Optometry and Vision Science*, *72*(2), 125–138.

Bunce, C., & Wormald, R. P. L. (2006). Leading causes of certification for blindness and partial sight in England & Wales. *BMC Public Health*, *6*(1), 58. http://doi.org/10.1186/1471-2458-6-58

Burr, D. C. (1980). Motion smear. *Nature*, *284*(5752), 164–165. http://doi.org/10.1038/284164a0

Burr, D. C., Morrone, M. C., & Spinelli, D. (1989). Evidence for edge and bar detectors in human vision. *Vision Research*, *29*(4), 419–431. http://doi.org/10.1016/0042-6989(89)90006-0

Burr, D. C., & Ross, J. A. (1982). Contrast sensitivity at high velocities. *Vision Research*, *22*(4), 479–484. http://doi.org/10.1016/0042-6989(82)90196-1

Burr, D. C., Ross, J. A., & Morrone, M. C. (1986a). Seeing objects in motion. *Proceedings of the Royal Society of London. Series B. Biological Sciences*, *227*(1247), 249–265.

Burr, D. C., Ross, J. A., & Morrone, M. C. (1986b). Smooth and sampled motion. *Vision Research*, *26*(4), 643–652. http://doi.org/10.1016/0042-6989(86)90012-X

Campbell, F. W., & Gubisch, R. W. (1966). Optical quality of the human eye. *The Journal of Physiology*, *186*(3), 558–578. http://doi.org/10.1113/jphysiol.1966.sp008056

Cao, D., Zele, A. J., & Pokorny, J. (2007). Linking impulse response functions to reaction time: Rod and cone reaction time data and a computational model. *Vision Research*, *47*(8), 1060–1074. http://doi.org/10.1016/j.visres.2006.11.027

Carrasco, M., Williams, P. E., & Yeshurun, Y. (2002). Covert attention increases spatial resolution with or without masks: Support for signal enhancement. *Journal of Vision*, *2*(6), 4. http://doi.org/10.1167/2.6.4

Cavanagh, P., Holcombe, A. O., & Chou, W. (2008). Mobile computation : Spatiotemporal integration of the properties of objects in motion. *Journal of Vision*,

8, 1–23. http://doi.org/10.1167/8.12.1.Introduction

Chong, E., Familiar, A. M., & Shim, W. M. (2016). Reconstructing representations of dynamic visual objects in early visual cortex. *Proceedings of the National Academy of Sciences of the United States of America*, *113*(5), 1453–8. http://doi.org/10.1073/pnas.1512144113

Chung, S. T. L. (2004). Reading speed benefits from increased vertical word spacing in normal peripheral vision. *Optometry and Vision Science*, *81*(7), 525–35.

Chung, S. T. L. (2012). Dependence of reading speed on letter spacing in central vision loss. *Optometry and Vision Science*, *89*(9), 1288–98. http://doi.org/10.1097/OPX.0b013e318264c9dd

Chung, S. T. L., & Bedell, H. E. (1998). Vernier and letter acuities for low-pass filtered moving stimuli. *Vision Research*, *38*(13), 1967–1982.

Chung, S. T. L., & Bedell, H. E. (2003). Velocity dependence of Vernier and letter acuity for band-pass filtered moving stimuli. *Vision Research*, *43*(6), 669–682.

Chung, S. T. L., Jarvis, S. H., Woo, S. Y., Hanson, K., & Jose, R. T. (2008). Reading speed does not benefit from increased line spacing in AMD patients. *Optometry and Vision Science*, *85*(9), 827–33. http://doi.org/10.1097/OPX.0b013e31818527ea

Chung, S. T. L., Legge, G. E., & Tjan, B. S. (2002). Spatial-frequency characteristics of letter identification in central and peripheral vision. *Vision Research*, *42*(18), 2137–2152. http://doi.org/10.1016/S0042-6989(02)00092-5

Chung, S. T. L., Levi, D. M., & Bedell, H. E. (1996). Vernier in motion: what accounts for the threshold elevation? *Vision Research*, *36*(16), 2395–2410.

Chung, S. T. L., Mansfield, J. S., & Legge, G. E. (1998). Psychophysics of reading. XVIII. The effect of print size on reading speed in normal peripheral vision. *Vision Research*, *38*(19), 2949–2962. http://doi.org/10.1016/S0042-6989(98)00072-8

Coleman, H. R., Chan, C., Ferris, F. L., & Chew, E. Y. (2008). Age-related macular degeneration. *The Lancet*, *372*(9652), 1835–1845. http://doi.org/10.1016/S0140-6736(08)61759-6

Collewijn, H., van der Mark, F., & Jansen, T. C. (1975). Precise recording of human eye movements. *Vision Research*, *15*(3), 447–IN5. http://doi.org/10.1016/0042-6989(75)90098-X

Cowey, A., & Rolls, E. T. (1974). Human cortical magnification factor and its relation to visual acuity. *Experimental Brain Research*, *21*(5), 447–454.

Crossland, M. D., Culham, L. E., Kabanarou, S. A., & Rubin, G. S. (2005). Preferred retinal locus development in patients with macular disease. *Ophthalmology*, *112*, 1579–1585. http://doi.org/10.1016/j.ophtha.2005.03.027

Crossland, M. D., Culham, L. E., & Rubin, G. S. (2004). Fixation stability and reading speed in patients with newly developed macular disease. *Ophthalmic & Physiological Optics*, *24*(4), 327–33. http://doi.org/10.1111/j.1475-1313.2004.00213.x

Culham, L. E., Fitzke, F. W., Timberlake, G. T., & Marshall, J. (1992). Use of scrolled text in a scanning laser ophthalmoscope to assess reading performance at different retinal locations. *Ophthalmic & Physiological Optics*, *12*(3), 281–286.

Curcio, C. A. (2001). Photoreceptor topography in ageing and age-related maculopathy. *Eye*, *15*(3), 376–383. http://doi.org/10.1038/eye.2001.140

Curcio, C. A., & Allen, K. A. (1990). Topography of ganglion cells in human retina. *The Journal of Comparative Neurology*, *300*(1), 5–25. http://doi.org/10.1002/cne.903000103

Curcio, C. A., Millican, C. L., Allen, K. A., & Kalina, R. E. (1993). Aging of the human photoreceptor mosaic: evidence for selective vulnerability of rods in central retina. *Investigative Ophthalmology & Visual Science*, *34*(12), 3278–3296.

Curcio, C. A., Sloan, K., Packer, O., Hendrickson, A. E., & Kalina, R. E. (1987). Distribution of cones in human and monkey retina: individual variability and radial asymmetry. *Science*, *236*(4801), 579–582. http://doi.org/10.1126/science.3576186

Curcio, C. A., Sloan, K. R., Kalina, R. E., & Hendrickson, A. E. (1990). Human photoreceptor topography. *Journal of Comparative Neurology*, *292*(4), 497–523.

de Lange, H. (1958). Research into the Dynamic Nature of the Human Fovea→Cortex Systems with Intermittent and Modulated Light I Attenuation Characteristics with White and Colored Light. *Journal of the Optical Society of America*, *48*(11), 777. http://doi.org/10.1364/JOSA.48.000777

Dimitrov, P. N., Guymer, R. H., Zele, A. J., Anderson, A. J., & Vingrys, A. J. (2008). Measuring Rod and Cone Dynamics in Age-Related Maculopathy. *Investigative Opthalmology & Visual Science*, *49*(1), 55. http://doi.org/10.1167/iovs.06-1048

Engbert, R., & Kliegl, R. (2003). Binocular Coordination in Microsaccades. In J. Hyona, R. Radach, & H. Deubel (Eds.), *The Mind's Eye: Cognitive and Applied Aspects of Eye Movement Research* (1st ed., pp. 103–119). Amsterdam: Elsevier.

Engbert, R., & Kliegl, R. (2004). Microsaccades keep the eyes' balance during fixation. *Psychological Science*, *15*(6), 431–6. http://doi.org/10.1111/j.0956-7976.2004.00697.x

Engbert, R., & Mergenthaler, K. (2006). Microsaccades are triggered by low retinal image slip. *PNAS*, *103*(18), 7192–7197.

Evans, J. R., Fletcher, A. E., & Wormald, R. P. L. (2004). Causes of visual impairment in people aged 75 years and older in Britain: an add-on study to the MRC Trial of Assessment and Management of Older People in the Community. *British Journal of Ophthalmology*, *88*(3), 365–370. http://doi.org/10.1136/bjo.2003.019927

Fahle, M., Biester, A., & Morrone, C. (2001). Spatiotemporal interpolation and quality of apparent motion. *Journal of the Optical Society of America A*, *18*(11), 2668. http://doi.org/10.1364/JOSAA.18.002668

Fahle, M., & Poggio, T. (1981). Visual Hyperacuity: Spatiotemporal Interpolation in Human Vision. *Proceedings of the Royal Society B: Biological Sciences*, *213*(1193), 451–477. http://doi.org/10.1098/rspb.1981.0075

Falkenberg, H. K., Rubin, G. S., & Bex, P. J. (2007). Acuity, crowding, reading and fixation stability. *Vision Research*, *47*(1), 126–35. http://doi.org/10.1016/j.visres.2006.09.014

Ferris, F. L., Kassoff, A., Bresnick, G. H., & Bailey, I. (1982). New Visual Acuity Charts for Clinical Research. *American Journal of Ophthalmology*, *94*(1), 91–96. http://doi.org/10.1016/0002-9394(82)90197-0

Fine, E. M., & Peli, E. (1995). Scrolled and rapid serial visual presentation texts are read at similar rates by the visually impaired. *Journal of the Optical Society of America A*, *12*(10), 2286. http://doi.org/10.1364/JOSAA.12.002286

Fine, E. M., & Peli, E. (1998). Benefits of rapid serial visual presentation (RSVP) over scrolled text vary with letter size. *Optometry and Vision Science*, *75*(3), 191–196.

Fischer, B., & Weber, H. (1993). Express saccades and visual attention. *Behavioral and Brain Sciences*, *16*(3), 553. http://doi.org/10.1017/S0140525X00031575

Fishman, G. A., Farber, M., Patel, B. S., & Derlacki, D. J. (1987). Visual Acuity Loss in Patents with Stargardt's Macular Dystrophy. *Ophthalmology*, *94*(7), 809–814. http://doi.org/10.1016/S0161-6420(87)33533-X

Fletcher, D. C., & Schuchard, R. A. (1997). Preferred Retinal Loci Relationship to Macular Scotomas in a Low-vision Population. *Ophthalmology*, *104*(4), 632–638. http://doi.org/10.1016/S0161-6420(97)30260-7

Frisén, L. (1986). Vanishing optotypes: new type of acuity test letters. *Archives of Ophthalmology*, *104*(8), 1194–1198.

Frisén, L. (2010). Scope of super-resolution in central vision. *British Journal of Ophthalmology*, *94*(1), 97–100.

Frisén, L. (2012). Performance of a Rapid Rarebit Central-Vision Test with Optic Neuropathies. *Optometry and Vision Science*, *89*(8), 1192–1195. http://doi.org/10.1097/OPX.0b013e318264f406

Frisén, L., & Quigley, H. A. (1984). Visual acuity in optic atrophy: a quantitative clinicopathological analysis. *Graefe's Archive for Clinical and Experimental Ophthalmology*, *222*(2), 71–74. http://doi.org/10.1007/BF02150634

Ghafour, I. M., Allan, D., & Foulds, W. S. (1983). Common causes of blindness and visual handicap in the west of Scotland. *British Journal of Ophthalmology*, *67*(4), 209–213. http://doi.org/10.1136/bjo.67.4.209

Ghasemi Falavarjani, K., & Nguyen, Q. D. (2013). Adverse events and complications associated with intravitreal injection of anti-VEGF agents: a review of literature. *Eye*, *27*(7), 787–794. http://doi.org/10.1038/eye.2013.107

Green, D. M. (1990). Stimulus selection in adaptive psychophysical procedures. *The Journal of the Acoustical Society of America*, *87*(6), 2662. http://doi.org/10.1121/1.399058

Haberthy, C., & Yu, D. (2016). Effects of Temporal Modulation on Crowding, Visual Span, and Reading. *Optometry and Vision Science*, *93*(6), 579–587. http://doi.org/10.1097/OPX.0000000000000848

Hamel, C. P. (2007). Cone rod dystrophies. *Orphanet Journal of Rare Diseases*, *2*(1), 7. http://doi.org/10.1186/1750-1172-2-7

Hammer, D. X., Ferguson, R. D., Magill, J. C., White, M. A., Elsner, A. E., & Webb, R. H. (2003). Tracking scanning laser ophthalmoscope (TSLO). In F. Manns, P. G. S÷derberg, & A. Ho (Eds.), (p. 208). International Society for Optics and Photonics. http://doi.org/10.1117/12.477974

Hammett, S. T. (1997). Motion blur and motion sharpening in the human visual system. *Vision Research*, *37*(18), 2505–2510. http://doi.org/10.1016/S0042-6989(97)00059-X

Hammett, S. T., Georgeson, M. A., & Gorea, A. (1998). Motion blur and motion sharpening: temporal smear and local contrast non-linearity. *Vision Research*, *38*(14), 2099–2108. http://doi.org/10.1016/S0042-6989(97)00430-6

He, S., Cavanagh, P., & Intriligator, J. (1996). Attentional resolution and the locus of visual awareness. *Nature*, *383*(6598), 334–7. http://doi.org/10.1038/383334a0

Hennig, M. H., & Wörgötter, F. (2003). Eye micro-movements improve stimulus detection beyond the nyquist limit in the peripheral retina. In *NIPS*.

Hirsch, J., & Curcio, C. A. (1989). The spatial resolution capacity of human foveal retina. *Vision Research*, *29*(9), 1095–1101. http://doi.org/10.1016/0042-6989(89)90058-8

Hogendoorn, H., Carlson, T. A., & Verstraten, F. A. J. (2008). Interpolation and extrapolation on the path of apparent motion. *Vision Research*, *48*(7), 872–881. http://doi.org/10.1016/j.visres.2007.12.019

Holcombe, A. O. (2009). Seeing slow and seeing fast: two limits on perception. *Trends in Cognitive Sciences*, *13*(5), 216–21. http://doi.org/10.1016/j.tics.2009.02.005

Hussain, Z., Webb, B. S., Astle, A. T., & McGraw, P. V. (2012). Perceptual learning reduces crowding in amblyopia and in the normal periphery. *Journal of Neuroscience*, *32*(2), 474–80. http://doi.org/10.1523/JNEUROSCI.3845-11.2012

Jackson, G. R., Owsley, C., & Curcio, C. A. (2002). Photoreceptor degeneration and dysfunction in aging and age-related maculopathy. *Ageing Research Reviews*, *1*(3), 381–396. http://doi.org/10.1016/S1568-1637(02)00007-7

Jennings, J. A. M., & Charman, W. N. (1981). Off-axis image quality in the human eye. *Vision Research*, *21*(4), 445–455. http://doi.org/10.1016/0042-6989(81)90091-2

Johnson, C. A., & Casson, E. J. (1995). Effects of Luminance, Contrast, and Blur on Visual Acuity. *Optometry and Vision Science*, *72*(12), 864–869.

Johnson, C. A., Keltner, J. L., & Balestrery, F. (1978). Effects of target size and eccentricity on visual detection and resolution. *Vision Research*, *18*(9), 1217–1222. http://doi.org/10.1016/0042-6989(78)90106-2

Kaiser, M. K., Adelstein, B. D., Anderson, M. R., Beutter, B. R., Ahumada, A. J., & McCann, R. S. (2014, April 29). Stroboscopic image modulation to reduce the visual blur of an object being viewed by an observer experiencing vibration. USA.

Kandil, F. I., & Lappe, M. (2007). Spatio-Temporal Interpolation Is Accomplished by Binocular Form and Motion Mechanisms. *PLoS ONE*, *2*(2), e264. http://doi.org/10.1371/journal.pone.0000264

Kanizsa, G. (1979). *The Organisation of Vision*. New York: Praeger.

Kellman, P. J., Yin, C., & Shipley, T. F. (1998). A common mechanism for illusory and occluded object completion. *Journal of Experimental Psychology: Human Perception and Performance*, *24*(3), 859–869.

Kelly, D. H. (1979). Motion and vision. II. Stabilized spatio-temporal threshold surface, *69*(10), 1340–1349.

Kelly, D. H. (1984). Retinal inhomogeneity. I. Spatiotemporal contrast sensitivity. *Journal of the Optical Society of America. A, Optics and Image Science*, *1*(1), 107–113. http://doi.org/10.1364/JOSAA.1.000107

Kelly, D. H. (1985). Visual processing of moving stimuli. *Journal of the Optical Society of America A*, *2*(2), 216–225.

Khuu, S. K., & Kalloniatis, M. (2015). Spatial summation across the central visual field: implications for visual field testing. *Journal of Vision*, *15*(1), 15.1.6. http://doi.org/10.1167/15.1.6

Klein, R., Klein, B. E. K., Knudtson, M. D., Meuer, S. M., Swift, M., & Gangnon, R. E. (2007). Fifteen-Year Cumulative Incidence of Age-Related Macular Degeneration: The Beaver Dam Eye Study. *Ophthalmology*, *114*(2), 253–262. http://doi.org/10.1016/j.ophtha.2006.10.040

Koenderink, J. J., Bouman, M. A., Bueno de Mesquita, E., & Slappendel, S. (1978a). Perimetry of contrast detection thresholds of moving spatial sine wave patterns. IV. The influence of the mean retinal illuminance. *Journal of the Optical Society of America*, *68*(1970), 860–865. http://doi.org/10.1364/JOSA.68.000860

Koenderink, J. J., Bouman, M. A., Bueno de Mesquita, E., & Slappendel, S. (1978b). Perimetry of contrast detection thresholds of moving spatial sine wave patterns II. The far peripheral visual field (eccentricity 0-50). *Journal of the Optical Society of America*, *68*(6), 850. http://doi.org/10.1364/JOSA.68.000850

Koenderink, J. J., Bouman, M. A., de Mesquita, A. E., & Slappendel, S. (1978). Perimetry of contrast detection thresholds of moving spatial sine wave patterns: I. The near peripheral visual field (eccentricity 0°-8°). *Journal of the Optical Society of America*, *68*(6), 845–849.

Kowler, E., & Steinman, R. M. (1980). Small saccades serve no useful purpose: Reply to a letter by R. W. Ditchburn. *Vision Research*, *20*(3), 273–276. http://doi.org/10.1016/0042-6989(80)90113-3

Krauskopf, J., Cornsweet, T. N., & Riggs, L. A. (1960). Analysis of eye movements during monocular and binocular fixation. *Journal of the Optical Society of America*, *50*.

Kuehni, R. G. (2016). How many object colors can we distinguish? *Color Research & Application*, *41*(5), 439–444. http://doi.org/10.1002/col.21980

Kumar, G., & Chung, S. T. L. (2014). Characteristics of Fixational Eye Movements in People with Macular Disease. *Investigative Ophthalmology & Visual Science*, iovs.14-14608-. http://doi.org/10.1167/iovs.14-14608

Land, M. F. (1969). Movements of the retinae of jumping spiders (Salticidae: Dendryphantinae) in response to visual stimuli. *Journal of Experimental Biology*, *51*(2), 471–493.

Land, M. F. (1999). Motion and vision: Why animals move their eyes. *Journal of Comparative Physiology A*, *185*(4), 341–352. http://doi.org/10.1007/s003590050393

Latham, K., & Whitaker, D. (1996). A Comparison of Word Recognition and Reading Performance in Foveal and Peripheral Vision. *Vision Research*, *36*(17), 2665–2674. http://doi.org/10.1016/0042-6989(96)00022-3

Lee, K. K., & Markowitz, S. N. (2010). Scotoma size reduction as an adaptive strategy in age-related macular degeneration. *Canadian Journal of Ophthalmology. Journal Canadien D'ophtalmologie*, *45*(4), 393–8. http://doi.org/10.3129/i10-021

Legge, G. E., & Bigelow, C. A. (2011). Does print size matter for reading? A review of findings from vision science and typography. *Journal of Vision*, *11*(5), 1–22. http://doi.org/10.1167/11.5.8

Legge, G. E., Cheung, S. H., Chung, S. T. L., Lee, H. W., Gefroh, J., & Kwon, M. (2008). Training peripheral vision to read. In J. Rieser, D. Ashmead, F. Ebner, & A. Corn (Eds.), *Blindness and brain plasticity in navigation and object perception* (pp. 209–226). New York, NY: Lawrence Erlbaum Associates.

Legge, G. E., Mansfield, J. S., & Chung, S. T. L. (2001). Psychophysics of reading: XX. Linking letter recognition to reading speed in central and peripheral vision. *Vision Research*, *41*(6), 725–743. http://doi.org/10.1016/S0042-6989(00)00295-9

Legge, G. E., Rubin, G. S., & Luebker, A. (1987). Psychophysics of reading—V. The role of contrast in normal vision. *Vision Research*, *27*(7), 1165–1177. http://doi.org/10.1016/0042-6989(87)90028-9

Legge, G. E., Rubin, G. S., Pelli, D. G., & Schleske, M. M. (1985). Psychophysics of reading—II. Low vision. *Vision Research*, *25*(2), 253–265. http://doi.org/10.1016/0042-6989(85)90118-X

Levi, D. M. (1996). Pattern perception at high velocities. *Current Biology*, *6*(8), 1020–1024.

Levi, D. M. (2008). Crowding--an essential bottleneck for object recognition: a mini-review. *Vision Research*, *48*(5), 635–54. http://doi.org/10.1016/j.visres.2007.12.009

Lim, L. S., Mitchell, P., Seddon, J. M., Holz, F. G., & Wong, T. Y. (2012). Age-related macular degeneration. *The Lancet*, *379*(9827), 1728–38. http://doi.org/10.1016/S0140-6736(12)60282-7

Lin, Z., & He, S. (2012). Emergent filling in induced by motion integration reveals a high-level mechanism in filling in. *Psychological Science*, *23*(12), 1534–41. http://doi.org/10.1177/0956797612446348

Macedo, A. F., Crossland, M. D., & Rubin, G. S. (2011). Investigating Unstable Fixation in Patients with Macular Disease. *Investigative Ophthalmology and Visual Science*, *52*(3), 1275–1280.

Macedo, A. F., Nascimento, S. M. C., Gomes, A. O. S., & Puga, A. T. (2007). Fixation in patients with juvenile macular disease. *Optometry and Vision Science : Official Publication of the American Academy of Optometry*, *84*(9), 852–858. http://doi.org/10.1097/OPX.0b013e3181559beb

Mansfield, J. S., Ahn, S. J., Legge, G. E., & Luebker, A. (1993). A new reading-acuity chart for normal and low vision. In *Ophthalmic and Visual Optics/Noninvasive Assessment of the Visual System, OSA Technical Digest Series* (Vol. 3, pp. 232–235). Washington, DC: Optical Society of America.

Mansfield, J. S., Legge, G. E., & Bane, M. C. (1996). Psychophysics of reading. XV: Font effects in normal and low vision. *Investigative Ophthalmology & Visual Science*, *37*(8), 1492–1501.

Markowitz, S. N., & Aleykina, N. (2010). The relationship between scotoma displacement and preferred retinal loci in low-vision patients with age-related macular degeneration. *Canadian Journal of Ophthalmology*, *45*(1), 58–61. http://doi.org/10.3129/i09-244

Martinez-Conde, S. (2006a). Chapter 8: Fixational eye movements in normal and pathological vision. *Progress in Brain Research*, *154*, 151–176. http://doi.org/10.1016/S0079-6123(06)54008-7

Martinez-Conde, S. (2006b). Fixational eye movements in normal and pathological vision. *Progress in Brain Research*, *154*, 151–76. http://doi.org/10.1016/S0079-6123(06)54008-7

Martinez-Conde, S., Macknik, S. L., & Hubel, D. H. (2004). The role of fixational eye movements in visual perception. *Nature Reviews Neuroscience*, *5*(3), 229–240.

Martinez-Conde, S., Macknik, S. L., Troncoso, X. G., & Dyar, T. A. (2006). Microsaccades Counteract Visual Fading during Fixation. *Neuron*, *49*(2), 297–305.

Mateeff, S., Popov, D., & Hohnsbein, J. (1993). Multi-aperture viewing: perception of figures through very small apertures. *Vision Research*, *33*(17), 2563–2567. http://doi.org/10.1016/0042-6989(93)90135-J

Mehta, S. (2015). Age-Related Macular Degeneration. *Primary Care: Clinics in Office Practice*, *42*(3), 377–391. http://doi.org/10.1016/j.pop.2015.05.009

Metra, A. B., Vingrys, A. J., & Badcock, D. R. (1993). Calibration of a color monitor for visual psychophysics. *Behavior Research Methods. Instruments. & Computers*, *25*(3), 371–383.

Morgan, M. J., & Watt, R. J. (1983). On the failure of spatiotemporal interpolation: A filtering model. *Vision Research*, *23*(10), 997–1004. http://doi.org/10.1016/0042-6989(83)90010-X

Muckli, L., Kohler, A., Kriegeskorte, N., & Singer, W. (2005). Primary Visual Cortex Activity along the Apparent-Motion Trace Reflects Illusory Perception. *PLoS Biology*, *3*(8), e265. http://doi.org/10.1371/journal.pbio.0030265

Murakami, I., & Cavanagh, P. (1998). A jitter after-effect reveals motion-based stabilization of vision. *Nature*, *395*(6704), 798–801. http://doi.org/10.1038/27435

Naito, T., Sato, H., & Osaka, N. (2010). Direction anisotropy of human motion perception depends on stimulus speed. *Vision Research*, *50*(18), 1862–1866. http://doi.org/10.1016/j.visres.2010.06.007

Nishida, S. (2004). Motion-Based Analysis of Spatial Patterns by the Human Visual System. *Current Biology*, *14*(1), 830–839.

Nishida, S., Watanabe, J., Kuriki, I., & Tokimoto, T. (2007). Human visual system integrates color signals along a motion trajectory. *Current Biology*, *17*(4), 366–72.

Nothdurft, H. C. (1991). *Texture segmentation and pop-out from orientation contrast*. *Vision Research* (Vol. 31).

Palmer, E. M., Kellman, P. J., & Shipley, T. F. (2006). A theory of dynamic occluded and illusory object perception. *Journal of Experimental Psychology*, *135*(4), 513–541.

Park, S., Park, M., & Kang, M. (2003). Super-resolution image reconstruction: a technical overview. *Signal Processing Magazine*, *IEEE*(20), 21–36.

Peirce, J. W. (2007). PsychoPy - Psychophysics software in Python. *Journal of Neuroscience Methods*, *162*(1–2), 8–13.

Pelli, D. G., Robson, J. G., & Wilkins, A. J. (1988). The design of a new letter chart for measuring contrast sensitivity. *Clinical Vision Sciences*, *2*(3), 187–198.

Pelli, D. G., Tillman, K. A., Freeman, J., Su, M., Berger, T. D., & Majaj, N. J. (2007). Crowding and eccentricity determine reading rate. *Journal of Vision*, *7*(2), 1–36. http://doi.org/10.1167/7.2.20

Pelli, D. G., & Zhang, L. (1991). Accurate control of contrast on microcomputer displays. *Vision Research*, *31*(7–8), 1337–1350. http://doi.org/10.1016/0042-6989(91)90055-A

Perneger, T. V. (1998). What's wrong with Bonferroni adjustments. *British Medical Journal*, *316.7139*, 1236–1238.

Pointer, J. S., & Hess, R. F. (1989). The contrast sensitivity gradient across the human visual field: With emphasis on the low spatial frequency range. *Vision Research*, *29*(9), 1133–1151. http://doi.org/10.1016/0042-6989(89)90061-8

Polyak, S. L. (1941). *The Retina*. Chicago: University of Chicago Press.

Previc, F. H. (2011). Functional specialization in the lower and upper visual fields in humans: Its ecological origins and neurophysiological implications. *Behavioral and Brain Sciences*, *13*(3), 519–542. http://doi.org/10.1017/S0140525X00080018

Rabb, M. F., Tso, M. O. M., & Fishman, G. A. (1986). Cone-Rod Dystrophy: A Clinical and Histopathologic Report. *Ophthalmology*, *93*(11), 1443–1451. http://doi.org/10.1016/S0161-6420(86)33547-4

Rabin, J. (1994). Luminance Effects on Visual Acuity and Small Letter Contrast Sensitivity. *Optometry and Vision Science*, *71*(11), 685–688.

Ransom-Hogg, A., & Spillmann, L. (1980). Perceptive field size in fovea and periphery of the light- and dark-adapted retina. *Vision Research*, *20*(3), 221–228. http://doi.org/10.1016/0042-6989(80)90106-6

Ratliff, F., & Riggs, L. A. (1950). Involuntary motions of the eye during monocular fixation. *Journal of Experimental Psychology*, *40*(6), 687–701. http://doi.org/10.1037/h0057754

Rees, A. L., Kabanarou, S. A., Culham, L. E., & Rubin, G. S. (2005). Can retinal eccentricity predict visual acuity and contrast sensitivity at the PRL in AMD patients? *International Congress Series*, *1282*, 694–698. http://doi.org/10.1016/j.ics.2005.05.172

Regan, D., & Beverley, K. I. (1983). Visual fields described by contrast sensitivity, by acuity, and by relative sensitivity to different orientations. *Investigative Ophthalmology and Visual Science*, *24*, 754–759.

Reich, L. N., & Ekabutr, M. (2002). The effects of optical defocus on the legibility of the Tumbling-E and Landolt-C. *Optometry & Vision Science*, *79*(6), 389–393. http://doi.org/10.1097/00006324-200206000-00013

Riggs, L. A., Armington, J. C., & Ratliff, F. (1954). Motions of the retinal image during fixation. *Journal of the Optical Society of America*, *44*(4), 315–21.

Riggs, L. A., & Ratliff, F. (1951). Visual Acuity and the Normal Tremor of the Eyes. *Science*, *114*(2949).

Riggs, L. A., Ratliff, F., Cornsweet, J. C., & Cornsweet, T. N. (1953). The disappearance of steadily fixated visual test objects. *Journal of the Optical Society of America*, *43*(6), 495–501.

Rijsdijk, J. P., Kroon, J. N., & van der Wildt, G. J. (1980). Contrast sensitivity as a function of position on the retina. *Vision Research*, *20*(3), 235–241. http://doi.org/10.1016/0042-6989(80)90108-X

Robson, J. G. (1966). Spatial and temporal contrast sensitivity functions of the visual system. *Journal of the Optical Society of America A*, *56*, 1141–1142.

Rodieck, R. W. (1983). Raster-based colour stimulators. In J. D. Mollon & L. T. Sharpe (Eds.), *Colour vision* (1st ed., pp. 133–144). London: Academic Press.

Rosenfeld, P. J., Brown, D. M., Heier, J. S., Boyer, D. S., Kaiser, P. K., Chung, C. Y., & Kim, R. Y. (2006). Ranibizumab for Neovascular Age-Related Macular Degeneration. *New England Journal of Medicine*, *355*(14), 1419–1431. http://doi.org/10.1056/NEJMoa054481

Rossi, E. A., & Roorda, A. (2010). The relationship between visual resolution and cone spacing in the human fovea. *Nature Neuroscience*, *13*(2), 156–7. http://doi.org/10.1038/nn.2465

Rovamo, J., Virsu, V., Laurinen, P., & Hyvärinen, L. (1982). Resolution of gratings oriented along and across meridians in peripheral vision. *Investigative Ophthalmology and Visual Science*, *23*(5), 666–670.

Roy, M., & Kaiser-Kupfer, M. (1990). Second eye involvement in age-related macular degeneration: a four-year prospective study. *Eye*, *4*, 813–818.

Rubin, G. S., & Feely, M. (2009). The Role of Eye Movements During Reading in Patients with Age-Related Macular Degeneration (AMD). *Neuro-Ophthalmology*, *33*(3), 120–126. http://doi.org/10.1080/01658100902998732

Rubin, G. S., & Turano, K. (1992). Reading without saccadic eye movements. *Vision Research*, *32*(5), 895–902. http://doi.org/10.1016/0042-6989(92)90032-E

Rubin, G. S., & Turano, K. (1994). Low vision reading with sequential word presentation. *Vision Research*, *34*(13), 1723–1733. http://doi.org/10.1016/0042-6989(94)90129-5

Rucci, M., Iovin, R., Poletti, M., & Santini, F. (2007). Miniature eye movements enhance fine spatial detail. *Nature*, *447*(7146), 852–855. http://doi.org/10.1038/nature05866

Ruddock, K. H. (1965). The effect of age upon colour vision—II. changes with age in light transmission of the ocular media. *Vision Research*, *5*(1), 47–58. http://doi.org/10.1016/0042-6989(65)90074-X

Scherzer, T. R., & Ekroll, V. (2012). Occlusion improves the interpolation of sampled motion. *Vision Research*, *62*, 17–25. http://doi.org/10.1016/j.visres.2012.02.015

Schiller, P. H., Sandell, J. H., & Maunsell, J. H. R. (1986). Functions of the ON and OFF channels of the visual system. *Nature*, *322*(6082), 824–825. http://doi.org/10.1038/322824a0

Scholl, B. J., & Pylyshyn, Z. W. (1999). Tracking multiple items through occlusion: clues to visual objecthood. *Cognitive Psychology*, *38*(2), 259–90. http://doi.org/10.1006/cogp.1998.0698

Schuchard, R. A. (2005). Preferred retinal loci and macular scotoma characteristics in

patients with age-related macular degeneration. *Canadian Journal of Ophthalmology. Journal Canadien D'ophtalmologie*, *40*(3), 303–312. http://doi.org/10.1016/S0008-4182(05)80073-0

Seiple, W., Szlyk, J. P., McMahon, T. T., Pulido, J., & Fishman, G. A. (2005). Eye-Movement Training for Reading in Patients with Age-Related Macular Degeneration. *Investigative Opthalmology & Visual Science*, *46*(8), 2886. http://doi.org/10.1167/iovs.04-1296

Shah, N., Dakin, S. C., Dobinson, S., Tufail, A., Egan, C. A., & Anderson, R. S. (2016). Visual acuity loss in patients with age-related macular degeneration measured using a novel high-pass letter chart. *British Journal of Ophthalmology*, *100*(10), 1346–52. http://doi.org/10.1136/bjophthalmol-2015-307375

Shima, N., Markowitz, S. N., & Reyes, S. V. (2010). Concept of a functional retinal locus in age-related macular degeneration. *Canadian Journal of Ophthalmology. Journal Canadien D'ophtalmologie*, *45*(1), 62–6. http://doi.org/10.3129/i09-236

Shioiri, S., & Cavanagh, P. (1990). ISI produces reverse apparent motion. *Vision Research*, *30*(5), 757–768. http://doi.org/10.1016/0042-6989(90)90101-P

Shipley, T. F., & Cunningham, D. W. (2001). Perception of occluding and occluded objects over time: Spatiotemporal segmentation and unit formation. In T. F. Shipley & P. J. Kellman (Eds.), *From fragments to objects: Segmentation and grouping in vision* (pp. 557–585). Amsterdam: Elsevier.

Simpson, T. L., Barbeito, R., & Bedell, H. E. (1986). The effect of optical blur on visual acuity for targets of different luminances. *Ophthalmic & Physiological Optics : The Journal of the British College of Ophthalmic Opticians (Optometrists)*, *6*(3), 279–81.

Sloan, L. L. (1959). New test charts for the measurement of visual acuity at far and near distances. *American Journal of Ophthalmology*, *48*, 807.

Stappers, P. J. (1989). Forms can be recognized from dynamic occlusion alone. *Perceptual and Motor Skills*, *68*(1), 243–51. http://doi.org/10.2466/pms.1989.68.1.243

Stevenson, S. B., Cormack, L. K., & Schor, C. M. (1989). Hyperacuity, superresolution and gap resolution in human stereopsis. *Vision Research*, *29*(11), 1597–1605. http://doi.org/10.1016/0042-6989(89)90141-7

Strasburger, H., Rentschler, I., & Juettner, M. (2011). Peripheral vision and pattern recognition: A review. *Journal of Vision*, *11*(5), 13–13. http://doi.org/10.1167/11.5.13

Swanson, W. H., Ueno, T., Smith, V. C., & Pokorny, J. (1987). Temporal modulation sensitivity and pulse-detection thresholds for chromatic and luminance perturbations. *Journal of the Optical Society of America A*, *4*(10).

Thibos, L. N., & Anderson, R. S. (2004). The filtered Fourier difference spectrum predicts psychophysical letter discrimination in the peripheral retina. *Spatial Vision*, *17*(1), 5–15. http://doi.org/10.1163/156856804322778242

Thibos, L. N., Cheney, F. E., & Walsh, D. J. (1987). Retinal limits to the detection and resolution of gratings. *Journal of the Optical Society of America A*, *4*(8), 1524–1529.

Thibos, L. N., Still, D. L., & Bradley, A. (1996). Characterization of spatial aliasing and contrast sensitivity in peripheral vision. *Vision Research*, *36*(2), 249–258. http://doi.org/10.1016/0042-6989(95)00109-D

Thibos, L. N., Walsh, D. J., & Cheney, F. E. (1987). Vision beyond the resolution limit: Aliasing in the periphery. *Vision Research*, *27*(12), 2193–2197.

Timberlake, G. T., Peli, E., Essock, E. A., & Augliere, R. A. (1987). Reading with a macular scotoma. II. Retinal locus for scanning text. *Investigative Ophthalmology & Visual Science*, *28*(8), 1268–1274.

Toet, A., & Levi, D. M. (1992). The two-dimensional shape of spatial interaction zones in the parafovea. *Vision Research*, *32*(7), 1349–1357. http://doi.org/10.1016/0042-6989(92)90227-A

Torgesen, J. K., Wagner, R. K., & Rashotte, C. A. (1999). *Test of word reading efficiency*. Austin, TX: Pro-Ed.

Treisman, A. M., & Gelade, G. (1980). A feature-integration theory of attention. *Cognitive Psychology*, *12*(1), 97–136. http://doi.org/10.1016/0010-0285(80)90005-5

Treutwein, B., & Strasburger, H. (1999). Fitting the psychometric function. *Perception & Psychophysics*, *61*(1), 87–106. http://doi.org/10.3758/BF03211951

Troxler, D. (1804). Über das Verschwinden gegebener Gegenstände innerhalb unseres Gesichtskreises. *Ophthalmologische Bibliothek*, *2*(2), 1–53.

Van De Grind, W. A., Koenderink, J. J., Van Doorn, A. J., Milders, M. V, & Voerman, H. (1993). Inhomogeneity and anisotropies for motion detection in the monocular visual field of human observers. *Vision Research*, *33*(8), 1089–1107. http://doi.org/10.1016/0042-6989(93)90242-O

Van Nes, F. L., & Bouman, M. A. (1967). Spatial Modulation Transfer in the Human Eye. *Journal of the Optical Society of America*, *57*(3), 401. http://doi.org/10.1364/JOSA.57.000401

Van Nes, F. L., Koenderink, J. J., Nas, H., & Bouman, M. A. (1967). Spatiotemporal Modulation Transfer in the Human Eye. *Journal of the Optical Society of America*, *57*(9), 1082. http://doi.org/10.1364/JOSA.57.001082

Van Santen, J. P. H., & Sperling, G. (1985). Elaborated Reichardt detectors. *Journal of the Optical Society of America A*, *2*(2), 300. http://doi.org/10.1364/JOSAA.2.000300

Velez-Montoya, R., Oliver, S. C. N., Olson, J. L., Fine, S. L., Quiroz-Mercado, H., & Mandava, N. (2014). Current knowledge and trends in age-related macular degeneration. *Retina*, *34*(3), 423–441. http://doi.org/10.1097/IAE.0000000000000036

Vol, I. A., Pavlovskaja, M. B., & Bondarko, V. M. (1990). Similarity between Fourier transforms of objects predicts their experimental confusions. *Perception & Psychophysics*, *47*(1), 12–21. http://doi.org/10.3758/BF03208160

Walker, R., Bryan, L., Harvey, H., Riazi, A., & Anderson, S. J. (2016). The value of Tablets as reading aids for individuals with central visual field loss: an evaluation of eccentric reading with static and scrolling text. *Ophthalmic and Physiological Optics*, *36*(4), 459–464. http://doi.org/10.1111/opo.12296

Wang, Y. Z., Bradley, A., & Thibos, L. N. (1997a). Aliased Frequencies Enable the Discrimination of Compound Gratings in Peripheral Vision. *Vision Research*, *37*(3), 283–290.

Wang, Y. Z., Bradley, A., & Thibos, L. N. (1997b). Interaction between sub- and supra-Nyquist spatial frequencies in peripheral vision. *Vision Research*, *37*(18), 2545–2552. http://doi.org/10.1016/S0042-6989(97)00065-5

Watson, A. B. (2013). High Frame Rates and Human Vision: A View Through the Window of Visibility. *SMPTE Motion Imaging Journal*, *122*(2), 18–32. http://doi.org/10.5594/j18266

Watson, A. B., & Ahumada, A. J. (2005). A standard model for foveal detection of spatial contrast. *Journal of Vision*, *5*(9), 6–6. http://doi.org/10.1167/5.9.6

Watson, A. B., Ahumada, A. J., & Farrell, J. E. (1986). Window of visibility: a psychophysical theory of fidelity in time-sampled visual motion displays. *Journal of the Optical Society of America A*, *3*(3), 300. http://doi.org/10.1364/JOSAA.3.000300

Watson, L. M., Strang, N. C., Scobie, F., Love, G. D., Seidel, D., & Manahilov, V. (2012). Image jitter enhances visual performance when spatial resolution is impaired. *Investigative Ophthalmology and Visual Science*, *53*(10), 6004–6010. http://doi.org/10.1167/iovs.11-9157

Wertheimer, M. (1912). Experimentelle Studien über das Sehen von Bewegung (Experimental studies on seeing motion). *Zeitschrift Für Psychologie*, *61*(1), 161–265.

Westheimer, G. (1979). Scaling of Visual Acuity Measurements. *Archives of Ophthalmology*, *97*(2), 327–330. http://doi.org/10.1001/archopht.1979.01020010173020

Westheimer, G. (1982). The spatial grain of the perifoveal visual field. *Vision Research*, *22*(1), 157–162. http://doi.org/10.1016/0042-6989(82)90177-8

Westheimer, G. (1987). Visual Acuity and Hyperacuity: Resolution, Localization, Form. *Optometry & Vision Science*, *64*(8), 567–573.

Westheimer, G. (2009). Visual acuity: Information theory, retinal image structure and resolution thresholds. *Progress in Retinal and Eye Research*, *28*(3), 178–186.

Westheimer, G., & Beard, B. L. (1998). Orientation dependency for foveal line stimuli: detection and intensity discrimination, resolution, orientation discrimination and vernier acuity. *Vision Research*, *38*(8), 1097–1103.

Westheimer, G., & McKee, S. P. (1975). Visual acuity in the presence of retinal-image motion. *Journal of the Optical Society of America A*, *65*(7), 847–850.

Whittaker, S. G., Budd, J., & Cummings, R. W. (1988). Eccentric fixation with macular scotoma. *Investigative Ophthalmology & Visual Science*, *29*(2), 268–278.

Whittaker, S. G., & Cummings, R. W. (1990). Foveating saccades. *Vision Research*, *30*(9), 1363–1366. http://doi.org/10.1016/0042-6989(90)90009-A

Wichmann, F. A., & Hill, N. J. (2001a). The psychometric function: I. Fitting, sampling, and goodness of fit. *Perception & Psychophysics*, *63*(8), 1293–1313. http://doi.org/10.3758/BF03194544

Wichmann, F. A., & Hill, N. J. (2001b). The psychometric function: II. Bootstrap-based confidence intervals and sampling. *Perception & Psychophysics*, *63*(8), 1314–1329. http://doi.org/10.3758/BF03194545

Williams, D. R. (1985). Aliasing in human foveal vision. *Vision Research*, *25*(2), 195–205. http://doi.org/10.1016/0042-6989(85)90113-0

Williams, D. R. (1986). Seeing through the photoreceptor mosaic. *Trends in Neurosciences*, *9*, 193–198.

Williams, D. R. (1988). Topography of the foveal cone mosaic in the living human eye. *Vision Research*, *28*(3), 433–454. http://doi.org/10.1016/0042-6989(88)90185-X

Williams, D. R., Artal, P., Navarro, R., McMahon, M. J., & Brainard, D. H. (1996). Off-axis optical quality and retinal sampling in the human eye. *Vision Research*, *36*(8), 1103–1114. http://doi.org/10.1016/0042-6989(95)00182-4

Winther, C., & Frisén, L. (2010). A compact rarebit test for macular diseases. *British Journal of Ophthalmology*, *94*(3), 324–7. http://doi.org/10.1136/bjo.2009.164749

Wong, T. Y., Liew, G., & Mitchell, P. (2007). Clinical update: new treatments for age-related macular degeneration. *The Lancet*, *370*(9583), 204–206.

http://doi.org/10.1016/S0140-6736(07)61104-0

Xu, R., & Bradley, A. (2015). IURead: a new computer-based reading test. *Ophthalmic and Physiological Optics*, *35*(5), 500–513. http://doi.org/10.1111/opo.12233

Yang, J., Wright, J., Huang, T. S., & Ma, Y. (2010). Image Super-Resolution Via Sparse Representation. *IEEE Transactions on Image Processing*, *19*(11), 2861–2873.

Yanoff, M., & Sassani, J. W. (2009). *Ocular Pathology* (6th ed.). Elsevier Health Sciences.

Yarbus, A. L. (1967). Eye movements during perception of complex objects. In *Eye Movements and Vision* (pp. 171–211). New York: Springer. http://doi.org/10.1007/978-1-4899-5379-7

Yellott, J. I. (1983). Spectral consequences of photoreceptor sampling in the rhesus retina. *Science*, *221*(4608), 382–385. http://doi.org/10.1126/science.6867716

Zele, A. J., Cao, D., & Pokorny, J. (2008). Rod–cone interactions and the temporal impulse response of the cone pathway. *Vision Research*, *48*(26), 2593–2598. http://doi.org/10.1016/j.visres.2008.04.003

Zuber, B. L., Stark, L., & Cook, G. (1965). Microsaccades and the Velocity-Amplitude Relationship for Saccadic Eye Movements. *Science*, *150*(3702).

Appendices

Appendix 1

Two different analysis techniques are used to estimate resolution thresholds in this thesis. For a description of both, refer to sections 2.5.2 and 2.5.3. In order to ensure the analysis procedure has no effect on the estimated resolution threshold, a comparison was made between thresholds as estimated by the two procedures. The data compared were from Experiment 1.1.

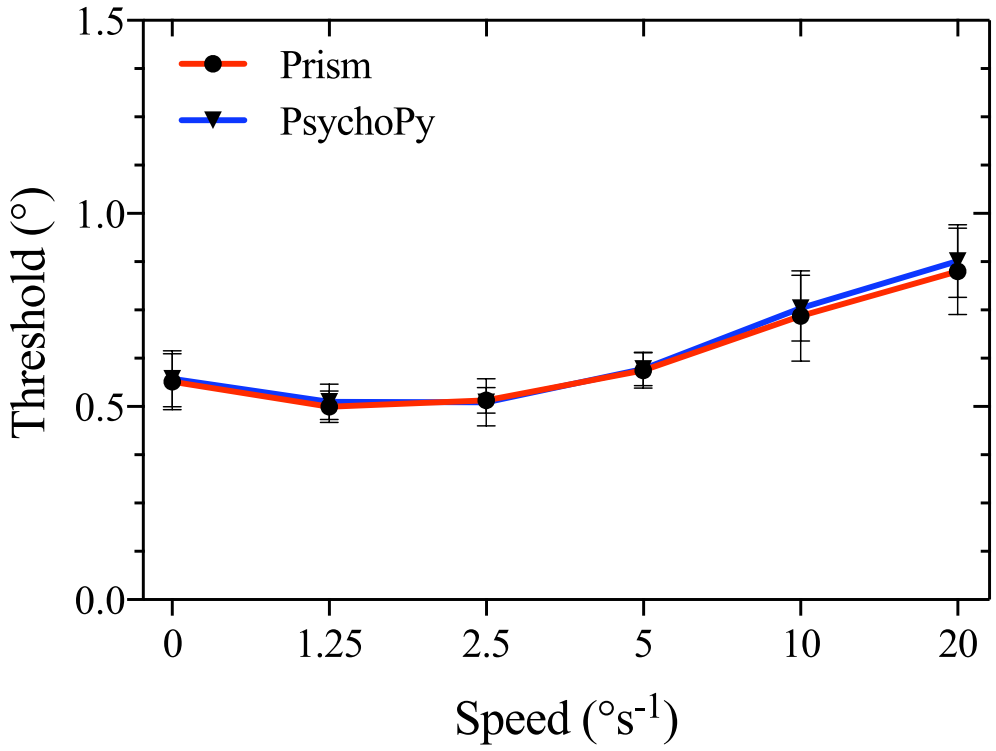

Figure 70: Threshold target size as a function of speed for smoothly moving targets (Experiment 1.1), as calculated using different analysis techniques.

Figure 70 does not show clear differences between threshold estimation techniques. The root mean square deviation (RMSD) between the different binning procedures is

calculated using Equation 11, and thereby the normalised RMSD (NRMSD) using Equation 12.

$$RMSD = \sqrt{\frac{\sum_{c=1}^{n}\left(T_{1,c}-T_{2,c}\right)^2}{n}} \tag{11}$$

$$NRMSD = \frac{RMSD}{\bar{T}} \tag{12}$$

Where $T_{1,c}$ and $T_{2,c}$ are the resolution thresholds calculated by the Prism and PsychoPy methods for condition c, respectively. The NRMSD between the two methods was calculated as 0.068.

Appendix 2

Different groups of observers participated in Experiment 3.2.1 and Experiment 3.3 (Chapter 5). However, for both groups, resolution thresholds were calculated for unmodulated targets at 10° in the periphery, at speeds 0-20°s^{-1}.

Eight observers (mean age 22.75 years, *SD* 2.31 years) participated in Experiment 3.2.1, and eight participants (mean age 24.00 years, *SD* 2.93 years) participated in Experiment 3.3.

Figure 71 shows a comparison of resolution thresholds for these conditions between the two groups.

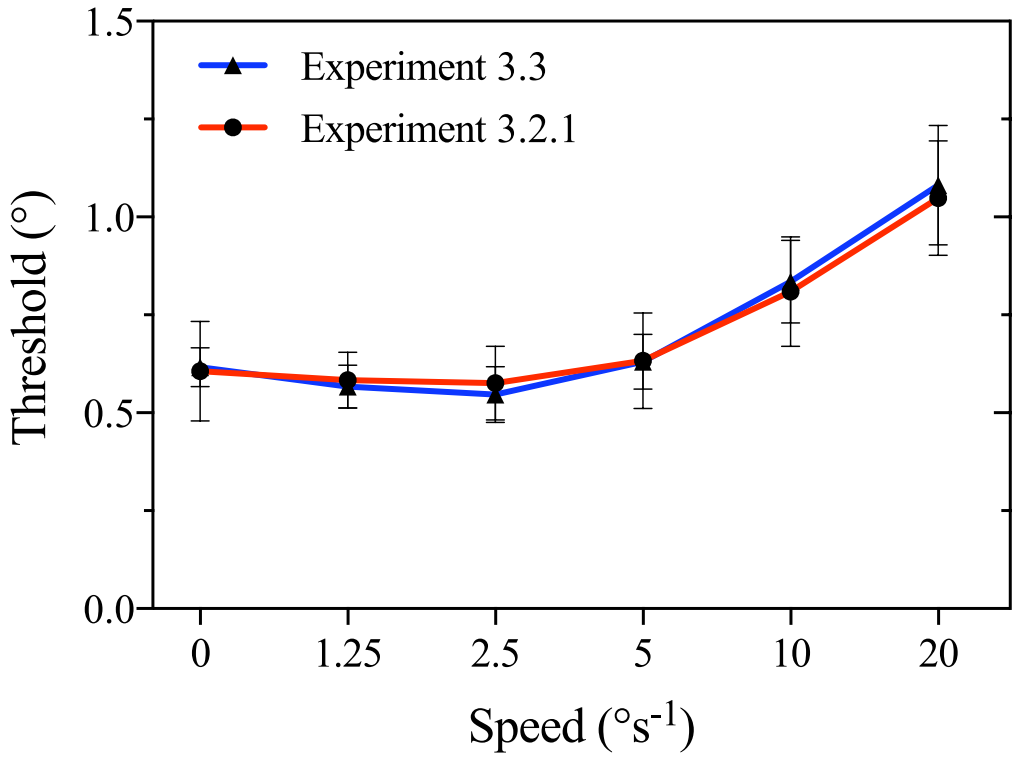

Figure 71: showing resolution thresholds for targets moving along isoeccentric arcs at 10° in the periphery, at speeds 0-20°s^{-1} for two groups of observers.

Figure 71 indicates that the differences between thresholds for the two groups are very low across the range of speeds. A two-way ANOVA confirmed that there was no significant difference between groups ($F(1,84)=0.18$, $p>.05$). The effect of target speed remained, however: as target speed increases, resolution thresholds rise significantly ($F(5,84)=38.40$, $p<.0001$). No significant interaction was reported ($F(5,84)=0.14$, $p>.05$).

Appendix 3

In Experiment 4.1.2 it was shown that, at high amplitude target jitter, temporal subsampling can improve resolution for targets restrained to an isoeccentric arc. One potential explanation for this result concerns the temporal response function of the photoreceptor cells stimulated by the targets. In order to examine whether this explanation is supported by the observers' data, a comparison was made between resolution thresholds for jittering targets, and the absolute distance between the locations of successive target presentations. For a full explanation of the motivation for this analysis, refer to section 6.4.

The difference in target position between frames was calculated for the example stimulus used in Figure 47 and Figure 48. The Euclidian distance was calculated between successive frames for targets with unrestricted (varying) eccentricity, and for targets restricted to an isoeccentric arc, 10° from fixation. In the unmodulated condition, the target was displayed on every video frame, whereas in the subsampled condition, the target was displayed on every sixth video frame (with blank intervals of 66.7ms). The data in Figure 72 are reanalysed from Experiment 4.1.1 and 4.1.2. For a detailed description of the stimulus, procedure, and observers, refer to section 6.2.1.

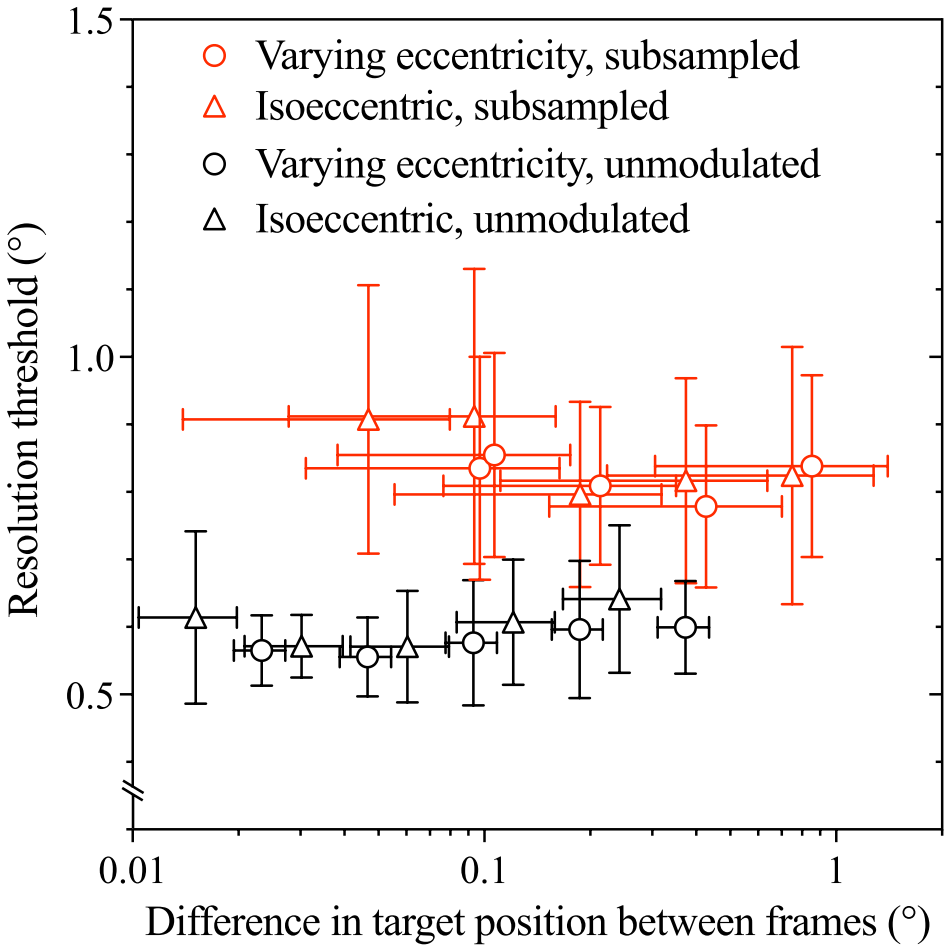

Figure 72: resolution thresholds for jittering targets as a function of the average distance between the locations of the target on successive presentations. Data is reanalysed from Experiment 4.1.1 and 4.1.2. Red data points indicate the temporally subsampled condition, whereas black targets indicate the unmodulated condition. Circles refer to data from Experiment 4.1.1, whereby the target eccentricity was unrestricted. Triangles refer to data from Experiment 4.1.2, in which the target was restrained to an isoeccentric arc. The data points are the mean resolution thresholds across observers. Vertical error bars indicate the between-subjects 95%CI of thresholds, while the horizontal error bars are the 95%CI of the mean distance between frames. 24 changes in target position were analysed, from one observer.

Figure 72 shows a clear separation between resolution thresholds for the unmodulated and subsampled conditions. However, there is no such separation between isoeccentric and unrestrained targets. If the difference in target position between

frames was driving the improvement in resolution thresholds for subsampled targets at high amplitude jitter in Experiment 4.1.2, it would be expected that the thresholds for the unmodulated and subsampled targets would converge in this analysis. Since this is not the case, this explanation is not supported.